U. PORTO

DOUTORAMENTO

BIOLOGIA MOLECULAR E CELULAR

Dissecting the interplay between kinetochores and centrosomes for mitotic fidelity

Nelson Machado Leça

D
2025



U. PORTO

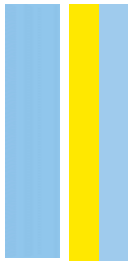
Nelson Machado Leça. Dissecting the interplay between kinetochores and centrosomes for mitotic fidelity



D.ICBAS **2025**

Dissecting the interplay between kinetochores and centrosomes for mitotic fidelity
Nelson Machado Leça

SEDE ADMINISTRATIVA
INSTITUTO DE CIÊNCIAS BIOMÉDICAS ABEL SALAZAR
FACULDADE DE CIÊNCIAS



NELSON MACHADO LEÇA

DISSECTING THE INTERPLAY BETWEEN KINETOCHORES AND CENTROSOMES FOR MITOTIC FIDELITY

Tese de Candidatura ao grau de Doutor em Biologia Molecular e Celular;
Programa Doutoral da Universidade do Porto (Instituto de Ciências Biomédicas Abel Salazar da Universidade do Porto)
i3S – Instituto de Investigação e Inovação em Saúde

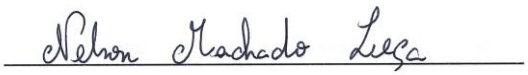
Orientador – Professor Doutor Carlos Conde
Categoria – Professor Auxiliar
Afiliação – i3S – Instituto de Investigação e Inovação em Saúde; IBMC – Instituto de Biologia Molecular e Celular; ICBAS – Instituto de Ciências Biomédicas Abel Salazar, Universidade do Porto

Co-orientador – Doutor Eurico Morais de Sá
Categoria – Investigador Principal
Afiliação – i3S – Instituto de Investigação e Inovação em Saúde; IBMC – Instituto de Biologia Molecular e Celular

Co-orientador – Professor Doutor Claudio Sunkel
Categoria – Professor Catedrático
Afiliação – i3S – Instituto de Investigação e Inovação em Saúde; IBMC – Instituto de Biologia Molecular e Celular; ICBAS – Instituto de Ciências Biomédicas Abel Salazar, Universidade do Porto

DECLARAÇÃO

Declaro que a presente tese é de minha autoria e não foi utilizada previamente noutro curso ou unidade curricular, desta ou de outra instituição. As referências a outros autores (afirmações, ideias, pensamentos) respeitam escrupulosamente as regras da atribuição, e encontram-se devidamente indicadas no texto e nas referências bibliográficas, de acordo com as normas de referenciação. Tenho consciência de que a prática de plágio e auto-plágio constitui um ilícito académico.



(Nelson Machado Leça)

PREFACE

The work presented in this thesis was mainly performed at Cell Division and Genomic Stability (CDGS) group at the Institute for Research and Innovation in Health (i3S), University of Porto, under the supervision of Prof. Carlos Conde, and co-supervision of Dr. Eurico Morais de Sá and Prof. Claudio Sunkel. This work was performed in collaboration with the research groups coordinated by Prof. Thomas Maresca, Prof. Marin Barisic, Prof. Tanja Bange and Prof. Andrea Musacchio.





Nelson Machado Leça is the recipient of a PhD Grant (SFRH/BD/136526/2018) from Fundação para a Ciência e a Tecnologia (FCT). Nelson Machado Leça was awarded a Fulbright Portugal grant to develop part of the work in UMASS-Amherst, in the laboratory of Thomas J. Maresca. Nelson Machado Leça was also supported by a PhD scholarship under the NEUROSENSE project (HORIZON-EIC-2021-PATHFINDEROPEN-01; Project number 101047131). The research leading to the results present in this thesis was supported by national funds under FCT—Fundação para a Ciência e a Tecnologia, I.P., under the project UIDB/04293/2020 and by the project "Cancer Research on Therapy Resistance: From Basic Mechanisms to Novel Targets" – NORTE-01-0145-FEDER-000051, supported by Norte Portugal Regional Operational Programme (NORTE 2020), under the PORTUGAL 2020 Partnership Agreement, through the European Regional Development Fund (ERDF). This work was supported by an NIH grant (GM107026) to Thomas J. Maresca. Work in Tanja Bange's lab was supported by funding from the Deutsche Forschungsgemeinschaft (DFG) (project number: 5041140321) and from the Friedrich-Baur Stiftung. Tanja Bange is also thankful for funding by LMU Munich's Institutional Strategy LMUexcellent within the framework of the German Excellence Initiative and MS instrumentation by the DFG (INST 86/1800-1 FUGG for MSR). Work in Marin Barisic's lab was supported by the Novo Nordisk Foundation (NNF19OC0058504), the Independent Research Fund Denmark (3101-00075B), and the Lundbeck Foundation (R434-2023-431).







ORIGINAL PUBLICATIONS

This thesis contains results from the following original publication (Appendix):

Leça, N., Barbosa, F., Rodriguez-Calado, S., Verza, A. E., Moura, M., Pedroso, P. D., Pinto, I., Artes, E., Bange, T., Sunkel, C. E., Barisic, M., Maresca, T. J., Conde, C. (2025). Proximity-based activation of AURORA A by MPS1 potentiates error correction. *Current Biology*. Volume 35, Issue 8, 1935 - 1947.e8

Other publications to which I contributed within the scope of this thesis:

Mesquita, P., Coelho, A., Ribeiro, A.S., Póvoas, L.F.C., de Oliveira, C., Leça, N., Silva, S., Ferreira, D., Pádua, D., Coelho, R., Jerónimo, C., Paredes, J., Conde, C., Pereira, B., Almeida, R. (2025) The RNA-binding protein YTHDF3 affects gastric cancer cell migration and response to paclitaxel by regulating EZRIN. *Gastric Cancer*. 2025 Sep;28(5):760-775. doi: 10.1007/s10120-025-01620-y. Epub 2025 May 14. PMID: 40366509; PMCID: PMC12378723.

Moura, M., Barbosa, J., Pinto, I., Leça, N., Cunha-Silva, S., Verza, A. E., Pedroso, P. D., Lemaire, S., Duro, J., Silva, M., Oliveira, A., Reis, R., Nilsson, J., Sunkel, C. E., Musacchio, A., Bollen, M., Conde, C. (2024). POLO kinase inhibits Protein Phosphatase 1 to promote the Spindle Assembly Checkpoint and prevent aneuploidy. *Current Biology*.

This manuscript was accepted for publication in Current Biology and is currently *in press*.

AGRADECIMENTOS

Chegado o fim desta importante etapa da minha vida, quero agradecer a todos os que contribuíram de variadas formas para a conclusão do meu doutoramento.

Ao Carlos, por ter apostado num jovem de 20 anos que timidamente lhe enviou um email a perguntar se poderia acompanhar algum dos trabalhos a decorrer no seu laboratório, porque gostaria de contactar mais de perto com as técnicas de Biologia Molecular. E por, desde aí, me ter orientado por mais de 10 anos. Por me desafiar todos os dias a fazer melhor, por me fazer sentir um estudante competente e apoiado e pela confiança que depositou em mim. Pelas várias oportunidades que me proporcionou, pelas longas discussões em busca da próxima pergunta ou experiência para avançar os projetos científicos que tínhamos em mãos. Pelo muito que me fez crescer e evoluir cientificamente. E, claro, por todos os momentos não científicos que partilhamos, que não esquecerei, e por trabalhar ativamente para que o seu grupo seja uma equipa.

Ao Eurico por ter aceitado coorientar-me, por me ter ajudado a iniciar no mundo da Genética da *Drosophila* e por estar sempre disponível a responder a alguma dúvida ou a reunir para nos ajudar neste projeto.

Ao Professor Claudio por ter aceitado coorientar-me, por ser – e cito – "a pain in the neck" e pelas longas e produtivas discussões científicas que em muito contribuíram para a minha evolução e para evolução do meu trabalho.

À Ana, à Sofia e à Margarida por me fazerem sentir que a minha jornada e a delas ao longo do doutoramento eram uma só.

A todos os membros dos grupos Cell Division and Genomic Stability e Epithelial Polarity and Cell Division por fazerem do laboratório um divertido local de trabalho, pelas conversas e pelas discussões científicas. Vim para este laboratório pela vontade de aprender, fiquei pela vontade de explorar estes temas e pela vontade de estar com estas pessoas.

Ao Tom por me ter recebido no seu laboratório durante uns meses e por me ter ajudado a ambientar-me a um novo país.

A todas as pessoas que contribuíram para o trabalho aqui apresentado.

Aos meus amigos pelas partilhas, pela preocupação e pela amizade. E por perceberem que não consigo estar com eles tanto quanto gostaria.

Aos meus pais por durante mais de 30 anos cultivarem e alimentarem o meu interesse pela Ciência e pelo Conhecimento. Por todas as idas aos jardins zoológicos, oceanário, museus e caminhadas pela Natureza. Por me apoiarem em todas as etapas e em todas as decisões da minha vida, pelo respeito e pelo carinho.

À Margarida, pela simpatia demonstrada quando cheguei ao laboratório e por pacientemente me ensinar todas as técnicas que precisava de conhecer. Pela confiança que depositou em mim, desde o início. Pela amizade. Por aceitar partilhar a vida comigo e por me fazer sentir um homem com muita sorte. Pela compreensão demonstrada sempre que tive de trabalhar fora de horas. Por estar sempre ao meu lado nos bons e maus momentos. Por ser um exemplo de inteligência, competência, dedicação, preocupação e amor. Por todos os momentos, conversas e partilhas. Por me apoiar em todos os momentos e decisões e por ser a minha “safety net” ao longo deste percurso. E, finalmente, por partilhar comigo a experiência biológica mais importante da minha vida.

ABSTRACT

Faithful cell division relies on mitotic chromosomes becoming bioriented with each pair of sister kinetochores bound to microtubules oriented toward opposing spindle poles. Erroneous kinetochore-microtubule attachments often form during early mitosis but are destabilized through the phosphorylation of outer kinetochore proteins by centromeric AURORA B kinase (ABK) and centrosomal AURORA A kinase (AAK), thus allowing for re-establishment of attachments until biorientation is achieved. MPS1-mediated phosphorylation of NDC80 has also been shown to directly weaken the kinetochore-microtubule interface in yeast. In human cells, MPS1 has been proposed to transiently accumulate at end-on attached kinetochores and phosphorylate SKA3 to promote microtubule release. Whether MPS1 directly targets NDC80 and/or promotes the activity of AURORA kinases in metazoans remains unclear. Here, we report a novel mechanism involving communication between kinetochores and centrosomes, wherein MPS1 acts upstream of AAK to promote error correction. MPS1 on pole-proximal kinetochores phosphorylates the C-lobe of AAK, thereby increasing its activation at centrosomes. This proximity-based activation ensures the establishment of a robust AAK activity gradient that locally destabilizes mal-oriented kinetochores near spindle poles. Accordingly, MPS1 depletion from *Drosophila* cells causes severe chromosome misalignment and erroneous kinetochore-microtubule attachments, which can be rescued by tethering either MPS1 or constitutively active AAK mutants to centrosomes. Proximity-based activation of AAK by MPS1 also occurs in human cells to promote AAK-mediated phosphorylation of the NDC80 N-terminal tail. These findings uncover an MPS1-AAK crosstalk that is required for efficient error correction, showcasing the ability of kinetochores to modulate centrosome outputs to ensure proper chromosome segregation.

RESUMO

A fidelidade da divisão celular depende da biorientação dos cromossomas mitóticos, em que cada cinetocoros irmão está ligado a microtúbulos orientados para polos opostos do fuso mitótico. Ligações erradas entre o cinetocoro e os microtúbulos formam-se geralmente durante o início da mitose, mas são destabilizadas pela fosforilação das proteínas do cinetocoro externo pela cinase centromérica AURORA B (ABK) e pela cinase centrossomal AURORA A (AAK), permitindo assim o restabelecimento das ligações até que a biorientação seja atingida. A fosforilação de NDC80 mediada por MPS1 também demonstrou enfraquecer diretamente a interface cinetocoro-microtúbulo em leveduras. Em células humanas, foi proposto que MPS1 acumula-se transientemente em cinetocoros ligados à extremidade de microtúbulos e fosforila SKA3 para promover a libertação de microtúbulos. Ainda não é claro se o MPS1 tem como alvo direto o NDC80 e/ou promove a atividade das cinases AURORA A e AURORA B nos metazoários. Aqui, reportamos um novo mecanismo que envolve a comunicação entre cinetocoros e centrossomas, em que o MPS1 atua a montante da AAK para promover a correção de erros nas ligações entre cinetocoros e microtúbulos. O MPS1, nos cinetocoros próximos ao polo do fuso, fosforila o lobo C da AAK, aumentando assim o seu nível de ativação nos centrossomas. Esta ativação baseada na proximidade dos cinetocoros garante o estabelecimento de um gradiente robusto de atividade de AAK que destabiliza localmente as ligações dos cinetocoros mal orientados junto aos polos do fuso. Consequentemente, a depleção de MPS1 em células de *Drosophila* causa um desalinhamento cromossómico significativo e ligações erradas entre cinetocoros e microtúbulos, que podem ser recuperadas ao ligar MPS1 ou mutantes de AAK constitutivamente ativos aos centrossomas. A ativação de AAK baseada na proximidade de MPS1 também ocorre em células humanas para promover a fosforilação mediada por AAK da cauda N-terminal do NDC80. Estas descobertas revelam uma interação entre MPS1 e AAK necessária para a correção eficiente de erros na ligação cinetocoro-microtúbulos, demonstrando a capacidade dos cinetocoros de modular a sinalização produzida pelos centrossomas para garantir uma segregação cromossómica adequada.

TABLE OF CONTENTS

DECLARAÇÃO ..... **III**

PREFACE ..... **V**

ORIGINAL PUBLICATIONS ..... **VII**

AGRADECIMENTOS ..... **IX**

ABSTRACT ..... **XI**

RESUMO ..... **XIII**

TABLE OF CONTENTS ..... **XV**

FIGURE AND TABLE INDEX ..... **XVII**

ABBREVIATIONS ..... **XXI**

CHAPTER 1 ..... **1**

GENERAL INTRODUCTION 1

Cell cycle overview 3

Mitosis 4

Kinetochore-microtubule attachments 6

Kinetochore-microtubule attachments regulation 8

AURORA kinase family 11

AURORA B kinase 12

AURORA A kinase 16

MPS1 kinase 20

Aim of the work 23

CHAPTER 2 ..... **25**

MATERIALS AND METHODS 25

Experimental models *27*

Drosophila Cell Lines 27

Human Cell Lines 27

Method details *27*

RNAi-mediated depletion and drug treatments 27

Transgene constructs and S2 cell transfection 28

FRET-based AURORA kinase sensor 29
Live cell imaging 30
Immunofluorescence imaging and analysis 30
Antibodies 32
Recombinant Protein Production 33
In vitro kinase assay and mass-spectrometry 35
In vitro AAK T337/T360 antibody validation 36
NDC80 bonsai phosphorylation assay 36
Western blotting and gel staining 37
AlphaFold 3 predictions 38
Quantification and statistical analysis *38*
Statistical analysis 38

CHAPTER 3 43

RESULTS | Proximity-based activation of AURORA A by MPS1 potentiates error correction 43
Introduction 45
Polar chromosomes promote AAK activation at centrosomes in an MPS1-dependent manner 46
MPS1-mediated phosphorylation of AAK C-lobe potentiates AAK auto-activation 53
Activation of AAK by MPS1 is required for efficient error correction and chromosome congression 61
Proximity-based activation of AAK by MPS1 is conserved in human cells 71

CHAPTER 4 79

GENERAL DISCUSSION 79

REFERENCES 89

APPENDIX 113

ORIGINAL PUBLICATION 113

FIGURE AND TABLE INDEX

CHAPTER 1 | INTRODUCTION

Figure 1. Kinetochore-microtubule attachment configurations. 7

Figure 2. Schematic representation of the four distinct AAK complexes. 18

CHAPTER 2 | MATERIALS AND METHODS

Table 1 – Main resources used in this thesis 39

CHAPTER 3 | RESULTS

Figure 3. AAK activation levels peak in prophase and prometaphase in *Drosophila* S2 cells in an MPS1-dependent manner. 46

Figure 4. AAK activation is increased by the presence of misaligned and unattached kinetochores, regardless of mitotic duration. 47

Figure 5. Kinetochore MPS1 is required for mitotic activation of AAK at centrosomes. 48

Figure 6. Kinetochore MPS1 is dispensable for mitotic ABK activation at centromeres. 49

Figure 7. γ-TUBULIN and D-TACC phosphorylation (TACCS863Ph) levels at centrosomes are reduced in prometaphase cells depleted of MPS1. 50

Figure 8. AAK activation levels are increased by the presence of kinetochores in the vicinity of the centrosome. 51

Figure 9. Polar chromosomes potentiate centrosomal AAK activity in an MPS1-dependent manner. 52

Figure 10. MPS1-mediated phosphorylation of AAK potentiates its auto-activation *in vitro*. 54

Figure 11. MPS1 phosphorylates AAK C-lobe at the conserved T337/T360. 55

Figure 12. AAK T360 phosphorylation by MPS1 is detectable *in vitro* and in *Drosophila* S2 cells. 56

Figure 13. MPS1 overexpression potentiates centrosomal AAK auto-phosphorylation in metaphase *Drosophila* S2 cells. 58

Figure 14. AAK T360 phosphorylation by MPS1 is required for proper centrosomal AAK prometaphase activation in *Drosophila* S2 cells. 59

Figure 15. AAK T360 phosphorylation by MPS1 increases AAK T-loop auto-phosphorylation levels. 60

Figure 16. Centrosomal MPS1 or AAK phosphomimetic mutant (T360D) restore chromosome congression defects caused by MPS1 depletion in *Drosophila* S2 cells. 62

Figure 17. AAK T360 phosphorylation by MPS1 is required for timely chromosome congression in *Drosophila* S2 cells. 63

Figure 18. Centrosomal MPS1, AAK phosphomimetic mutant (T360D) or constitutively active AAK (T311D) restore defects in the correction of KT-MT attachments caused by MPS1 depletion in *Drosophila* S2 cells. 64

Figure 19. AAK T360 phosphorylation by MPS1 is required for efficient correction of erroneous KT-MT attachments in *Drosophila* S2 cells. 65

Figure 20. The defects in error correction and chromosome congression caused by MPS1 depletion are not caused by compromised centrosome function. 67

Figure 21. NDC80 phosphorylation by AAK is potentiated by MPS1 in *Drosophila* S2 cells. 69

Figure 22. NDC80 phosphorylation by AAK is potentiated by MPS1 *in vitro*. 70

Figure 23. Kinetochore – centrosome distance can be manipulated in RPE1 cells using CENP-Ei or siSpindly. 71

Figure 24. Decrease in kinetochore – centrosome distance increases AAK activation levels in RPE1 cells in an MPS1-dependent manner. 72

Figure 25. AAK activation profile in mitosis is conserved in RPE1 cells, except in prophase. 73

Figure 26. Decrease in kinetochore – centrosome distance increases NDC80 phosphorylation by AAK in hRPE1 cells in an MPS1-dependent manner. 75

Figure 27. Proposed model for proximity-based activation of AAK by MPS1 as a strategy to potentiate error correction of polar chromosomes and ensure chromosome congression. 76

Figure 28. AlphaFold 3 prediction models of the structural changes caused by AAK T360 phosphorylation. 77

ABBREVIATIONS

γ-TuRC	γTUBULIN ring-like complex
AAK	AURORA A kinase
ABK	AURORA B kinase
ACK	AURORA C kinase
APC/C	Anaphase promoting complex/cyclosome
Arg	Arginine
Asp	Aspartic acid
Asn	Asparagine
ATP	Adenosine triphosphate
CENP	Centromere protein
CDE	Cycle-dependent element
CDK	Cyclin-dependent kinase
CHR	Cycle gene homology region
CIN	Chromosomal instability
CPC	Chromosome passenger complex
DNA	Deoxyribonucleic acid
EGFP	Enhanced green fluorescent protein
FRET	Förster/Fluorescence Resonance Energy Transfer
G1	Gap phase 1
G2	Gap phase 2
Gln	Glutamine
Glu	Glutamic acid
H	Histone
KIF	Kinesin family member
KMN	KNL1-MIS12-NDC80
KT	Kinetochore
Leu	Leucine
Lys	Lysine
M	Mitosis
MAP	Microtubule-associated protein
MCAK	Mitotic centromere-associated kinesin
MCC	Mitotic checkpoint complex
MELT	Methionine – Glutamic acid – Leucine – Threonine

Met	Methionine
MT	Microtubule
MTOC	Microtubule-organizing centre
NEB	Nuclear envelope breakdown
PBS	Phosphate buffered saline
PCM	Pericentriolar material
PLK	POLO-like kinase
PP	Protein phosphatase
PTM	Post-translational modification
RNAi	Ribonucleic acid interference
RPE1	Retinal pigment epithelial1
S	DNA synthesis phase
SAC	Spindle assembly checkpoint
Ser	Serine
SLiM	Short linear motif
Thr	Threonine
TPR	Tetratricopeptide repeat

CHAPTER 1

GENERAL INTRODUCTION

Cell cycle overview

In 1665, Robert Hooke published the book *Micrographia* in which he listed several drawings of small biological structures he had observed using a compound microscope. One of the highlights of these is the clear illustration of walled cavities he observed when looking at sections of cork and that Hooke coined as "cells" (from the Latin *cella* – small room or cubicle). For the next 180 years, work from many scientists like Nehemiah Grew, Marcello Malpighi, Jan Swammerdam and Anton van Leeuwenhoek have bolstered the idea that plants' and animals' biological tissue were composed of cells, while work from Leeuwenhoek and Abraham Trembley described single-celled organisms and their reproduction through fission. All of these developments in cell biology led Matthias Schleiden and Theodor Schwann, in 1839, to postulate what has become known as the Cell Theory: (i) all living organisms are composed of one or more cells, (ii) the cell is the basic unit of structure and organization in organisms, and (iii) cells arise from pre-existing cells, this latter one being proposed in 1855 by Rudolf Virchow with the epigram *omnis cellula e cellula*, meaning "all cells arise from other cells" (Nurse, 2000). In 1882, Walther Flemming published the book Zellsubstanz, Kern und Zelltheilung ("Cell substance, nucleus and cell division") in which he describes the process of nuclear and cell division that gives rise to two daughter cells with one nucleus each. Flemming named this process mitosis (from the Greek word *mitos*: threads) to account for the thread-like structures he described as being separated along their longitudinal axis, that have come to be later known as chromosomes (Flemming, 1965; Mitchison & Salmon, 2001). Since then, countless studies have been conducted that showed that cell division is a key process in heredity, proliferation, growth and development of multicellular organisms. However, to ensure the formation of daughter cells carrying the same genomic content, cells must replicate their chromosomes and then equally segregate them to each of the daughter nuclei. To achieve these goals, cells undergo a series of sequential events collectively known as Cell Cycle. The Cell Cycle typically consists of four phases: G1 (for gap), S-Phase (for DNA synthesis), G2 and M-phase (for mitosis). The two major events of the cell cycle are genome replication, which occurs in the S-phase and duplicated genome segregation, which occurs in the M-phase (Nurse, 2000). The division of the chromosomes along their longitudinal axis in mitosis, like anticipated by Flemming, ensures that each daughter cell receives an equal set of chromatids. This is a key hallmark of mitosis that warrants a stable transmission of the genomic content along successive generations. Theodor Boveri, as early as 1902, described the compromised development of doubly fertilised sea urchin eggs as a consequence of alterations in chromosome content. Boveri proceeded to postulate that a wrong set of chromosomes (a condition known as aneuploidy) could highly increase the

chance of tumour development (Boveri, 2008). Progression through the cell cycle is coordinated by the chronological activation of Cyclin-Dependent Kinases (CDKs), whose catalytic activity depends on the association with specific Cyclins that accumulate in the cell during specific periods of the cell cycle. The oscillation of Cyclins concentration throughout the cell cycle is a consequence of cell cycle-regulated transcription and protein degradation, which are, in turn, also dependent on CDK activity. This feedback loop generates a regulatory network that contributes for a sequential and unidirectional progression of the cell cycle (Fisher, 2012; Matthews et al., 2022; Simmons et al., 2008). At any given moment, Cyclin-associated CDKs phosphorylate various substrates on serine or threonine residues and induce events that regulate the cell cycle progression. The G2-M transition occurs due to the accumulation of CYCLIN A and CYCLIN B that then associate with CDK1, resulting in increased CDK1 activity (mainly CDK1:CYCLIN B). Once a threshold of CDK1 activity is achieved, several of CDK1:CYCLIN B substrates are phosphorylated triggering mitotic entry (Blethrow et al. 2008; Dephoure et al., 2008; Matthews et al., 2022).

Mitosis

Mitosis begins at prophase with the reorganisation of the nuclear content, during which the chromatin rearranges into the X-shaped condensed chromosomes, in which the thread-like sister chromatids are kept together at the centromere level, by ring-shaped protein complexes of COHESIN. The previously duplicated centrosomes separate and start nucleating microtubules (MTs) that contribute to build the mitotic spindle. In higher eukaryotes, nuclear envelop breakdown (NEB) starts – in opposition to lower eukaryotes that go through a so-called closed mitosis – allowing microtubules to start interacting with chromosomes and marking the beginning of prometaphase. In prometaphase, the mitotic spindle is assembled as an intricate network of microtubules emanating from the centrosomes (microtubules minus-ends). The microtubules plus-ends may then interact with different structures, dictating the role of that microtubule in the spindle: (i) astral microtubules are anchored to the cell cortex and help with the positioning and orientation of the mitotic spindle; (ii) interpolar and central microtubules extend to the centre of the spindle and ensure interconnectivity between the spindle poles; and (iii) kinetochore microtubules (K-fibres) interact with proteinaceous structures called kinetochores (KTs) that assemble on the centromere of each chromatid. Once the bipolar mitotic spindle is correctly assembled and the microtubules start to interact with kinetochores, the chromosomes move towards the centre of the spindle, a process known as chromosome congression. Metaphase is achieved when all chromosomes are at the spindle equator with kinetochores from each

pair attached to microtubules emanating from opposite spindle poles (chromosome biorientation). At this point the cell is ready to irreversibly commit to exit mitosis, by transitioning to anaphase. This transition is marked by the polyubiquitination of two critical proteins – CYCLIN B and SECURIN – followed by their quick proteasome-mediated degradation (Musacchio, 2015). These proteins are polyubiquitinated by the E3-ubiquitin ligase named anaphase-promoting complex/cyclosome (APC/C) that must be kept inactive up to this point to ensure faithful chromosome segregation (Musacchio, 2015). For that, a surveillance mechanism named spindle assembly checkpoint (SAC) has evolved that monitors the state of kinetochore attachment to microtubules of the mitotic spindle (Musacchio, 2015). The SAC effector is the mitotic checkpoint complex (MCC), a complex formed by MAD2, BUBR1, BUB3 and CDC20, that inhibits the APC/C until all kinetochores are bound to microtubules, and the SAC is satisfied (Musacchio, 2015). The degradation of CYCLIN B results in the inactivation of CDK1:CYCLIN B and commits the cell to anaphase and mitotic exit. At the same time, the degradation of SECURIN releases the protease SEPARASE that will target and cleave the COHESIN rings keeping sister chromatids together, allowing their separation (Musacchio, 2015). In anaphase, the separation of sister chromatids is ensured by microtubule-driven chromosome movement towards opposite spindle poles. Telophase is the last mitotic stage and features chromatin decondensation and re-assembly of the nuclear envelope around the two DNA clumps accumulated around each spindle pole, giving rise to two daughter nuclei with equal DNA content. Mitosis is then usually followed by the physical division of the cytoplasm, named cytokinesis, resulting in the formation of two daughter cells.

The ultimate goal of mitosis is the equal distribution of the previously replicated chromosomes, to ensure that each of the daughter cells receives exactly one copy of each chromosome, thus keeping the same genome content as the mother cell. Mitotic fidelity is safeguarded by a number of molecular mechanisms that regulate spindle assembly, microtubule dynamics, kinetochore-microtubule (KT-MT) attachments, chromosome congression and chromosome segregation.

At the beginning of prometaphase, the mitotic spindle is assembled by the polymerization of α and β-TUBULIN subunits available in the cytoplasm that arise from the disassembly of the interphase microtubule structures. Because spontaneous microtubule nucleation from αβ-TUBULIN dimers is energetically unfavorable, to ensure a timely spindle assembly, multiple microtubule nucleation pathways must be used by the cell around different structures like centrosomes, kinetochores and other microtubules (Valdez et al., 2023).

In cells that have centrosomes, these localize at spindle poles, working as microtubule-organizing centre (MTOC) and expand their pericentriolar material (PCM) by the recruitment and accumulation of specific proteins. This process is called centrosome maturation and is regulated by POLO-LIKE KINASE 1 (PLK1) and AURORA A kinase activity (Haren et al., 2009; Lee & Rhee, 2011). This cascade of events culminates in the recruitment of γ-TUBULIN ring-like complexes (γ-TuRC) and the activation of microtubule nucleation at the centrosome level (Gomez-Ferreria et al., 2007; Haren et al., 2009; Joukov et al., 2014).

Kinetochore-driven microtubule nucleation was initially proposed as a safeguard mechanism to accommodate the failure of other microtubule nucleation pathways (Khodjakov et al., 2000; Khodjakov et al., 2003; Maiato et al., 2004). However, multiple studies have now shown that kinetochores catalyse the formation of microtubules and that this process is required for timely chromosome biorientation (Maiato et al., 2004; Renda et al., 2022; Sikirzhytski et al., 2018).

Kinetochore-microtubule attachments

Faithful chromosome segregation relies on proper kinetochore-microtubule attachments that relay the forces applied by the spindle to chromosomes required for chromosome congression in prometaphase and chromosome segregation in anaphase. It was proposed initially that, in the beginning of prometaphase, microtubules grow and shrink in a very dynamic fashion, until a microtubule plus-end randomly interacts with a kinetochore becoming then more stable (Hill, 1985; Holy & Leibler, 1994; Kirschner & Mitchison,1986). This has become known as the “search-and-capture” model and was later supported by the observations that in live cells highly dynamic microtubules are stabilised after binding to kinetochores (Hayden et al., 1990). This is also supported by the fact that K-fibres turn-over much slower than astral microtubules (Mitchison et al., 1986). Once attached to microtubules, kinetochores are brought to the equatorial plane of the spindle by microtubule growth-driven movement and the help of motor proteins like CENP-E and DYNEIN that help sliding chromosomes along microtubules (Figure 1) (Barisic et al., 2014; Hyman & Mitchison, 1991). Importantly, the lateral interactions between kinetochores and microtubules driven by motor proteins are clearly different from the “end-on” attachments required for proper segregation. In this configuration, microtubule plus-ends are immersed in the kinetochore mesh allowing efficient transmission of the forces generated by microtubule dynamics to accomplish chromosome segregation (Figure 1). It is therefore critical that lateral interactions are converted to end-on attachments (Maiato et al., 2017).

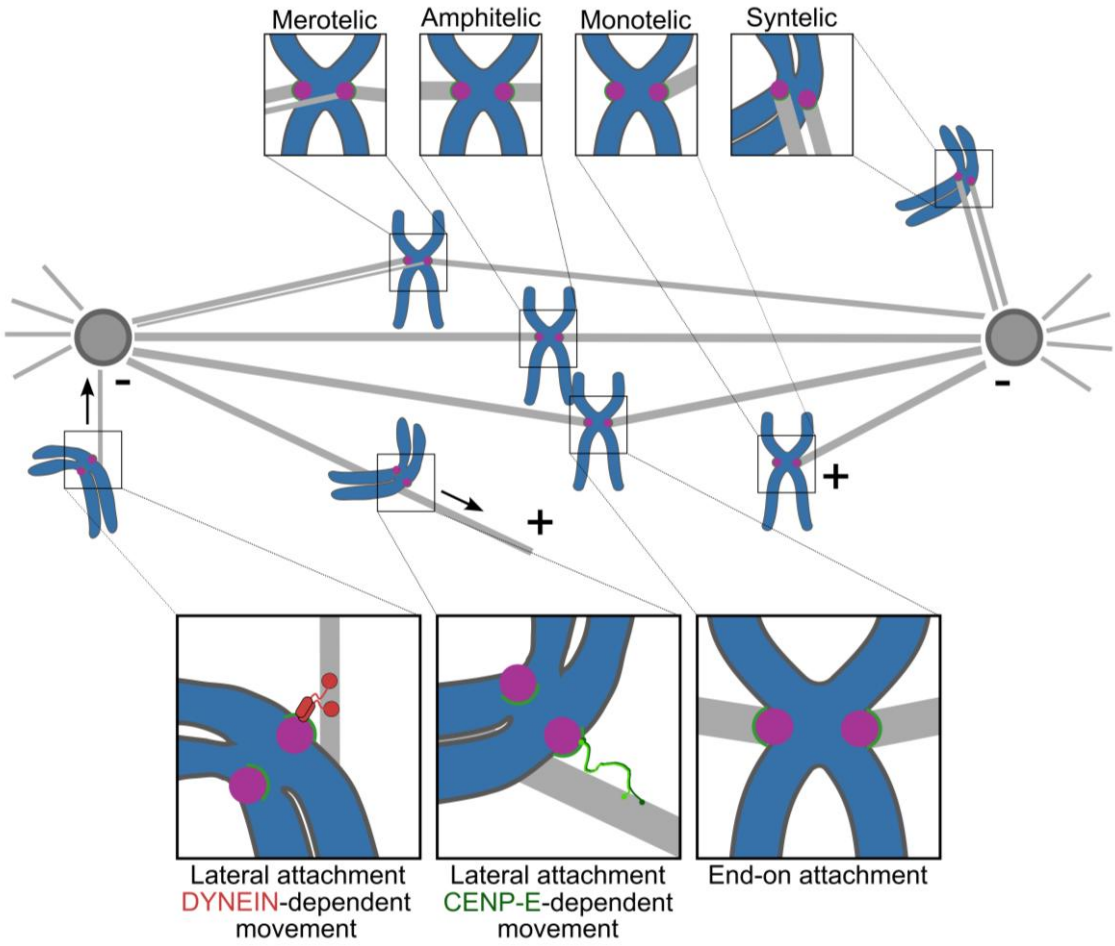


Figure 1. Kinetochore-microtubule attachment configurations.

Schematic representation of different kinetochore-microtubule attachment configurations that can be established throughout mitosis. Both merotelic and syntelic attachments must be destabilised and corrected into amphitelic attachments before anaphase onset to prevent chromosome mis-segregation. DYNEIN and CENP-E promote the congression and bio-orientation of a subset of chromosomes by mediating lateral kinetochore-microtubule attachments and promoting minus-end directed movement of peripheral chromosomes and plus-end directed movement of polar chromosome, respectively. Lateral kinetochore-microtubule interactions are converted in load-bearing end-on attachments.

To ensure proper chromosome segregation, at the anaphase onset, all kinetochores must be correctly attached to microtubule plus-ends and sister kinetochores must be bound to microtubules from opposite spindle poles (amphitelic attachments) (Figure 1). However, in early prometaphase, due to the stochastic nature of microtubule polymerization/depolymerization and their probing of the cytoplasm to find kinetochores, incorrect kinetochore-microtubule attachments are formed often. Erroneous kinetochore-microtubule attachments are usually classified as merotelic or syntelic (Figure 1). Merotelic attachments are configurations where one kinetochore is bound to microtubules emanating from both spindle poles. Configurations where both sister kinetochores are attached to

microtubules from the same pole are called syntelic. If left unchecked until anaphase, erroneous kinetochore-microtubule attachments jeopardize mitotic fidelity. Also, the transient state in which only one of the sister kinetochores is attached to microtubules is often called monotelic attachment (Figure 1). In the case of monotelic and syntelic configurations, both sister chromatids would be pulled to the same daughter nucleus, resulting in aneuploidy for both daughter cells. Merotelic kinetochores can still be separated, but in a slower fashion than amphitelic kinetochores resulting in so-called "lagging chromosomes". Lagging chromosomes are known to be one of the causes for the formation of micronuclei which have been described as a driver of chromosomal rearrangement through chromothripsis (Cimini et al., 2003; Cimini et al., 2004; Crasta et al., 2012; Fenech et al., 2011; Thompson & Compton, 2011). Monotelic attachments, due to the presence of one unattached kinetochore, promote the formation of MCC (the APC/C inhibitor) and therefore prevent the transition to anaphase until attachments are made. The SAC response is also activated by syntelic configurations in spite of both kinetochores being attached to microtubules. In this situation, the SAC signalling is triggered, in an ABK-dependent manner, by the lack of tension of these attachments that can be perceived by low inter-kinetochore distance (Lampson et al., 2004; Liu et al., 2009; Nezi & Musacchio, 2009). On the other hand, merotelic attachments have both kinetochores bound to microtubules and under tension by microtubule pulling forces towards opposite spindle poles. For these reasons, merotelic attachments often go undetected by the SAC (Nezi & Musacchio, 2009). To ensure these attachments do not persist through anaphase, error correction mechanisms have evolved to either destabilize erroneous attachments or convert them to amphitelic before the metaphase to anaphase transition (Lampson & Grishchuk, 2017).

Kinetochore-microtubule attachments regulation

Computational simulations together with experimental observations revealed how simple mechanisms are hardwired to significantly favour the formation of amphitelic attachments (Bakhoum et al., 2009b; Loncarek et al., 2007; Paul et al., 2009; Zaytsev & Grishchuk, 2015). To start with, structural orientation of sister kinetochores facing opposite directions may entail geometric constrains to the attachment of both kinetochores to microtubules emanating from the same spindle pole (Loncarek et al., 2007). This is a possible explanation for the observation that even chromatids featuring merotelicly attached kinetochores still segregate to the correct side of the spindle. When at the spindle equator, merotelic kinetochores are more likely to build more robust K-fibres towards the proximal spindle pole, than to the distal one. The difference in microtubule pulling forces in anaphase will then

favour the movement of the chromatid towards the correct spindle pole, granted in a slower fashion (lagging chromosome). Regardless, at the beginning of mitosis, kinetochores may be positioned in orientations or regions of the cell that increase the likelihood that both sister kinetochores bind to microtubules from the same pole (syntelic) or expose one kinetochore to interactions with microtubules from both poles (merotelic) (Magidson et al., 2015; Zaytsev & Grishchuk, 2015). It is therefore required that additional mechanisms are in place to destabilize incorrect attachments and promote amphitelic attachments.

As previously mentioned, kinetochore-bound microtubules are more stable than non-kinetochore microtubules, nonetheless, they still exhibit an intrinsic turnover that helps in promoting the establishment of correct attachments (Godek et al., 2015; Zaytsev & Grishchuk, 2015). The dynamic turnover of microtubules results in multiple consecutive events of attachment and detachment at the interface between the microtubule bundles and the kinetochores. As a consequence of chromosome congression to the spindle equator and sister kinetochores orientation towards opposite spindle poles, this permanent shuffle leans towards a selective substitution of initially formed improper interactions with correct attachments. Work with mammalian cells has shown that the decrease of CDK1:CYCLIN A levels from prometaphase to metaphase culminates in a reduction of microtubule turnover (Kabeche & Compton, 2013). Importantly, abnormal hyper-stability of kinetochore-microtubule attachments correlates with an increased number of mis-segregation events in human cancer (Bakhoum et al., 2009b). Moreover, destabilizing kinetochore-microtubule attachments by overexpression of the microtubule-depolymerizing kinesins KIF2B or MCAK decreases the number of mis-segregation events in cells featuring chromosomal instability (CIN) (Bakhoum et al., 2009a). These results emphasize the critical role that microtubule turnover has on the accuracy of chromosome segregation. However, the kinetochore-microtubule attachments become progressively more stable through mitotic progression, as the number of microtubules interacting with a kinetochore (microtubule occupancy) increases. The increase in microtubule occupancy results in the decrease of the SAC signalling and is most likely needed to ensure the formation of robust K-fibre bundles and ensure efficient chromosome segregation in anaphase.

Notably, the establishment of bi-oriented attachments further stabilizes kinetochore-microtubule attachments. Early experimental chromosome micromanipulation revealed that microtubules attached to kinetochores are stabilised when tension is applied by pulling the chromosome in the opposite direction with a micro-needle (Nicklas & Koch, 1969). Subsequent work has shown that higher tension correlates with higher microtubule occupancy, hinting at a decrease in microtubule turnover as tension is built at the kinetochore-microtubule interface (King & Nicklas, 2000). Additionally, kinetochore-

microtubule interactions were tested resorting to laser-trapped beads coated with kinetochore proteins from budding yeast and microtubule assembled from pig brain TUBULIN. This approach revealed that forces exerted on the attachments can modulate their stability and microtubule dynamics, for example, increasing the tension on the attachment resulted in increased attachment stability and slower microtubule depolymerization (Akiyoshi et al., 2010; Umbreit et al., 2012; Volkov et al., 2018). Although all these intrinsic mechanisms regarding kinetochore architecture and microtubule dynamics are in place, erroneous kinetochore-microtubule attachments may still persist, and additional molecular players and mechanisms are required to ensure their correction.

The kinetochore is a macromolecular complex comprising dozens of different components that contribute to multiple aspects of mitotic fidelity. The proteins of the inner kinetochore are usually involved in the binding to the centromeric DNA, whereas outer kinetochore proteins are usually responsible for the kinetochore-microtubule interface. The outer kinetochore core is the so-called KMN network which is assembled by the interaction of 3 complexes: KNL1 complex (KNL1c), MIS12 complex (MIS12c) and NDC80 complex (NDC80c). The NDC80c includes four proteins (NDC80, NUF2, SPC24, SPC25), binds directly to microtubules and is critical for the establishment of end-on attachments (Hsu & Toda, 2011; Maure et al., 2011; Tang et al, 2013; Wimbish et al, 2020; Zhang et al, 2012). The interaction between the outer kinetochore and microtubules is further enhanced by additional microtubule-associated proteins (MAPs) like the ones that constitute the DAM1 complex (DAM1c) in yeast, or the spindle- and kinetochore- associated complex (SKAc) in mammals. Importantly, both MAPs and NDC80 are known to be regulated by phosphorylation of mitotic Serine/Threonine (Ser/Thr) kinases like AURORA B, AURORA A and MPS1 (DeLuca et al., 2018; Krenn & Musacchio, 2015; Lampson & Grishchuk, 2017; Maciejowski et al., 2017; Sarangapani et al., 2021; Ye et al., 2015). These phosphorylations are predicted to induce the disruption of the attachments or depolymerization of the microtubules (DeLuca et al., 2018; Krenn & Musacchio, 2015; Lampson & Grishchuk, 2017; Maciejowski et al., 2017; Sarangapani et al., 2021; Ye et al., 2015; Zaytsev et al., 2015). Therefore, they are regarded as critical for the correction of erroneous kinetochore-microtubule attachments. The current model envisions that after the phosphorylation of some of these substrates, the microtubule is released from the kinetochore and that results in an unattached kinetochore that will then interact with other microtubules. This cycle of attachment-release then repeats until a proper attachment is formed, the chromosome is bi-oriented and the attachment stabilised (Foley & Kapoor, 2013). While the kinetochore is unattached, it catalyses the formation of the MCC, preventing anaphase onset until a proper attachment is formed. The establishment of

amphitelic kinetochore-microtubule attachments is a decisive step to prepare the cell to commit to mitotic exit, while ensuring chromosome segregation fidelity. It is, therefore, essential that mechanisms responsible for converting improper kinetochore-microtubule interactions into correct attachments are in place to prevent mis-segregation and aneuploidy.

AURORA kinase family

AURORAs are a family of Ser/Thr kinases that are critical in the regulation of mitotic fidelity with functions in many processes like mitotic entry, centrosome maturation, kinetochore-microtubule attachments, the mitotic checkpoint and spindle orientation. Phylogenetical analyses suggest that the members of the AURORA kinase family evolved from a common ancestor gene from *Urochordata* (Willems et al., 2018). The ancestral gene, called *Ipl1* (Increase-In-Ploidy 1), has been identified in the budding yeast *S. cerevisiae* and shares about 40% of identity with the human AURORA A (Willems et al., 2018). In non-mammalian higher eukaryotes (like *C. elegans*, *D. Melanogaster* and *X. laevis*) this family has two orthologs: AURORA A kinase (AAK) and AURORA B kinase (ABK). In mammals, the duplication of the ancestor gene that encodes ABK resulted in two the paralogs ABK and AURORA C kinase (ACK) which are closely related (Brown et al., 2004; Chan et al., 1993; Glover et al., 1995; Roghi et al., 1998; Schumacher et al., 1998; Willems et al., 2018). Because ACK is exclusively expressed in mammals, mainly expressed in meiotically active cells and has no described functions in error correction of kinetochore-microtubule attachments in mitosis, it will not be discussed as thoroughly in this piece (Bernard et al., 1998; Khan et al., 2011; Tang et al., 2006; Tseng et al., 1998; Yang et al., 2010). AURORA kinases are mainly constituted by 3 domains: the N-terminal domain, the kinase domain (the catalytically active domain) and the C-terminal domain, constituted by the last ~20 amino acids, unstructured and less conserved amongst the AURORA members (Naso et al., 2021; Willems et al, 2018).

As expected, the kinase domain is the most conserved domain between AURORA proteins. It is comprised of a β-stranded N-terminal lobe and an α-helical C-terminal lobe that are connected by a hinge region that has a key role in the formation of the catalytic active site (Cheetham et al., 2002). The C-terminal lobe of the kinase domain includes a well-conserved residue that when phosphorylated results in a change in conformation that correlates with the gain of the kinase activity (Bayliss et al., 2017; Dodson et al., 2010; Giet et al., 1999; Tang et al., 2017). In humans this residue is positioned at Thr288 for AAK (Thr311 in *Drosophila*) and Thr232 for ABK (Thr209 in *Drosophila*) and is often referred to

as activation T-loop. Notably, this domain is decorated with multiple short linear motifs (SLiMs) that serve as degrons to signal proteasome-mediated protein degradation. The ATP molecule required for the phosphorylation reaction binds to a deep cleft between the two lobes that constitutes the ATP-binding pocket (Cheetham et al, 2002). This is usually the region targeted by chemical inhibitors (like MNL8237 for AAK and ZM447439 for ABK) that compete with ATP for binding rendering the kinase inactive (Ditchfield et al, 2003; Sells et al., 2008).

The non-catalytic N- and C-terminal domains exhibit higher variability between species and carry a number of degrons that are recognized by APC/C^{CDH1} to prompt the protein for proteosome-mediated degradation in the following G1 (Arlot-Bonnemains et al., 2001; Bolanos-Garcia et al. 2005; Carmena & Earnshaw, 2003; Castro et al., 2002). The C-terminal domain carries regions that intervene in the interaction with co-factors important for protein conformation and, therefore, activity. On the other hand, the N-terminal domain which is less conserved among AURORA kinases bears the regions that bind AURORA partners that dictate their subcellular localization. Interestingly, targeting of AAK to ABK localization, and vice-versa, showed that they are capable of substituting (at least partially) each other's functions, suggesting their functional divergence is most likely dictated by spatial compartmentalization caused by the N-terminal variances (Li et al., 2015). AAK and ABK transcription is regulated by cell cycle-dependent elements (CDE) and cell cycle gene homology regions (CHR). AURORAS transcription occurs mainly in the G2/M transition (Crosio et al., 2002; Tanaka et al., 2002; Vader et al., 2008).

AURORA B kinase

ABK is part of the multi-subunit chromosome passenger complex (CPC) together with INCENP, BOREALIN and SURVIVIN. INCENP binds the three other components with ABK interacting with INCENP's C-terminal region and conferring the catalytical activity of the complex. On the other hand, BOREALIN and SURVIVIN bind the N-terminal region that instruct the subcellular localization of the CPC (Carmena et al., 2012; Krenn & Musacchio, 2015). In early mitosis, the CPC localizes at the centromere by direct interaction between SURVIVIN and histone H3 and indirect interaction between BOREALIN and histone H2A. These interactions require a prior phosphorylation by HASPIN and BUB1 kinases on histones H3 at Thr3 and H2A at Thr120, respectively (Baron et al., 2016; Bekier et al., 2015; De Antoni et al., 2012; Kelly et al., 2010; Wang et al., 2010; Wang et al., 2012; Yamagishi et al., 2010). After anaphase onset, the CPC localizes to the spindle midzone where it regulates processes related to cytokinesis (Carmena et al., 2012). Importantly, many

studies have detected the presence of an active pool of the CPC at kinetochores of mammalian cells in early prometaphase that then progressively decreases, resulting in exclusively centromeric accumulation of the complex at late prometaphase and metaphase (Broad et al., 2020; Caldas et al., 2013; DeLuca et al., 2011; Posch et al., 2010). ABK activation is a complex process involving multiple events, initiated by ABK binding to INCENP, that induces low levels of kinase activity. Following this step, ABK phosphorylates INCENP in a C-terminal TSS (threonine-serine-serine) motif and finally itself on its activation T-loop Thr232, rendering the kinase in its fully activated state (Bishop et al., 2002; Honda et al., 2003). Because both phosphorylation events are likely to occur in *trans*, ABK activation is thought to be promoted by the accumulation of the CPC at centromeres (Sessa et al., 2005). Accordingly, the increase in the local concentration of the complex, even in ectopic localizations was shown to stimulate ABK activation (Kelly et al., 2007; Wang et al., 2011). Besides auto-phosphorylation other mechanisms were shown to regulate ABK activation and localization by targeting other CPC components. Different studies have demonstrated that MPS1, PLK1 and CDK1 phosphorylate BOREALIN, SURVIVIN and INCENP, respectively. Together, these mechanisms contribute to the proper performance of AURORA B kinase during mitosis (Carmena et al., 2012; Krenn & Musacchio, 2015). ABK activity is critical for mitotic fidelity specifically, among other functions, by regulating the kinetochore-microtubule attachments. As previously discussed, the stochastic nature of the microtubule growth and the randomness of their interaction with kinetochores often result in early erroneous attachments. To correct these attachments, multiple cycles of attachment-detachment may have to be made until a proper attachment is formed. The first AURORA gene (*Ipl1*) was described in a genetic screen in *S. cerevisiae* searching for genes that were key for the maintenance of ploidy (Chan & Botstein, 1993). Early studies revealed that a strain carrying a mutation for this gene was unable to successfully segregate sister chromatids to opposing poles, a defect reasoned to be caused by issues in kinetochore-microtubule attachment turnover (Biggins et al., 1999; Tanaka et al., 2002). Later studies in mammalian cells reported defects in chromosome alignment and the accumulation of syntelic and merotelic kinetochore-microtubule attachments when ABK was either depleted by RNAi or chemically inhibited (Cimini et al., 2006; Ditchfield et al., 2003; Hauf et al., 2003). Importantly, coupling live cell imaging and temporal control of ABK activity using reversible chemical inhibition revealed that restoring ABK activity resulted in the selective depolymerization of K-fibres associated with mal-oriented attachments, instead of the microtubule release initially anticipated (Lampson et al., 2004; Tanaka et al., 2002). However, the detachment model is most likely the one that better describes how merotelic attachments are resolved (Cimini et al., 2006). While syntelic attachments are usually formed and corrected early in mitosis, merotelic attachments often persist even in

chromosomes aligned at the metaphase plate (Gregan et al., 2011). Moreover, to turn merotelic to amphitelic attachments it is required that microtubules connected to the farthest spindle pole are released from the kinetochore, while keeping the microtubules emanating from the closest spindle pole. A recent study has shed light into how the variance in inter-kinetochore tension linked to different attachment configurations may regulate ABK effect on kinetochore-microtubule attachment turnover (Chen et al., 2021). Using optogenetic tools to recruit and activate ABK at specific kinetochores, it was shown that at syntelic (tensionless) kinetochores, ABK induces microtubule depolymerization with no detachment from the kinetochore, bringing the kinetochore closer to the spindle pole, like previously described (Chen et al., 2021; Lampson et al., 2004). However, when this procedure is applied to kinetochores under increased tension, ABK activation induces microtubule detachment from the kinetochore. This result likely reveals the underlying mechanism of correction of erroneous attachments under tension, like merotelic (Chen et al., 2021). It would be interesting to explore whether these two distinct inter-kinetochore tension conformations induce different effects on ABK substrates that could explain whether microtubules are targeted for release or depolymerization. The consensus sequence described as the target for ABK phosphorylation is Arg/Lys-X-Ser/Thr-h (being "X" any amino acid and "h" a hydrophobic or aromatic amino acid) and several kinetochore- or centromere-localised ABK substrates have been identified (Carmena et al., 2012; Cheeseman et al., 2002; Kettenbach et al., 2011; Krenn & Musacchio, 2015; Lampson & Cheeseman, 2011). The main ABK substrate in the mechanism of error correction is NDC80c due to its core function in the direct interaction between kinetochores and the microtubule plus tips. *In vitro* studies have shown that ABK directly phosphorylates the N-terminal tail of NDC80 (HEC1 in human) on multiple conserved residues (Akiyoshi et al., 2009; Cheeseman et al., 2006; Ciferri et al., 2008; DeLuca et al., 2006). Some of these sites were shown to be phosphorylated, in mammalian cells, in early mitosis, decreasing significantly as chromosomes bi-orient (DeLuca et al, 2011). The phosphorylation of these residues is thought to disrupt the electrostatic interactions between this domain and the negatively charged C-terminal ends of TUBULIN, therefore decreasing the affinity between NDC80c and microtubules (Ciferri et al., 2008; Miller et al., 2008). Accordingly, phospho-mimetic mutants of NDC80/HEC1 for these residues are unable to establish stable end-on attachments with microtubules in mammalian cells (Alushin et al., 2012; Guimaraes et al., 2008; Yoo et al., 2018; Zaytsev et al., 2014). These observations suggest that ABK-mediated phosphorylation of NDC80/HEC1 is a major mechanism of error correction by inducing mal-oriented attachments turnover. Accordingly, expression of non-phosphorylatable versions of NCD80/HEC1 for these sites resulted in the accumulation of erroneous kinetochore-microtubule attachments (DeLuca et al., 2011; Sundin et al., 2011).

Besides NDC80c, ABK intervenes in the regulation of kinetochore-microtubule attachments by phosphorylating other MAPs like DAM1c, SKAc, KIF2B and MCAK. KIF2B and MCAK are two microtubule depolymerases that regulate microtubule turnover at the kinetochore level in prometaphase and metaphase, respectively (Bakhoum et al., 2009a; Godek et al., 2015). Notably, the phosphorylation of these microtubule depolymerases by ABK was shown to be important for their recruitment to the kinetochore and function (Andrews et al., 2004; Bakhoum et al., 2009a; Ritter et al., 2015). The DAM1c is a key component in the kinetochore-microtubule interface in budding yeast. It is not part of the kinetochore, instead it localizes at the microtubule plus tip when a lateral kinetochore-microtubule attachment is formed. It then, interacts with NDC80c to help in the establishment of the kinetochore-microtubule end-on attachment (Kalantzaki et al., 2015; Kitamura et al., 2007; Tanaka, K. et al., 2007). This complex assembles in a ring-like oligomer around microtubules *in vitro* and assists the NDC80c in relaying the microtubule-driven forces to the kinetochore (Gestaut et al., 2008; Grishchuk et al., 2008; Miranda et al., 2005; Westermann et al., 2005; Westermann et al., 2006). To correct improper kinetochore-microtubule attachments, IPL1 (the AURORA kinase in yeast) phosphorylates, besides NDC80, components of the DAM1c, disrupting the interaction (Cheeseman et al., 2002). Studies in metazoans have shown that the SKAc also tracks with microtubule plus ends and that it also contributes to the interaction between NDC80c and microtubules (Helgeson et al., 2018; Schmidt et al., 2012). For this reason, the SKAc has been proposed as the functional ortholog of the DAM1c in higher eukaryotes. However, the SKAc is seemingly absent in some higher eukaryotic species, like *D. melanogaster*. Its depletion was shown to cause mitotic defects mirroring defects observed in phenotypes with loss of kinetochore-microtubule interactions, highlighting the importance of this complex to the establishment of stable end-on attachments (Amin et al., 2019; Thomas et al., 2017). Interestingly, the SKA complex regulates and is regulated by ABK (Redli et al., 2016). Like for the DAM1c, ABK phosphorylation of SKA1 and SKA3 disrupts the interaction between the SKA complex and NDC80 (Chan et al., 2012). On the other hand, the SKA complex itself promotes ABK activity (Redli et al., 2016). Importantly, the SKA complex is allowed to progressively accumulate through prometaphase as protein phosphatase 1 (PP1) starts being recruited to the kinetochore, counteracting ABK activity and promoting end-on attachments (Redli et al., 2016).

Unlike some other kinases, ABK has no described targeting motifs on its substrates. Moreover, ABK activity gradient has its peak at the centromere and decreases along the centromere-kinetochore axis. This led to the hypothesis that ABK effects over its substrates are likely limited by physical constrains such as the distance between the kinase and the

substrate. Because bi-oriented chromosomes are subject to opposite pulling forces, the distance between their kinetochores and the centromeres (where ABK localizes) is bigger than on mal-oriented chromosomes. One of the prevailing models proposes that this distance could work as an indication of the configuration of the attachments and, therefore proper attachments would be less likely to be disrupted by the phosphorylation of ABK substrates at the kinetochore-microtubule interface (Akiyoshi et al., 2010; Liu et al., 2009; Tanaka et al., 2002). This results in progressively less phosphorylation of ABK substrates like NDC80 as bi-orientation is achieved in each chromosome, promoting the establishment and stabilization of proper end-on attachments and mitotic fidelity.

AURORA A kinase

As previously discussed, the major functional and substrates divergence between AAK and ABK is most likely dictated by their distinct subcellular localizations induced by their clearly different N-terminal regions (Hochegger et al., 2013; Li et al., 2015). Unlike ABK and the ancestor AURORA kinase IPL1, AAK localizes mainly at the centrosomes and pole proximal microtubules (Giet et al., 2001). AAK has been implicated in multiple key roles in mitosis, namely, centrosome maturation and separation, mitotic entry, spindle orientation and error correction (Barr et al., 2007; Berdnik & Knoblich, 2002; Chmátal et al., 2015; DeLuca et al., 2018; Hannak et al., 2001; Johnston et al., 2009; Joukov & De Nicolo, 2018; Palazzo et al., 1999; Ye et al., 2015). As expected, to accurately execute all these functions, multiple proteins are involved in the regulation of AAK localization and activity (Asteriti et al., 2015; Barr et al., 2007; Joukov & De Nicolo, 2018).

Importantly, AAK can work as part of four distinct complexes (Figure 2). (i) In the cytoplasm, BORA, previously phosphorylated on Ser112 by CDK1:CYCLIN A, binds unphosphorylated and inactive AAK. The phosphorylated BORA domain substitutes in *trans* AAK T-loop phosphorylation in promoting AAK active kinase domain conformation (Tavernier et al., 2021a). Moreover, BORA associates AAK and POLO/PLK1 in G2 phase and promotes the phosphorylation of POLO/PLK1 T182/T210 activating T-loop by AAK (Hutterer et al., 2006; Macurek et al., 2008; Seki et al., 2008). POLO/PLK1 then phosphorylates multiple substrates resulting in CDK1 activation and mitotic entry. CDK1 then phosphorylates BORA further enhancing its ability to bind POLO/PLK1 and promote its activation by AAK (Figure 2) (Tavernier et al., 2015; Thomas et al., 2016; Vigneron et al., 2018). (ii) At least in vertebrates, AAK associates with centrosomal protein 192 (CEP192) that recruits it to the centrosome. Experimental evidence suggests this complex oligomerizes and the accumulation of the kinase at the centrosomes is suggested to facilitate the trans-auto-

phosphorylation of its activation T-loop (Joukov et al., 2010; Joukov et al., 2014; Littlepage et al., 2002; Tavernier et al., 2021b; Walter et al., 2000). Importantly, although AAK recruitment to centrosomes in invertebrates is observed, the CEP192 ortholog, spindle-defective protein 2 (SPD-2) is yet to be confirmed to interact with AAK in *Drosophila* or *C. elegans*. Therefore, there may be another protein working as the AAK centrosomal cofactor (Joukov & De Nicolo, 2018). Once active at centrosomes, AAK phosphorylates multiple proteins contributing to the cascade of events required for centrosome maturation and separation and centrosome-driven microtubule nucleation and pole anchoring (Figure 2) (Joukov et al, 2014; Meng et al., 2015). Besides the roles in centrosome maturation and separation, centrosomal AAK has also been implicated in the regulation of spindle orientation. Briefly, in *Drosophila*, AAK was shown to phosphorylate lethal giant larvae (LGL) to trigger its release from the cortex at mitotic entry and partner of inscuteable (PINS) – LGN in mammals – to trigger the cortical recruitment of discs large (DLG) to help in astral microtubule capturing (Bell et al., 2015; Carvalho et al., 2015; Johnston et al., 2009). Moreover, work in human cells, revealed that nuclear mitotic apparatus (NuMA) is phosphorylated by AAK triggering its release from the spindle poles and accumulation at the cortex. This accumulation helps on the assembly of the conserved cortical complex Gαi/LGN/NuMA required for the cortical recruitment and processivity of the DYNEIN motor protein that orients the spindle by pulling astral microtubules (di Pietro et al., 2016; Gallini et al., 2016; Polverino et al., 2021). (iii) AAK associates with targeting protein XKLP2 (TPX2) that mediates the binding of AAK to the pole-proximal microtubules. Interestingly, multiple studies suggest that this pool of AAK does not seem to be activated by T-loop phosphorylation. Firstly, the T-loop autophosphorylation seems to require centrosome accumulation of AAK in *Xenopus* and mammalian cells (Joukov et al., 2010; Joukov et al., 2014), Second, unlike the centrosome-associated AAK, the microtubule-bound (TPX2-associated) pool of AAK is not phosphorylated on its T-loop in mammalian cells and adding TPX2 to frog extracts does not increase significantly AAK T-loop phosphorylation (Joukov et al., 2014; Ohashi et al., 2006). And lastly, structural data suggests that TPX2-binding and T-loop phosphorylation produce distinct conformational changes to AAK T-loop (Cyphers et al., 2017; Ruff et al., 2018; Zorba et al., 2014). Taken together, these results suggest that this pool of AAK is activated by TPX2 binding-mediated allostery. This complex mainly contributes to microtubule nucleation and bundling (Figure 2). (iv) AAK has also been observed at centromeres, in human cells, interacting with INCENP and TPX2 (Katayama et al., 2008). The initial evidence suggests that this pool of active AAK is a key component in promoting the recruitment of γ-TUBULIN and to trigger microtubule nucleation in the vicinity of chromatin/kinetochores (Katayama et al., 2008). Additionally, more recently, a study revealed that this pool of AAK is also responsible for the correction of erroneous

kinetochore-microtubule attachments (Figure 2). Specifically, observations in human cells, revealed that AAK could also phosphorylate the NDC80 N-terminal tail, alongside ABK (DeLuca et al., 2018). Moreover, chemical inhibition assays revealed that some phosphorylation sites in NDC80/HEC1 are preferentially phosphorylated by AAK or ABK. Ser69, for example, is mainly phosphorylated by AAK (DeLuca et al., 2018). Importantly, the expression of a non-phosphorylatable mutant of HEC1 for this residue resulted in a metaphase delay and in an increase in segregation errors during anaphase (DeLuca et al., 2018).

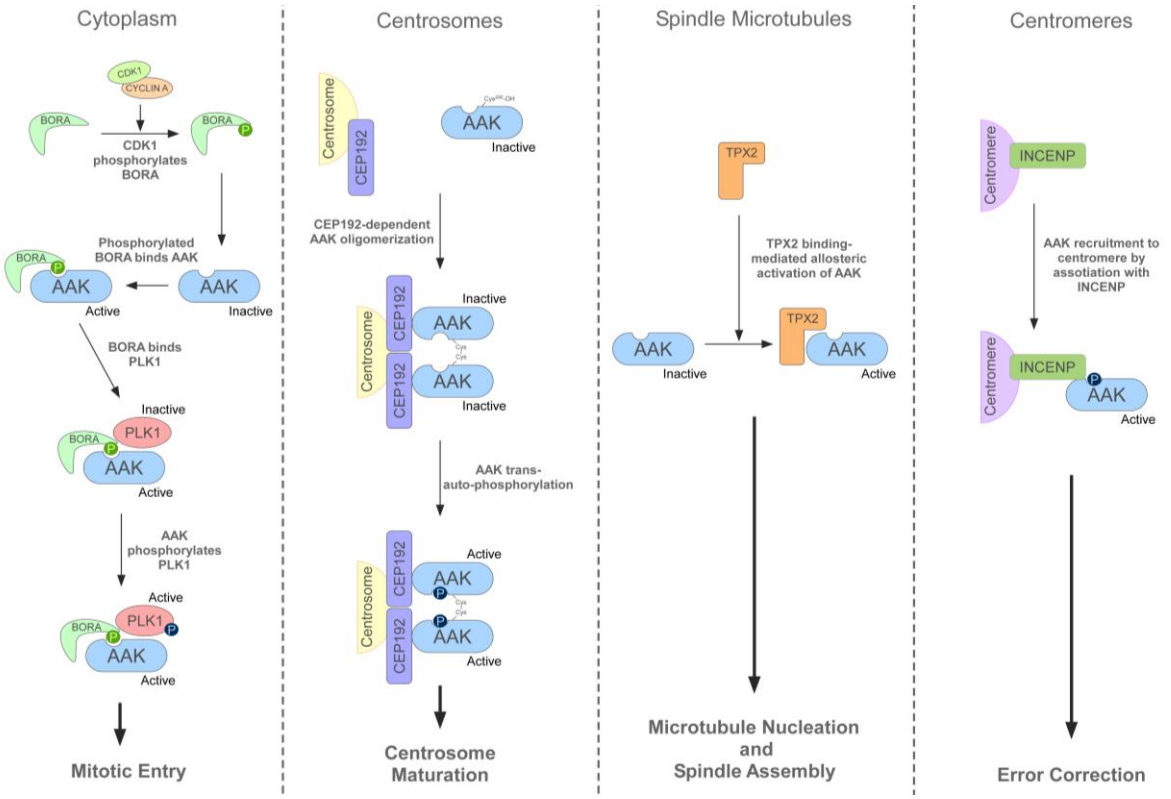


Figure 2. Schematic representation of the four distinct AAK complexes.

AAK can work as part of four distinct complexes. In the cytoplasm, BORA, previously phosphorylated on Ser112 by CDK1:CYCLIN A, binds unphosphorylated and inactive AAK. The phosphorylated BORA domain substitutes in *trans* AAK T-loop phosphorylation in promoting AAK active kinase domain conformation. BORA mediates the interaction of AAK and PLK1 in G2 phase and promotes the phosphorylation of PLK1 activating T-loop by AAK, promoting mitotic entry. (ii) AAK is recruited to the centrosome by interaction with centrosomal protein 192 (CEP192). Centrosomal accumulation of AAK drives its oligomerization and facilitates the auto-phosphorylation *in trans* of its activation T-loop. Once active at centrosomes, AAK phosphorylates multiple proteins contributing to the cascade of events required for centrosome maturation. (iii) TPX2 mediates the binding of AAK to pole-proximal microtubules. Additionally, TPX2 works as an allosteric modulator that imposes conformational changes to AAK that induce its activation at microtubules. This complex mainly contributes to microtubule nucleation and bundling. (iv) AAK can interact with INCENP and localize at centromeres. This pool of AAK was shown to be active and phosphorylate NDC80c for the correction of erroneous kinetochore-microtubule attachments.

Notably, a role in error correction has also been described for centrosomal AAK. Besides the centromere-based correction of kinetochore-microtubule attachments, multiple studies have now identified a similar centrosome-based mechanism regulated by AAK (Barisic et al., 2014; Chmátal et al., 2015; Ye et al., 2015). A number of proteins localised at or near kinetochores initially thought to be only phosphorylated by ABK, have now been shown to be also phosphorylated by AAK, like the centromere protein E (CENP-E) kinesin. CENP-E is a kinesin that transports cargo along microtubules preferentially in a plus end-directed movement. Importantly, syntelic chromosomes are prone to accumulate in the periphery of the cell in the vicinity of the only spindle pole they are attached to. In this scenario, kinetochore-associated DYNEIN induces a poleward movement on the polar chromosome, opposing polar ejection forces, that brings the chromosome closer to the centrosome. At some point, kinetochore-associated CENP-E becomes close enough to be phosphorylated by centrosomal AAK resulting in its dissociation from PP1 and an increased preference for binding to stable central spindle microtubules instead of astral microtubules (Kim et al., 2010). Once attached to stable microtubules, the plus end-directed sliding of CENP-E, transports the associated chromosome towards the cell equator helping in the congression of polar chromosomes (Barisic et al., 2015). To complement this model, two independent studies have demonstrated a direct function of centrosomal AAK in the correction of erroneous kinetochore-microtubule attachments (Chmátal et al., 2015; Ye et al., 2015). Specifically, these two studies show that kinetochores of polar chromosomes have their attachments to microtubules destabilised in an AAK activity-dependent manner (Chmátal et al., 2015; Ye et al., 2015). This is possible due to a centrosome-centred AAK activity gradient that is able to reach these pole-proximal kinetochores and phosphorylate NDC80 in its N-terminal tail on sites that had been previously implicated in the reducing the affinity to microtubules (Chmátal et al., 2015; Ye et al., 2015). Taken together, these results highlight AAK as a critical protein in the correction of pole-proximal syntelic attachments. It triggers the destabilization of erroneous attachments and promotes the CENP-E-mediated transport of these chromosomes to the central spindle region. By this two-step approach, AAK prevents the accumulation of chromosomes near the poles – where syntelic attachments are prone to be formed – and promotes their congression to the equatorial plane of the spindle – where bi-oriented attachments are more likely to be formed. Once at the spindle equator, kinetochores become out of reach from the centrosomal AAK, which has no longer an influence on NDC80 and therefore the attachments are more easily stabilised.

MPS1 kinase

Monopolar spindle 1 (MPS1) is a dual-specificity Ser/Thr kinase that acts as the most upstream regulator of the SAC (McAinsh & Kops, 2023; Musacchio, 2015). MPS1 was initially described in budding yeast and named so because its mutation resulted in cells unable to duplicate their spindle pole body (Weiss & Winey, 1996). MPS1 roles in the SAC, though somewhat variable on a species-by-species basis, are evolutionarily conserved and very well detailed (He et al., 1998; Komaki and Schnittger, 2016; Liu & Winey, 2012; Pachis & Kops et al., 2018). However, a growing body of studies has provided new insights that highlight an emerging role of MPS1 in error correction as well.

MPS1 is mainly composed by two domains: an N-terminal α-helical region containing the tetratricopeptide repeat (TPR) motif and a C-terminal region comprising the catalytically active kinase domain (Bolanos-Garcia, 2025). A comparative analysis of multiple MPS1 substrates suggests that the most likely consensus motif for MPS1 phosphorylation is E/D/N/Q at -2 position relative to the S/T, resembling the motif described for POLO/PLK1 kinase phosphorylation (Dou et al., 2011).

MPS1 recruitment to unattached kinetochores is key in its well-described function regulating the SAC and is mediated by direct binding of its N-terminal domain to NDC80c and promoted by ABK activity (Conde et al., 2013; Nijenhuis et al., 2013; Santaguida et al., 2011; Saurin et al., 2011). The accumulation of the kinase at the kinetochore is hypothesised to bolster the trans-auto-phosphorylation of its activation T-loop to induce full kinase activity (Kang et al., 2007; Sacristan & Kops, 2015). Once active, MPS1 phosphorylates the kinetochore protein Spc105/KNL1 in its Met-Glu-Leu-Thr (MELT) motifs to promote the hierarchical recruitment of additional SAC proteins essential for the assembly of the MCC (London et al., 2012; Primorac et al., 2013; Shepperd et al., 2012; Vleugel et al., 2015; Yamagishi et al., 2012). On the other hand, while it has long been appreciated that MPS1 contributes to error correction in human cells, defining whether it plays a direct or indirect role in the process has proven difficult. In yeast, a study hinted at an MPS1 role in tension-dependent sister-kinetochore biorientation independent of ABK (Maure et al., 2007). However, initial evidence in metazoans suggested that MPS1 could contribute to error correction indirectly via activation of centromeric AURORA B kinase (ABK) (Jelluma et al., 2008a; Kwiatkowski et al., 2010; van der Waal et al., 2012). More recently, a group of studies have uncovered direct roles of MPS1 in the correction of improper kinetochore-microtubule interactions.

In spite of the technical difficulties in clearly splitting MPS1 functions in error correction and other error correction pathways, an increasingly number of observations suggests that

MPS1 acts directly on error correction (Bolanos-Garcia, 2025). Resorting to a chemically tuned kinetochore-targeting assay, work in human cells revealed that recruitment of MPS1 to metaphase kinetochores resulted in kinetochore-microtubule attachments destabilization and loss of chromosome alignment (Maciejowski et al., 2017). Importantly, this effect on the kinetochore-microtubule interactions happened independently of ABK activity. Following up on this, phospho-proteomic analysis identified Ser34 from SKA3, from the SKAc, as a target of MPS1 phosphorylation localised at the kinetochore-microtubule interface (Maciejowski et al., 2017). Phosphomimetic mutations of the identified site resulted in the destabilization of K-fibres in cells and hindered the ability of the SKAc in converting from lattice diffusion to end-on interaction with microtubules *in vitro* (Maciejowski et al., 2017). These results suggest a role for MPS1 in error correction by the phosphorylation of the SKAc to disrupt improper attachments. Interestingly, studies in yeast have revealed that MPS1 phosphorylation of the DAM1c (functional ortholog of the SKAc in yeast) increases the load bearing capacity of the kinetochore-microtubule interface and help in stabilizing attachments (Meyer et al., 2018; Shimogawa et al., 2006). More recently, taking advantage of a laser trap assay that allows the measurement of the strength of attachment between isolated kinetochores and single microtubules *in vitro* (Akiyoshi et al., 2010; Sarangapani et al., 2013), a study in yeast uncovered new insights underlying MPS1 functions in error correction (Sarangapani et al., 2021). To untangle MPS1 effects on attachments from ABK contributions, the work resorted to previously described kinetochore particles that copurify together with MPS1 and lack any other kinase activity (London et al., 2012). *In vitro* and *in vivo* data show that NDC80 is directly phosphorylated my MPS1 in its N-terminal tail at that those phosphorylations result in weaken kinetochore-microtubule attachments (Sarangapani et al., 2021). Moreover, this phosphorylation is increased in cohesion-deficient kinetochores suggesting that the phosphorylation is increased in kinetochores that lack tension (Sarangapani et al., 2021). Finally, phospho-mimetic and phospho-defective mutations of the identified site in NDC80 revealed that these MPS1 phosphorylations contribute to error correction and mitotic fidelity (Sarangapani et al., 2021). Additionally, in human cells, a pool of MPS1 was shown to transiently localize to end-on attached kinetochores prior to microtubule destabilization and error correction (Hayward et al., 2022).

Interestingly, studies in vertebrates have also revealed that MPS1 can regulate the localization of the motor protein CENP-E (Espeut et al., 2008; Hewitt et al., 2010). Moreover, MPS1 phosphorylation relieves CENP-E from its auto-inhibitory conformation and helps in its motility activity (Espeut et al., 2008). Due to the relevance of CENP-E motor activity in chromosome congression, this could be an additional indirect contribution of MPS1 for chromosome bi-orientation.

Importantly, MPS1 localization and activation is higher at unattached kinetochores and decreases as the microtubule occupancy at that particular kinetochore increases due to a competition between MPS1 and microtubules for NDC80c binding (Hiruma et al., 2015; Ji et al., 2015). This competition was suggested to be a hardwired mechanism to progressively attenuate the SAC signalling. Importantly, this could also be the underlying mechanism that shuts down the activity of the kinetochore pool of MPS1 towards its kinetochore-microtubule interface substrates as proper end-on kinetochore-microtubule attachments are formed. Alternatively, a balanced interplay between ABK kinase and PP2A-B56 and phosphatase activities has also been proposed as a fine-tuned mechanism of MPS1 accumulation/release from the kinetochore (Hayward et al., 2022). Regardless, it is clear that MPS1 accumulation at kinetochores is reduced as kinetochore-microtubule end-on attachments and biorientation are achieved. MPS1 is then inactivated by the dephosphorylation of its activation T-loop by PP1 or PP2A (Hayward et al., 2019; Moura et al., 2017). The inactivation of MPS1, once proper attachments are formed, allows the stabilization of the attachments, the activation of the APC/C and accurate chromosome segregation.

Efficient error correction in yeast and human cells relies on direct phosphorylation of kinetochore-microtubule attachment factors and MAPs by MPS1 and both AURORA kinases. However, whether MPS1 directly targets NDC80 and/or promotes the activity of AURORA kinases in metazoans are open questions.

Drosophila melanogaster offers a unique model to further dissect error correction because key players in the pathway (MPS1, AURORA kinases, and the NDC80 complex) are conserved, but the kinetochore composition in flies is divergent relative to human and budding yeast in notable ways. For example, flies do not have a functional SKA complex but, like humans, possess centrosome-enriched AURORA A kinase (AAK) and centromere/kinetochore-localized ABK, while budding yeast has a single AURORA kinase ortholog (IPL1). AURORA kinases play a conserved role in error correction by targeting NDC80, but the localization of AAK and ABK imparts a spatial component to error correction that is likely absent in budding yeast. Indeed, AAK contributes to a polar error correction pathway in flies and mammals via phosphorylation of NDC80 at pole-proximal kinetochores (Chmátal et al., 2015; Ye et al., 2015). In flies, MPS1 also localizes to microtubule-attached kinetochores (Moura et al., 2017), but if it contributes to error correction, then it does so in the absence of the SKA complex and in the presence of spatial cues from AURORA kinases.

Aim of the work

The establishment of proper kinetochore-microtubule attachments is critical for the fidelity of chromosome segregation. Due to the stochastic nature of the microtubule dynamics in search of kinetochores, erroneous kinetochore-microtubule interactions are often formed during early mitosis. To achieve the needed amphitelic configuration, mal-oriented attachments must be disrupted to make kinetochores available to new attachments. The attachment/detachment cycle repeats until proper attachments are formed. Several mechanisms work together to ensure that kinetochore-microtubule interactions are dynamically adjusted within a limited range to promote the correction of erroneous attachments, while favouring the stabilization of proper end-on attachments. While centromeric AURORA B and centrosomal AURORA A are key kinases in the correction of mal-oriented kinetochore-microtubule interactions, MPS1 has, more recently, been shown to directly play important roles in error correction pathways, as well. MPS1-mediated phosphorylation of NDC80 has been shown to directly weaken the kinetochore-microtubule interface in yeast. In human cells, MPS1 has been proposed to transiently accumulate at end-on attached kinetochores and phosphorylate SKA3 to promote microtubule release. Whether MPS1 directly targets NDC80 and/or promotes the activity of AURORA kinases in metazoans remains unclear. Therefore, the main goal of this thesis was to further understand MPS1 contributions to the correction of erroneous kinetochore-microtubule attachments. This objective was addressed by combining *in vitro* biochemistry assays with cell biology studies using *Drosophila melanogaster* S2 cells and human RPE1 cells.

CHAPTER 2

MATERIALS AND METHODS

This chapter is based on the STAR METHODS section of the following published paper and has been reproduced here with the permission of the copyright holder (Appendix). Modifications to the published version have been made. The text and resources table have been subjected to minor changes and are therefore maintained for the most part as included in the published manuscript.

Leça, N., Barbosa, F., Rodriguez-Calado, S., Verza, A. E., Moura, M., Pedroso, P. D., Pinto, I., Artes, E., Bange, T., Sunkel, C. E., Barisic, M., Maresca, T. J., Conde, C. (2025). Proximity-based activation of AURORA A by MPS1 potentiates error correction. Current Biology. Volume 35, Issue 8, 1935 - 1947.e8

.

Experimental models

Drosophila Cell Lines

The experiments have been conducted in male *Drosophila* S2 cells (S2-DGRC, RRID: CVCL_TZ72) cultured at 25°C in Schneider's Insect Medium (Sigma-Aldrich) supplemented with 10% FBS. This cell line has been authenticated by DGRC.

Human Cell Lines

The experiments have been conducted in female hTERT RPE-1 (ATCC, RRID: CVCL_4388) cultured in DMEM/F12 supplemented with 10% FBS and cultured at 37°C in humidified conditions with 5% CO2. This cell line has been authenticated by ATCC.

Method details

RNAi-mediated depletion and drug treatments

For protein depletion in *Drosophila* S2 cells, dsRNA synthesis was performed using TranscriptAid T7 High Yield Transcription Kit (ThermoFischer), according to the manufacturer's instructions, at 37°C for 16h. The incubation with dsRNA was performed at 25°C for 1h in non-supplemented Schneider's Insect Medium (Sigma-Aldrich) followed by 96h-120h of cell culture in Schneider's Insect Medium (Sigma-Aldrich) supplemented with 10% FBS, as previously described (Conde et al., 2013). The PCR product used as template to produce MPS1 RNAi was amplified with the set of primers MPS1F (5′-TAATACGACTCACTATAGGGTCTTCCAAACACCTATGACG-3′) and MPS1R (5′-TAATACGACTCACTATAGGGCGTTTAGATATCCCTGCACCA-3′) (Table 1). The PCR product used as template to produce AAK 5′UTR RNAi was amplified with AAK5′_F (5′-TAATACGACTCACTATAGGGAGAACTTGCCATTCGCCTCATC-3′) and AAK5′_R (5′-TAATACGACTCACTATAGGGAGAGACGGCACGGCACAGGCACTCG-3′) (Table 1). The PCR product used as template to produce AAK 3′UTR RNAi was amplified with AAK3′_F (5′-TAATACGACTCACTATAGGGAGAACACATTCTTGTTTAATTTTC-3′) and AAK3′_R (5′-TAATACGACTCACTATAGGGAGAGAAAACACACACAAACTTT-3′) (Table 1). The PCR product used as template to produce NDC80 RNAi was amplified with NDC80F (5′-TAATACGACTCACTATAGGGTTTGATCCGGATGTTTTGTTGTAGTTC-3′) and NDC80R (5′-TAATACGACTCACTATAGGGTTTTTTAATTTGAAAACAAAGAATACTCTT-3′) (Table 1). The PCR product used as template

to produce CDC27 RNAi was amplified with CDC27F (5′-TAATACGACTCACTAT AGGGAACAATAGC-3′) and CDC27R (5′-TAATACGACTCACTATAGGGTCTTCATGTAG AATTGCATGGC-3′) (Table 1). The PCR product used as template to produce γ-TUBULIN RNAi was amplified with γTub RNAiF (5'-TAATACGACTCACTATAGTTTTCTCATGACAG GCTACACG-3') and γTub RNAiR (5'-TAATACGACTCACTATAGGGTCACAGATCGACTA TCCTCC-3') (Table 1). At selected time points, cells were collected and processed for immunofluorescence or time-lapse microscopy. When required, cells were subjected to several drug treatments before being collected and processed for analysis. To promote microtubule depolymerization, cells were incubated for 2 h with 30 μM colchicine (Sigma-Aldrich). To inhibit the proteasome, cells were incubated for 3 h with 20 μM MG132 (Calbiochem).

For siRNA-mediated depletion experiments in human RPE-1 cells, cells were transfected in OptiMEM (Thermo Fisher) with Lipofectamine RNAiMAX (Thermo Fisher) with 40 nM siRNAs for 48 h – siSpindly: 5′-GAAAGGGUCUCAAA CUGAA-3′, siControl (non-targeting control siRNA): 5′- UGGUUUACAUGUCGACUAA-3′ (Table 1). Where indicated, monopolar spindles were induced by inhibiting Eg5 using 5 μM S-Trityl-L-Cysteine (STLC; Santa Cruz Biotechnology) which was added to the medium 5 h before fixation. CENP-E was inhibited by adding 200 nM GSK923295 (MedChemExpress) to the medium 1 h before fixation. MPS1 was inhibited by adding 500 nM Cp5 (Koch et al., 2016) (a gift from René Medema, Oncode Institute, The Netherlands Cancer Institute, The Netherlands) to the medium 1 h before fixation. To avoid mitotic exit after MPS1 inhibition, the proteasome was inhibited by adding 5 μM MG132 (Sigma) to the medium 1 h before MPS1 inhibition. To depolymerize microtubules, 2 μM nocodazole (Sigma) was added 2 h before fixation. For inhibition of AAK and ABK, 250 nM MLN-8054 (Selleck Chemicals) and 4 μM ZM447439 (AstraZeneca) were respectively added to the cells 2 h before fixation.

Transgene constructs and S2 cell transfection

EGFP-MPS1^{WT}, H2B-GFP and mCherry-α-TUBULIN constructs were previously characterized (Conde et al., 2013). For the generation of the expression vector mCherry-MPS1^{WT}, mCherry cDNA was amplified by PCR and inserted into the EGFP-MPS1 construct, by FastCloning (Li et al., 2011), in replacement of previously removed EGFP. EGFP-AAK^{WT} and FLAG-AAK^{WT} constructs were generated by PCR amplification of AAK cDNA and insertion into modified versions of pENTR entry vector through FastCloning (Li et al., 2011). Entry clones were then used for Gateway recombination (Thermo Fischer Scientific) together with pHGW (for EGFP-AAK constructs) or pHFMW (for FLAG-AAK

constructs) destination vectors (heat-shock inducible promoter, N-terminal EGFP or FLAG tag, respectively). To generate FLAG-AAK^{K183I}, EGFP-AAK^{T311D}, EGFP-AAK^{T360A}, EGFP-AAK^{T360D} and EGFP-AAK$^{K183I/T360D}$ versions, either FLAG-AAK^{WT} or EGFP-AAK^{WT} expression vectors had their codons corresponding to K183, T311, T360, T360 and K183 and T360 changed by site-directed mutagenesis with a primer harbouring the desired mutation to Isoleucine (I), Aspartate (D), Alanine (A), Aspartate (D) and Isoleucine (I) and Aspartate (D), respectively. The PCR reactions were performed with Phusion polymerase (Thermo Fisher Scientific). To generate the EGFP-MPS1^{WT}-CM2 and EGFP-AAK-CM2 constructs, the CM2 domain of CENTROSOMIN (CNN) cDNA was amplified by PCR and was inserted in the C-terminal region of the available EGFP-MPS1^{WT} and EGFP-AAK constructs, respectively, by FastCloning (Li et al., 2011). Stable transfection of indicated vectors into S2 cells was performed using Effectene Transfection Reagent (Qiagen, Hilden, Germany), according to the manufacturer's instructions. To induce EGFP-MPS1^{WT}, mCh-MPS1^{WT} and EGFP-MPS1^{WT}-CM2 expression, S2 cells were incubated overnight with 200 µM $CuSO_4$ at 25°C. To induce the expression of either AAK constructs cells were heat-shocked for 30 min at 37°C and allowed to rest for at least 6 h before being processed for immunofluorescence or live cell imaging.

FRET-based AURORA kinase sensor

S2 cells stably expressing the CM2-FRET reporter, GFP-H2B and either mCherry-α-TUBULIN or mCherry-MPS1 were seeded onto Concanavalin A- (ConA) (Sigma-Aldrich) treated 35 mm glass bottom petri dishes (Cellvis) for 1 hour prior to bringing the volume of Schneider's media up to 2 mL. Cells were then imaged at 24°C on a TiE inverted microscope (Nikon) equipped with an iXON EMCCD camera (Andor Technology) using a 100x 1.4 NA Plan Apo violet-corrected series differential interference contrast objective (Nikon). Metamorph software (Molecular Devices) was used to control the imaging system. Mitotic cells and the best focal plane were identified on the RFP channel (mCherry-α-TUBULIN or mCherry-MPS1). After acquiring the RFP image, sequential images of mTurquoise2, mVenus, and FRET (ECFP excitation, EYFP emission) were taken with equal exposure times (200 ms). Over-expression of MPS1 was induced by overnight incubation with 200 µM $CuSO_4$. AAK was inhibited by treating the seeded cells in the chamber for 1 hour in 100 nM MLN8237 (Selleck Chemicals) prior to FRET imaging. Background-corrected fluorescence intensities for mTurquoise2 and FRET were measured in Metamorph software by subtraction of local background using a duplicate area. The reported FRET emission ratios represent the ratios of the background corrected FRET

signal over the background corrected mTurquoise2 signal and values were normalized against the mean prometaphase FRET emission ratio for each biological replicate.

Live cell imaging

For live imaging of S2 cells, cells were plated onto µ-Dish 35 mm, high Glass Bottom dishes (Ibidi) previously treated with 0.2 mg/mL ConA (Sigma-Aldrich). Images were obtained at 30s intervals up to a maximum of 90min. All images were acquired at 25°C with either a spinning disc confocal system (Revolution; Andor) equipped with an electron multiplying charge-coupled device camera (iXonEM+; Andor) and a CSU-22 unit (Yokogawa) based on an inverted microscope (IX81; Olympus) driven by iQ software (Andor) or a Nikon ECLIPSE Ti2 (Nikon, Japan) equipped with Crest X-Light V3 spinning disk confocal system (Crest CrestOptics, Italy) and Kinetix 25 (Photometrics) camera driven by NIS elements 5.5 (Nikon, Japan) software. The microscopes are served with two laser lines, 488 and 561 nm, for the excitation of EGFP/GFP and mCherry, respectively. Time-lapse imaging of z stacks with 0.8 µm steps covering the entire volume of the cell was collected, and image sequence analysis and video assembly were done with Fiji software (https://fiji.sc/). The time each polar chromosome spent closer to the spindle pole than to the metaphase plate was quantified.

Immunofluorescence imaging and analysis

For immunofluorescence analysis of kinetochore-microtubule attachments in S2 cells, 10^5 cells were seeded onto coverslips previously treated with 0.2 mg/mL ConA (Sigma-Aldrich). For detection of calcium-stable k-fibers, cells were permeabilized for 120 seconds in a buffer containing 100 mM Pipes (pH 6.8), 1 mM MgCl2, 0.1 mM $CaCl_2$, and 0.1% Triton X-100 and then fixed for 10 min in the same buffer supplemented with 4% formaldehyde as previously described (Kapoor et al., 2000) followed by immunostaining. For immunofluorescence analysis of AAK^{T311Ph}, AAK^{T360Ph} or $NDC80^{S67Ph}$ levels in correlation to the distance between the centrosome and its closest kinetochore in S2 cells, 10^5 cells were seeded onto coverslips previously treated with 0.2 mg/mL ConA (Sigma-Aldrich), processed for fixation in 4% paraformaldehyde in PBS for 12 min and further extracted for 8 min with 0.1% Triton X-100 in PBS, followed by immunostaining. For immunofluorescence analysis of AAK^{T311Ph} and ABK^{T209Ph} levels, 10^5 cells were centrifuged onto slides for 5 min, at 239 g, and processed for fixation in 4% paraformaldehyde in PBS for 12 min and further extracted for 8 min with 0.1% Triton X-100 in PBS, followed by immunostaining. Immunostaining of S2

cells was performed as previously described (Conde et al., 2013). Blocking was performed in 1xPBS, 10% fetal bovine serum, 0.05% Tween 20 at room temperature for 1h. Primary antibody incubations were prepared in blocking solution and incubated at 4°C overnight, followed by three 10-min washes in 1xPBS, 0.05% Tween. Secondary antibody incubations were prepared in blocking solution and incubated at room temperature for 1h, followed by three 10-min washes in 1xFBS, 0,05% Tween. Slides were then mounted using Vectashield mounting medium for fluorescence with DAPI (Vector Laboratories, Burlingame, CA). Images were collected in a Leica Scanning Confocal SP8 inverted microscope (Leica Microsystems). For immunofluorescence analysis of human cells, cells were grown on 12 mm round cover glasses (Menzel Glaser) and fixed by ice-cold methanol at -20°C for 4 minutes. DAPI was used at 1 µg/mL (Sigma) for DNA counterstaining. For quantification of centrosome to kinetochore distance, as well as for AAK and HEC1 phosphorylation status, images were acquired using a Plan-Apochromat DIC 63x/1.4 NA oil objective mounted on an inverted Zeiss Axio Observer Z1 microscope (Marianas Imaging Workstation from 3i-Intelligent Imaging and Innovations Inc.) equipped with a Hamamatsu ORCA-Flash4.0 v2 sCMOS Camera (Hamamatsu Photonics). Representative images were acquired using LSM700 confocal microscope (Carl Zeiss Inc.) mounted on a Zeiss-Axio imager Z1 equipped with alpha-Plan-Apochromat 100x/1.46 oil DIC M27 and plan-apochromat 63×/1.40 oil DIC M27 objective (Carl Zeiss Inc.) and Zen 2010 B SP1 software (Carl Zeiss, Inc.). In S2 cells, the distance (in 3D) between the centrosome and its closest kinetochore was calculated using the measured values of the distance in the XY plane and the distance in the Z-axis (number of slices x Z-step). For immunofluorescence quantification, the mean fluorescence intensity of kinetochore or centrosome proteins was measured within a specific predefined region of interest (ROI) where individual kinetochores or centrosomes could fit. The kinetochores were identified based on their constitutive marker CID. The centrosomes were identified based on either their constitutive marker DPLP or, when stated, the transfected FLAG-AAK or EGFP-AAK versions. After background subtraction, identified as a region in the cell with no kinetochores or centrosomes, the intensities of the proteins of interest were determined relative to the respective constitutive markers, unless stated otherwise. Control values were averaged and used for normalization of values determined in the different biological conditions tested.

In human cells, kinetochore to centrosome distance and HEC1^{S69Ph} signal quantification on kinetochores in fixed cells were both measured using a custom routine written in MATLAB 8.2 (Mathworks). For analysis of kinetochore to centrosome distance, Pericentrin signal at centrosomes and CENP-C signal at kinetochores were used to determine the three-dimensional distance between the midpoint between the centrioles and the centroids of a

kinetochore. For HEC1^{S69Ph} quantification on kinetochores, intensities were determined by quantification of pixel gray levels of the focused z plane within a ROI. Background fluorescence was measured outside the ROI and subtracted. For quantifications at kinetochores, the ROI encompassed a single kinetochore measuring the signal intensity of HEC1^{S69Ph} at the kinetochores. HEC1^{S69Ph} intensity was quantified relative to CENP-C fluorescence. HEC1^{S69Ph}/CENP-C intensity ratios were subsequently normalized to control median value. At least 200 kinetochores from 10 different cells in each of three independent experiments were measured in both quantifications.

For AAK^{T288Ph} quantification at centrosomes, intensities were determined by measuring the signal intensity of AAK^{T288Ph} and total AAK in ImageJ software. Protein signal was quantified by drawing a circle closely along the total AAK staining at centrosomes and using the same ROI for AAK^{T288Ph} quantification. The ROI were adjusted in every cell to accurately match the total AAK staining. AAK^{T288Ph} intensity was quantified relative to total AAK fluorescence. AAK^{T288Ph}/AAK intensity ratios were subsequently normalized to control median value. At least 25 cells in each of three independent experiments were used for the quantifications.

Antibodies

Rabbit polyclonal anti-phospho(ph)Thr360-AAK (AAK^{T360Ph}) was raised against a phosphorylated peptide SKNYDE[pT]YKKIL, generated by Eurogentec, Seraing, Belgium. The primary antibodies used for immunofluorescence in S2 cells were rabbit anti-phosphorylated Thr360-AURORA A (AAK^{T360Ph}, this study) used at 1:500; mouse anti-α-TUBULIN B512 (Sigma-Aldrich) used at 1:5000; rat anti-CID (Rat4) used at 1:500; chicken anti-GFP (#ab13970, Abcam, Cambridge, UK) used at 1:2000; rabbit anti-CENP-C (Rb1; a gift from Christian Lehner, University of Zurich, Switzerland) used at 1:3000 (Heeger et al., 2005); guinea pig anti-MPS1 (Gp15; a gift from Scott Hawley, The Stowers Institute for Medical Research, USA) used at 1:250 (Gilliland et al., 2007); rabbit anti-phosphorylated Thr232-AURORA B (ABK^{T232Ph}, Rockland, Lim-erik, PA) used at 1:1000; rabbit anti-phosphorylated Thr288-AURORA A (AAK^{T288Ph}, C39D8, mAb #3079, Cell Signaling Technology, Danvers, MA, USA) used at 1:500; chicken anti-DPLP (a gift from Mónica Bettencourt-Dias, Instituto Gulbenkian de Ciencia, Portugal) used at 1:2000 (Rodrigues-Martins et al., 2007); mouse anti-FLAG (F1804, Sigma-Aldrich) used at 1:500; mouse anti-γ-TUBULIN (GTU-88, T5326 Sigma-Aldrich) used at 1:250; rabbit anti-phosphorylated Ser863-D-TACC (D-TACC^{S863Ph}, a gift from Jordan Raff) used at 1:500 (Barros et al., 2005). Alexa secondary antibodies were used according to the manufacturer's instructions.

The primary antibodies used for immunofluorescence in human cells were guinea pig anti-CENP-C (PD030, MBL) used at 1:1000, mouse anti-Pericentrin (ab28144, Abcam) used at 1:1000, mouse anti-AURORA A (ab13824, Abcam) used at 1:200, rabbit anti-phosphorylated Thr288 AURORA A (AAK^{T288Ph}) (C39D8 #3079, Cell Signalling) used at 1:1600 and rabbit anti-phosphorylated Ser69-HEC1 ($HEC1^{S69Ph}$, a gift from Jennifer DeLuca, Colorado State University, USA) used at 1:3000 (DeLuca et al., 2018). Goat anti-Mouse IgG (H + L) Highly Cross-Adsorbed Secondary Antibody, Alexa Fluor 568; Goat anti-Rabbit IgG (H + L) Highly Cross-Adsorbed Secondary Antibody, Alexa Fluor 488; and Goat anti-Guinea Pig IgG (H + L) Highly Cross-Adsorbed Secondary Antibody, Alexa Fluor 647 (Invitrogen) secondary antibodies were used at 1:1000.

The primary antibodies used for Western blotting analysis were rabbit anti-phosphorylated Thr360-AURORA A (AAK^{T360Ph}, this study) used at 1:250, rabbit anti-phosphorylated Thr676-MPS1 ($MPS1^{T676Ph}$,[49]; a gift from Geert Kops, Oncode Institute, Hubrecht Institute, The Netherlands) used at 1:2000; rabbit anti-phosphorylated Thr288-AURORA A (AAK^{T288Ph}, C39D8, mAb #3079, Cell Signaling Technology, Danvers, MA, USA) used at 1:1000; mouse anti-α-TUBULIN (DM1a, sc-32293, Santa Cruz Biotechnology) used at 1:10000; guinea pig anti-MPS1 (Gp15, a gift from Scott Hawley, The Stowers Institute for Medical Research, USA) used at 1:5000 (Gilliland et al., 2007); mouse anti-AURKA antibody (BD #610938, 4/IAK1) used at 1:1000, rabbit anti-AURKA pT288, AURKB pT232, AURKC pT198 (Cell Signalling #2914, D13A11) used at 1:1000, mouse anti-GST (Novagen/Millipore #71097-3) used at 1:1000, mouse anti-NDC80 (Gene Tex (via Biozol) # GTX 70268-100, 9G3.23), rabbit anti-phosphorylated Ser55-NDC80 ($NDC80^{S55Ph}$, Invitogen #PA5-85846) used at 1:1000.

Recombinant Protein Production

For the mass spectrometry analysis, the catalytic domain of either human or *Drosophila* AAK wild-type or kinase-dead (AAK^{K162I} in human or AAK^{K183I} in *Drosophila*) were fused with N-terminal MBP. To generate these constructs, human and *Drosophila* AAK cDNAs were used as template to amplify the regions corresponding to the amino acids 126-403 and 144-411, respectively. The PCR products were introduced in pMal-c2 (New England Biolabs) expression vector through FastCloning (Li et al., 2011). Recombinant vectors were subsequently transformed into BL21-star competent cells, and expression was induced overnight at 15°C by the addition of 0.05 mM IPTG. Lysates were sonicated and clarified by centrifugation at 4°C. The recombinant proteins were then incubated with MBP amylose magnetic beads (New England Biolabs) for 1 h at 4°C and washed with 200 mM NaCl,

20 mM Tris–HCl, 1 mM EDTA, 1 mM DTT, pH 7.4 and eluted in Column Buffer supplemented with 10 mM Maltose. The same protocol was followed for expression and purification of MBP protein alone.

To produce human MBP-AAK-8xHis for *in vitro* kinase assays with bonsai NDC80 complex, a PCR product containing the sequence encoding full length human AAK was inserted into the BamHI/XhoI sites of a pETDuet-1 vector modified as described by Pan et al. (Pan et al., 2017) by Gibson assembly (Gibson et al., 2009). All PCR amplifications were performed with Phusion High Fidelity PCR master mix (Thermo Fisher Scientific, Waltham, US-MA). The ligation and PCR products were used to transform Omnimax competent bacteria (Invitrogen Corporation, Waltham, US-MA), and cells harboring plasmids were kept under antibiotic selection. The final DNA construct was validated by Sanger sequencing. The sequence encoding GST-MPS1-6xHis was subcloned into BamHI/HindIII sites of a pLIB vector for insect cell expression. The construct expressing bonsai NDC80 complex was generated previously (Ciferri et al., 2008).

Expression of human wild-type (WT) and non-phosphorylatable T337 mutant (T337A) MBP-AAK-6xHis was carried out in *E. coli* BL21CodonPlus(DE3)-RIL cells (Agilent Products, Santa Clara, US-CA) grown in 2 L Terrific Broth (TB). Protein expression was induced with 0.1 mM IPTG at 18°C for 18 hours. Cells were pelleted, snap-frozen, and stored at -80°C. All purification steps were performed on ice or at 4°C. Cells expressing MBP-AAK-6xHis were resuspended in purification buffer (20 mM Tris-HCl pH 8, 500 mM NaCl, 1 mM TCEP) with added DNase (Roche, Basel, Switzerland) and protease inhibitors (Serva Electrophoresis GmbH, Heidelberg, Germany). Cells were lysed via sonication, and the lysate clarified by centrifugation (85,000×g, 30 min). The supernatant was incubated with 2 mL cOmplete His-tag NiNTA beads (Roche) pre-equilibrated in purification buffer for 2 hours with agitation. Beads were washed with 60 mL wash buffer (20 mM Tris-HCl pH 8, 500 mM NaCl, 1 mM TCEP, 20 mM Imidazole) using a 10-mL gravity column (Thermo Fisher Scientific). Protein was eluted using 300 mM imidazole in purification buffer. Following concentration by centrifugation, the protein was injected into a Superdex 200 10/600 (Cytiva, Marlborough, US-MA). Eluted fractions were analyzed by SDS-PAGE and Coomassie blue staining; the purest fractions were concentrated, spun down and snap-frozen to be stored at -80°C. GST-MPS1-6xHis and mCherry-MPS1-6xHis had been previously expressed and purified as described by Raisch et al. (Raisch et al., 2022). Expression and purification of NDC80^{bonsai} had been previously done by Ciferri et al. (Ciferri et al., 2008).

In vitro kinase assay and mass-spectrometry

For *in vitro* kinase assays, recombinant human or *Drosophila* MBP-fused catalytic domain of wild-type or kinase-dead AAK, or 70nM of N-terminal His6-tagged, recombinant full-length human active AAK (#14-511 Merck Millipore, Germany) were incubated either in the presence or the absence of 14nM of N-terminal GST-fused active HsMPS1/TTK (SignalChem, Richmond, Canada) at 30°C for 30 min in a total volume of 30 µL kinase reaction buffer (5 mM MOPS, pH 7.2, 2.5 mM b-glycerol-phosphate, 5 mM $MgCl_2$, 1 mM EGTA, 0.4 mM EDTA, 0.25 mM DTT, 0.1 mM ATP. For inhibition of HsMPS1/TTK activity, Compound 5 (Cp5) (gift from René Medema, Oncode Institute, The Netherlands Cancer Institute, The Netherlands) (Koch et al., 2016) was added to the reaction at a final concentration of 100 nM. For AAK inhibition, MLN8237 (Selleck Chemicals) was added to the reaction at a final concentration of 100 nM. For Western blot analysis of AAK phosphorylation levels, reactions were stopped by addition of Laemmli sample buffer (4% SDS, 10% mercaptoetanol, 0.125 M Tris-HCl, 20% glycerol, 0.004% bromophenol blue) and heated for 5 min at 95°C. Peptides were resolved in a 10% SDS-PAGE. The activating auto-phosphorylation on T676 of human MPS1/TTK and the activating auto-phosphorylation on T288 of human AAK were detected by western blotting with phospho-specific antibodies. Total protein levels were detected by silver staining of the gel.

For identification of phosphorylated residues, the reaction was stopped by addition of 6 M urea and analyzed by liquid chromatography (LC) coupled to a mass spectrometer (LC/MS-MS). Samples were digested with LysC/Trypsin and prepared for LC-MS/MS analysis as previously described (Rappsilber et al., 2007). Peptides (100 ng) were separated on an EASY-nLC 1000 HPLC system (Thermo Fisher Scientific) with a 45 min gradient from 5–60% acetonitrile with 0.1% formic acid and directly sprayed via a nano-electrospray source in an Orbitrap Exploris 480 (Thermo Fisher Scientific). The MS was operated in data-dependent mode, acquiring one survey scan and subsequently 20 MS/MS scans (Olsen et al., 2007). Resulting raw files were processed with MaxQuant software (v.2.0.1.0) using a database composed of the BL21-DE3 proteome (uniprot release 2024), *Drosophila* AAK, human TTK and common contaminants. Oxidation (M) and phosphorylation (STY) were given as variable modifications and carbamidomethylation (C) as fixed modification (Cox & Mann, 2008). A false discovery rate cut-off of 1% was applied at the peptide, and protein levels and as well on phosphorylated peptides. Samples were run at least twice as technical replicates. Phosphosites were extracted from the phosphor(STY).txt output table. The MS/MS spectrum of pT360 was visualized and exported from MaxQuant.

In vitro AAK T337/T360 antibody validation

To test the sensitivity and specificity of the T337/T360 antibody produced in this study in detecting the AAK phosphorylation by MPS1, 200 nM of MBP-AAK (WT or T337A) was incubated either in the presence or absence of 200 nM mCherry-MPS1, previously obtained by Raisch et al. (Raisch et al., 2022), at 30°C for 30 min in a total volume of 40 µL kinase reaction buffer (5 mM MOPS, pH 7.2, 2.5 mM b-glycerol-phosphate, 5 mM $MgCl_2$, 1 mM EGTA, 0.4 mM EDTA, 0.25 mM DTT, 0.1 mM ATP. For inhibition of HsMPS1/TTK activity, Cp5 (gift from René Medema, Oncode Institute, The Netherlands Cancer Institute, The Netherlands) was added to the reaction at a final concentration of 100 nM. For Western blot analysis of AAK T337/T360 phosphorylation levels, reactions were stopped by addition of Laemmli sample buffer (4% SDS, 10% mercaptoetanol, 0.125 M Tris-HCl, 20% glycerol, 0.004% bromophenol blue) and heated for 5 min at 95°C. Peptides were resolved in an 8% SDS-PAGE. The T337 AAK phosphorylation by MPS1 was detected by Western blotting with the phospho-specific antibody produced in this study. Total protein levels were detected by Coomassie staining.

NDC80 bonsai phosphorylation assay

To test *in vitro* MPS1-mediated potentiation of HEC1/NDC80 phosphorylation by AAK, recombinant MBP-AAK-8xHis at a concentration of 5 µM was pre-incubated for 18 hours at 10°C with 1 mM MnCl2 and 200 nM λ-PP (produced in house) to remove T-loop phosphorylation. Subsequently, MBP-AAK-8xHis was diluted at a final concentration of 70 nM and incubated with $NDC80^{bonsai}$ (500 nM), with or without GST-MPS1 (70 nM) for 30 min. Reactions were carried out at 30°C in the presence of 5 µM sodium orthovanadate, and started by adding a mix of ATP (final concentration of 2.5 mM) and MgCl2 (5 mM) to a 40 µL solution of proteins in reaction buffer (50 mM Hepes, pH 7.5, 150 mM NaCl, 1 mM TCEP). Reactions were stopped by addition of 5x Laemmli sample buffer (4% SDS, 10% β-mercaptoethanol, 0.125 M Tris-HCl, 20% glycerol, 0.004% bromophenol blue). Proteins were resolved by 15% SDS-PAGE. The auto-phosphorylation of T288 on MBP-AAK-8xHis and the phosphorylation of S55 on HEC1 were detected by Western blotting with phospho-specific antibodies. Total protein levels were detected by Western blotting or Coomassie blue staining of the gel.

Western blotting and gel staining

For *in vitro* kinase assays in Figure 10, Coomassie staining of proteins resolved by SDS–PAGE was first conducted to determine comparable amounts of recombinant protein in solution to be used in the kinase assays. For Western blotting analysis, resolved proteins were transferred to a nitrocellulose membrane, using the iBlot Dry Blotting System (Thermo Fisher Scientific) according to the manufacturer's instructions. Membranes were incubated for at least 1 h at room temperature in blocking solution (5% powder milk in PBS1×, 0.05% Tween 20). All primary and secondary antibodies were diluted in the blocking solution. Membranes were incubated with primary antibody solutions overnight at 4°C under constant stirring and washed three times in PBS1×, 0.05% Tween 20 for 10 min each. Then, membranes were incubated with secondary antibody solutions for 1 h at room temperature under constant stirring. Secondary antibodies were conjugated to horseradish peroxidase (Jackson Immuno Research, UK). The blots were visualized by ECL detection and exposure to X-ray films (Fuji Medical X-Ray Film). Silver staining was conducted by gel fixation (in 30% ethanol, 10% acetic acid solution) for 2 h, followed by washing in 20% ethanol solution for 20 min and washing in water for 10 min. Then, the gel was incubated for 1min in 0,2g/L sodium thiosulfate, followed by a quick rinse with water and a 30 min incubation with 2g/L silver nitrate at 4°C. After a quick rinse with water, the gel was incubated with developer solution (10mg/L sodium thiosulfate, 0,025% formaldehyde, 30g/L sodium carbonate). When the adequate degree of staining was achieved, the development was stopped by adding a 50g/L Tris-base, 2,5% acetic acid solution.

For *in vitro* NDC80^{bonsai} phosphorylation assays in Figure 22, proteins were transferred onto nitrocellulose membranes using the TransBlot Turbo transfer system (BioRad Laboratories, Hercules, US-CA) as per the manufacturer’s protocol. Membranes were blocked for 1 hour at room temperature in 5% milk dissolved in TBS 1x, 0.1% Tween 20. Primary antibodies, diluted in the blocking solution, were incubated overnight at 4°C with constant stirring. Membranes were washed three times (10 min each) with TBS 1×, 0.1% Tween 20, followed by a 1-hour incubation at room temperature with horseradish peroxidase-conjugated secondary antibodies (Amersham/Cytiva, catalog #NXA931-1ML, 1:10000 dilution) in TBS 1×, 0.1% Tween 20. Blots were visualized via ECL detection, and images were acquired using the ChemiDoc MP System (BioRad) with Image Lab 5.1 software.

AlphaFold 3 predictions

AlphaFold 3 (Abramson et al., 2024) was used to model the structure of *Drosophila melanogaster* AAK and the impact of T360 phosphorylation and T360A and T360D mutations. Models were obtained by inputting the kinase domain sequence (154-406 amino acids) of *Drosophila* AAK (Q9VGF9) as a single copy 'Protein' together with a single ADP 'Ligand' and two Mg2+ 'Ion' copies. Similarly, the mutants were obtained in the same conditions, but with either Alanine (A) or Aspartic acid (D) replacing Threonine (T) in amino acid position 360. For the Phospho-threonine (pT) model, the appropriate PTM was added onto the original sequence. For each of the five output models, ClashScore analysis and T-loop Confidence scores were assessed in SwissModel to determine the best model for each prediction. Confidence scores can be found in Figure 28C. All images of structures were processed on RCSB PBD - 3D view, where alignments are overall cartoon chain superpositions with ball and stick highlights on aa360, aa317, aa311 and molecular surface of the structure. The color coding was set as cyan blue for AAK^{WT}, yellow for AAK^{T360A}, red for AAK^{T360D} and orange for AAK^{pT360}.

Quantification and statistical analysis

Statistical analysis

All statistical analysis was performed using GraphPad Prism V10.0 (GraphPad Software, Inc.). Values were considered statistically different whenever $P < 0.05$. P values: ns, not significant; $^{*}< 0.05$; $^{**}< 0.01$; $^{***}< 0.001$; $^{****}< 0.0001$. *Drosophila* cells and western blot data are presented as median ± interquartile range or mean ± SD. Statistical analysis was performed using a Kruskal–Wallis test for multiple comparisons or Mann-Whitney test when comparing between two conditions. Details on the specific test, the sample sizes and what is shown are indicated in the respective figure legends. Human cells data points were assessed for normality using the D'Agostino & Pearson test. Based on the results, statistical significance was evaluated either by Student's t-test (unpaired, two-tailed for normally distributed data) or the Mann-Whitney U-test (unpaired, two-tailed for non-normally distributed data). Variances were compared using the F-test, and Welch's correction was applied when variances were unequal. Detailed information on statistical significance for each condition can be found in the figures and their legends.

Table 1 – Main resources used in this thesis

REAGENT or RESOURCE	SOURCE	IDENTIFIER
Antibodies		
Anti AURORA A T360Ph, rabbit	This study	N/A
Anti α-TUBULIN B512, mouse	Sigma-Aldrich	RRID: AB_477582
Anti CID, rat	Conde et al., 2013	Clone Rat4
Anti GFP, chicken	Abcam	RRID: AB_300798
Anti CENP-C, rabbit	Heeger et al., 2005	Clone Rb1
Anti MPS1, guinea pig	Gilliland et al., 2007	RRID: AB_2567774
Anti AURORA B T232Ph, rabbit	Rockland	RRID: AB_2061641
Anti AURORA A T288Ph, rabbit	Cell Signaling Technology	RRID: AB_2061481
Anti DPLP, chicken	Rodrigues-Martins et al., 2007	N/A
Anti FLAG, mouse	Sigma-Aldrich	RRID: AB_262044
Anti γ-TUBULIN GTU-88, mouse	Sigma-Aldrich	RRID: AB_532292
Anti D-TACC S863Ph, rabbit	Barros et al., 2005	N/A
Anti CENP-C, guinea pig	MBL	RRID: AB_10693556
Anti PERICENTRIN, mouse	Abcam	RRID: AB_2160664
Anti AURORA A, mouse	Abcam	RRID: AB_300667
Anti HEC1 S69Ph, rabbit	DeLuca et al., 2018	N/A
Anti MPS1 T676Ph, rabbit	Jelluma et al., 2008b	N/A
Anti α-TUBULIN DM1a, mouse	Santa Cruz Biotechnology	RRID: AB_628412
Anti AURORA A, mouse	BD	RRID: AB_398252
Anti AURORA B T232Ph, rabbit	Cell Signaling Technology	RRID: AB_2061631
Anti GST, mouse	Sigma-Aldrich	RRID: AB_10807767
Anti NDC80, mouse	Gene Tex	RRID: AB_371632
Anti NDC80 S55Ph, rabbit	Invitrogen	RRID: AB_2792966
Anti chicken Alexa Fluor 488	Invitrogen	RRID: AB_142924
Anti chicken Alexa Fluor 647	Invitrogen	RRID: AB_2535866
Anti rabbit Alexa Fluor 488	Invitrogen	RRID: AB_2576217
Anti rabbit Alexa Fluor 568	Invitrogen	RRID: AB_10563566
Anti rabbit Alexa Fluor 647	Invitrogen	RRID: AB_2536183
Anti rat Alexa Fluor 647	Invitrogen	RRID: AB_141778
Anti guinea pig Alexa Fluor 488	Invitrogen	RRID: AB_2534117
Anti guinea pig Alexa Fluor 568	Invitrogen	RRID: AB_141954
Anti guinea pig Alexa Fluor 647	Invitrogen	RRID: AB_141882
Anti mouse Alexa Fluor 488	Invitrogen	RRID: AB_2534088

Anti mouse Alexa Fluor 568	Invitrogen	RRID: AB_144696
Anti mouse Alexa Fluor 647	Invitrogen	RRID: AB_162542
Anti rabbit HRP conjugated	Jackson ImmunoResearch	RRID: AB_2313567
Anti guinea pig HRP conjugated	Invitrogen	RRID: AB_2535546
Anti mouse HRP conjugated	Jackson ImmunoResearch	RRID: AB_10015289
Anti rabbit HRP conjugated	GE Healthcare	RRID: AB_772191
Anti mouse HRP conjugated	GE Healthcare	RRID: AB_772193
Bacterial and virus strains		
E. coli BL21CodonPlus(DE3)-RIL	Agilent Products	CAT#200131
E. coli DH5α competent cells	ThermoFischer	CAT#EC0112
E. coli Omnimax competent bacteria	Invitrogen	CAT#C854003
E. coli BL21(DE3) competente bacteria	ThermoFischer	CAT#C601003
Chemicals, peptides, and recombinant proteins		
Protease inhibitors cOmplete cocktail	Roche	CAT#11697498001
Phosphatase inhibitor cocktail 3	Sigma-Aldrich	CAT#P0044
MG132 proteasome inhibitor	Sigma-Aldrich	CAS 133407
Colchicine	Sigma-Aldrich	CAS 64-86-8
Nocodazole	Sigma-Aldrich	CAS 31430-18-9
MLN8054	Selleck Chemicals	CAT#S1100
MLN8237	Selleck Chemicals	CAT#S1133
Compound5 (Cp5)	Koch et al., 2016	N/A
ZM447439	AstraZeneca	CAS 331771-20-1
GSK923295	MedChemExpress	CAT#HY-10299
STLC Eg-5 inhibitor	Santa Cruz Biotechnology	CAS 2799-07-7
Aurora A Protein, active	Merck, Millipore	CAT#14-511
Recombinant Human Mps1/TTK Protein	SignalChem	CAT#T20-10G
Vectashield Antifade Mounting Medium with DAPI	Vector Laboratories	CAT#H-1200
NDC80^{bonsai}	Cifferi et al., 2008	N/A
MBP-AAK WT	This study	N/A
MBP-AAK T337A	This study	N/A
mCherry-MPS1	Raisch et al., 2022	N/A
GST-MPS1-6xHis	Raisch et al., 2022	N/A
Concanavalin A	SigmaAldrich	CAT#C5275
Deposited data		
Mass spectrometry data	This study	Pride Archive: PXD056173

Experimental models: Cell lines		
Drosophila: S2 cells	DGRC	RRID: CVCL_TZ72
Human: hTERT RPE-1	ATCC	RRID: CVCL_4388
Oligonucleotides		
MPS1F (5'- TAATACGACTCACTATAG GGTC TTCCAAACACCTATGACG-3′)	This study	N/A
MPS1R (5′-TAATACGACTCACTATAG GGCGTT TAGATATCCCTGCACCA-3′)	This study	N/A
AAK5′_F (5′-TAATACGACTCACTATA GGGAGAACTTGCCATTCGCCTCATC-3′)	This study	N/A
AAK5′_R (5′-TAATACGACTCACTATA GGGAGAGACGGCACGGCACAGGCACTC G-3′)	This study	N/A
AAK3′_F (5′-TAATACGACTCACTATA GGAGAACACATTCTTGTTTAATTTTC-3′)	This study	N/A
AAK3′_R (5′-TAATACGACTCACTATA GGGAGAGAAAACACACACAAACTTT-3′)	This study	N/A
NDC80F (5′-TAATACGACTCACTATA GGGTTTGATCCGGATGTTTTGTTGTAGTT C-3′)	This study	N/A
NDC80R (5′-TAATACGACTCACTATA GGGTTTTTTAATTTGAAAACAAAGAATACT CTT-3′)	This study	N/A
CDC27F (5′-TAATACGACTCACTAT AGGGAACA ATAGC-3′)	This study	N/A
CDC27R (5′-TAATACGACTCACTATA GGGTCTTCATGTAGAATTGCATGGC-3′)	This study	N/A
gTub RNAiF (5'-TAATACGACTCACTA TAGTTTTCTCATGACAGGCTACACG-3')	This study	N/A
gTub RNAiR (5'-TAATACGACTCACT ATAGGGTCACAGATCGACTATCCTCC-3')	This study	N/A
siSpindly: (5′- GAAAGGGUCUCAAACUGAA-3′)	Eibes et al., 2023	N/A
siControl: (5′- UGGUUUACAUGUCGACUAA-3′)	Eibes et al., 2023	N/A
Recombinant DNA		
pGFP-Histone2B	Conde et al., 2013	N/A
pAc-mCherry-α-TUBULIN	Conde et al., 2013	N/A
pCENP-C-CM2-AuroraFRETsensor	This study	N/A
pHGW-AAK^{WT}	This study	N/A
pMT-mCherry-MPS1	This study	N/A
pHGW-AAK^{T360A}	This study	N/A

pHGW-AAK^{T360D}	This study	N/A
pMT-EGFP-MPS1^{WT}-CM2	This study	N/A
pHGW-AAK^{WT}-CM2	This study	N/A
pHGW-AAK^{T311D}-CM2	This study	N/A
pHGW-AAK^{T360D}-CM2	This study	N/A
pHGW-AAK$^{K183I/T360D}$-CM2	This study	N/A
pHFMW-AAK^{WT}	This study	N/A
pHFMW-AAK^{K183I}	This study	N/A
pMT-EGFP-MPS1	Conde et al., 2013	N/A
pMalc-AAK 126-403	This study	N/A
pMalc-AAK 126-403 K162I	This study	N/A
pMalc-AAK 144-411	This study	N/A
pMalc-AAK 144-411 K183I	This study	N/A
pETDuet-AAK WT	Pan et al., 2017	N/A
pETDuet-AAK T337A	This study	N/A
pLIB-GST-MPS1	Raisch et al., 2022	N/A
pLIB-mCherry-MPS1	Raisch et al., 2022	N/A
pGEX6P-2rbs-NDC80^{bonsai}	Ciferri et al., 2008	N/A
Software and algorithms		
Fiji software	ImageJ	RRID:SCR_002285
AlphaFold3	Abramson et al., 2024	RRID:SCR_025454
GraphPad Prism 10.2.3	GraphPad Software Inc.	RRID:SCR_002798
KT-SP distance measurement custom routine	Barisic et at., 2014	N/A
Other		
µ-Dish 35mm, high Glass Bottom	Ibidi	CAT#81158
35 mm glass bottom petri dishes	Cellvis	CAT#D35-20-0-N
12 mm round cover glasses	Menzel Glaser	CAT#MENZCB0012 0RA020
Superdex® 200 SEC column	GE Healthcare	CAT#GE28-9909-44
TranscriptAid T7 High Yield Transcription Kit	(ThermoFischer)	CAT#K0441
MBP amylose magnetic beads	New England Biolabs	CAT#E8035S

CHAPTER 3

RESULTS

Proximity-based activation of AURORA A by MPS1 potentiates error correction

This chapter is based on the following published scientific article and has been reproduced here with the permission of the copyright holder (Appendix). Modifications to the published version have been made, with figures and results presented differently than the ones included in the published manuscript. The text has only been subjected to minor changes and is therefore maintained for the most part as included in the published manuscript:

Leça, N., Barbosa, F., Rodriguez-Calado, S., Verza, A. E., Moura, M., Pedroso, P. D., Pinto, I., Artes, E., Bange, T., Sunkel, C. E., Barisic, M., Maresca, T. J., Conde, C. (2025). Proximity-based activation of AURORA A by MPS1 potentiates error correction. *Current Biology*. Volume 35, Issue 8, 1935 - 1947.e8

Carlos Conde conceptualized the study, and Thomas J. Maresca wrote the original manuscript draft with contributions from Carlos Conde. Carlos Conde and Thomas J. Maresca coordinated the work. Carlos Conde designed the experiments, with contributions from me, Claudio E. Sunkel, Marin Barisic and Thomas J. Maresca. Data acquisition and analysis: I performed most of the experiments and analysed most data presented in Figures 3-21, with contributions from Francisca Barbosa, Margarida Moura, and Inês Pinto; Ariana E. Verza performed the *in vitro* assays presented in Figure 22. Sergi Rodriguez-Calado performed the experiments and analysed the data presented in Figures 23-26; Elena Artes and Tanja Bange performed the mass spectrometry analysis; and Paulo D. Pedroso generated the Alphafold models and performed the *in vitro* assays presented in Figure 12A. João Barbosa generated the model presented in Figure 27. Data interpretation was mostly done by me and Carlos Conde with contributions from Claudio E. Sunkel, Marin Barisic and Thomas J. Maresca.

Introduction

While it has long been appreciated that MPS1 contributes to error correction in human cells, defining whether it plays a direct or indirect role in the process has proven difficult. Initial evidence suggested that MPS1 could contribute to error correction indirectly via activation of centromeric AURORA B kinase (ABK) (Jelluma et al., 2008a; Kwiatkowski et al., 2010; van der Waal et al., 2012); however, other studies concluded that MPS1 acted downstream of ABK (Santaguida et al., 2010) and reported that MPS1 inhibition did not reduce ABK's ability to phosphorylate known substrates in cells (Hewitt et al., 2010; Maciejowski et al., 2010). A direct role for kinetochore-associated MPS1 in error correction was later supported by the identification of kinetochore-microtubule attachment factors as MPS1 substrates in human and budding yeast. In humans, a pool of MPS1 localizes to end-on attached kinetochores prior to error correction (Hayward et al., 2022) and MPS1-mediated phosphorylation of the SKA complex, which accumulates at end-on attachments to stabilize them, hinders its association with dynamic microtubules *in vitro*, and is required for error correction in cells (Maciejowski et al., 2017). Similarly, in budding yeast, phosphorylation of the attachment factor NDC80 by kinetochore-associated MPS1 weakens the binding of kinetochore particles to microtubules *in vitro* and contributes to error correction and accurate chromosome segregation *in vivo* (Sarangapani et al., 2021). Thus, efficient error correction in yeast and humans relies on direct inputs from both MPS1 and AURORA kinases via phosphorylation of kinetochore-microtubule attachment factors. However, whether MPS1 directly targets NDC80 and/or promotes the activity of AURORA kinase in metazoans are open questions.

Drosophila melanogaster offers a unique model to further dissect error correction because key players in the pathway (MPS1, AURORA kinases, and the NDC80 complex) are conserved, but kinetochore composition in flies is divergent relative to human and budding yeast in notable ways. For example, flies do not have a functional SKA complex but, like humans, possess centrosome-enriched AURORA A kinase (AAK) and centromere/kinetochore-localized ABK, while budding yeast has a single AURORA kinase ortholog (Ipl1). AURORA kinases play a conserved role in error correction by targeting NDC80, but the localization of AAK and ABK imparts a spatial component to error correction that is likely absent in budding yeast. Indeed, AAK contributes to a polar error correction pathway in flies and mammals via phosphorylation of NDC80 at pole-proximal kinetochores (Chmátal et al., 2015; Ye et al., 2015). In flies, MPS1 also localizes to microtubule-attached kinetochores (Moura et al., 2017), but if it contributes to error correction, then it does so in the absence of the SKA complex and in the presence of spatial cues from AURORA kinases.

Polar chromosomes promote AAK activation at centrosomes in an MPS1-dependent manner

The activation status of AURORA kinases throughout the cell cycle was assessed in D. melanogaster S2 cells using antibodies against the phosphorylated T-loops of ABK (ABK^{T209Ph}) and AAK (AAK^{T311Ph}), the latter of which was distinguished from cross-reactive ABK^{T209Ph} by its colocalization with the *Drosophila* pericentrin-like protein (DPLP). Active AAK^{T311Ph} was undetectable at interphase centrosomes but increased significantly during mitosis, peaking in prophase and declining from prometaphase through metaphase and anaphase (Figures 3A and 3B).

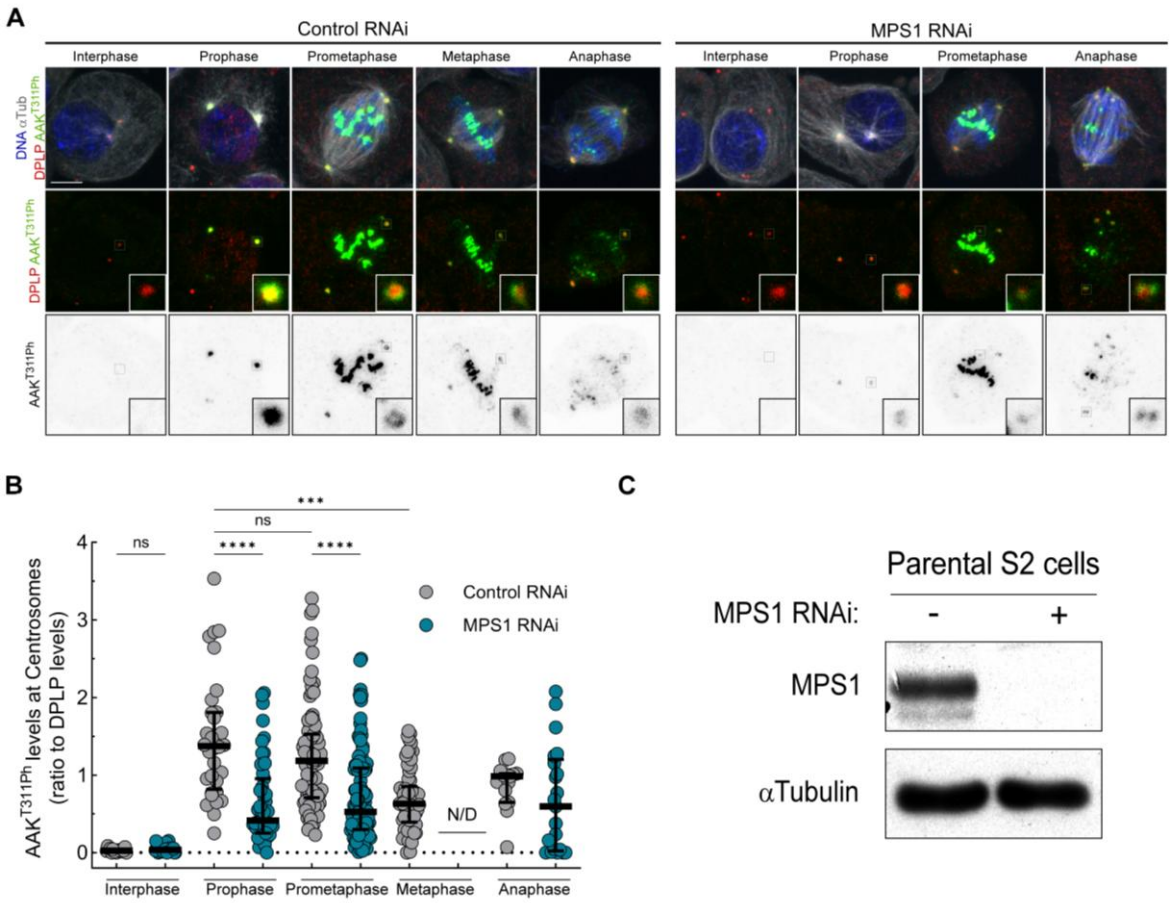


Figure 3. AAK activation levels peak in prophase and prometaphase in *Drosophila* S2 cells in an MPS1-dependent manner.

(A) Representative immunofluorescence images of AAK T311 phosphorylation (AAK^{T311Ph}) in control and MPS1-depleted *Drosophila* S2 cells in the indicated cell cycle stages. Insets depict magnifications of selected centrosomes.

(B) Quantification of the levels of AAK T311 phosphorylation (AAK^{T311Ph}) relative to DPLP at centrosomes of control and MPS1-depleted *Drosophila* S2 cells in the indicated cell cycle stages, as presented in (A). All values were normalized to the mean value determined for prometaphase control cells, which was set to 1. n ≥ 15 centrosomes for each condition from 2 biological replicates.

(C) Western blot showing MPS1 depletion in parental *Drosophila* S2 cells as presented in (A).

Data information: Data in (B) are presented as median ± interquartile range. Statistical analysis was performed using a Kruskal–Wallis test for multiple comparisons. P values: ns, not significant; *p < 0.05; **p < 0.01; ***p < 0.001; ****p < 0.0001. Scale bar: 5 µm.

MG132-treated cells in prometaphase or co-treated with colchicine to depolymerize microtubules exhibited comparable levels of AAK^{T311Ph} that were significantly higher than AAK^{T311Ph} levels in MG132-arrested metaphase cells (Figures 4A and 4B). This suggests that AAK activation is increased by the presence of misaligned and unattached kinetochores, regardless of mitotic duration.

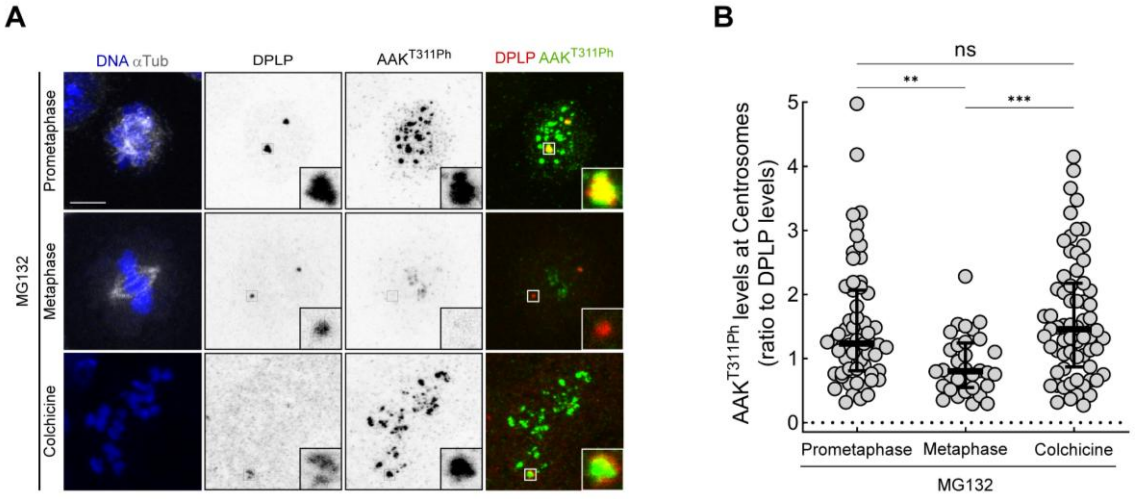


Figure 4. AAK activation is increased by the presence of misaligned and unattached kinetochores, regardless of mitotic duration.

(A) Representative immunofluorescence images of AAK T311 phosphorylation (AAK^{T311Ph}) levels in MG132-treated *Drosophila* S2 cells in the indicated conditions. Insets depict magnifications of selected centrosomes.

(B) Quantification of the levels of AAK T311 phosphorylation (AAK^{T311Ph}) relative to DPLP at centrosomes in the indicated conditions, as presented in (A). All values were normalized to the mean value determined for prometaphase control cells treated with MG132, which was set to 1. n ≥ 32 centrosomes for each condition from 2 biological replicates.

Data information: Data in (B) are presented as median ± interquartile range. Statistical analysis was performed using a Kruskal–Wallis test for multiple comparisons. P values: ns, not significant; *p < 0.05; **p < 0.01; ***p < 0.001; ****p < 0.0001. Scale bar: 5 µm.

Interestingly, robust activation of AAK required MPS1 activity as AAK^{T311Ph} levels at centrosomes remained low throughout mitosis in cells depleted of MPS1 relative to controls (Figures 3A-3C).

The effect of MPS1 depletion on AAK activation was next examined following depolymerization of microtubules with colchicine since MPS1 becomes enriched at

unattached kinetochores via direct interaction with the NDC80 complex (Dou et al., 2015; Hiruma et al., 2015; Ji et al., 2015; Parnell et al., 2024; Pleuger et al., 2024; Zahm & Harrison, 2024). High levels of AAK^{T311Ph} were observed in control cells, but AAK activation was significantly compromised following depletion of either MPS1 or NDC80, which mislocalized MPS1 from kinetochores (Figures 5A-5C).

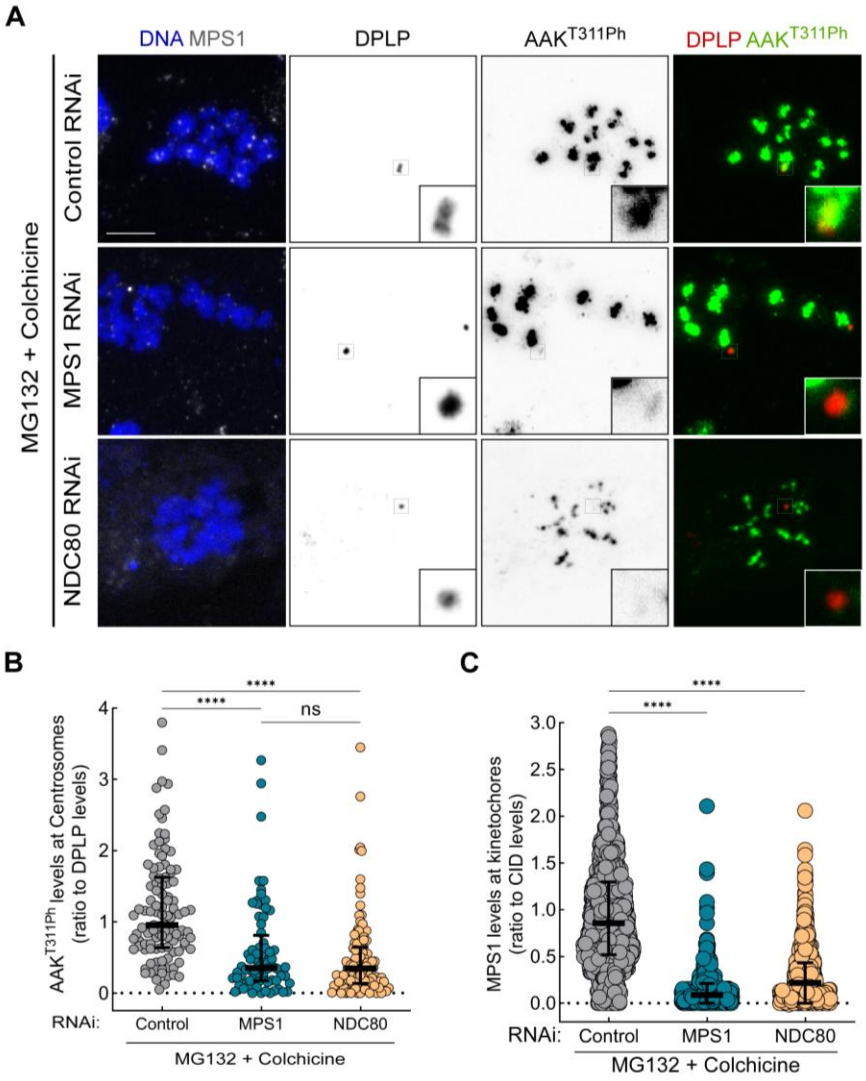


Figure 5. Kinetochore MPS1 is required for mitotic activation of AAK at centrosomes.

(A) Representative immunofluorescence images of AAK T311 phosphorylation (AAK^{T311Ph}) in control, MPS1-depleted, or NDC80-depleted *Drosophila* S2 cells treated with 20 µM MG132 for 3 h and 30 µM colchicine for 2 h. Insets depict magnifications of selected centrosomes. Technical replicates were also stained for MPS1 and CID to quantify the kinetochore levels of MPS1. The quantification and the corresponding representative immunofluorescence images are presented in (C) and (Figure 6A), respectively.

(B) Quantification of the levels of AAK T311 phosphorylation (AAK^{T311Ph}) relative to DPLP at centrosomes of control, MPS1-depleted, and NDC80-depleted *Drosophila* S2 cells treated with 20 µM MG132 for 3 h and 30 µM colchicine for 2 h in the indicated conditions, as presented in (A). All values were normalized to the mean value determined for control cells, which was set to 1. n ≥ 72 centrosomes for each condition from 2 biological replicates.

(C) Quantification of the levels of MPS1 relative to CID at kinetochores in MG132 and colchicine-treated *Drosophila* S2 cells in the indicated conditions, as presented in (Figure 6A). All values were normalized to the mean value determined for control cells treated with MG132 and colchicine, which was set to 1. n ≥ 796 kinetochores for each condition from 2 biological replicates.

Data information: Data in (B) and (C) are presented as median ± interquartile range. Statistical analysis was performed using a Kruskal–Wallis test for multiple comparisons. P values: ns, not significant; *$p < 0.05$; **$p < 0.01$; ***$p < 0.001$; ****$p < 0.0001$. Scale bar: 5 μm.

Thus, kinetochore-associated MPS1 at misaligned and unattached kinetochores was required for the efficient activation of centrosomal AAK in mitosis. It was noteworthy that the effect of inhibiting MPS1 was specific to AAK because ABK^{T209Ph} levels at centromeres remained high throughout mitosis or following colchicine treatment in MPS1- and NDC80-depleted cells relative to control RNAi-treated cells (Figures 6A–6D).

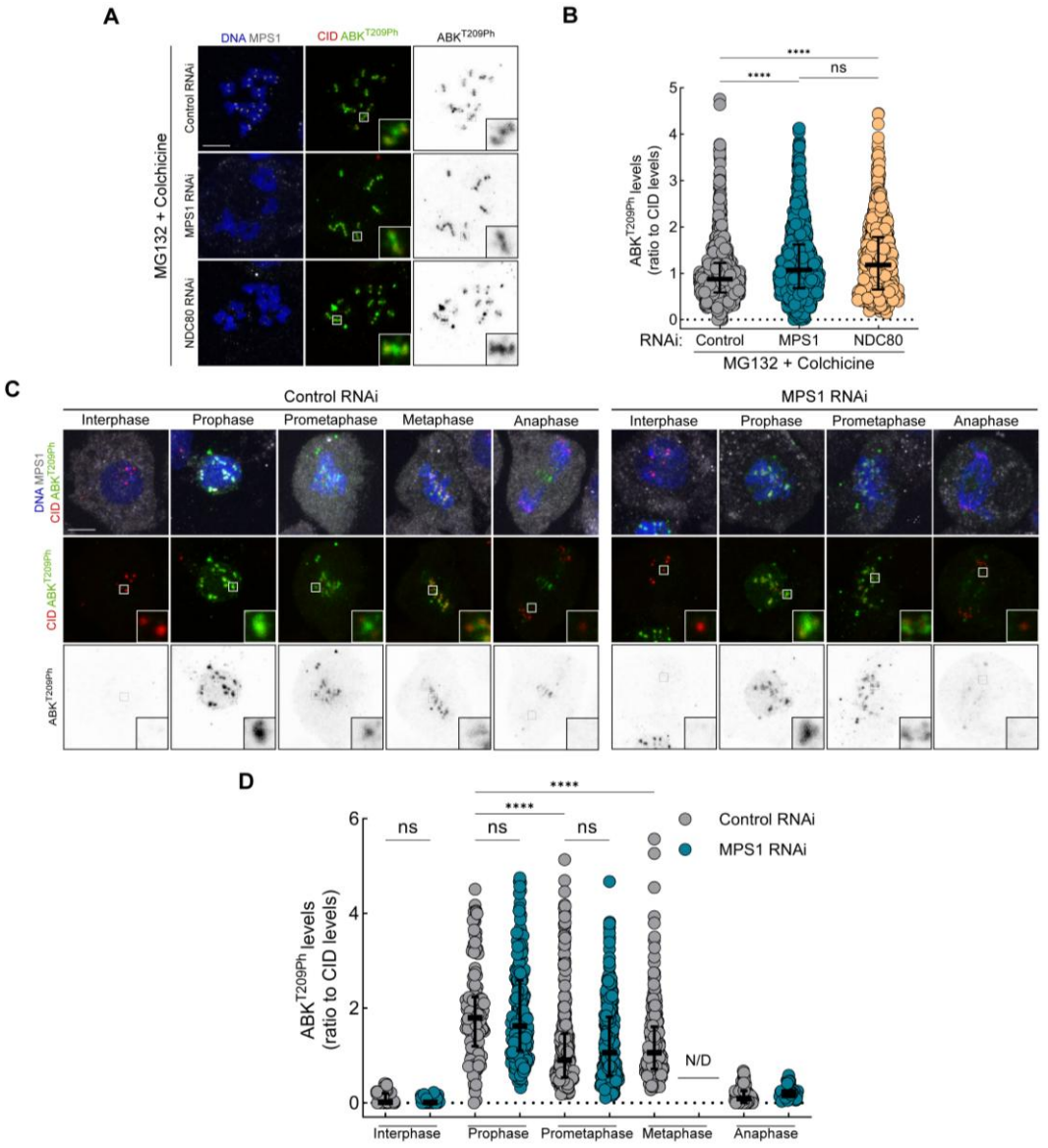


Figure 6. Kinetochore MPS1 is dispensable for mitotic ABK activation at centromeres.

(A) Representative immunofluorescence images of ABK T209 phosphorylation (ABK^{T209Ph}) and MPS1 levels in MG132 and colchicine-treated *Drosophila* S2 cells in the indicated conditions. Insets depict magnifications of selected kinetochores. This immunofluorescence staining was performed in technical replicates that were used for the immunofluorescence and quantification of AAK^{T311Ph} centrosomal levels presented in (Figures 5A and 5B).

(B) Quantification of the levels of ABK T209 phosphorylation (ABK^{T209Ph}) relative to CID at kinetochores/centromeres in the indicated conditions, as presented in (A). All values were normalized to the mean value determined for control cells treated with MG132 and colchicine, which was set to 1. n ≥ 796 kinetochores for each condition, from 2 biological replicates.

(C) Representative immunofluorescence images of ABK T209 phosphorylation (ABK^{T209Ph}) in control and MPS1-depleted *Drosophila* S2 cells in the indicated cell cycle stages. Insets depict magnifications of selected kinetochores/centromeres.

(D) Quantification of the levels of ABK T209 phosphorylation (ABK^{T209Ph}) relative to CID at kinetochores/centromeres of control and MPS1-depleted *Drosophila* S2 cells in the indicated cell cycle stages, as presented in (C). All values were normalized to the mean value determined for prometaphase control cells, which was set to 1. n ≥ 45 kinetochores for each condition from 2 biological replicates.

Data information: Data in (B) and (D) are presented as median ± interquartile range. Statistical analysis was performed using a Kruskal–Wallis test for multiple comparisons. P values: ns, not significant; *p < 0.05; **p < 0.01; ***p < 0.001; ****p < 0.0001. Scale bar: 5 μm.

Consistent with impaired AAK activity, the phosphorylation of D-TACC on S863, an established substrate of AAK (Barros et al., 2005), and the accumulation of γ-TUBULIN (Berdnik & Knoblich, 2002; Giet et al., 2002; Hannak et al., 2001) were reduced at centrosomes of MPS1-depleted prometaphase cells (Figures 7A-7C).

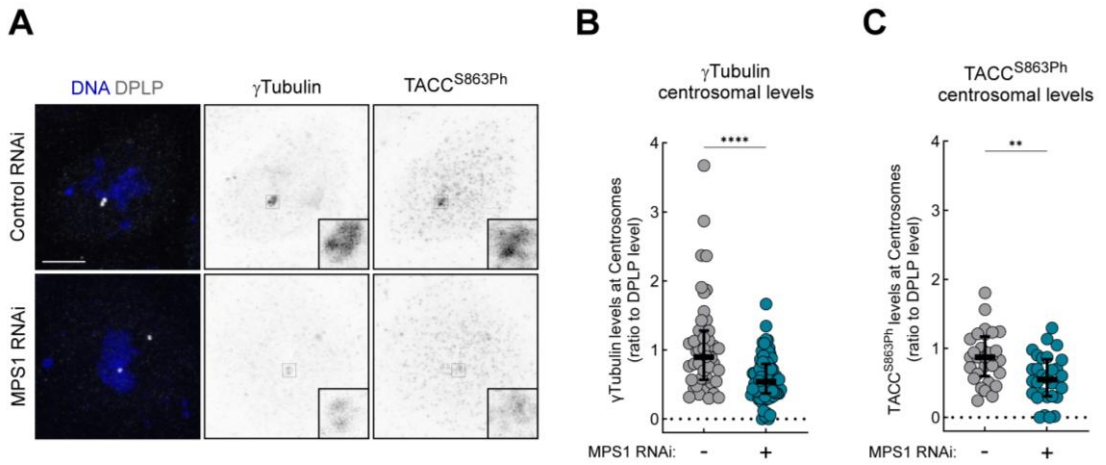


Figure 7. γ-TUBULIN and D-TACC phosphorylation (TACCS863Ph) levels at centrosomes are reduced in prometaphase cells depleted of MPS1.

(A) Representative immunofluorescence images of γ-TUBULIN and D-TACC phosphorylation at S863 (TACC^{S863Ph}) in prometaphase control and MPS1-depleted *Drosophila* S2 cells. Insets depict magnifications of selected centrosomes.

(B) Quantification of the levels of γ-TUBULIN relative to DPLP at centrosomes of prometaphase control and MPS1-depleted *Drosophila* S2 cells, as presented in (A). All values were normalized to

the mean value determined for prometaphase control cells, which was set to 1. n ≥ 29 centrosomes for each condition from 2 biological replicates.

(C) Quantification of the levels of D-TACC phosphorylation at S863 (TACC^{S863Ph}) relative to DPLP at centrosomes of prometaphase control and MPS1-depleted *Drosophila* S2 cells, as presented in (A). All values were normalized to the mean value determined for prometaphase control cells, which was set to 1. n ≥ 44 centrosomes for each condition, from 2 biological replicates.

Data information: Data in (B) and (C) are presented as median ± interquartile range. Statistical analysis was performed using a Mann-Whitney test. P values: ns, not significant; *p < 0.05; **p < 0.01; ***p < 0.001; ****p < 0.0001. Scale bar: 5 μm.

Centrosomal AAK^{T311Ph} levels were plotted as a function of distance to the nearest kinetochore to assess whether there was a spatial component to the MPS1-dependent activation of AAK. There was a clear correlation between the extent of AAK activation at centrosomes and proximity to kinetochores such that higher levels of centrosomal AAK^{T311Ph} were measured when kinetochores were present within an ~1 μm radius of the centrosome (Figure 8). While the spatial effect was observed in both colchicine and untreated cells, the extent of kinetochore-proximal AAK activation was generally higher in colchicine-treated cells, consistent with there being elevated levels of MPS1 at unattached kinetochores.

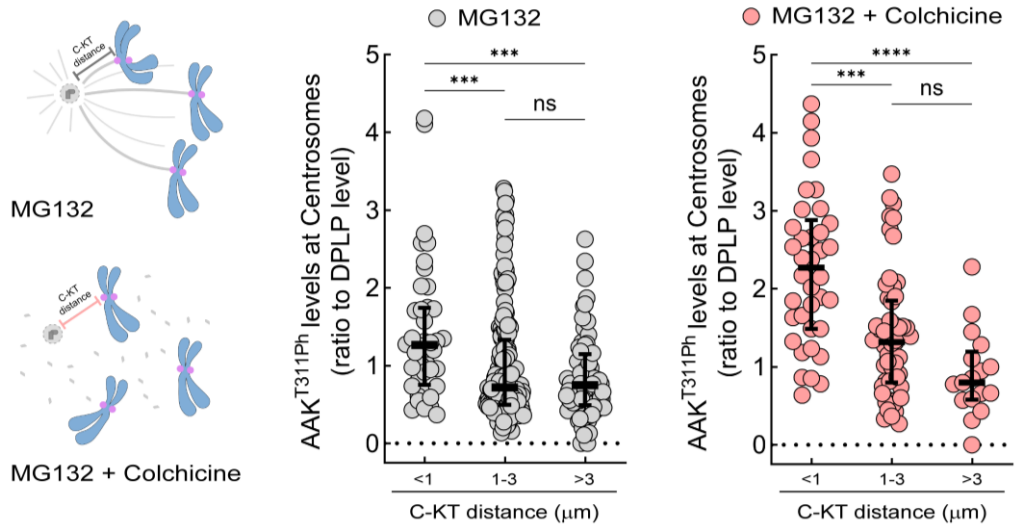


Figure 8. AAK activation levels are increased by the presence of kinetochores in the vicinity of the centrosome.

Quantification of the levels of AAK T311 phosphorylation (AAK^{T311Ph}) relative to DPLP at each centrosome versus the 3D distance between that centrosome and the closest kinetochore (measured as indicated in the schematic representation at the left) of control *Drosophila* S2 cells treated with 20 μM MG132 for 3 h (grey) or cells treated with and 20 μM MG132 for 3 h and 30 μM colchicine for 2 h (salmon), as presented in (Figures 4A and 4B). Centrosomes to kinetochore (C-KT) distances were organized in 3 different column ranges: less than 1 μm (<1), between 1 and 3 μm (1–3), and above 3 μm (>3). All values were normalized to the mean value determined for prometaphase control cells treated with 20 μM MG132 for 3 h, which was set to 1. n ≥ 17 centrosomes for each condition from 2 biological replicates.

Data information: Data are presented as median ± interquartile range. Statistical analysis was performed using a Kruskal–Wallis test for multiple comparisons. P values: ns, not significant; *p < 0.05; **p < 0.01; ***p < 0.001; ****p < 0.0001.

A fluorescence resonance energy transfer (FRET)-based biosensor for AURORA kinase activity (Fuller et al., 2008; Ye et al., 2015) was next used to study if MPS1-dependent activation of centrosomal AAK affected phosphorylation of downstream substrates. The reporter, which undergoes a conformational change upon phosphorylation that results in reduced FRET efficiency (Violin et al., 2003), was tethered to centrosomes via an N-terminal fusion to the CM2 domain of CENTROSOMIN (Feng et al., 2017) (Figure 9A). Centrosome targeting put the reporter in close proximity to AAK, but higher phosphorylation (lower FRET) of the reporter was observed at centrosomes with nearby polar chromosomes (Figure 9B).

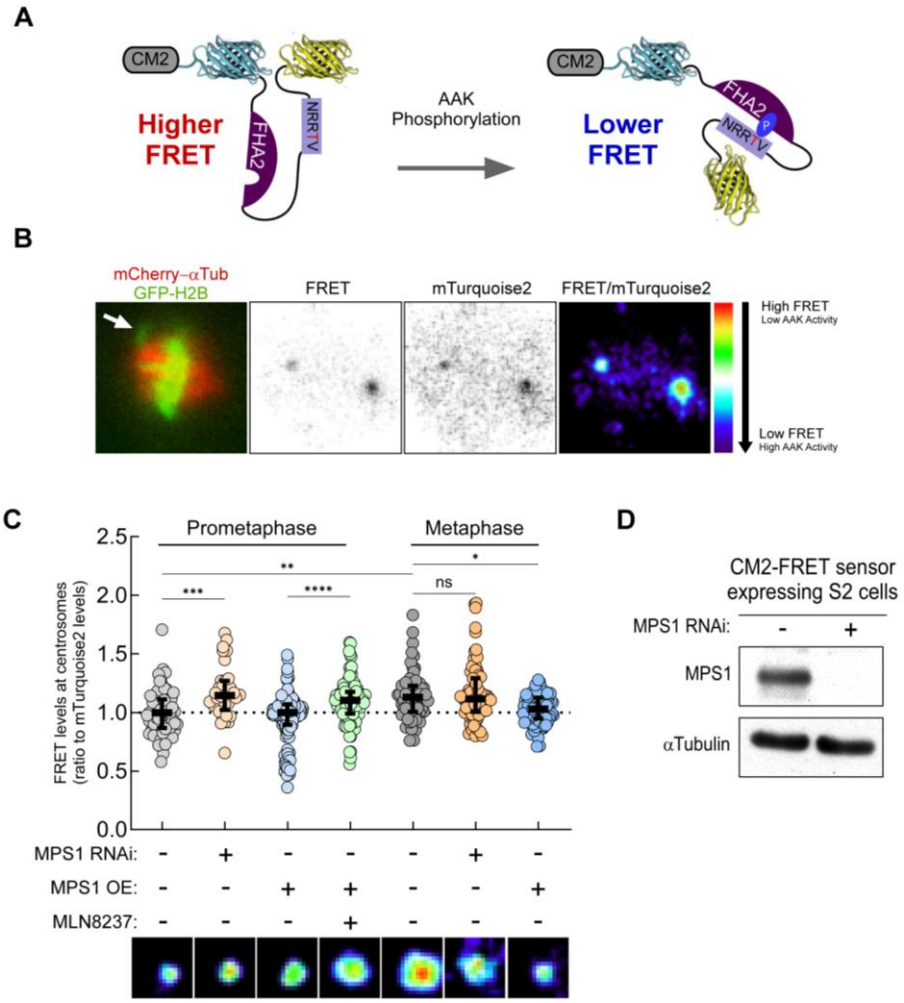


Figure 9. Polar chromosomes potentiate centrosomal AAK activity in an MPS1-dependent manner.

(A) Schematic of the centrosome-targeted CM2-AURORA FRET sensor used in (B) and (C).

(B) Representative images of the FRET reporter in a control cell with one polar chromosome (white arrow) near the left centrosome. The FRET emission ratio images ''FRET/mTurquoise2'' are pseudo-colored, according to the color wedge in display. All images are from a single selected Z-slice in the indicated channels.

(C) Quantification of the levels of FRET emission relative to total mTurquoise2 levels at centrosomes of cells and representative FRET emission ratio images FRET/mTurquoise2 pseudo-colored in the indicated conditions. All images are from a single selected Z-slice and depict magnifications of selected centrosomes from the indicated conditions. All values were normalized to the mean value determined for prometaphase control cells, which was set to 1. n ≥ 32 centrosomes for each condition from 3 biological replicates.

(D) Western blot showing MPS1 depletion in S2 cells expressing CM2-FRET sensor as presented in (C).

Data information: Data in (C) are presented as median ± interquartile range. Statistical analysis was performed using a Kruskal-Wallis test for multiple comparisons. ns, not significant; *$p < 0.05$, **$p < 0.01$, ***$p < 0.001$, ****$p < 0.0001$.

Quantification of FRET emission ratios in prometaphase revealed a significant decrease in phosphorylation (higher FRET) of the reporter following MPS1 depletion (Figures 9C and 9D). FRET emission ratios were comparable in control and MPS1 overexpressing (MPS1 OE) prometaphase cells, suggesting that the centrosome-targeted sensor approaches maximal phosphorylation in prometaphase. Phosphorylation of the reporter in MPS1 OE prometaphase cells required AAK activity since treatment with the inhibitor MLN8237 at a concentration previously determined to specifically inhibit AAK in *Drosophila* S2 cells (Ye et al., 2015) decreased phosphorylation of the reporter to the same extent as that measured in MPS1-depleted cells (Figure 9C). Consistent with the prior observation of decreased AAK activation at centrosomes in metaphase (Figures 3A and 3B), the CM2-fused reporter exhibited reduced phosphorylation at metaphase centrosomes of control and MPS1-depleted cells (Figure 9C). However, overexpression of MPS1 increased phosphorylation of the reporter in metaphase to comparable levels as that measured in prometaphase cells (Figure 9C). Taken together, these findings support the conclusion that the proximity-based activation of AAK at centrosomes by MPS1 potentiates the phosphorylation of downstream AAK substrates.

MPS1-mediated phosphorylation of AAK C-lobe potentiates AAK auto-activation

In vitro kinase assays with purified human orthologs of His-AAK and GST-MPS1 were employed to gain mechanistic insights into how MPS1 activates AAK. Co-incubation of AAK with MPS1 resulted in an ~4-fold increase in the phosphorylation of AAK activation loop

(AAK^{T288Ph}, equivalent to *Drosophila* AAK^{T311Ph}), which was reduced by half in the presence of the MPS1 inhibitor Cp5 (Koch et al., 2016) (Figures 10A and 10B). The AAK inhibitor MLN8237 prevented MPS1-induced AAK activation, indicating that MPS1 does not directly phosphorylate the T-loop (T288) but rather stimulates its auto-phosphorylation.

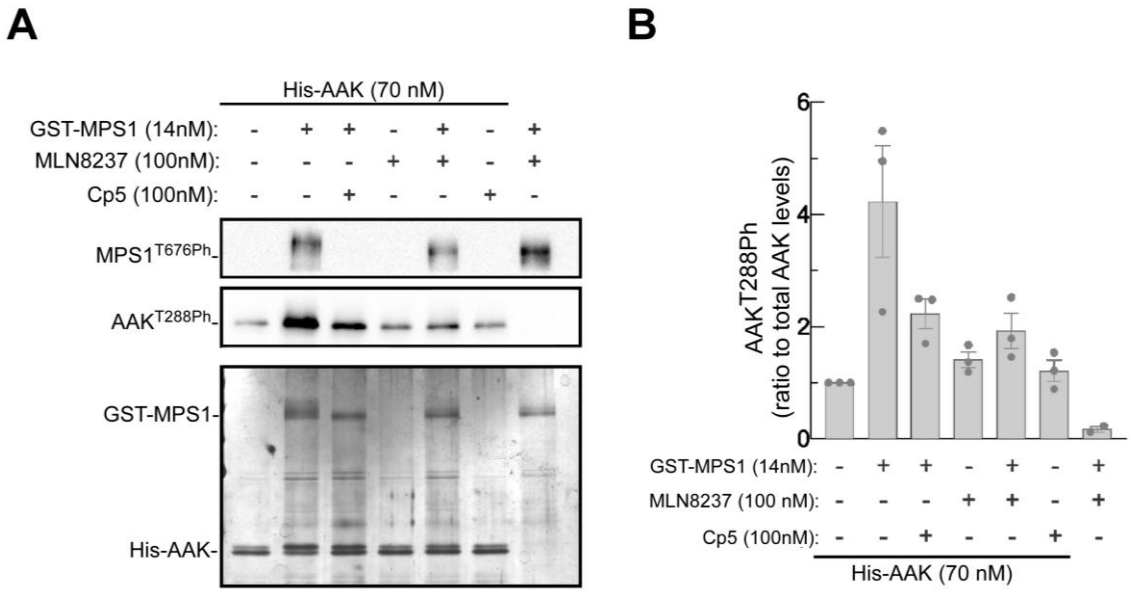


Figure 10. MPS1-mediated phosphorylation of AAK potentiates its auto-activation *in vitro*.

(A) *In vitro* kinase assay with purified human orthologs of AAK and MPS1. Western blot analysis of human AAK T288 activating T-loop auto-phosphorylation (AAK^{T288Ph}) and human MPS1 T676 activating T-loop auto-phosphorylation (MPS1^{T676Ph}). Recombinant His6-AAK was incubated with 100 µM ATP during 30 min at 30ºC in the indicated conditions. Total protein levels were assessed by gel silver staining.

(B) Quantification of human AAK T288 activating T-loop phosphorylation (AAK^{T288Ph}) blot intensity relative to total AAK levels in the indicated conditions, as presented in (A). All values were normalized to the mean value determined for basal AAK T288 phosphorylation, which was set to 1. The bars indicate the mean intensities, and the dots indicate the measurements from triplicates.

Data information: Data in (B) are presented as mean ± SD.

Mass spectrometry of *in vitro* phosphorylated AAK identified a putative MPS1 target site located at a conserved residue (T337/T360 in human and *Drosophila* AAK, respectively) that is predicted by AlphaFold3 to be positioned in the C-lobe αG-helix with close proximity to the T-loop (Figures 11A–11C).

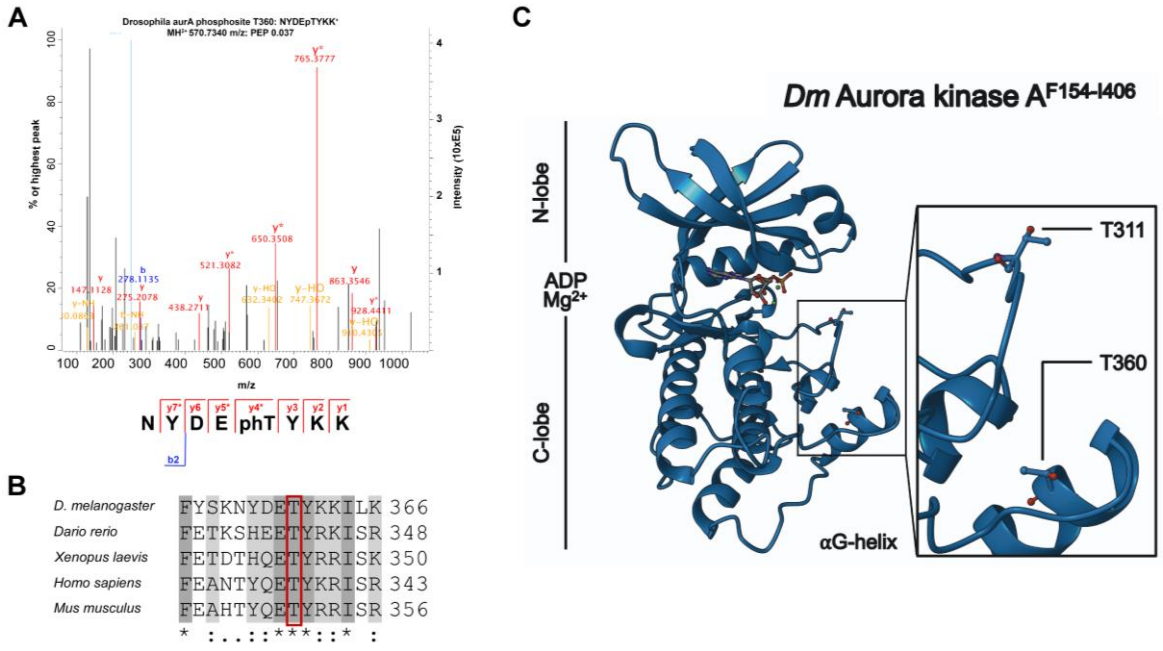


Figure 11. MPS1 phosphorylates AAK C-lobe at the conserved T337/T360.

(A) MS/MS spectrum of the phosphorylated T360 peptide of *Drosophila* AAK. *In vitro* phosphorylation of AAK by MPS1 was analyzed by MS and the MS/MS spectra were extracted from MaxQuant. Peaks corresponding to b- (blue) and y- (red and yellow) ions are annotated in the spectrum and peptide below. Fragment ions are labelled with their corresponding m/z value. Ions marked * indicate neutral losses (water or ammonia) or posttranslational modifications. The highest peak was set to 100%. Peptide mass, phosphorylation site and PEP (posterior error probability) are indicated.

(B) Clustal Omega (EMBL-EBI) local sequence alignment for the indicated AAK orthologues. Residues conservation: (*), fully conserved; (:), strongly similar properties; (.), weakly similar properties. MPS1-mediated phosphorylation of Threonine 360 (T360) in *Drosophila* AAK was identified by MS analysis after *in vitro kinase* assays. The identified residue is conserved in AAK orthologues (red rectangular box).

(C) AlphaFold 3 model of the kinase domain (154-406aa) of *Drosophila melanogaster* AAK (Q9VGF9) in crystal-like conditions (ADP and two Mg^{2+} ions).

We raised a phospho-specific antibody that confirmed by immunoblotting the phosphorylation of AAK^{WT} at T337 (T337Ph) upon incubation with MPS1 *in vitro* (Figure 12A). As expected, the T337Ph signal failed to be detected when T337 was converted to alanine (AAK^{T337A}) or when Cp5 was added to the reaction (Figure 12A). To test if MPS1 phosphorylates AAK at T360 in *Drosophila* S2 cells, we used the phospho-specific antibody for immunofluorescence analysis. Centrosomal signal of T360 phosphorylation (T360Ph) was readily detected in prometaphase cells but became significantly reduced in metaphase or upon depletion of MPS1 (Figures 12B and 12C). Mirroring AAK T-loop activation, the levels of T360Ph at centrosomes were positively correlated with the proximity of kinetochores in an MPS1-dependent manner (Figures 12B and 12D). Depleting AAK, or replacing the endogenous protein with an unphosphorylatable

mutant for T360 (T360A), also compromised T360Ph staining, which further validated the specificity of the antibody in S2 cells (Figures 12E and 12F). Collectively, these results support the conclusion that centrosomal AAK is phosphorylated at T360 by kinetochore-proximal MPS1.

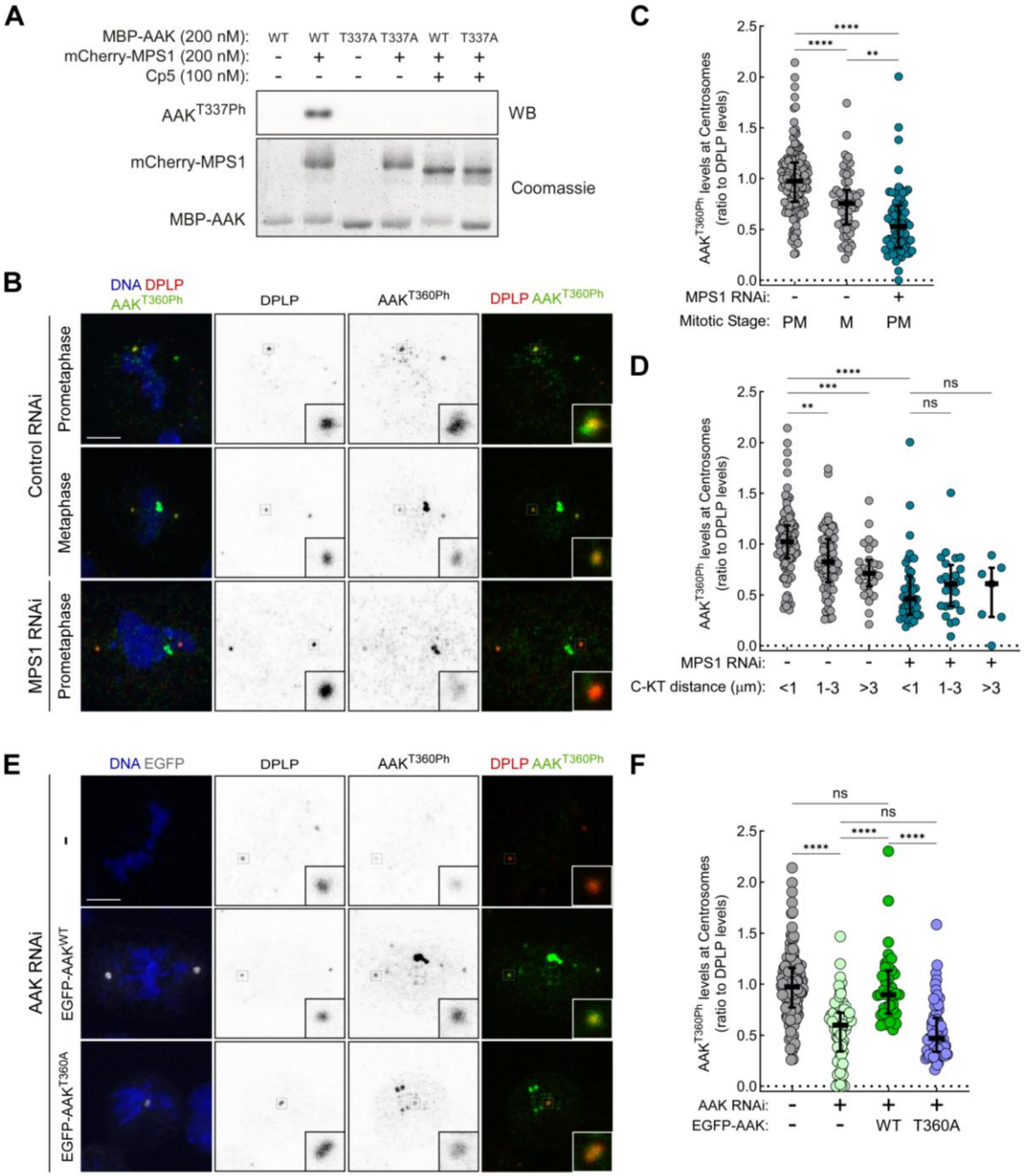


Figure 12. AAK T360 phosphorylation by MPS1 is detectable *in vitro* and in *Drosophila* S2 cells.

(A) *In vitro* kinase assay with purified human MBP-AAK and mCherry-MPS1. Western blot analysis of AAK T337 phosphorylation (AAK^{T337Ph}) using the phospho-specific antibody produced in this study. Recombinant human wild-type (WT) or non-phosphorylatable T337 mutant (T337A) MBP-AAK was

incubated with or without human mCherry-MPS1 for 30 min at 30ºC. MPS1 was inhibited (when indicated) with Cp5. Total protein levels were detected by Coomassie staining.

(B) Representative immunofluorescence images of AAK T360 phosphorylation (AAK^{T360Ph}) in prometaphase and metaphase control *Drosophila* S2 cells and prometaphase cells depleted of MPS1. Insets depict magnifications of selected centrosomes.

(C) Quantification of the levels of AAK T360 phosphorylation (AAK^{T360Ph}) relative to DPLP at centrosomes of prometaphase and metaphase control *Drosophila* S2 cells and prometaphase cells depleted of MPS1, as presented in (B). All values were normalized to the mean value determined for control prometaphase cells, which was set to 1. n ≥ 56 centrosomes for each condition from 2 biological replicates.

(D) Quantification of the levels of AAK T360 phosphorylation (AAK^{T360Ph}) relative to DPLP at centrosomes of control *Drosophila* S2 cells and cells depleted of MPS1 in the indicated conditions. Centrosomes presented in (C) were organized in 3 different columns representing ranges of distance to the closest kinetochore: less than 1 µm (<1), between 1 and 3 µm (1–3), and above 3 µm (>3). All values were normalized to the mean value determined for control prometaphase cells, as presented in (C), which was set to 1. n ≥ 7 centrosomes for each condition from 2 biological replicates.

(E) Representative immunofluorescence images of AAK T360 phosphorylation (AAK^{T360Ph}) levels in prometaphase *Drosophila* S2 cells depleted of endogenous AAK and expressing EGFP-AAK^{WT} or EGFP-AAK^{T360A}. Insets depict magnifications of selected centrosomes. These results are part of the experiment presented in (B), (C) and (D). The immunofluorescence image of the control parental S2 cell is presented in (B).

(F) Quantification of the levels of AAK T360 phosphorylation (AAK^{T360Ph}) relative to DPLP at centrosomes of prometaphase control *Drosophila* S2 cells as presented in (B), cells depleted of endogenous AAK and cells depleted of endogenous AAK and expressing EGFP-AAK^{WT} or EGFP-AAK^{T360A}, as presented in (E). These results are part of the experiment presented in (B), (C) and (D). The values for controls are the same as presented in (B), (C) and (D). All values were normalized to the mean value determined for prometaphase control cells, which was set to 1. n ≥ 39 centrosomes for each condition, from 2 biological replicates.

Data information: Data in (C), (D) and (F) are presented as median ± interquartile range. Statistical analysis was performed using a Kruskal-Wallis test for multiple comparisons. ns, not significant; *$p < 0.05$, **$p < 0.01$, ***$p < 0.001$, ****$p < 0.0001$. Scale bar, 5 µm.

A series of cell-based assays were next employed to test whether MPS1 stimulates AAK auto-phosphorylation of the T-loop (AAK^{T311Ph}) via phosphorylation of T360 in S2 cells. Consistent with the FRET results, MPS1 OE caused a significant increase in AAK^{T311Ph} at metaphase centrosomes relative to controls (Figures 13A and 13B). Loss of AAK activation upon MPS1 OE in AAK-depleted cells (Figures 13A and 13B) could be rescued by expression of wild type (WT) but not kinase-dead (K183I) AAK (Figures 13C and 13D).

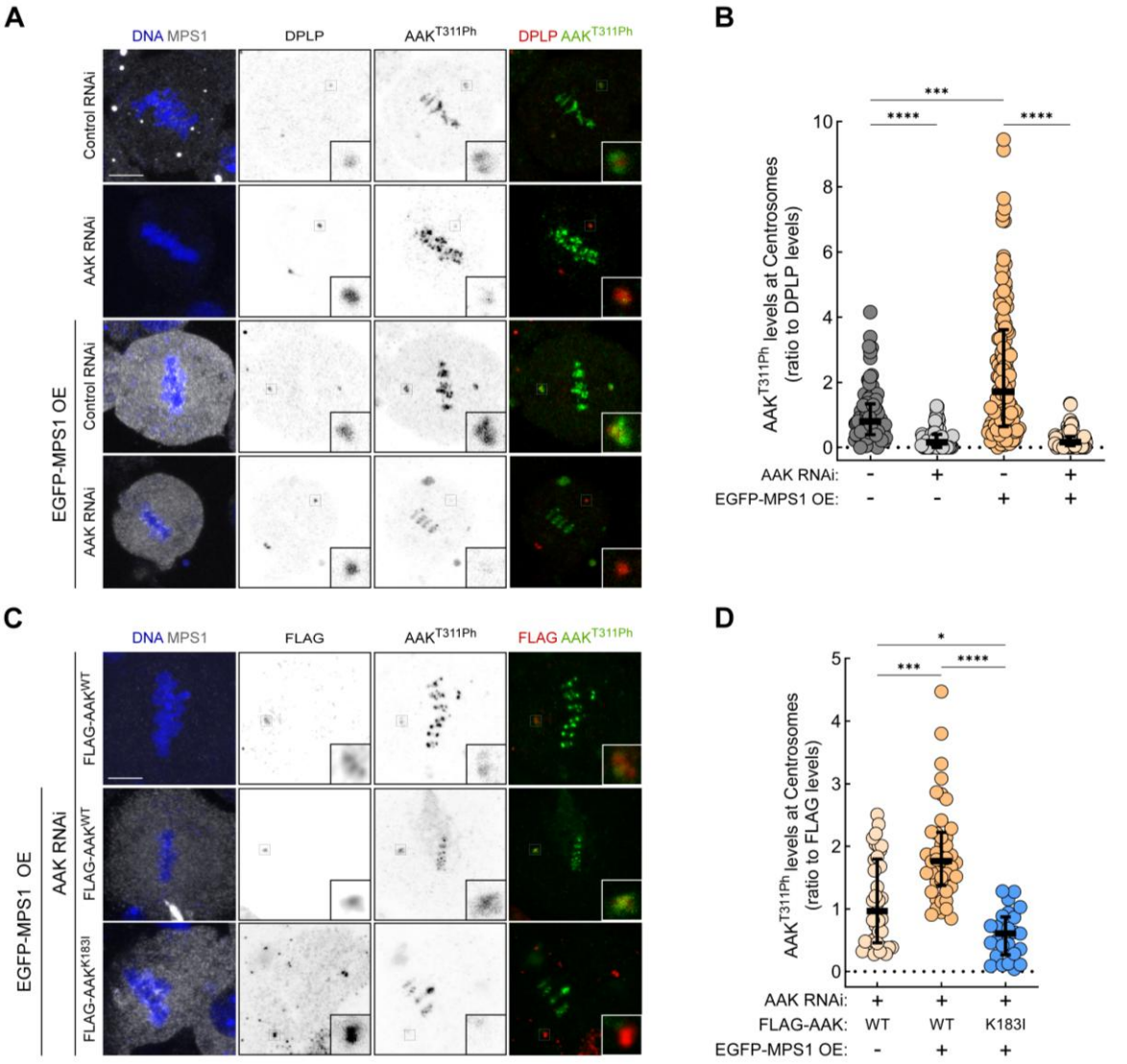


Figure 13. MPS1 overexpression potentiates centrosomal AAK auto-phosphorylation in metaphase *Drosophila* S2 cells.

(A) Representative immunofluorescence images of AAK T311 phosphorylation (AAK^{T311Ph}) levels in metaphase *Drosophila* S2 cells in the indicated conditions. Insets depict magnifications of selected centrosomes.

(B) Quantification of the levels of AAK T311 phosphorylation (AAK^{T311Ph}) relative to DPLP at centrosomes of metaphase *Drosophila* S2 cells in the indicated conditions, as presented in (A). All values were normalized to the mean value determined for control cells expressing endogenous levels of MPS1, which was set to 1. n ≥ 71 centrosomes for each condition, from 2 biological replicates.

(C) Representative immunofluorescence images of AAK T311 phosphorylation (AAK^{T311Ph}) in metaphase *Drosophila* S2 cells depleted of endogenous AAK and expressing FLAG-AAK^{WT} or FLAG-AAK^{K183I} in the indicated conditions. Insets depict magnifications of selected centrosomes.

(D) Quantification of the levels of AAK T311 phosphorylation (AAK^{T311Ph}) relative to FLAG at centrosomes of metaphase *Drosophila* S2 cells depleted of endogenous AAK and expressing FLAG-AAK^{WT} or FLAG-AAK^{K183I} in the indicated conditions, as presented in (C). All values were normalized to the mean value determined for cells expressing FLAG-AAK^{WT} and endogenous levels of MPS1, which was set to 1. n ≥ 25 centrosomes for each condition, from 2 biological replicates.

Data information: Data in (B) and (D) are presented as median ± interquartile range. Statistical analysis was performed using a Kruskal-Wallis test for multiple comparisons. P values: ns, not significant; *$p < 0.05$; **$p < 0.01$; ***$p < 0.001$; ****$p < 0.0001$. Scale bar: 5 µm.

Importantly, expression of the AAK non-phosphorylatable T360A mutant (AAK^{T360A}), predicted to have a similar structure as AAK^{WT} (Figure 14A), also failed to rescue MPS1-mediated activation of AAK in either prometaphase or metaphase cells (Figures 14B and 14C).

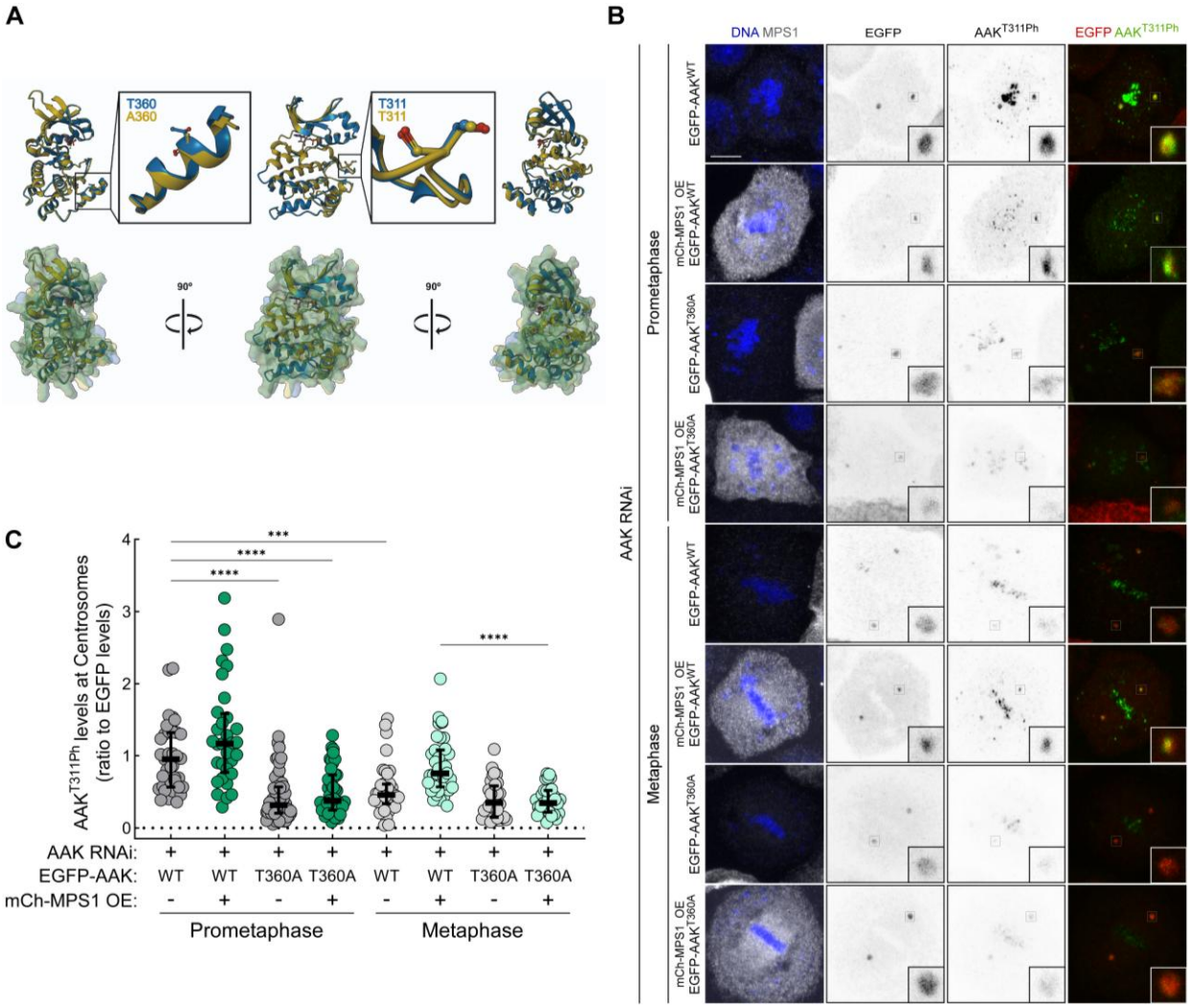


Figure 14. AAK T360 phosphorylation by MPS1 is required for proper centrosomal AAK prometaphase activation in *Drosophila* S2 cells.

(A) Superposed AlphaFold 3 models of *Drosophila* AAK^{WT} (cyan) and AAK^{T360A} (yellow) showing that the T360A mutation is not predicted to induce structural changes on the αG-helix, nor on the T-loop.

(B) Representative immunofluorescence images of AAK T311 phosphorylation (AAK^{T311Ph}) in prometaphase or metaphase *Drosophila* S2 cells depleted of endogenous AAK and expressing EGFP-AAK^{WT} or EGFP-AAK^{T360A} in the indicated conditions. Insets depict magnifications of selected centrosomes. EGFP-AAK^{WT} cells expressing endogenous MPS1 or overexpressing mCherry-MPS1

(OE) were imaged in the same coverslip. EGFP-AAK^{T360A} cells expressing endogenous MPS1 or overexpressing mCherry-MPS1 (OE) were imaged in the same coverslip.

(C) Quantification of the levels of AAK T311 phosphorylation (AAK^{T311Ph}) relative to EGFP at centrosomes of prometaphase or metaphase *Drosophila* S2 cells depleted of endogenous AAK and expressing EGFP-AAK^{WT} or EGFP-AAK^{T360A} in the indicated conditions, as presented in (B). All values were normalized to the mean value determined for prometaphase cells expressing EGFP-AAK^{WT} and endogenous levels of MPS1, which was set to 1. n ≥ 32 centrosomes for each condition from 2 biological replicates.

Data information: Data in (C) are presented as median ± interquartile range. Statistical analysis was performed using a Kruskal–Wallis test for multiple comparisons. P values: ns, not significant; *p < 0.05; **p < 0.01; ***p < 0.001; ****p < 0.0001. Scale bar: 5 μm.

Conversely, the phospho-mimetic mutation of T360 to aspartic acid (AAK^{T360D}) was sufficient to retain elevated levels of AAK T-loop phosphorylation in metaphase and restore AAK activation in prometaphase cells depleted of MPS1 (Figures 15A and 15B). Thus, phosphorylation of the conserved AAK T360 residue by MPS1 promotes auto-phosphorylation of the AAK T-loop (T311) and hence efficient kinase activation *in vitro* and in cells.

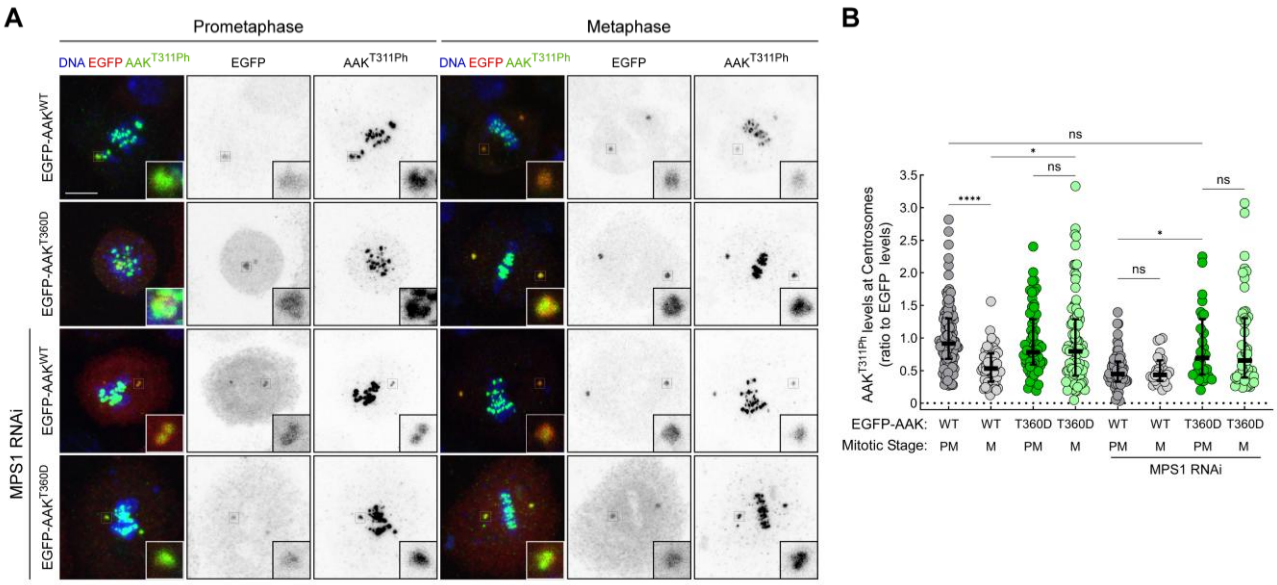


Figure 15. AAK T360 phosphorylation by MPS1 increases AAK T-loop auto-phosphorylation levels.

(A) Representative immunofluorescence images of AAK T311 phosphorylation (AAK^{T311Ph}) in prometaphase or metaphase *Drosophila* S2 cells expressing EGFP-AAK^{WT} or EGFP-AAK^{T360D} and expressing endogenous MPS1 or depleted of endogenous MPS1 in the indicated conditions. Insets depict magnifications of selected centrosomes.

(B) Quantification of the levels of AAK T311 phosphorylation (AAK^{T311Ph}) relative to EGFP at centrosomes of prometaphase or metaphase *Drosophila* S2 cells expressing EGFP-AAK^{WT} or EGFP-AAK^{T360D} and expressing endogenous MPS1 or depleted of endogenous MPS1 in the indicated conditions, as presented in (A). All values were normalized to the mean value determined for

prometaphase cells expressing EGFP-AAK^{WT} and endogenous levels of MPS1, which was set to 1. n ≥ 27 centrosomes for each condition from 2 biological replicates.

Data information: Data in (B) are presented as median ± interquartile range. Statistical analysis was performed using a Kruskal–Wallis test for multiple comparisons. P values: ns, not significant; *p < 0.05; **p < 0.01; ***p < 0.001; ****p < 0.0001. Scale bar: 5 μm.

Activation of AAK by MPS1 is required for efficient error correction and chromosome congression

The functional contributions of proximity-based activation of AAK by MPS1 to cell division were evaluated by live- and fixed-cell analyses of mitotic S2 cells. To isolate potential chromosome alignment and error correction functions of MPS1 from its role as a checkpoint kinase in *D. melanogaster* (Conde et al., 2013), cells were arrested in mitosis via RNAi of the APC/C subunit CDC27 (Huang and Raff, 2002; Lamb et al., 1994; Tugendreich et al., 1995). Cells efficiently aligned their chromosomes on a metaphase plate upon depletion of CDC27; however, co-depleting MPS1 impaired timely chromosome congression and increased the abundance of persistent polar chromosomes (Figures 16A and 16B). The congression defect in CDC27/MPS1 co-depleted cells was rescued by centrosomal targeting (via C-terminal fusions to CM2) of either WT MPS1 (MPS1^{WT}-CM2) or a phospho-mimetic mutant of AAK in which the previously identified MPS1 site (T360) was mutated to aspartic acid (AAK^{T360D}-CM2) (Figures 16A and 16B). The rescue of chromosome alignment required AAK kinase activity since cells expressing a kinase-dead (K183I) version of AAK^{T360D}-CM2 (AAK$^{K183I/T360D}$-CM2) failed to effectively congress their chromosomes (Figures 16A and 16B).

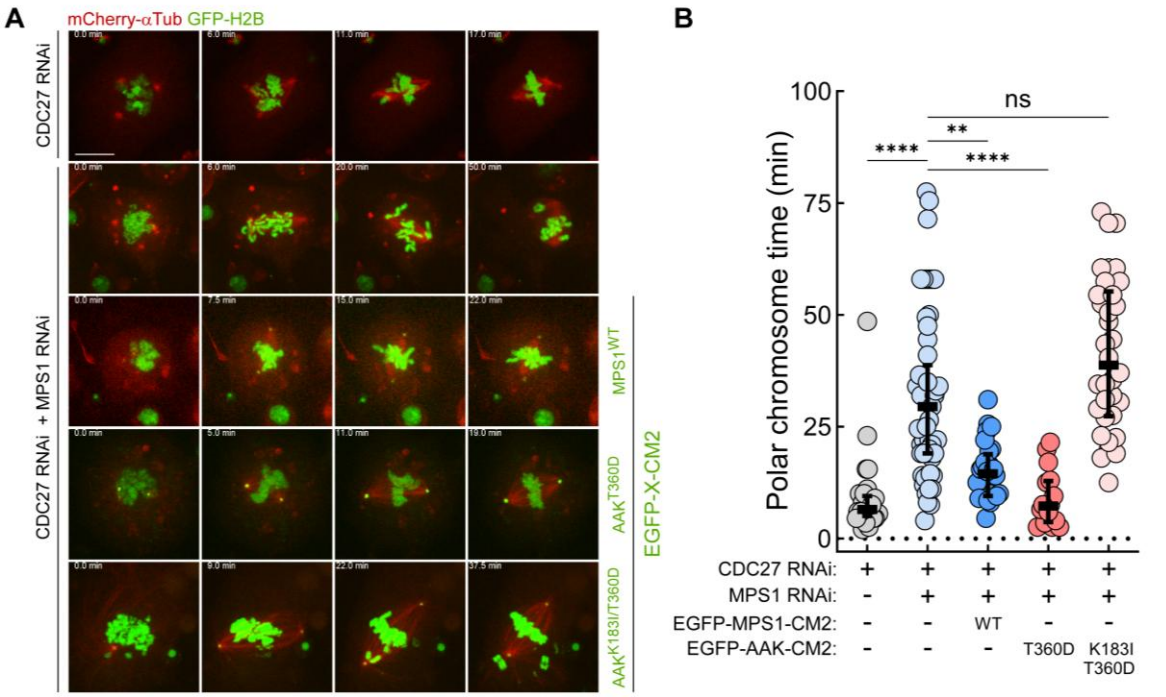


Figure 16. Centrosomal MPS1 or AAK phosphomimetic mutant (T360D) restore chromosome congression defects caused by MPS1 depletion in *Drosophila* S2 cells.

(A) Selected stills of representative mitotic progression movies of CDC27-depleted or CDC27/MPS1 co-depleted *Drosophila* S2 cells stably expressing GFP-H2B, mCherry-α-TUBULIN, and the indicated EGFP-tagged and CM2-fused transgenes (EGFP-X-CM2).

(B) Quantifications of the congression time of individual polar chromosomes (time each chromosome was retained near the spindle pole) in the conditions indicated in (A). n ≥ 16 polar chromosomes followed through time for each condition from at least 2 biological replicates.

Data information: Data in (B) are presented as median ± interquartile range. Statistical analysis was performed using a Kruskal–Wallis test for multiple comparisons. P values: ns, not significant; *p < 0.05; **p < 0.01; ***p < 0.001; ****p < 0.0001. Scale bar: 5 μm.

As expected, co-depletion of AAK and CDC27 delayed chromosome congression (Figures 17A and 17B). This defect was rescued by the expression of EGFP-AAK^{WT} and EGFP-AAK^{T360D} but not by the non-phosphorylatable T360A AAK mutant (EGFP-AAK^{T360A}) (Figures 17A and 17B). These results support the conclusion that MPS1-mediated phosphorylation of AAK T360 is required for efficient chromosome congression.

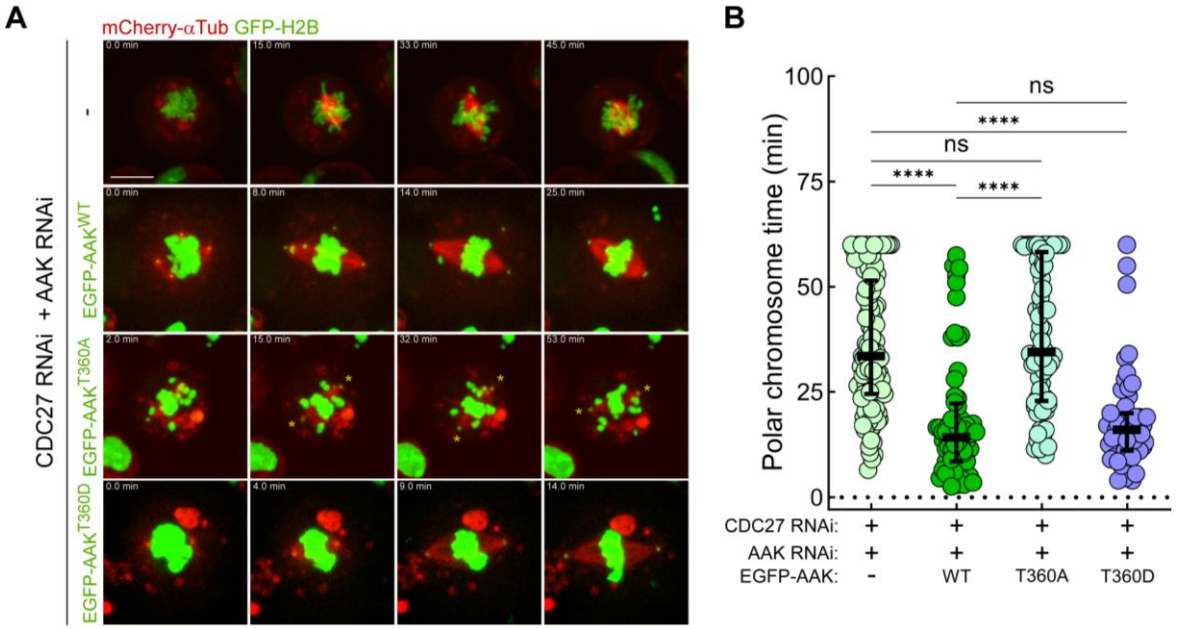


Figure 17. AAK T360 phosphorylation by MPS1 is required for timely chromosome congression in *Drosophila* S2 cells.

(A) Selected stills of representative mitotic progression movies of CDC27/AAK co-depleted *Drosophila* S2 cells stably expressing GFP-H2B, mCherry-α-TUBULIN, and the indicated transgenes. Asterisks indicate the centrosomes in the EGFP-AAK^{T360A} condition.

(B) Quantifications of the congression time of individual polar chromosomes (time each chromosome was retained near the spindle pole) in the conditions indicated in (A). n ≥ 51 polar chromosomes followed through time for each condition from at least 3 biological replicates.

Data information: Data in (B) are presented as median ± interquartile range. Statistical analysis was performed using a Kruskal–Wallis test for multiple comparisons. P values: ns, not significant; *p < 0.05; **p < 0.01; ***p < 0.001; ****p < 0.0001. Scale bar: 5 μm.

The attachment status of kinetochores was next assessed by analyzing confocal Z-sections of chromosomes (DAPI), kinetochores (CENP-C), and microtubules (α-TUBULIN) in calcium-treated fixed cells to assess error correction (Figures 18A–18D and 19A–19D). Chromosomes were scored as (1) bioriented when each sister kinetochore was clearly associated with microtubules oriented toward opposing spindle poles, (2) syntelic when sister kinetochore pairs were clearly attached to microtubules from the same spindle pole, and (3) pinned when the kinetochore pair was within 1 μm of the spindle pole regardless of whether its attachment status could be clearly discerned. While a vast majority of chromosomes were bioriented in CDC27-depleted cells, co-depletion of CDC27 and MPS1 resulted in a significant increase in the frequency of syntelic and pinned chromosomes, revealing that MPS1 is required for error correction in fly cells (Figures 18A–18D). The error correction defect in CDC27/MPS1 RNAi cells could be rescued by expressing centrosome-tethered MPS1^{WT}-CM2 but not AAK^{WT}-CM2 (Figures 18A–18D). Co-depletion of AAK

hindered MPS1^{WT}-CM2 capacity to promote chromosome alignment and biorientation, further supporting the conclusion that MPS1 acts upstream of AAK in the pole-based error correction pathway (Figures 18A–18D). The requirement for MPS1 to potentiate AAK-mediated error correction could be bypassed in CDC27/MPS1 co-depleted cells by centrosomal targeting of either the T-loop (T311D) or C-lobe (T360D) AAK-CM2 phospho-mimetic mutants but not the catalytic dead AAK$^{K183I/T360D}$-CM2 version (Figures 18A–18D).

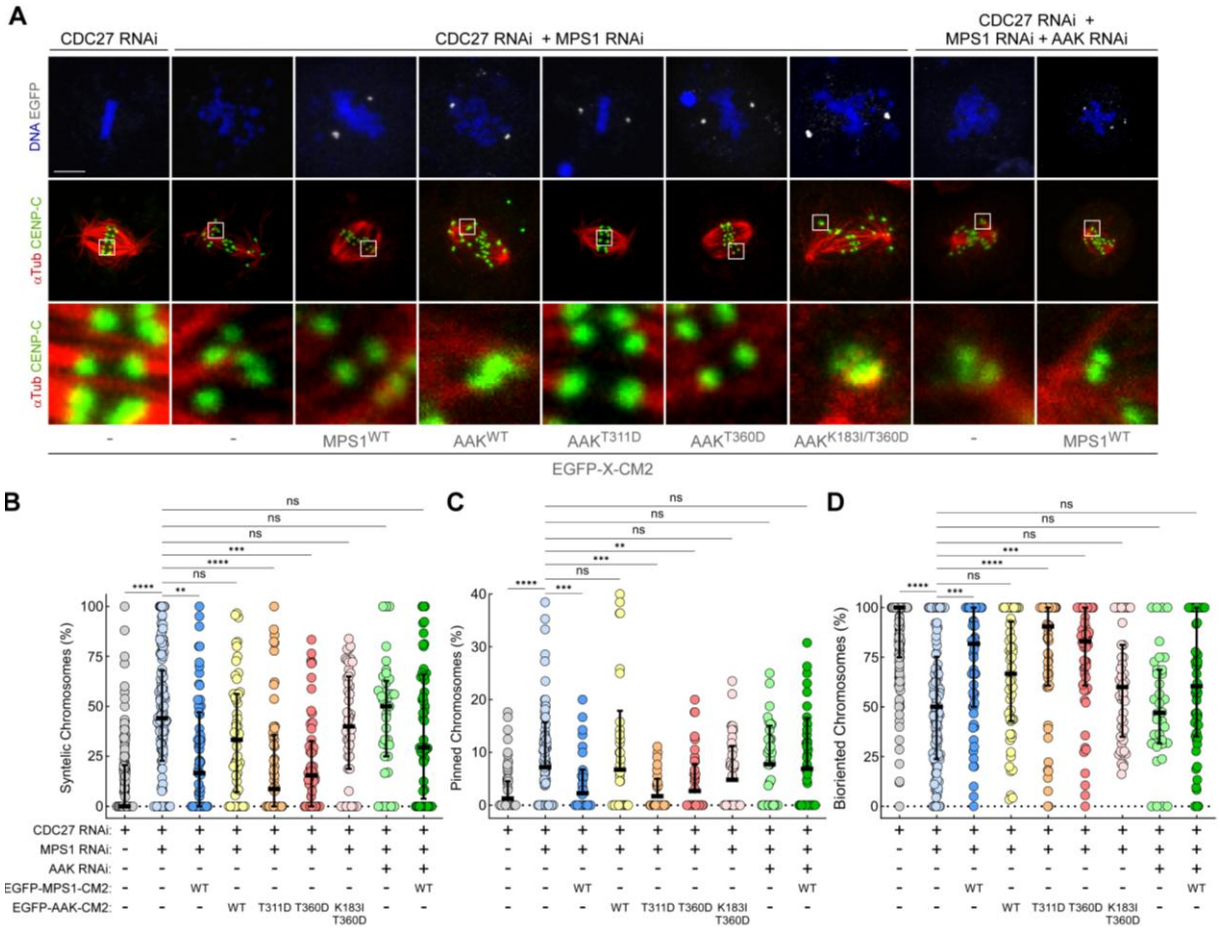


Figure 18. Centrosomal MPS1, AAK phosphomimetic mutant (T360D) or constitutively active AAK (T311D) restore defects in the correction of KT-MT attachments caused by MPS1 depletion in *Drosophila* S2 cells.

(A) Representative immunofluorescence images of mitotic *Drosophila* S2 cells expressing the indicated EGFP-tagged and CM2-fused transgenes (EGFP-X-CM2) and depleted of the indicated proteins. Insets depict magnifications of selected Z-steps of sister-kinetochores in amphitelic or syntelic attachment configurations.

(B) Percentage of syntelic kinetochore-microtubule attachments per cell in the indicated conditions, as presented in (A). n ≥ 36 cells for each condition from at least 2 biological replicates.

(C) Percentage of chromosomes pinned to centrosomes/spindle poles per cell in the indicated conditions, as presented in (A). n ≥ 36 cells for each condition from at least 2 biological replicates.

(D) Percentage of bioriented chromosomes per cell in the indicated conditions, as presented in (A). n ≥ 36 cells for each condition from at least 2 biological replicates.

Data information: Data in (B) and (D) are presented as median ± interquartile range. Data in (C) are presented as mean ± SD. Statistical analysis was performed using a Kruskal–Wallis test for multiple comparisons. P values: ns, not significant; *$p < 0.05$; **$p < 0.01$; ***$p < 0.001$; ****$p < 0.0001$. Scale bar: 5 μm.

To directly test the requirement of AAK T360 phosphorylation for error correction, we co-depleted CDC27 and endogenous AAK and evaluated kinetochore-microtubule attachments upon the expression of untethered versions of AAK. Contrasting with EGFP-AAK^{WT} and EGFP-AAK^{T360D}, the non-phosphorylatable EGFP-AAK^{T360A} mutant failed to restore chromosome biorientation and alignment in S2 cells depleted of endogenous AAK (Figures 19A–19D).

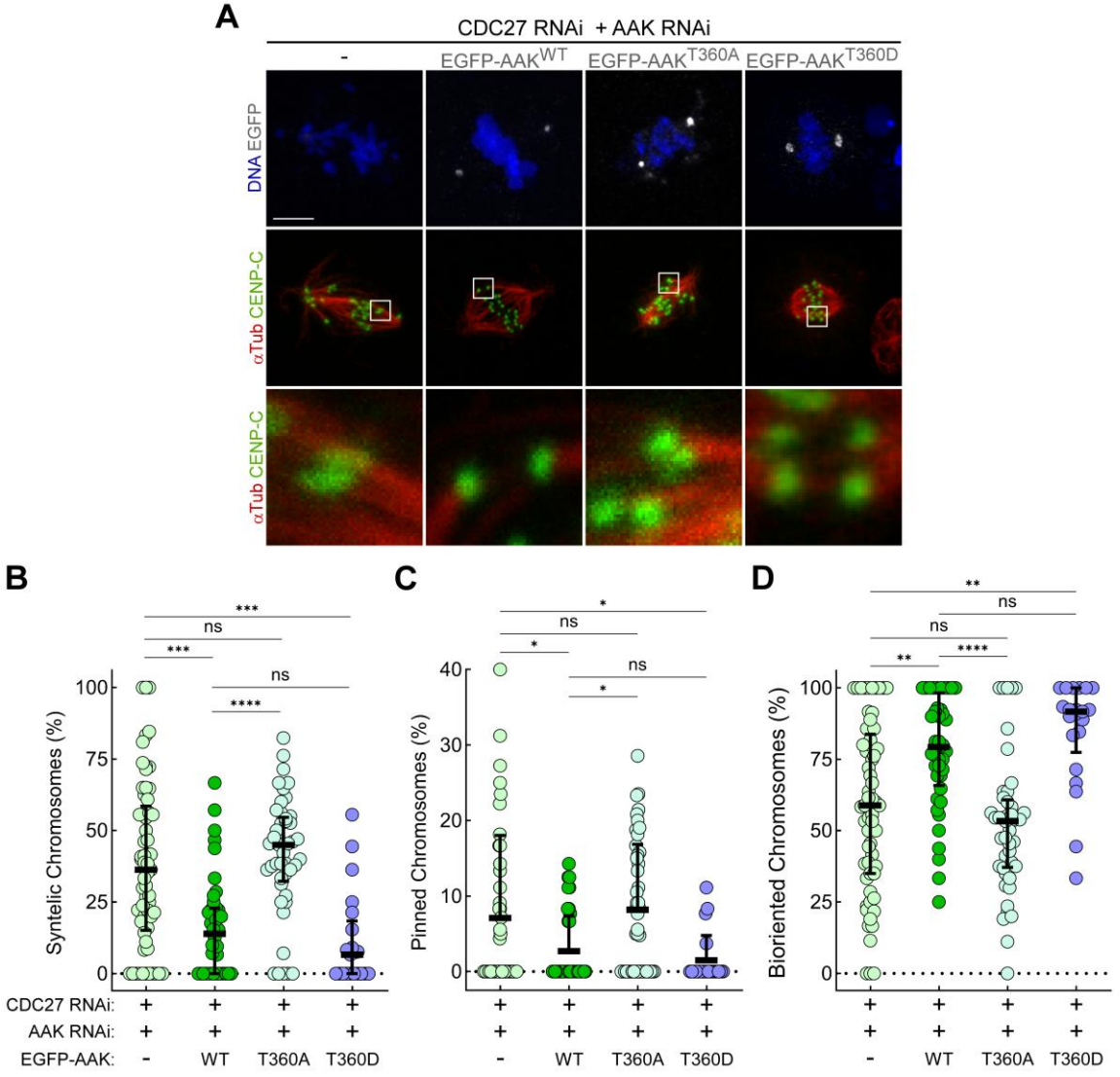


Figure 19. AAK T360 phosphorylation by MPS1 is required for efficient correction of erroneous KT-MT attachments in *Drosophila* S2 cells.

(A) Representative immunofluorescence images of CDC27/AAK co-depleted *Drosophila* S2 cells expressing EGFP-tagged AAK^{WT}, AAK^{T360A}, and AAK^{T360D}. Insets depict magnifications of selected Z-steps of sister-kinetochores in amphitelic or syntelic attachment configurations.

(B) Percentage of syntelic kinetochore-microtubule attachments per cell in the indicated conditions, as presented in (A). n ≥ 21 cells for each condition from at least 2 biological replicates.

(C) Percentage of chromosomes pinned to centrosomes/spindle poles per cell in the indicated conditions, as presented in (A). n ≥ 21 cells for each condition, from at least 2 biological replicates.

(D) Percentage of bioriented chromosomes per cell in the indicated conditions, as presented in (A). n ≥ 21 cells for each condition from at least 2 biological replicates.

Data information: Data in (B) and (D) are presented as median ± interquartile range. Data in (C) are presented as mean ± SD. Statistical analysis was performed using a Kruskal–Wallis test for multiple comparisons. P values: ns, not significant; *$p < 0.05$; **$p < 0.01$; ***$p < 0.001$; ****$p < 0.0001$. Scale bar: 5 μm.

Given that MPS1 depletion hindered the accumulation of γ-TUBULIN and D-TACC S863 phosphorylation at centrosomes (Figures 7A-7C), it was possible that the mitotic defects observed in the absence of MPS1-dependent AAK activation stemmed from an attenuation of centrosome maturation and function. However, S2 cells partially depleted of γ-TUBULIN, which formed abnormal mitotic spindles (Figure 20A) but maintained robust AAK activation (Figures 20C–20E), successfully aligned their chromosomes and established proper kinetochore-microtubule attachments as efficiently as control cells (Figures 20A, 20B, and 20F–20I). This finding suggests that compromised microtubule nucleation and polymerization at the centrosome play a minor role in the observed accumulation of erroneous kinetochore-microtubule attachments and chromosome misalignment in S2 cells that fail to fully activate AAK.

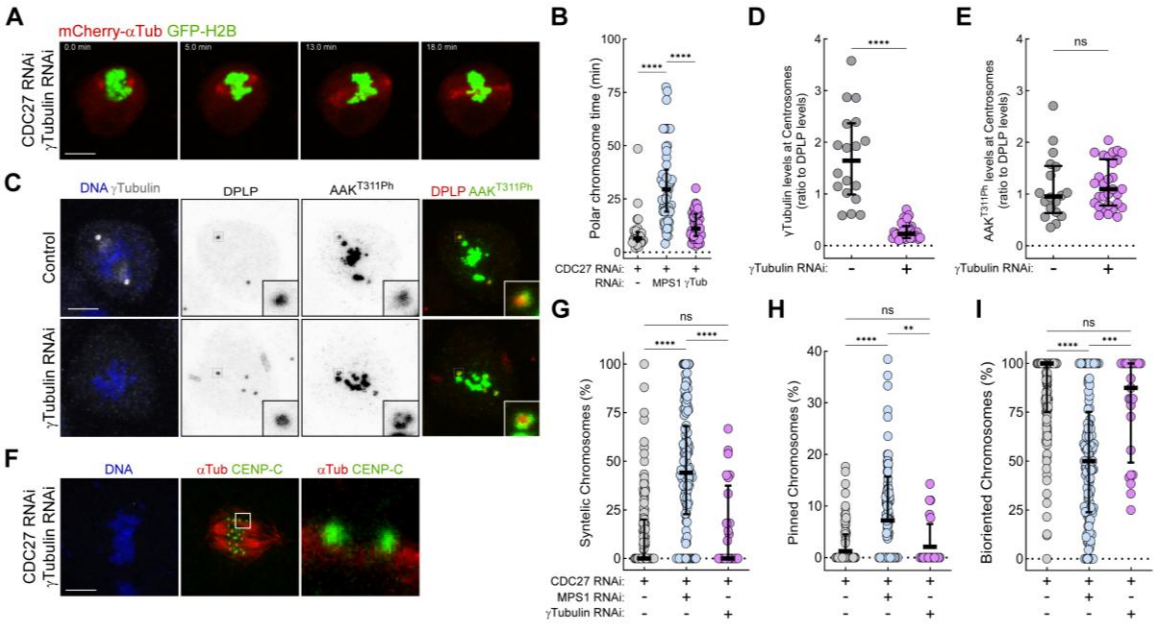


Figure 20. The defects in error correction and chromosome congression caused by MPS1 depletion are not caused by compromised centrosome function.

(A) Selected stills of representative mitotic progression movies of CDC27/γ-TUBULIN co-depleted *Drosophila* S2 cells stably expressing GFP-H2B, mCherry-α-TUBULIN. These results are part of the experiment presented in Figure 16.

(B) Quantifications of the congression time of individual polar chromosomes (time each chromosome was retained near the spindle pole) in the condition presented in (A). These results are part of the experiment presented in Figure 16. The values for controls and MPS1-depleted cells are the same as presented in Figure 16B and are depicted to facilitate comparison. n ≥ 16 polar chromosomes followed through time for each condition from at least 2 biological replicates.

(C) Representative immunofluorescence images of AAK T311 phosphorylation (AAK^{T311Ph}) and γ-TUBULIN levels in prometaphase *Drosophila* S2 cells in the indicated conditions. Insets depict magnifications of selected centrosomes.

(D) Quantification of the levels of γ-TUBULIN relative to DPLP at centrosomes of prometaphase *Drosophila* S2 control cells in the indicated conditions, as presented in (C). All values were normalized to the mean value determined for prometaphase control cells, which was set to 1. n ≥ 18 centrosomes for each condition from 2 biological replicates.

(E) Quantification of the levels of AAK T311 phosphorylation (AAK^{T311Ph}) relative to DPLP at centrosomes of prometaphase *Drosophila* S2 in the indicated conditions, as presented in (C). All values were normalized to the mean value determined for prometaphase control cells, which was set to 1. n ≥ 18 centrosomes for each condition from 2 biological replicates.

(F) Representative immunofluorescence images of CDC27/γ-TUBULIN co-depleted mitotic *Drosophila* S2 cells. Insets depict magnifications of selected Z-steps of sister-kinetochores in amphitelic or syntelic attachment configurations. These results are part of the experiment presented in Figure 18.

(G) Percentage of syntelic kinetochore-microtubule attachments per cell in the indicated conditions, as presented in (F) and Figure 18A. These results are part of the experiment presented in Figure 18. The values for controls and MPS1-depleted cells are the same as presented in Figure 18B and are depicted to facilitate comparison. n ≥ 25 cells for each condition from at least 2 biological replicates.

(H) Percentage of chromosomes pinned to centrosomes/spindle poles per cell in the indicated conditions, as presented in (F) and Figure 18A. These results are part of the experiment presented in Figure 18. The values for controls and MPS1-depleted cells are the same as presented in Figure 18C and are depicted to facilitate comparison. n ≥ 25 cells for each condition from at least 2 biological replicates.

(I) Percentage of bioriented chromosomes per cell in the indicated conditions, as presented in (F) and Figure 18A. These results are part of the experiment presented in Figure 18. The values for controls and MPS1-depleted cells are the same as presented in Figure 18D and are depicted to facilitate comparison. n ≥ 25 cells for each condition from at least 2 biological replicates.

Data information: Data in (B), (D), (E), (G), (H) and (I) are presented as median ± interquartile range. Statistical analysis in (B), (G), (H) and (I) was performed using a Kruskal–Wallis test for multiple comparisons. Statistical analysis in (D) and (E) was performed using a Mann-Whitney test. P values: ns, not significant; *p < 0.05; **p < 0.01; ***p < 0.001; ****p < 0.0001. Scale bar: 5 µm.

Collectively, the data demonstrate that the AAK-mediated error correction pathway is impaired in cells depleted of MPS1 or expressing AAK harbouring the T360A mutation. AAK targets a number of the same sites on the N-terminal tail of NDC80 as ABK, but S69 on HEC1 (human NDC80) is preferentially phosphorylated by AAK (DeLuca et al., 2018). Thus, we used a phospho-specific antibody against the equivalent phosphorylation on *Drosophila* NDC80 (NDC80^{S67Ph}) to evaluate whether it requires MPS1-mediated phosphorylation of AAK T360. Kinetochore levels of NDC80^{S67Ph} were elevated in prometaphase cells and decreased as chromosomes congressed to the metaphase plate (Figures 21A and 21B). Consistent with impaired error correction, depletion of MPS1 or expression of the EGFP-AAK^{T360A} mutant significantly compromised the phosphorylation of NDC80 at S67 regardless of kinetochore proximity to the spindle pole (Figures 21A–21C).

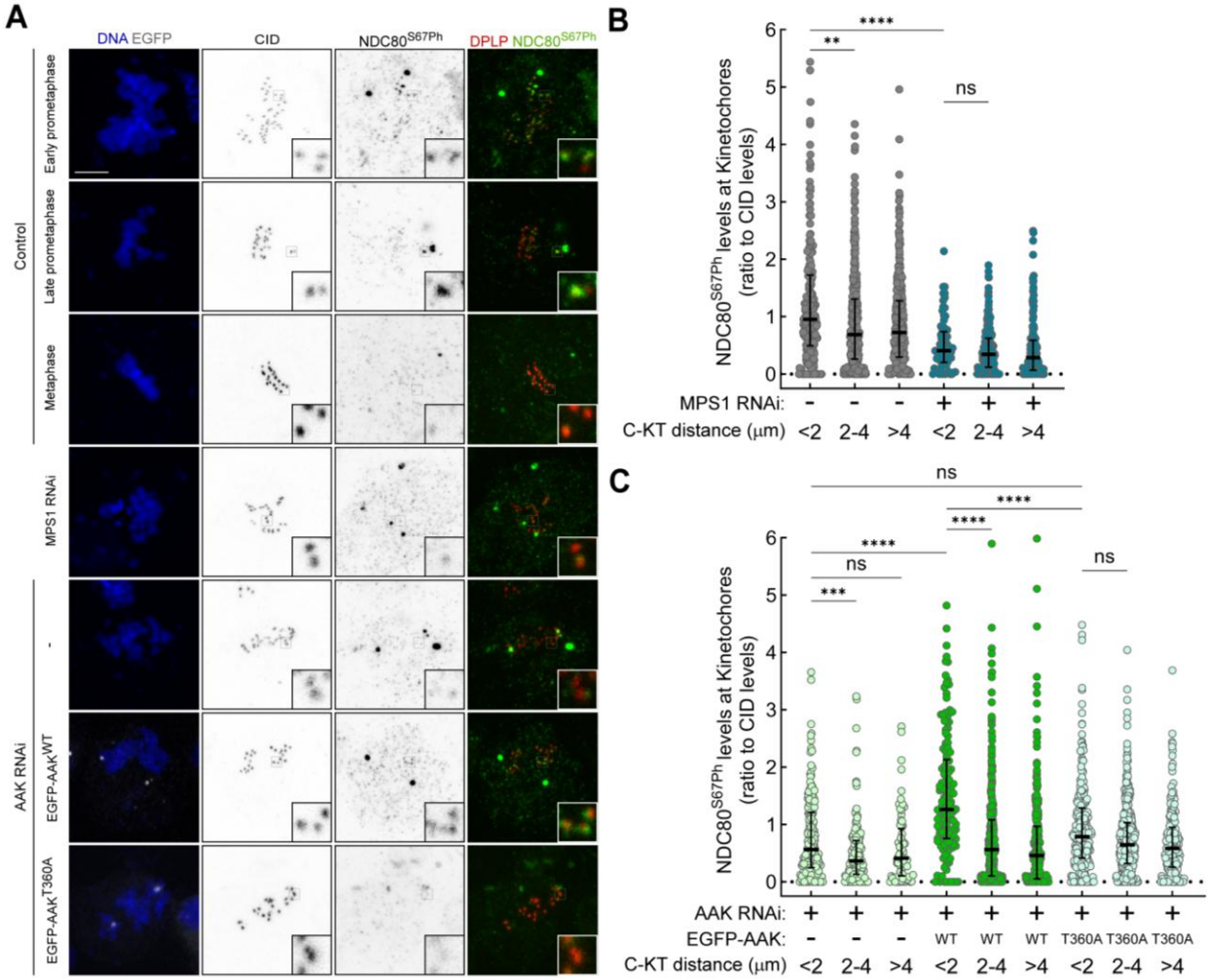


Figure 21. NDC80 phosphorylation by AAK is potentiated by MPS1 in *Drosophila* S2 cells.

(A) Representative immunofluorescence images of NDC80 S67 phosphorylation (NDC80^{S67Ph}) in control *Drosophila* S2 in early prometaphase, late prometaphase and metaphase cells, prometaphase cells depleted of MPS1, or prometaphase cells depleted of AAK and expressing EGFP-AAK^{WT} or EGFP-AAK^{T360A}. Insets depict magnifications of selected centrosomes.

(B) Quantification of the levels of NDC80 S67 phosphorylation (NDC80^{S67Ph}) relative to CID at kinetochores of prometaphase and metaphase *Drosophila* S2 control cells and cells depleted of MPS1 in the indicated conditions, as presented in (A). Kinetochores were organized in 3 different columns representing ranges of distance to the closest centrosome: less than 2 μm (<2); between 2 μm and 4 μm (2-4) and above 4 μm (>4). All values were normalized to the mean value determined for prometaphase control cells, which was set to 1. n ≥ 72 kinetochores for each condition from 2 biological replicates.

(C) Quantification of the levels of NDC80 S67 phosphorylation (NDC80^{S67Ph}) relative to CID at kinetochores of prometaphase and metaphase *Drosophila* S2 depleted of endogenous AAK or depleted of endogenous AAK and expressing either AAK^{WT} or AAK^{T360A} in the indicated conditions, as presented in (A). Kinetochores were organized in 3 different columns representing ranges of distance to the closest centrosome: less than 2 μ m (<2); between 2 μ m and 4 μ m (2-4) and above 4 μ m (>4). All values were normalized to the mean value determined for prometaphase control cells, as presented in (L), which was set to 1. n $\geq$ 72 kinetochores for each condition from 2 biological replicates.

Data information: Data in (B) and (C) are presented as median ± interquartile range. Statistical analysis in (B) and (C) was performed using a Kruskal–Wallis test for multiple comparisons. P values: ns, not significant; *p < 0.05; **p < 0.01; ***p < 0.001; ****p < 0.0001. Scale bar: 5 μm.

To test whether MPS1 directly potentiates AAK-mediated phosphorylation of NDC80/HEC1 N-terminal tail, we performed an *in vitro* kinase assay with recombinant bonsai NDC80 complex as a substrate (Ciferri et al., 2008) and probed for the phosphorylation of HEC1 at S55, another well-established AAK phosphorylation site (DeLuca et al., 2018). In accordance with its activation status, AAK capacity to phosphorylate S55 increased dramatically when co-incubated with MPS1 (Figures 22A and 22B). These findings support the conclusion that pole-based error correction in fly cells is carried out by AAK activated via phosphorylation of its C-lobe (T360) by MPS1 and further validate results from the FRET reporter, indicating that phosphorylation of downstream AAK targets is potentiated by MPS1.

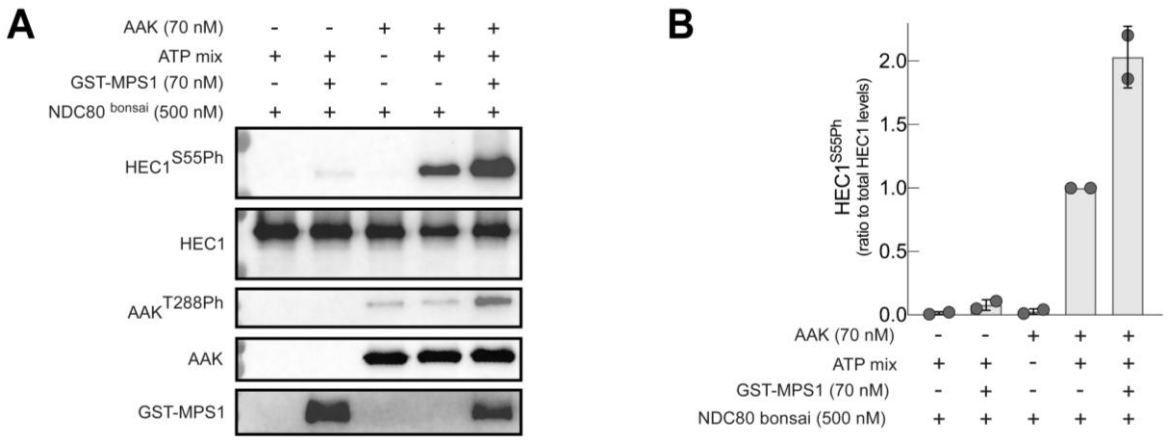


Figure 22. NDC80 phosphorylation by AAK is potentiated by MPS1 *in vitro*.

(A) *In vitro* kinase assay with purified human orthologues of AAK and MPS1 and NDC80^{bonsai}. Western blot analysis of human AAK T288 activating T-loop auto-phosphorylation (AAK^{T288Ph}) and human HEC1 S55 phosphorylation (HEC1^{S55Ph}) using phospho-specific antibodies. Previously dephosphorylated recombinant MBP-AAK-8xHis was incubated with NDC80^{bonsai}, with or without GST-MPS1 for 30 min at 30ºC. Total protein levels were detected by Western blotting.

(B) Quantification of HEC1 S55 phosphorylation (HEC1^{S55Ph}) blot intensity relative to total HEC1 levels in the indicated conditions, as presented in (A). All values were normalized to the mean value determined for HEC1 S55 phosphorylation in the presence of AAK and ATP and in the absence of MPS1 (lane 4), which was set to 1. The bars indicate the mean intensities; the dots indicate the measurements from duplicates.

Data information: Data in (B) are presented as mean ± SD.

Proximity-based activation of AAK by MPS1 is conserved in human cells

To examine if proximity-based activation of AAK by MPS1 is conserved outside *D. melanogaster*, the extent of AAK activation was evaluated under experimental conditions where the positioning of kinetochores relative to centrosomes/spindle poles could be manipulated in human RPE-1 cells (Barisic et al., 2014). When compared with control monopolar spindles (S-trityl-L-cysteine [STLC] treatment), kinetochores were positioned closer to the monopole center upon inhibition of the kinetochore-associated motor CENP-E with GSK923295 (CENP-Ei), while depletion of the DYNEIN adaptor Spindly (siSpindly) positioned kinetochores further from the monopole center (Figures 23A–23C).

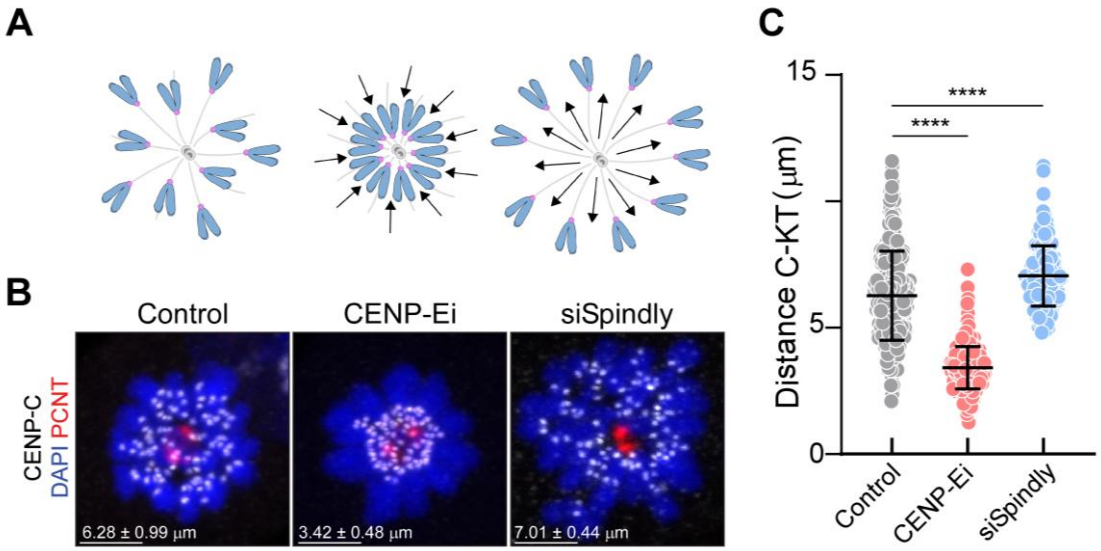


Figure 23. Kinetochore – centrosome distance can be manipulated in RPE1 cells using CENP-Ei or siSpindly.

(A) Schematic representation of the monopolar spindle assay used to assess AAK^{T288Ph} and HEC1^{S69Ph} changes in response to the distance between centrosomes and kinetochores.

(B) Representative immunofluorescence images of STLC-treated RPE-1 cells in control, CENP-E inhibited (CENP-Ei), and Spindly depleted (siSpindly) conditions.

(C) Quantification of centrosome (PCNT)-kinetochore (CENP-C) (C-KT) distances of STLC-treated RPE-1 cells in the indicated conditions, as presented in (B).

Data information: Data are presented in (C) as mean ± SD. Statistical analysis was performed using a Mann-Whitney non-parametric t test. ns, not significant; *$p < 0.05$, **$p < 0.01$, ***$p < 0.001$, ****$p < 0.0001$. n ≥ 75 cells for each condition. Scale bar, 5 µm.

Consistent with there being spatial crosstalk between kinetochores and centrosomes, AAK activation (AAK^{T288Ph}) levels at centrosomes/spindle poles were significantly increased in the CENP-Ei cells and significantly reduced in the siSpindly cells relative to control cells (Figures 24A and 24B). Active AAK^{T288Ph} signal at centrosomes was significantly reduced

compared with controls in nocodazole- (Figures 24C and 24D) and STLC-treated cells (Figures 24E and 24F) when MPS1 was inhibited with Cp5 (MPS1i). Importantly, inhibiting MPS1 prevented the increase in AAK activation in CENP-Ei monopoles (Figures 24E and 24F). Thus, the potentiation in AAK activation observed when kinetochores were positioned closer to centrosomes in human RPE-1 cells required MPS1 activity.

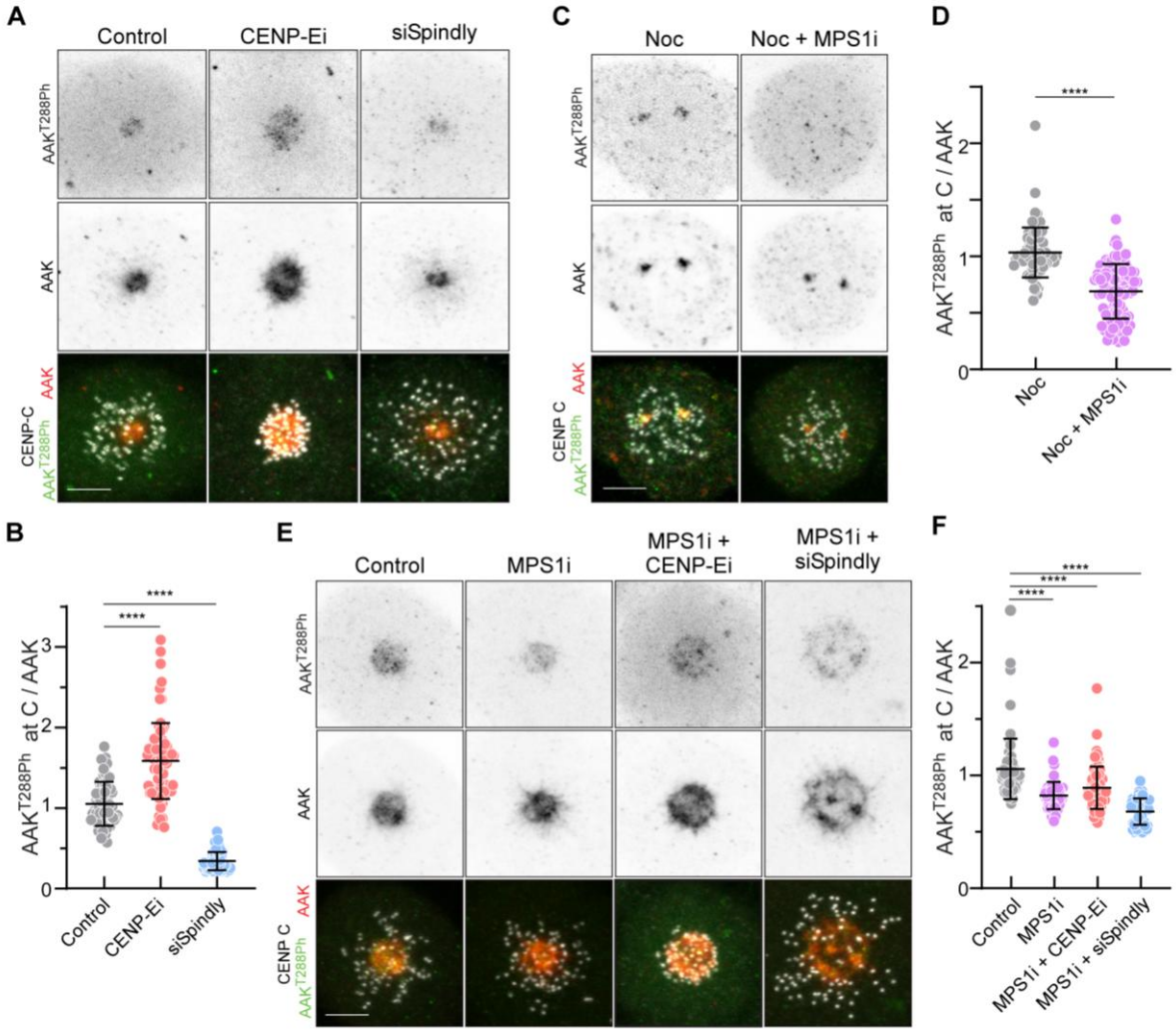


Figure 24. Decrease in kinetochore – centrosome distance increases AAK activation levels in RPE1 cells in an MPS1-dependent manner.

(A) Representative immunofluorescence images of AAK T288 phosphorylation (AAK^{T288Ph}) and AAK levels in STLC-treated RPE-1 cells in control, CENP-E inhibited (CENP-Ei), and Spindly depleted (siSpindly) conditions.

(B) Quantification of the levels of AAK T288 phosphorylation (AAK^{T288Ph}) relative to total AAK levels at centrosomes of STLC-treated RPE-1 cells in the indicated conditions, as presented in (A). All values were normalized to the median value determined for control cells, which was set to 1.

(C) Representative immunofluorescence images of AAK T288 phosphorylation (AAK^{T288Ph}) and AAK levels in nocodazole-treated RPE-1 cells in control and MPS1-inhibited (MPS1i) conditions. Proteasome was inhibited by MG132 to prevent mitotic exit after MPS1 inhibition.

(D) Quantification of the levels of AAK T288 phosphorylation (AAK^{T288Ph}) relative to total AAK levels at centrosomes of nocodazole-treated RPE-1 cells in the indicated conditions as presented in (C). All values were normalized to the median value determined for control cells, which was set to 1.

(E) Representative immunofluorescence images of AAK T288 phosphorylation (AAK^{T288Ph}) and AAK levels in STLC-treated RPE-1 cells in control, MPS1 inhibited (MPS1i), MPS1/CENP-E co-inhibited (MPS1i + CENP-Ei), and MPS1 inhibited in Spindly depleted background (MPS1i + siSpindly). In all conditions, the proteasome was inhibited with MG132.

(F) Quantification of the levels of AAK T288 phosphorylation (AAK^{T288Ph}) relative to total AAK levels at centrosomes of STLC-treated RPE-1 cells in the indicated conditions, as presented in (E). All values were normalized to the median value determined for control cells, which was set to 1.

Data information: Data are presented in (B), (D) and (F) as mean ± SD. Statistical analysis was performed using a Mann-Whitney non-parametric t test. ns, not significant; *$p < 0.05$, **$p < 0.01$, ***$p < 0.001$, ****$p < 0.0001$. n ≥ 75 cells for each condition. Scale bar, 5 µm.

Accordingly, the activation of AAK at centrosomes during an unperturbed mitosis peaked in prometaphase in an MPS1-dependent manner and decreased significantly in metaphase (Figures 25A and 25B). While the observations of centrosomal AAK activation in RPE-1 cells were broadly consistent with those from fly cells, one notable difference was in prophase cells, where AAK activation at centrosomes was high in fly cells but low in RPE-1 cells (Figures 25A and 25B). It is unclear why this is the case or if the AAK activation status fulfils unique prophase functions in fly versus human cells.

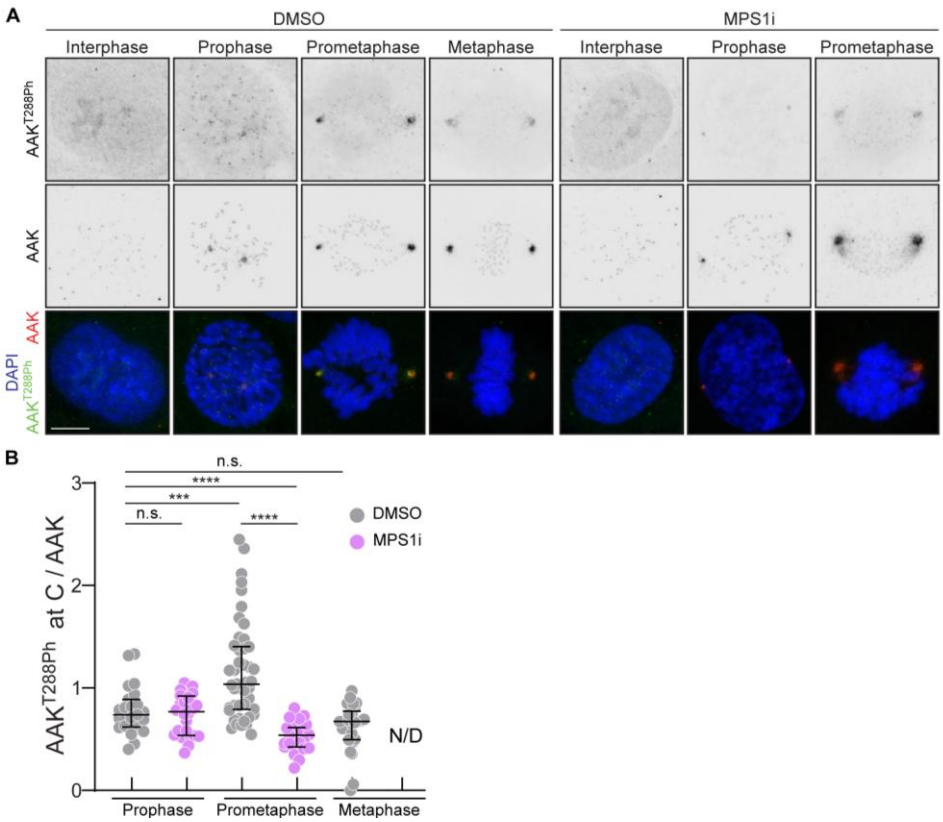


Figure 25. AAK activation profile in mitosis is conserved in RPE1 cells, except in prophase.

(A) Representative immunofluorescence images of AAK T288 phosphorylation (AAK^{T288Ph}) and AAK levels in RPE-1 cells in control and MPS1-inhibited (MPS1i) conditions in the indicated cell cycle stage.

(B) Quantification of the levels of AAK T288 phosphorylation (AAK^{T288Ph}) relative to total AAK levels at centrosomes of RPE1 cells in control and MPS1-inhibited (MPS1i) conditions in the indicated mitotic stages, as presented in (A). All values were normalized to the median value determined for control cells, which was set to 1.

Data information: Data are presented in (B) as mean ± SD. Statistical analysis was performed using a Mann-Whitney non-parametric t test. ns, not significant; $*p < 0.05$, $**p < 0.01$, $***p < 0.001$, $****p < 0.0001$. n ≥ 25 cells for each condition. Scale bar, 5 μm.

We then measured the extent of HEC1 phosphorylation at S69 ($HEC1^{S69Ph}$) as a function of kinetochore positioning within monopolar spindles. Consistent with the extent of AAK activation (AAK^{T288Ph} levels), phosphorylation of HEC1-S69 was increased in CENP-Ei cells and reduced in siSpindly cells relative to controls (Figures 26A and 26B). In nocodazole-treated cells, $HEC1^{S69Ph}$ levels were reduced to the same extent following inhibition of either MPS1 or AAK and to a lesser extent upon ABK inhibition, reflecting an upstream role of MPS1 in the preferential phosphorylation of HEC1-S69 by AAK (Figures 26C and 26D). Importantly, $HEC1^{S69Ph}$ levels were significantly reduced when MPS1 was inhibited, including in CENP-Ei cells that normally exhibited a significant increase in $HEC1^{S69Ph}$ levels (Figures 26E and 26F). Altogether, the data support the conclusion that kinetochore proximity-based activation of AAK by MPS1 potentiates phosphorylation of the bona fide error correction substrate HEC1 in human cells.

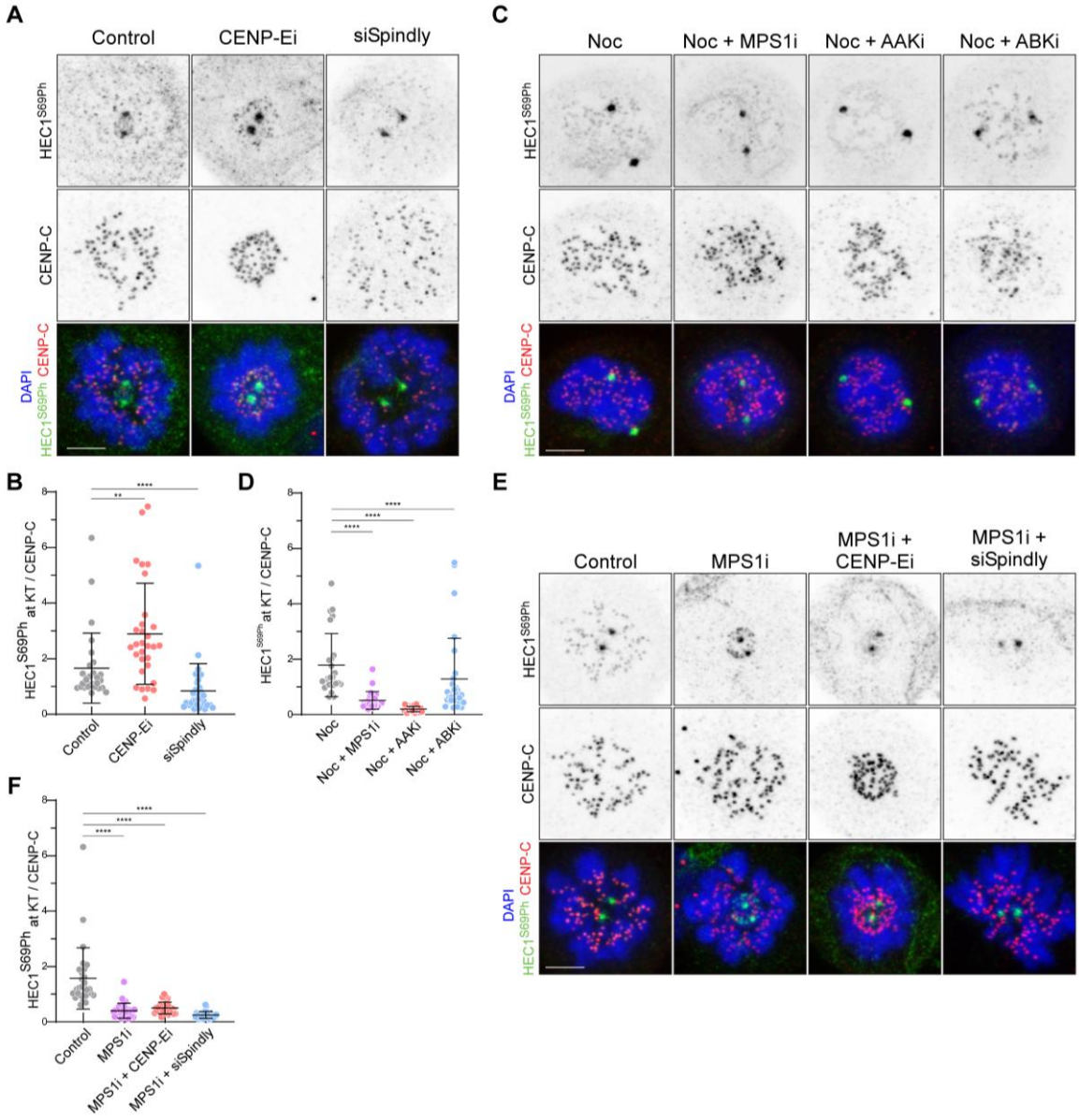


Figure 26. Decrease in kinetochore – centrosome distance increases NDC80 phosphorylation by AAK in hRPE1 cells in an MPS1-dependent manner.

(A) Representative immunofluorescence images of HEC1 S69 phosphorylation (HEC1^{S69Ph}) and CENP-C levels in STLC-treated RPE-1 cells in control, CENP-E inhibited (CENP-Ei), and Spindly depleted (siSpindly) conditions.

(B) Quantification of the levels of HEC1 S69 phosphorylation (HEC1^{S69Ph}) relative to CENP-C levels at kinetochores of STLC-treated RPE-1 cells in the indicated conditions, as presented in (A). All values were normalized to the median value determined for control cells, which was set to 1.

(C) Representative immunofluorescence images of HEC1 S69 phosphorylation (HEC1^{S69Ph}) and CENP-C levels in nocodazole-treated RPE-1 cells in control, MPS1-inhibited (MPS1i), AAK-inhibited (AAKi) and ABK-inhibited (ABKi) conditions. Proteasome was inhibited by MG132 to prevent mitotic exit after MPS1 inhibition.

(D) Quantification of the levels of HEC1 S69 phosphorylation (HEC1^{S69Ph}) relative to CENP-C levels at kinetochores of nocodazole-treated RPE-1 cells in the indicated conditions as presented in (C). All values were normalized to the median value determined for control cells, which was set to 1.

(E) Representative immunofluorescence images of HEC1 S69 phosphorylation (HEC1^{S69Ph}) and CENP-C levels in STLC-treated RPE-1 cells in control, MPS1 inhibited (MPS1i), MPS1/CENP-E co-inhibited (MPS1i + CENP-Ei), and MPS1 inhibited in Spindly depleted background (MPS1i + siSpindly). In all conditions the proteasome was inhibited with MG132.

(F) Quantification of the levels of HEC1 S69 phosphorylation (HEC1^{S69Ph}) relative to CENP-C levels at kinetochores of STLC-treated RPE-1 cells the indicated conditions, as presented in (E). All values were normalized to the median value determined for control cells, which was set to 1.

Data information: Data are presented in (B), (D) and (F) as mean ± SD. Statistical analysis was performed using a Mann-Whitney non-parametric t test. ns, not significant; *$p < 0.05$, **$p < 0.01$, ***$p < 0.001$, ****$p < 0.0001$. n ≥ 25 cells for each condition. Scale bar, 5 μm.

We propose a model whereby a proximity-dependent crosstalk between kinetochores and centrosomes/spindle poles promotes error correction (Figure 27). The model envisions that as erroneous kinetochore-microtubule interactions (e.g., a syntelic attachment) become positioned within the vicinity (~1 μm) of the spindle pole, kinetochore-recruited MPS1 phosphorylates AAK on a conserved site (T360 in flies) located in the αG-helix of the kinase C-lobe. Phosphorylation of the C-lobe, in turn, triggers auto-catalytic phosphorylation of the AAK T-loop to amplify an ~2 μm radius activity gradient (Chmátal et al., 2015; Ye et al., 2015; Ye & Maresca, 2015) to locally promote microtubule detachment via phosphorylation of kinetochore substrates such as the NDC80 complex.

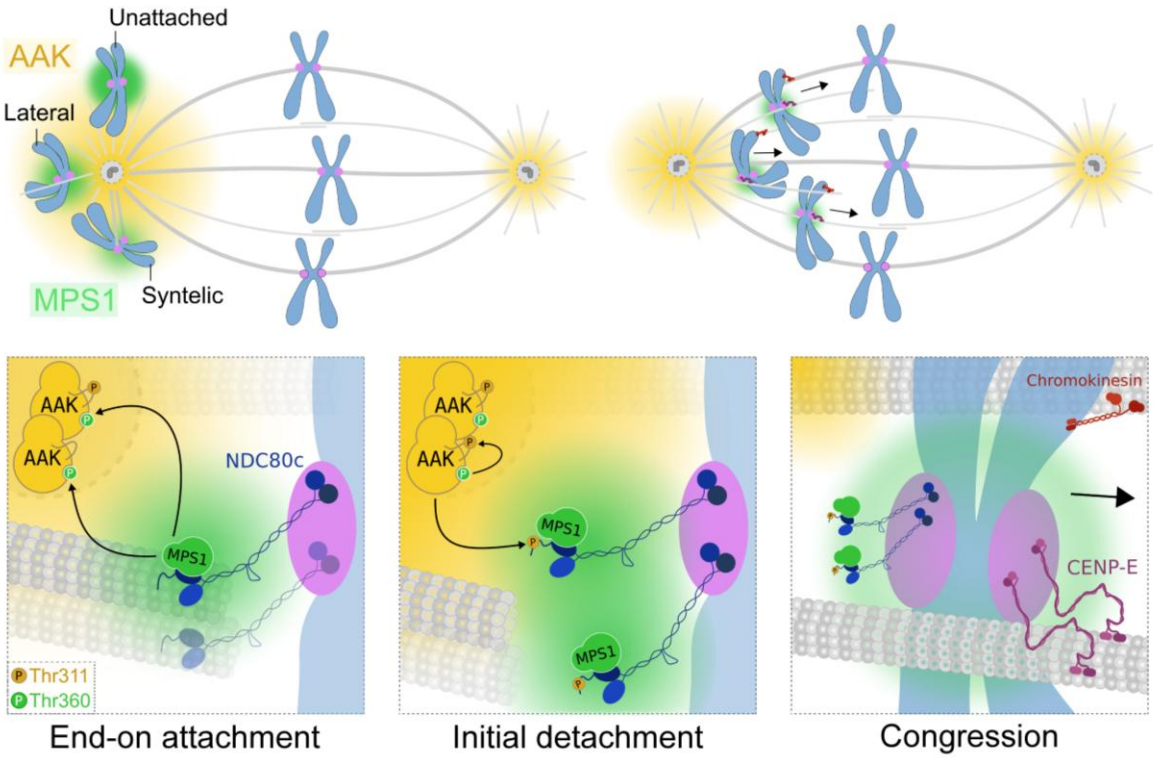


Figure 27. Proposed model for proximity-based activation of AAK by MPS1 as a strategy to potentiate error correction of polar chromosomes and ensure chromosome congression.

A pool of MPS1 recruited to kinetochores of polar chromosomes indirectly contributes to pole-based error correction by phosphorylating AAK on the conserved residue T360. This potentiates AAK activation at centrosomes and thereby its capacity to phosphorylate the N-terminal tail of HEC1/NDC80 at kinetochores to destabilize end-on attachments. This mechanism corrects and prevents syntelic kinetochore-microtubule interactions in the vicinity of centrosomes and ensures efficient chromosome congression.

AlphaFold3 predicts that phosphorylation of T360 causes an outward stretch of the αG-helix that pulls on the T-loop by interacting with D317 in a manner that could render the T-loop more flexible and leave the activating T311 more exposed for phosphorylation (Figures 28A–28C). Further investigation into the structural basis of this novel activation mechanism is warranted. Overall, our findings support the conclusion that a pool of MPS1 at kinetochores indirectly contributes to pole-based error correction through centrosomal AAK.

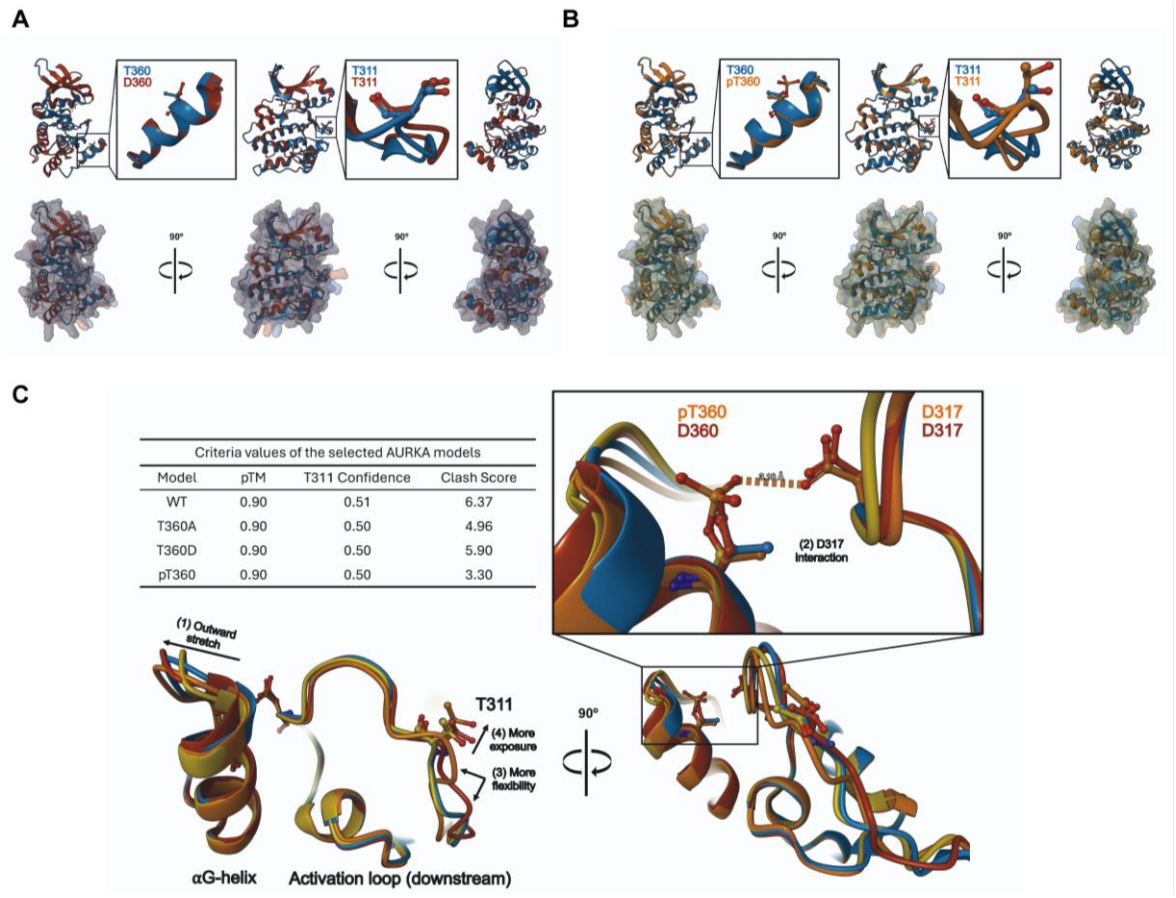


Figure 28. AlphaFold 3 prediction models of the structural changes caused by AAK T360 phosphorylation.

(A) Superposed AlphaFold 3 models of *Drosophila* AAK^{WT} (cyan) and AAK^{T360D} (red) showing that the T360D mutation is predicted to cause a displacement in the αG-helix, opening room for more flexibility of the T-loop and exposure of T311.

(B) Superposed AlphaFold 3 models of *Drosophila* AAK^{WT} (cyan) and AAK^{WT} phosphorylated in T360 (AAK^{pT360}) (orange) predicting that the phospho-threonine causes steric hindrance leading to αG-helix displacement and increased T-loop flexibility and exposure.

(C) The table shows the overall structure pTM, T-loop Confidence and ClashScore for the best models and underneath is presented the predicted model by which phosphorylation of T360 facilitates AAK T311 auto-phosphorylation. (AAK^{T360A} mutant Alphafold 3 model is depicted in Figure 14A).This model consists of four steps, (1) an outward stretch of the αG-helix that pulls on the T-loop by (2) interacting with D317 in manner that could (3) render the T-loop more flexible and (4) leave the activating T311 more exposed for phosphorylation.

CHAPTER 4

GENERAL DISCUSSION

This chapter contains part of the following published scientific article and has been reproduced here with the permission of the copyright holder (Appendix).

Leça, N., Barbosa, F., Rodriguez-Calado, S., Verza, A. E., Moura, M., Pedroso, P. D., Pinto, I., Artes, E., Bange, T., Sunkel, C. E., Barisic, M., Maresca, T. J., Conde, C. (2025). Proximity-based activation of AURORA A by MPS1 potentiates error correction. *Current Biology*. Volume 35, Issue 8, 1935 - 1947.e8

Cell division is a key process in life that is required for proliferation, growth, tissue repair, homeostasis and development of multicellular organisms. To ensure the formation of daughter cells carrying the same genomic content, cells must replicate their chromosomes during the S-phase and then equally segregate them to each of the daughter nuclei during mitosis. Mitosis is, therefore, a fundamental period of the cell cycle where several pathways must work jointly with precise coordination in space and time to ensure the even distribution of the genomic content between the two new nuclei. An essential step towards a faithful mitosis is the establishment of proper interactions between microtubules that constitute the mitotic spindle and kinetochores, the multi-protein complexes that assemble on the centromeric region of each chromatid.

These interactions allow the transduction of the forces applied by the mitotic spindle to generate chromosome movement. This is required to bring the chromosomes to the cell equator during prometaphase (chromosome congression) – ensuring a proper "metaphase plate" before chromatid separation can take place – and for efficient chromosome segregation during anaphase. By metaphase, it is essential that all sister kinetochores are bound to the plus tips of microtubules emanating from opposite spindle poles (amphitelic attachment). This attachment configuration warrants that chromosomes are separated along their longitudinal axis, being a chromatid from each pair inherited by each daughter cell. Failure in achieving this configuration results in an uneven distribution of chromosomes and gives rise to aberrant karyotypes in daughter cells. The abnormal number of chromosomes in a cell is known as aneuploidy and is a hallmark of cancer (Schukken & Foijer, 2018). To reduce the likelihood of chromosome mis-segregation, species evolved regulatory mechanisms that (1) monitor the attachment status of kinetochores (2) and correct erroneous attachments to promote chromosome biorientation.

In prometaphase, the spindle microtubules start interacting with the previously duplicated and condensed chromosomes, through kinetochores. Due to the microtubule dynamic polymerization/depolymerization cycles and the stochastic nature of their "search and capture" probing of the cytoplasm, both correct and incorrect attachments configurations can be established. Incorrect attachments include syntelic attachments – where both sister kinetochores are bound to microtubules connected to the same spindle pole – and merotelic attachments – where one kinetochore is bound to microtubules emanating from both spindle poles. If left unchecked, by the time anaphase takes place, syntelic attachments prevent the segregation of sister chromatids, being them inherited by the same daughter nucleus. On the other hand, merotelic attachments are likely to result in a lagging chromosome, which often ends up in the formation of a micronucleus, a known driver of chromothripsis and genome instability (Cimini et al., 2003; Cimini et al., 2004; Crasta et al., 2012; Fenech

et al., 2011; Thompson & Compton, 2011). It is therefore critical for mitotic fidelity, that these configurations are disrupted and subsequently converted and stabilized as amphitelic before chromosome segregation (Lampson & Grishchuk, 2017; Tanaka, 2010). The outer kinetochore is the main platform for end-on interactions with microtubule plus ends. The core of this structure is the KMN network, constituted by three subcomplexes: KNL1c, MIS12c and NDC80c (Musacchio and Desai, 2017). The NDC80c is elongated and works as the main microtubule receptor at the kinetochore. It interacts with microtubules plus tips via the CH domains, in the N-terminal regions of NDC80 and NUF2, that are preceded by a basic N-terminal unstructured tail (Alushin et al., 2010; Cheeseman et al., 2006; Ciferri et al., 2008).

To achieve stable end-on attachments, kinetochore-microtubule interactions are regulated on both the kinetochore and microtubule ends by multiple kinases and phosphatases (Lampson & Grishchuk, 2017; Moura & Conde, 2019; Sherwin & Wang, 2019). The basic N-terminal tail that precedes the NDC80/NUF2 CH domains is known to be phosphorylated on multiple sites by AAK and ABK decreasing the affinity between the kinetochore and microtubules (Chmátal et al., 2015; DeLuca et al., 2006; DeLuca et al., 2011; DeLuca et al., 2018; Guimaraes et al., 2008; Lampson et al.,2004; Ye et al., 2015). Other studies also described ABK ability to phosphorylate the functional orthologs SKAc, in human, and DAM1c, in yeast, reducing their affinity to bind NDC80c and hindering the stabilization of end-on attachments.

The idea that centrosomal AAK has a considerable contribution to the correction of erroneous kinetochore-microtubule attachments may not be intuitive at first. However, by the nature of syntelic attachments, when these are formed, the chromosome is likely to be positioned in the vicinity of the centrosome it is connected to by microtubule pulling forces. Once close to the centrosome, the kinetochores of the polar chromosome become under the zone of influence of the AAK gradient emanating from the centrosome (Chmátal et al., 2015; Ye et al., 2015). This allows the phosphorylation of NDC80 by AAK, resulting in the disruption of the erroneous kinetochore-microtubule end-on attachments (Chmátal et al., 2015; Ye et al., 2015). Once unattached, the kinetochores become available to interact with other microtubules. However, because of the close proximity between both sister kinetochores and this single centrosome (relative to the opposite spindle pole), new syntelic attachments are prone to form in this situation. To prevent endless cycles of syntelic attachment/detachment near the pole, kinetochores must interact laterally with microtubules through motor proteins like CENP-E (Barisic et al., 2015), that will then assist in the congression by transporting chromosomes along microtubules – in a plus-end directed way – to the spindle equator before new end-on attachments are formed. Notably, centrosomal

AAK was also shown to phosphorylate CENP-E. This phosphorylation dissociates PP1 from CENP-E and promotes its association with stable central spindle microtubules, instead of peripheric/astral microtubules (Kim et al., 2010). Once attached to microtubules, the plus end-directed sliding of CENP-E, transports the associated chromosome towards the cell equator helping in the congression of polar chromosomes (Barisic et al., 2015). This process is very well complemented by the ability that centrosomal AAK has to phosphorylate NDC80 at pole proximal kinetochores to correct erroneous attachments (Chmátal et al., 2015; Ye et al., 2015). AAK disrupts improper end-on attachments while promoting the congression of those polar chromosomes by lateral association between the kinetochore and microtubules through CENP-E. Once at the spindle equator, amphitelic attachments are more likely to form and be stabilised.

Besides the AURORA kinases, MPS1 was also shown to contribute to error correction. Initially, indirectly via the activation of centromeric ABK (Jelluma et al., 2008a; Kwiatkowski et al., 2010; van der Waal et al., 2012) and, more recently, by the direct phosphorylation of the SKAc, in human cells (Maciejowski et al., 2017), and by the direct phosphorylation of NDC80's N-terminal tail, in yeast (Sarangapani et al., 2021). In both cases, these phosphorylations result in the destabilization of kinetochore-microtubule attachments. Additionally, in human cells, a pool of MPS1 was shown to transiently localize to end-on attached kinetochores prior to microtubule destabilization and error correction (Hayward et al., 2022). Importantly, the disruption of kinetochore-microtubule attachments, results in unattached kinetochores that signal the lack of attachments by the accumulation of SAC proteins and assembly of the MCC, preventing mitotic exit until proper attachments are formed. Besides a direct effect on the kinetochore-microtubule attachments stability, MPS1 can also regulate both chromosome congression and biorientation through the motor protein CENP-E. MPS1 was shown to phosphorylate CENP-E, relieving it from its auto-inhibitory conformation and regulate its localization (Espeut et al., 2008; Hewitt et al., 2010).

These observations unravelled multiple mechanisms that evolved to regulate kinetochore-microtubule attachments. Interestingly, these regulatory pathways require not only kinases that localize at the kinetochores and centromeres but also rely on centrosomal AAK. Understanding why do kinases from these two subcellular localizations take part on error correction could further explain important mechanisms underlying the regulation of chromosome bi-orientation. To address this, some questions may be raised: (1) Why did a centrosomal error correction pathway evolve in parallel to the kinetochore/centromere pathways? (2) Is this only a consequence of the fact that AAK and ABK share very similar kinase domains for evolutionary reasons? (3) Are AAK and ABK specialized in different aspects of error correction? (4) What challenges and aspects of error correction are different

between species that only have one AURORA protein and species that express both AAK and ABK? Interestingly, in species like *S. cerevisiae*, cells undergo a closed mitosis, which does not favour the accumulation of chromosomes in the peripheral regions where centrosome-based error correction would be more relevant. *S. cerevisiae* only expresses one AURORA kinase (IPL1) that localizes at centromeres. Moreover, *S. cerevisiae* does not express a CENP-E homolog, further suggesting it does not rely on motor-driven congression of laterally attached kinetochores of polar chromosomes. Understanding whether these facts are intertwined could further explain the importance of evolving a centrosome-based error correction pathway.

The regulation of ABK activity towards the correction of mis-oriented kinetochore-microtubule attachments has been thoroughly investigated and detailed for many years. It would be interesting to further explore which pathways regulate the role of centrosomal AAK in error correction and whether these are distinct mechanisms from the ones that regulate other centrosomal AAK functions. Additionally, understanding whether there is a cross-talk between kinetochore/centromere-based and centrosome-based error correction pathways to coordinate their roles in promoting chromosome congression and bi-orientation could generate new insights in understanding the relevance of the evolution of two spatially compartmentalized pathways.

Our study sheds new light onto this matter by revealing a novel interaction by which kinetochore MPS1 promotes error correction in *Drosophila* cells indirectly by promoting AAK activity. Moreover, this proximity-based activation is conserved in human cells. This works as a crosstalk between kinetochores of polar chromosomes and centrosomes/spindle poles to promote centrosomal AAK-driven error correction.

Our work shows that centrosomal AAK activation levels peak in prophase/prometaphase. This high activation levels require MPS1 recruitment to kinetochores and close proximity between kinetochores and centrosomes. We show this both using a phospho-specific antibody and a centrosome-targeted FRET sensor that is phosphorylated by AAK. Importantly, in prometaphase, syntelic attachments are likely to form, specifically for chromosomes positioned in the periphery of the nucleus and close to a specific spindle pole after NEB (Mogilner & Craig, 2010). It is, therefore, critical that AAK activation is high at this stage in which the number of syntelic attachments that require correction is at its peak. However, our FRET data shows also that a single polar chromosome – in a cell where all other chromosomes are aligned at the metaphase plate – is enough to trigger significant centrosomal AAK activation (Figure 9B). Moreover, by probing for NDC80^{S67Ph} we observed that AAK activity towards its kinetochore substrate is significantly increased by a single polar

chromosome (Figure 21A Control, Late Prometaphase cell). These results show that not only AAK activation levels are increased in prometaphase – when most syntelic attachments are formed – but, also, it suggests that this mechanism grants high responsiveness to centrosomal AAK in the identification of the presence of polar chromosomes and in the correction of the syntelic attachments.

We show that MPS1 directly phosphorylates centrosome AAK on the conserved T360 (T337 in human AAK) located in the αG-helix of the kinase C-lobe. Phosphorylation of the C-lobe, in turn, triggers auto-catalytic phosphorylation of the AAK T-loop to amplify an ~2 µm radius activity gradient (Chmátal et al., 2015; Ye et al., 2015; Ye & Maresca, 2015) to locally promote microtubule detachment via phosphorylation of kinetochore substrates such as the NDC80 complex. According to AlphaFold3 predictions the phosphorylation of T360 causes an outward stretch of the αG-helix that pulls on the T-loop by interacting with D317 in a manner that could render the T-loop more flexible and leave the activating T311 more exposed for phosphorylation. Strikingly, a similar activation mechanism was described recently for the Ser/Thr CASEIN KINASE 1 (Cullati et al., 2022). Crystal structures and molecular dynamics simulations uncovered that a phosphorylation similar to the one we described – on a Threonine positioned in an αG-helix separated from the activation loop of the kinase by around 50aa and similar 3D configuration – resulted in increased plasticity of the substrate binding cleft of the kinase and affected the substrate specificity (Cullati et al., 2022). Whether AAK T337/T360 phosphorylation triggers a similar conformational change of the substrate binding cleft or modifies the plasticity of the activation T-loop that could increase the likelihood of its phosphorylation, remains unclear. Our results indicate that this phosphorylation is required for MPS1-driven activation of AAK. However, further investigation into the structural basis of this novel AAK activation mechanism is warranted.

Importantly, it has been proposed that the establishment of stable end-on attachments prevents recruitment of MPS1 to kinetochores because of mutually exclusive binding to either microtubules or MPS1 by the CH-domains of the NDC80 complex (Dou et al., 2015; Hiruma et al., 2015; Ji et al., 2015). However, recent reports propose that a pool of MPS1 still localizes to microtubule-attached kinetochores either through association with the NDC80 complex or other kinetochore receptors (Hayward et al., 2022; Moura et al., 2017). Three recent studies in budding yeast showed that MPS1 binds to regions in the CH-domains of the NDC80 complex that are on the opposite side of the microtubule binding region (Parnell et al., 2024; Pleuger et al., 2024; Zahm & Harrison, 2024) and, accordingly, purified budding yeast NDC80 complex was shown to simultaneously bind microtubules and MPS1 *in vitro* (Pleuger et al., 2024). It has been suggested that this interaction interface is conserved (Zahm & Harrison, 2024). If so, then this mechanism could explain how a

population of MPS1 remains at microtubule-attached metazoan kinetochores. Regardless of how it is recruited, we hypothesize that the residual MPS1 population on erroneously attached polar kinetochores activates AAK to promote their own correction.

An interesting feature of the crosstalk pathway described here is that it contains an intrinsic positive feedback loop since the destabilization of kinetochore-microtubule interactions by AAK-mediated phosphorylation of NDC80 would recruit more MPS1. Such a spatio-chemical feedback loop would heavily disfavour the production of end-on attached kinetochores in the vicinity of spindle poles. Thus, we speculate that MPS1-driven potentiation of AAK activity following nuclear envelope breakdown is important to minimize the formation of end-on attachments near the centrosomes, where syntelic attachments would otherwise be prone to accumulate due to the high density of nucleated microtubules. Instead, robust activation of AAK favours the formation of lateral attachments and facilitates motor activation of CENP-E (Eibes et al., 2023) to ensure timely chromosome congression toward the cell equator, where amphitelic attachments can form synchronously as a result of interactions between non-centrosomal short microtubules emanating from kinetochores and bundles of antiparallel microtubules (Chakraborty et al., 2019; Renda et al., 2022; Sikirzhytski et al., 2018).

Importantly, our work highlights the importance of AAK activation in error correction and polar chromosome congression, but it also suggests that high AAK activation levels should only be promoted in the presence of polar chromosomes as opposed to a permanent active mitotic state. In our experiments, centrosomal AAK activation levels are low when no MPS1 is recruited to kinetochores and/or when no chromosome is in the vicinity of the specific centrosome under assessment. These results suggest that basal AAK activity is intrinsically low, specially as the cell approaches metaphase, and only needs to be actively potentiated if chromosomes are nearby. One possibility is that permanent high AAK activity is detrimental for the fidelity of mitosis, specially as the cell approaches metaphase. In fact, most AAK roles seem to be specifically important in early mitosis. Importantly, AAK hyperactivation was shown to cause defects in the orientation of the mitotic spindle and chromosome segregation (Naso et al., 2024; Polverino et al., 2021; Polverino et al., 2024). These observations further highlight the relevance of evolving a pathway that locally triggers AAK activation in response to polar chromosomes, to correct the erroneous attachments and that can readily be switched off as soon as chromosome congression is achieved. Additional studies are required to further understand this kinetochore-driven centrosomal AAK regulation, for example by identifying the phosphatase that dephosphorylates AAK C-lobe, once kinetochores move away from the pole. Moreover, it would be important to understand whether the potentiation of centrosomal AAK activity by MPS1 is important for

other AAK roles at the centrosome level. And if so, it would be interesting to explore whether this proximity-based activation of AAK could be an underlying mechanism to coordinate centrosomal AAK activity levels with the mitotic stage itself.

It was recently shown that the level of tension across sister kinetochores influences the effect ABK has on that kinetochore pair (Chen et al, 2021). Resorting to optogenetics, ABK was acutely recruited to kinetochores and their movement was assessed as a readout for ABK effect on the kinetochore-microtubule interface (Chen et al, 2021). Whereas ABK recruitment to kinetochores under tension led to the release of the kinetochore-microtubule interaction, ABK recruitment to tensionless kinetochores resulted in the depolymerization of the microtubules, while maintaining the attachment (Chen et al, 2021). The authors hypothesize that this tension-dependent response may work as a mechanism to discern syntelic (tensionless) attachments from merotelic (under tension) attachments and assist in dealing with them differently. Merotelic attachments, usually allow the chromosome to be positioned at the spindle equator, because the kinetochore pair is still subjected to microtubule pulling forces from opposing spindle poles. Is this case, the release of kinetochore-microtubule attachments is a good strategy to deal with the improper configuration, because amphitelic attachments are likely to be formed on kinetochore pairs located at the spindle equator. However, chromosomes under syntelic attachments usually scatter around spindle poles. In this situation, microtubule release would leave chromosomes to be pushed away from the spindle by polar ejection forces. On the other hand, microtubule depolymerization pulls chromosomes toward the spindle, where they subsequently detach near the pole and congress by gliding along K-fibres of other chromosomes, as a consequence of AAK and CENP-E activities, respectively (Chmátal et al., 2015; Kapoor et al., 2006; Ye et al., 2015). It would be interesting to further dissect this depolymerization pathway, as some questions may be raised considering this result: (1) How is ABK (or its substrates) being regulated/influenced by tension to promote either microtubule detachment or microtubule depolymerization? (2) Is AAK the one disrupting the erroneous attachments once they get in the vicinity of the spindle pole, following ABK-driven microtubule depolymerization? (3) Can ABK disrupt these syntelic attachments near the poles in the absence of centrosomal AAK activity? (4) If so, what changed in ABK or its substrates to allow the switch between depolymerization and detachment? (5) Did this depolymerization mechanism evolve so AAK can assist ABK in correcting syntelic attachments? (6) Is ABK more tailored towards the disruption of merotelic attachments and AAK more suitable to deal with syntelic attachments? The answer to these questions could reveal new insights into whether AAK and ABK roles in error correction are similar and

simply spatially separated by their distinct localizations or whether they have evolved to tackle different challenges in kinetochore-microtubule attachments.

Overall, our findings support the conclusion that a pool of MPS1 at kinetochores indirectly contributes to pole-based error correction. This model is consistent with an earlier proposal that MPS1 plays an indirect role in error correction, with a notable difference being that the relevant downstream target of MPS1 is AAK rather than ABK (Jelluma et al., 2008a; Kwiatkowski et al., 2010; van der Waal et al., 2012). MPS1 clearly activated AAK in our cell-based assays, but consistent with prior findings (Hewitt et al., 2010; Maciejowski et al., 2010; Santaguida et al., 2010), we did not see evidence of MPS1-mediated ABK activation in cells despite the facts that (1) the centromere/kinetochore-localized ABK is closer than centrosomal AAK to kinetochore-bound MPS1, (2) the C-lobe threonine is present in ABK αG-helix, and (3) ABK is phosphorylated and activated by MPS1 *in vitro* (data not shown). Since constitutive ABK activation would be detrimental to forming stable attachments, kinetochore/centromere-associated protein phosphatases likely protect ABK from MPS1-mediated activation in cells. It would be interesting to understand whether these are the same phosphatases – in this case, associated with the centrosome – that dephosphorylate AAK C-lobe, once chromosome congression is achieved. Direct and indirect roles for MPS1 in error correction need not be mutually exclusive. In fact, it now appears that diverse organisms rely on each mechanism to different extents in carrying out error correction. Budding yeast utilize MPS1 to directly target the NDC80 complex without indirectly inducing error correction through activation of AURORA kinase (Sarangapani et al., 2021). Conversely, our work shows that activation of AAK-mediated error correction by kinetochore-recruited MPS1 is the dominant pathway in flies, although a direct role for MPS1 in error correction cannot be ruled out. Since we observed proximity-based activation of AAK by MPS1 in RPE-1 cells, efficient error correction in humans likely requires both indirect and direct pathways via MPS1-mediated phosphorylation of AAK and kinetochore-microtubule attachment factors, respectively. Future efforts to dissect the relative contributions of direct versus indirect roles of MPS1 in error correction are warranted, but the findings presented here define a novel and conserved mechanism by which polar kinetochores modulate centrosome-based activities to promote accurate chromosome segregation.

REFERENCES

Abramson, J., Adler, J., Dunger, J., Evans, R., Green, T., Pritzel, A., Ronneberger, O., Willmore, L., Ballard, A.J., Bambrick, J., et al. (2024). Accurate structure prediction of biomolecular interactions with AlphaFold 3. *Nature* 630, 493–500. https://doi.org/10.1038/s41586-024-07487-w.

Akiyoshi, B., Nelson, C. R., Ranish, J. A., & Biggins, S. (2009). Quantitative proteomic analysis of purified yeast kinetochores identifies a PP1 regulatory subunit. *Genes & development*, *23*(24), 2887–2899. https://doi.org/10.1101/gad.1865909

Akiyoshi, B., Sarangapani, K. K., Powers, A. F., Nelson, C. R., Reichow, S. L., Arellano-Santoyo, H., Gonen, T., Ranish, J. A., Asbury, C. L., & Biggins, S. (2010). Tension directly stabilizes reconstituted kinetochore-microtubule attachments. *Nature*, *468*(7323), 576–579. https://doi.org/10.1038/nature09594

Alushin, G. M., Ramey, V. H., Pasqualato, S., Ball, D. A., Grigorieff, N., Musacchio, A., & Nogales, E. (2010). The Ndc80 kinetochore complex forms oligomeric arrays along microtubules. *Nature*, *467*(7317), 805–810.

Alushin, G. M., Musinipally, V., Matson, D., Tooley, J., Stukenberg, P. T., & Nogales, E. (2012). Multimodal microtubule binding by the Ndc80 kinetochore complex. *Nature structural & molecular biology*, *19*(11), 1161–1167. https://doi.org/10.1038/nsmb.2411

Amin, M. A., Agarwal, S., & Varma, D. (2019). Mapping the kinetochore MAP functions required for stabilizing microtubule attachments to chromosomes during metaphase. *Cytoskeleton (Hoboken, N.J.)*, *76*(6), 398–412. https://doi.org/10.1002/cm.21559

Andrews, P. D., Ovechkina, Y., Morrice, N., Wagenbach, M., Duncan, K., Wordeman, L., & Swedlow, J. R. (2004). Aurora B regulates MCAK at the mitotic centromere. *Developmental cell*, *6*(2), 253–268. https://doi.org/10.1016/s1534-5807(04)00025-5

Arlot-Bonnemains, Y., Klotzbucher, A., Giet, R., Uzbekov, R., Bihan, R., & Prigent, C. (2001). Identification of a functional destruction box in the Xenopus laevis aurora-A kinase pEg2. *FEBS letters*, *508*(1), 149–152. https://doi.org/10.1016/s0014-5793(01)03048-4

Asteriti, I. A., De Mattia, F., & Guarguaglini, G. (2015). Cross-Talk between AURKA and Plk1 in Mitotic Entry and Spindle Assembly. *Frontiers in oncology*, *5*, 283. https://doi.org/10.3389/fonc.2015.00283

Bakhoum, S. F., Thompson, S. L., Manning, A. L., & Compton, D. A. (2009a). Genome stability is ensured by temporal control of kinetochore-microtubule dynamics. *Nature cell biology*, *11*(1), 27–35. https://doi.org/10.1038/ncb1809

Bakhoum, S. F., Genovese, G., & Compton, D. A. (2009b). Deviant kinetochore microtubule dynamics underlie chromosomal instability. *Current biology: CB*, *19*(22), 1937–1942. https://doi.org/10.1016/j.cub.2009.09.055

Barisic, M., Aguiar, P., Geley, S., and Maiato, H. (2014). Kinetochore motors drive congression of peripheral polar chromosomes by overcoming random arm-ejection forces. *Nat. Cell Biol.* 16, 1249–1256. https://doi.org/10.1038/ncb3060.

Barisic, M., Silva e Sousa, R., Tripathy, S. K., Magiera, M. M., Zaytsev, A. V., Pereira, A. L., Janke, C., Grishchuk, E. L., & Maiato, H. (2015). Mitosis. Microtubule detyrosination

guides chromosomes during mitosis. *Science (New York, N.Y.)*, *348*(6236), 799–803. https://doi.org/10.1126/science.aaa5175

Baron, A. P., von Schubert, C., Cubizolles, F., Siemeister, G., Hitchcock, M., Mengel, A., Schröder, J., Fernández-Montalván, A., von Nussbaum, F., Mumberg, D., & Nigg, E. A. (2016). Probing the catalytic functions of Bub1 kinase using the small molecule inhibitors BAY-320 and BAY-524. *eLife*, *5*, e12187. https://doi.org/10.7554/eLife.12187

Barr, A. R., & Gergely, F. (2007). Aurora-A: the maker and breaker of spindle poles. *Journal of cell science*, *120*(Pt 17), 2987–2996. https://doi.org/10.1242/jcs.013136

Barros, T.P., Kinoshita, K., Hyman, A.A., and Raff, J.W. (2005). Aurora A activates D-TACC-Msps complexes exclusively at centrosomes to stabilize centrosomal microtubules. *J. Cell Biol.* 170, 1039–1046. https://doi.org/10.1083/jcb.200504097.

Bayliss, R., Burgess, S. G., & McIntyre, P. J. (2017). Switching Aurora-A kinase on and off at an allosteric site. *The FEBS journal*, *284*(18), 2947–2954. https://doi.org/10.1111/febs.14069

Bekier, M. E., Mazur, T., Rashid, M. S., & Taylor, W. R. (2015). Borealin dimerization mediates optimal CPC checkpoint function by enhancing localization to centromeres and kinetochores. *Nature communications*, *6*, 6775. https://doi.org/10.1038/ncomms7775

Bell, G. P., Fletcher, G. C., Brain, R., & Thompson, B. J. (2015). Aurora kinases phosphorylate Lgl to induce mitotic spindle orientation in Drosophila epithelia. *Current biology : CB*, *25*(1), 61–68. https://doi.org/10.1016/j.cub.2014.10.052

Berdnik, D., & Knoblich, J.A. (2002). Drosophila Aurora-A is required for centrosome maturation and actin-dependent asymmetric protein localization during mitosis. *Curr. Biol.* 12, 640–647. https://doi.org/10.1016/s0960-9822(02)00766-2

Bernard, M., Sanseau, P., Henry, C., Couturier, A., & Prigent, C. (1998). Cloning of STK13, a third human protein kinase related to Drosophila aurora and budding yeast Ipl1 that maps on chromosome 19q13.3-ter. *Genomics*, *53*(3), 406–409. https://doi.org/10.1006/geno.1998.5522

Biggins, S., Severin, F.F., Bhalla, N., Sassoon, I., Hyman, A.A., and Murray, A.W. (1999). The conserved protein kinase Ipl1 regulates microtubule binding to kinetochores in budding yeast. *Genes Dev.* 13, 532–544. https://doi.org/10.1101/gad.13.5.532.

Bishop, J. D., & Schumacher, J. M. (2002). Phosphorylation of the carboxyl terminus of inner centromere protein (INCENP) by the Aurora B Kinase stimulates Aurora B kinase activity. *The Journal of biological chemistry*, *277*(31), 27577–27580. https://doi.org/10.1074/jbc.C200307200

Blethrow, J. D., Glavy, J. S., Morgan, D. O., & Shokat, K. M. (2008). Covalent capture of kinase-specific phosphopeptides reveals Cdk1-cyclin B substrates. *Proceedings of the National Academy of Sciences of the United States of America*, *105*(5), 1442–1447. https://doi.org/10.1073/pnas.0708966105

Bolanos-Garcia, V. M. (2005). Aurora kinases. *The international journal of biochemistry & cell biology*, *37*(8), 1572-1577.

Bolanos-Garcia V. M. (2025). Mps1 kinase functions in mitotic spindle assembly and error correction. *Trends in biochemical sciences*, *50*(5), 438–453. https://doi.org/10.1016/j.tibs.2025.02.005

Boveri T. (2008). Concerning the origin of malignant tumours by Theodor Boveri. Translated and annotated by Henry Harris. *Journal of cell science*, 121 Suppl 1, 1–84. https://doi.org/10.1242/jcs.025742

Broad, A. J., DeLuca, K. F., & DeLuca, J. G. (2020). Aurora B kinase is recruited to multiple discrete kinetochore and centromere regions in human cells. *The Journal of cell biology*, *219*(3), e201905144. https://doi.org/10.1083/jcb.201905144

Brown, J. R., Koretke, K. K., Birkeland, M. L., Sanseau, P., & Patrick, D. R. (2004). Evolutionary relationships of Aurora kinases: implications for model organism studies and the development of anti-cancer drugs. *BMC evolutionary biology*, *4*, 39. https://doi.org/10.1186/1471-2148-4-39

Caldas, G. V., DeLuca, K. F., & DeLuca, J. G. (2013). KNL1 facilitates phosphorylation of outer kinetochore proteins by promoting Aurora B kinase activity. *The Journal of cell biology*, *203*(6), 957–969. https://doi.org/10.1083/jcb.201306054

Carmena, M., & Earnshaw, W. C. (2003). The cellular geography of aurora kinases. *Nature reviews. Molecular cell biology*, *4*(11), 842–854. https://doi.org/10.1038/nrm1245

Carmena, M., Wheelock, M., Funabiki, H., & Earnshaw, W. C. (2012). The chromosomal passenger complex (CPC): from easy rider to the godfather of mitosis. *Nature reviews. Molecular cell biology*, *13*(12), 789–803. https://doi.org/10.1038/nrm3474

Carvalho, C. A., Moreira, S., Ventura, G., Sunkel, C. E., & Morais-de-Sá, E. (2015). Aurora A triggers Lgl cortical release during symmetric division to control planar spindle orientation. *Current biology : CB*, *25*(1), 53–60. https://doi.org/10.1016/j.cub.2014.10.053

Castro, A., Vigneron, S., Bernis, C., Labbé, J. C., Prigent, C., & Lorca, T. (2002). The D-Box-activating domain (DAD) is a new proteolysis signal that stimulates the silent D-Box sequence of Aurora-A. *EMBO reports*, *3*(12), 1209–1214. https://doi.org/10.1093/embo-reports/kvf241

Chakraborty, M., Tarasovetc, E.V., Zaytsev, A.V., Godzi, M., Figueiredo, A.C., Ataullakhanov, F.I., and Grishchuk, E.L. (2019). Microtubule end conversion mediated by motors and diffusing proteins with no intrinsic microtubule end-binding activity. *Nat. Commun.* 10, 1673. https://doi.org/10.1038/s41467-019-09411-7.

Chan, C. S., & Botstein, D. (1993). Isolation and characterization of chromosome-gain and increase-in-ploidy mutants in yeast. *Genetics*, *135*(3), 677–691. https://doi.org/10.1093/genetics/135.3.677

Chan, Y. W., Jeyaprakash, A. A., Nigg, E. A., & Santamaria, A. (2012). Aurora B controls kinetochore-microtubule attachments by inhibiting Ska complex-KMN network interaction. *The Journal of cell biology*, *196*(5), 563–571. https://doi.org/10.1083/jcb.201109001

Cheeseman, I. M., Anderson, S., Jwa, M., Green, E. M., Kang, J.s, Yates, J. R., 3rd, Chan, C. S., Drubin, D. G., & Barnes, G. (2002). Phospho-regulation of kinetochore-microtubule

attachments by the Aurora kinase Ipl1p. *Cell*, *111*(2), 163–172. https://doi.org/10.1016/s0092-8674(02)00973-x

Cheeseman, I.M., Chappie, J.S., Wilson-Kubalek, E.M., and Desai, A. (2006). The conserved KMN network constitutes the core microtubule-binding site of the kinetochore. *Cell* 127, 983–997. https://doi.org/10.1016/j.cell.2006.09.039.

Cheetham, G. M., Knegtel, R. M., Coll, J. T., Renwick, S. B., Swenson, L., Weber, P., Lippke, J. A., & Austen, D. A. (2002). Crystal structure of aurora-2, an oncogenic serine/threonine kinase. *The Journal of biological chemistry*, *277*(45), 42419–42422. https://doi.org/10.1074/jbc.C200426200

Chen, G. Y., Renda, F., Zhang, H., Gokden, A., Wu, D. Z., Chenoweth, D. M., Khodjakov, A., & Lampson, M. A. (2021). Tension promotes kinetochore-microtubule release by Aurora B kinase. *The Journal of cell biology*, *220*(6), e202007030. https://doi.org/10.1083/jcb.202007030

Chmátal, L., Yang, K., Schultz, R.M., and Lampson, M.A. (2015). Spatial regulation of kinetochore microtubule attachments by destabilization at spindle poles in meiosis I. *Curr. Biol.* 25, 1835–1841. https://doi.org/10.1016/j.cub.2015.05.013.

Ciferri, C., Pasqualato, S., Screpanti, E., Varetti, G., Santaguida, S., Dos Reis, G., Maiolica, A., Polka, J., De Luca, J.G., De Wulf, P., et al. (2008). Implications for kinetochore-microtubule attachment from the structure of an engineered Ndc80 complex. *Cell* 133, 427–439. https://doi.org/10.1016/j.cell.2008.03.020.

Cimini, D., Moree, B., Canman, J. C., & Salmon, E. D. (2003). Merotelic kinetochore orientation occurs frequently during early mitosis in mammalian tissue cells and error correction is achieved by two different mechanisms. *Journal of cell science*, *116*(Pt 20), 4213–4225. https://doi.org/10.1242/jcs.00716

Cimini, D., Cameron, L. A., & Salmon, E. D. (2004). Anaphase spindle mechanics prevent mis-segregation of merotelically oriented chromosomes. *Current biology: CB*, *14*(23), 2149–2155. https://doi.org/10.1016/j.cub.2004.11.029

Cimini, D., Wan, X., Hirel, C.B., and Salmon, E.D. (2006). Aurora kinase promotes turnover of kinetochore microtubules to reduce chromosome segregation errors. *Curr. Biol.* 16, 1711–1718. https://doi.org/10.1016/j.cub.2006.07.022.

Conde, C., Osswald, M., Barbosa, J., Moutinho-Santos, T., Pinheiro, D., Guimarães, S., Matos, I., Maiato, H., and Sunkel, C.E. (2013). Drosophila Polo regulates the spindle assembly checkpoint through Mps1-dependent BubR1 phosphorylation. *EMBO J.* 32, 1761–1777. https://doi.org/10.1038/emboj.2013.109.

Cox, J., and Mann, M. (2008). MaxQuant enables high peptide identification rates, individualized p.p.b.-range mass accuracies and proteome-wide protein quantification. *Nat. Biotechnol.* 26, 1367–1372. https://doi.org/10.1038/nbt.1511.

Crasta, K., Ganem, N. J., Dagher, R., Lantermann, A. B., Ivanova, E. V., Pan, Y., Nezi, L., Protopopov, A., Chowdhury, D., & Pellman, D. (2012). DNA breaks and chromosome pulverization from errors in mitosis. *Nature*, *482*(7383), 53–58. https://doi.org/10.1038/nature10802

Crosio, C., Fimia, G. M., Loury, R., Kimura, M., Okano, Y., Zhou, H., Sen, S., Allis, C. D., & Sassone-Corsi, P. (2002). Mitotic phosphorylation of histone H3: spatio-temporal regulation by mammalian Aurora kinases. *Molecular and cellular biology*, *22*(3), 874–885. https://doi.org/10.1128/MCB.22.3.874-885.2002

Cullati, S. N., Chaikuad, A., Chen, J. S., Gebel, J., Tesmer, L., Zhubi, R., Navarrete-Perea, J., Guillen, R. X., Gygi, S. P., Hummer, G., Dötsch, V., Knapp, S., & Gould, K. L. (2022). Kinase domain autophosphorylation rewires the activity and substrate specificity of CK1 enzymes. *Molecular cell*, *82*(11), 2006–2020.e8.

Cyphers, S., Ruff, E. F., Behr, J. M., Chodera, J. D., & Levinson, N. M. (2017). A water-mediated allosteric network governs activation of Aurora kinase A. *Nature chemical biology*, *13*(4), 402–408. https://doi.org/10.1038/nchembio.2296

De Antoni, A., Maffini, S., Knapp, S., Musacchio, A., & Santaguida, S. (2012). A small-molecule inhibitor of Haspin alters the kinetochore functions of Aurora B. *The Journal of cell biology*, *199*(2), 269–284. https://doi.org/10.1083/jcb.201205119

DeLuca, J.G., Gall, W.E., Ciferri, C., Cimini, D., Musacchio, A., and Salmon, E.D. (2006). Kinetochore microtubule dynamics and attachment stability are regulated by Hec1. *Cell* 127, 969–982. https://doi.org/10.1016/j.cell.2006.09.047.

DeLuca, K. F., Lens, S. M., & DeLuca, J. G. (2011). Temporal changes in Hec1 phosphorylation control kinetochore-microtubule attachment stability during mitosis. *Journal of cell science*, *124*(Pt 4), 622–634. https://doi.org/10.1242/jcs.072629

DeLuca, K.F., Meppelink, A., Broad, A.J., Mick, J.E., Peersen, O.B., Pektas, S., Lens, S.M.A., and DeLuca, J.G. (2018). Aurora A kinase phosphorylates Hec1 to regulate metaphase kinetochore-microtubule dynamics. *J. Cell Biol.* 217, 163–177. https://doi.org/10.1083/jcb.201707160.

Dephoure, N., Zhou, C., Villén, J., Beausoleil, S. A., Bakalarski, C. E., Elledge, S. J., & Gygi, S. P. (2008). A quantitative atlas of mitotic phosphorylation. *Proceedings of the National Academy of Sciences of the United States of America*, *105*(31), 10762–10767. https://doi.org/10.1073/pnas.0805139105

di Pietro, F., Echard, A., & Morin, X. (2016). Regulation of mitotic spindle orientation: an integrated view. *EMBO reports*, *17*(8), 1106–1130. https://doi.org/10.15252/embr.201642292

Ditchfield, C., Johnson, V. L., Tighe, A., Ellston, R., Haworth, C., Johnson, T., Mortlock, A., Keen, N., & Taylor, S. S. (2003). Aurora B couples chromosome alignment with anaphase by targeting BubR1, Mad2, and Cenp-E to kinetochores. *The Journal of cell biology*, *161*(2), 267–280. https://doi.org/10.1083/jcb.200208091

Dodson, C. A., Kosmopoulou, M., Richards, M. W., Atrash, B., Bavetsias, V., Blagg, J., & Bayliss, R. (2010). Crystal structure of an Aurora-A mutant that mimics Aurora-B bound to MLN8054: insights into selectivity and drug design. *The Biochemical journal*, *427*(1), 19–28. https://doi.org/10.1042/BJ20091530

Dou, Z., von Schubert, C., Körner, R., Santamaria, A., Elowe, S., & Nigg, E. A. (2011). Quantitative mass spectrometry analysis reveals similar substrate consensus motif for

human Mps1 kinase and Plk1. *PloS one*, *6*(4), e18793. https://doi.org/10.1371/journal.pone.0018793

Dou, Z., Liu, X., Wang, W., Zhu, T., Wang, X., Xu, L., Abrieu, A., Fu, C., Hill, D.L., and Yao, X. (2015). Dynamic localization of Mps1 kinase to kinetochores is essential for accurate spindle microtubule attachment. *Proc. Natl. Acad. Sci. USA* 112, E4546–E4555. https://doi.org/10.1073/pnas.1508791112.

Eibes, S., Rajendraprasad, G., Guasch-Boldu, C., Kubat, M., Steblyanko, Y., and Barisic, M. (2023). CENP-E activation by Aurora A and B controls kinetochore fibrous corona disassembly. *Nat. Commun.* 14, 5317. https://doi.org/10.1038/s41467-023-41091-2.

Espeut, J., Gaussen, A., Bieling, P., Morin, V., Prieto, S., Fesquet, D., Surrey, T., & Abrieu, A. (2008). Phosphorylation relieves autoinhibition of the kinetochore motor Cenp-E. *Molecular cell*, *29*(5), 637–643. https://doi.org/10.1016/j.molcel.2008.01.004

Fenech, M., Kirsch-Volders, M., Natarajan, A. T., Surralles, J., Crott, J. W., Parry, J., Norppa, H., Eastmond, D. A., Tucker, J. D., & Thomas, P. (2011). Molecular mechanisms of micronucleus, nucleoplasmic bridge and nuclear bud formation in mammalian and human cells. *Mutagenesis*, *26*(1), 125–132. https://doi.org/10.1093/mutage/geq052

Feng, Z., Caballe, A., Wainman, A., Johnson, S., Haensele, A.F.M., Cottee, M.A., Conduit, P.T., Lea, S.M., and Raff, J.W. (2017). Structural basis for mitotic centrosome assembly in flies. *Cell* 169, 1078–1089.e13. https://doi.org/10.1016/j.cell.2017.05.030.

Fisher R. P. (2012). The CDK Network: Linking Cycles of Cell Division and Gene Expression. *Genes & cancer*, *3*(11-12), 731–738. https://doi.org/10.1177/1947601912473308

Flemming W. (1965). CONTRIBUTIONS TO THE KNOWLEDGE OF THE CELL AND ITS VITAL PROCESSES. *The Journal of cell biology*, *25*(1), 3–69.

Foley, E. A., & Kapoor, T. M. (2013). Microtubule attachment and spindle assembly checkpoint signalling at the kinetochore. *Nature reviews. Molecular cell biology*, *14*(1), 25–37. https://doi.org/10.1038/nrm3494

Fuller, B.G., Lampson, M.A., Foley, E.A., Rosasco-Nitcher, S., Le, K.V., Tobelmann, P., Brautigan, D.L., Stukenberg, P.T., and Kapoor, T.M. (2008). Midzone activation of aurora B in anaphase produces an intracellular phosphorylation gradient. *Nature* 453, 1132–1136. https://doi.org/10.1038/nature06923.

Gallini, S., Carminati, M., De Mattia, F., Pirovano, L., Martini, E., Oldani, A., Asteriti, I. A., Guarguaglini, G., & Mapelli, M. (2016). NuMA Phosphorylation by Aurora-A Orchestrates Spindle Orientation. *Current biology : CB*, *26*(4), 458–469. https://doi.org/10.1016/j.cub.2015.12.051

Gestaut, D. R., Graczyk, B., Cooper, J., Widlund, P. O., Zelter, A., Wordeman, L., Asbury, C. L., & Davis, T. N. (2008). Phosphoregulation and depolymerization-driven movement of the Dam1 complex do not require ring formation. *Nature cell biology*, *10*(4), 407–414. https://doi.org/10.1038/ncb1702

Gibson, D.G., Young, L., Chuang, R.Y., Venter, J.C., Hutchison, C.A., 3rd, and Smith, H.O. (2009). Enzymatic assembly of DNA molecules up to several hundred kilobases. *Nat. Methods* 6, 343–345. https://doi.org/10.1038/nmeth.1318.

Giet, R., & Prigent, C. (1999). Aurora/Ipl1p-related kinases, a new oncogenic family of mitotic serine-threonine kinases. *Journal of cell science*, *112 (Pt 21)*, 3591–3601. https://doi.org/10.1242/jcs.112.21.3591

Giet, R., & Glover, D. M. (2001). Drosophila aurora B kinase is required for histone H3 phosphorylation and condensin recruitment during chromosome condensation and to organize the central spindle during cytokinesis. *The Journal of cell biology*, *152*(4), 669–682. https://doi.org/10.1083/jcb.152.4.669

Giet, R., McLean, D., Descamps, S., Lee, M.J., Raff, J.W., Prigent, C., and Glover, D.M. (2002). Drosophila Aurora A kinase is required to localize D-TACC to centrosomes and to regulate astral microtubules. *J. Cell Biol.* 156, 437–451. https://doi.org/10.1083/jcb.200108135

Gilliland, W.D., Hughes, S.E., Cotitta, J.L., Takeo, S., Xiang, Y., and Hawley, R.S. (2007). The multiple roles of mps1 in Drosophila female meiosis. *PLoS Genet.* 3, e113. https://doi.org/10.1371/journal.pgen.0030113.

Glover, D. M., Leibowitz, M. H., McLean, D. A., & Parry, H. (1995). Mutations in aurora prevent centrosome separation leading to the formation of monopolar spindles. *Cell*, *81*(1), 95–105. https://doi.org/10.1016/0092-8674(95)90374-7

Godek, K. M., Kabeche, L., & Compton, D. A. (2015). Regulation of kinetochore-microtubule attachments through homeostatic control during mitosis. *Nature reviews. Molecular cell biology*, *16*(1), 57–64. https://doi.org/10.1038/nrm3916

Gomez-Ferreria, M. A., Rath, U., Buster, D. W., Chanda, S. K., Caldwell, J. S., Rines, D. R., & Sharp, D. J. (2007). Human Cep192 is required for mitotic centrosome and spindle assembly. *Current biology: CB*, *17*(22), 1960–1966. https://doi.org/10.1016/j.cub.2007.10.019

Gregan, J., Polakova, S., Zhang, L., Tolić-Nørrelykke, I. M., & Cimini, D. (2011). Merotelic kinetochore attachment: causes and effects. *Trends in cell biology*, *21*(6), 374–381. https://doi.org/10.1016/j.tcb.2011.01.003

Grishchuk, E. L., Efremov, A. K., Volkov, V. A., Spiridonov, I. S., Gudimchuk, N., Westermann, S., Drubin, D., Barnes, G., McIntosh, J. R., & Ataullakhanov, F. I. (2008). The Dam1 ring binds microtubules strongly enough to be a processive as well as energy-efficient coupler for chromosome motion. *Proceedings of the National Academy of Sciences of the United States of America*, *105*(40), 15423–15428. https://doi.org/10.1073/pnas.0807859105

Guimaraes, G. J., Dong, Y., McEwen, B. F., & Deluca, J. G. (2008). Kinetochore-microtubule attachment relies on the disordered N-terminal tail domain of Hec1. *Current biology : CB*, *18*(22), 1778–1784. https://doi.org/10.1016/j.cub.2008.08.012

Hannak, E., Kirkham, M., Hyman, A.A., and Oegema, K. (2001). Aurora-A kinase is required for centrosome maturation in Caenorhabditis elegans. *J. Cell Biol.* 155, 1109–1116. https://doi.org/10.1083/jcb.200108051.

Haren, L., Stearns, T., & Lüders, J. (2009). Plk1-dependent recruitment of gamma-tubulin complexes to mitotic centrosomes involves multiple PCM components. *PloS one*, *4*(6), e5976. https://doi.org/10.1371/journal.pone.0005976

Hauf, S., Cole, R. W., LaTerra, S., Zimmer, C., Schnapp, G., Walter, R., Heckel, A., van Meel, J., Rieder, C. L., & Peters, J. M. (2003). The small molecule Hesperadin reveals a role for Aurora B in correcting kinetochore-microtubule attachment and in maintaining the spindle assembly checkpoint. *The Journal of cell biology*, *161*(2), 281–294. https://doi.org/10.1083/jcb.200208092

Hayden, J. H., Bowser, S. S., & Rieder, C. L. (1990). Kinetochores capture astral microtubules during chromosome attachment to the mitotic spindle: direct visualization in live newt lung cells. *The Journal of cell biology*, *111*(3), 1039–1045. https://doi.org/10.1083/jcb.111.3.1039

Hayward, D., Bancroft, J., Mangat, D., Alfonso-Pérez, T., Dugdale, S., McCarthy, J., Barr, F. A., & Gruneberg, U. (2019). Checkpoint signaling and error correction require regulation of the MPS1 T-loop by PP2A-B56. *The Journal of cell biology*, *218*(10), 3188–3199. https://doi.org/10.1083/jcb.201905026

Hayward, D., Roberts, E., and Gruneberg, U. (2022). MPS1 localizes to end-on microtubule-attached kinetochores to promote microtubule release. *Curr. Biol.* 32, 5200–5208.e8. https://doi.org/10.1016/j.cub.2022.10.047.

He, X., Jones, M. H., Winey, M., & Sazer, S. (1998). Mph1, a member of the Mps1-like family of dual specificity protein kinases, is required for the spindle checkpoint in S. pombe. *Journal of cell science*, *111 (Pt 12)*, 1635–1647. https://doi.org/10.1242/jcs.111.12.1635

Heeger, S., Leismann, O., Schittenhelm, R., Schraidt, O., Heidmann, S., and Lehner, C.F. (2005). Genetic interactions of separase regulatory subunits reveal the diverged Drosophila Cenp-C homolog. *Genes Dev.* 19, 2041–2053. https://doi.org/10.1101/gad.347805.

Helgeson, L. A., Zelter, A., Riffle, M., MacCoss, M. J., Asbury, C. L., & Davis, T. N. (2018). Human Ska complex and Ndc80 complex interact to form a load-bearing assembly that strengthens kinetochore-microtubule attachments. *Proceedings of the National Academy of Sciences of the United States of America*, *115*(11), 2740–2745. https://doi.org/10.1073/pnas.1718553115

Hewitt, L., Tighe, A., Santaguida, S., White, A.M., Jones, C.D., Musacchio, A., Green, S., and Taylor, S.S. (2010). Sustained Mps1 activity is required in mitosis to recruit O-Mad2 to the Mad1-C-Mad2 core complex. *J. Cell Biol.* 190, 25–34. https://doi.org/10.1083/jcb.201002133.

Hill T. L. (1985). Theoretical problems related to the attachment of microtubules to kinetochores. *Proceedings of the National Academy of Sciences of the United States of America*, *82*(13), 4404–4408. https://doi.org/10.1073/pnas.82.13.4404

Hiruma, Y., Sacristan, C., Pachis, S.T., Adamopoulos, A., Kuijt, T., Ubbink, M., von Castelmur, E., Perrakis, A., and Kops, G.J.P.L. (2015). CELL DIVISION CYCLE. Competition between MPS1 and microtubules at kinetochores regulates spindle checkpoint signaling. *Science* 348, 1264–1267. https://doi.org/10.1126/science.aaa4055.

Hochegger, H., Hégarat, N., & Pereira-Leal, J. B. (2013). Aurora at the pole and equator: overlapping functions of Aurora kinases in the mitotic spindle. *Open biology*, *3*(3), 120185. https://doi.org/10.1098/rsob.120185

Holy, T. E., & Leibler, S. (1994). Dynamic instability of microtubules as an efficient way to search in space. *Proceedings of the National Academy of Sciences of the United States of America*, *91*(12), 5682–5685. https://doi.org/10.1073/pnas.91.12.5682

Honda, R., Körner, R., & Nigg, E. A. (2003). Exploring the functional interactions between Aurora B, INCENP, and survivin in mitosis. *Molecular biology of the cell*, *14*(8), 3325–3341. https://doi.org/10.1091/mbc.e02-11-0769

Hsu, K. S., & Toda, T. (2011). Ndc80 internal loop interacts with Dis1/TOG to ensure proper kinetochore-spindle attachment in fission yeast. *Current biology : CB*, *21*(3), 214–220. https://doi.org/10.1016/j.cub.2010.12.048

Huang, J.Y., and Raff, J.W. (2002). The dynamic localisation of the Drosophila APC/C: evidence for the existence of multiple complexes that perform distinct functions and are differentially localised. *J. Cell Sci.* 115, 2847–2856. https://doi.org/10.1242/jcs.115.14.2847.

Hutterer, A., Berdnik, D., Wirtz-Peitz, F., Zigman, M., Schleiffer, A., & Knoblich, J. A. (2006). Mitotic activation of the kinase Aurora-A requires its binding partner Bora. *Developmental cell*, *11*(2), 147–157. https://doi.org/10.1016/j.devcel.2006.06.002

Hyman, A. A., & Mitchison, T. J. (1991). Regulation of the direction of chromosome movement. *Cold Spring Harbor symposia on quantitative biology*, *56*, 745–750. https://doi.org/10.1101/sqb.1991.056.01.083

Jelluma, N., Brenkman, A.B., van den Broek, N.J.F., Cruijsen, C.W.A., van Osch, M.H.J., Lens, S.M.A., Medema, R.H., and Kops, G.J.P.L. (2008a). Mps1 phosphorylates Borealin to control Aurora B activity and chromosome alignment. *Cell* 132, 233–246. https://doi.org/10.1016/j.cell.2007.11.046.

Jelluma, N., Brenkman, A.B., McLeod, I., Yates, J.R., 3rd, Cleveland, D.W., Medema, R.H., and Kops, G.J.P.L. (2008b). Chromosomal instability by inefficient Mps1 auto-activation due to a weakened mitotic checkpoint and lagging chromosomes. *PLoS One* 3, e2415. https://doi.org/10.1371/journal.pone.0002415.

Ji, Z., Gao, H., and Yu, H. (2015). CELL DIVISION CYCLE. Kinetochore attachment sensed by competitive Mps1 and microtubule binding to Ndc80C. *Science* 348, 1260–1264. https://doi.org/10.1126/science. aaa4029.

Johnston, C. A., Hirono, K., Prehoda, K. E., & Doe, C. Q. (2009). Identification of an Aurora-A/PinsLINKER/Dlg spindle orientation pathway using induced cell polarity in S2 cells. *Cell*, *138*(6), 1150–1163. https://doi.org/10.1016/j.cell.2009.07.041

Joukov, V., De Nicolo, A., Rodriguez, A., Walter, J. C., & Livingston, D. M. (2010). Centrosomal protein of 192 kDa (Cep192) promotes centrosome-driven spindle assembly by engaging in organelle-specific Aurora A activation. *Proceedings of the National Academy of Sciences of the United States of America*, *107*(49), 21022–21027. https://doi.org/10.1073/pnas.1014664107

Joukov, V., Walter, J. C., & De Nicolo, A. (2014). The Cep192-organized aurora A-Plk1 cascade is essential for centrosome cycle and bipolar spindle assembly. *Molecular cell*, *55*(4), 578–591. https://doi.org/10.1016/j.molcel.2014.06.016

Joukov, V., & De Nicolo, A. (2018). Aurora-PLK1 cascades as key signaling modules in the regulation of mitosis. *Science signaling*, *11*(543), eaar4195. https://doi.org/10.1126/scisignal.aar4195

Kabeche, L., & Compton, D. A. (2012). Checkpoint-independent stabilization of kinetochore-microtubule attachments by Mad2 in human cells. *Current biology: CB*, *22*(7), 638–644. https://doi.org/10.1016/j.cub.2012.02.030

Kabeche, L., & Compton, D. A. (2013). Cyclin A regulates kinetochore microtubules to promote faithful chromosome segregation. *Nature*, *502*(7469), 110–113. https://doi.org/10.1038/nature12507

Kalantzaki, M., Kitamura, E., Zhang, T., Mino, A., Novák, B., & Tanaka, T. U. (2015). Kinetochore-microtubule error correction is driven by differentially regulated interaction modes. *Nature cell biology*, *17*(4), 530. https://doi.org/10.1038/ncb3153

Kang, J., Chen, Y., Zhao, Y., & Yu, H. (2007). Autophosphorylation-dependent activation of human Mps1 is required for the spindle checkpoint. *Proceedings of the National Academy of Sciences of the United States of America*, *104*(51), 20232–20237. https://doi.org/10.1073/pnas.0710519105

Kapoor, T.M., Mayer, T.U., Coughlin, M.L., and Mitchison, T.J. (2000). Probing spindle assembly mechanisms with monastrol, a small molecule inhibitor of the mitotic kinesin, Eg5. *J. Cell Biol.* 150, 975–988. https:// doi.org/10.1083/jcb.150.5.975.

Kapoor, T. M., Lampson, M. A., Hergert, P., Cameron, L., Cimini, D., Salmon, E. D., McEwen, B. F., & Khodjakov, A. (2006). Chromosomes can congress to the metaphase plate before biorientation. *Science (New York, N.Y.)*, *311*(5759), 388–391. https://doi.org/10.1126/science.1122142

Katayama, H., Sasai, K., Kloc, M., Brinkley, B. R., & Sen, S. (2008). Aurora kinase-A regulates kinetochore/chromatin associated microtubule assembly in human cells. *Cell cycle (Georgetown, Tex.)*, *7*(17), 2691–2704. https://doi.org/10.4161/cc.7.17.6460

Kelly, A. E., Sampath, S. C., Maniar, T. A., Woo, E. M., Chait, B. T., & Funabiki, H. (2007). Chromosomal enrichment and activation of the aurora B pathway are coupled to spatially regulate spindle assembly. *Developmental cell*, *12*(1), 31–43. https://doi.org/10.1016/j.devcel.2006.11.001

Kelly, A. E., Ghenoiu, C., Xue, J. Z., Zierhut, C., Kimura, H., & Funabiki, H. (2010). Survivin reads phosphorylated histone H3 threonine 3 to activate the mitotic kinase Aurora B. *Science (New York, N.Y.)*, *330*(6001), 235–239. https://doi.org/10.1126/science.1189505

Kettenbach, A. N., Schweppe, D. K., Faherty, B. K., Pechenick, D., Pletnev, A. A., & Gerber, S. A. (2011). Quantitative phosphoproteomics identifies substrates and functional modules of Aurora and Polo-like kinase activities in mitotic cells. *Science signaling*, *4*(179), rs5. https://doi.org/10.1126/scisignal.2001497

Khan, J., Ezan, F., Crémet, J. Y., Fautrel, A., Gilot, D., Lambert, M., Benaud, C., Troadec, M. B., & Prigent, C. (2011). Overexpression of active Aurora-C kinase results in cell transformation and tumour formation. *PloS one*, *6*(10), e26512. https://doi.org/10.1371/journal.pone.0026512

Khodjakov, A., Cole, R. W., Oakley, B. R., & Rieder, C. L. (2000). Centrosome-independent mitotic spindle formation in vertebrates. *Current biology: CB*, *10*(2), 59–67. https://doi.org/10.1016/s0960-9822(99)00276-6

Khodjakov, A., Copenagle, L., Gordon, M. B., Compton, D. A., & Kapoor, T. M. (2003). Minus-end capture of preformed kinetochore fibers contributes to spindle morphogenesis. *The Journal of cell biology*, *160*(5), 671–683. https://doi.org/10.1083/jcb.200208143

Khodjakov, A., & Pines, J. (2010). Centromere tension: a divisive issue. *Nature cell biology*, *12*(10), 919–923. https://doi.org/10.1038/ncb1010-919

Kim, Y., Holland, A. J., Lan, W., & Cleveland, D. W. (2010). Aurora kinases and protein phosphatase 1 mediate chromosome congression through regulation of CENP-E. *Cell*, *142*(3), 444–455. https://doi.org/10.1016/j.cell.2010.06.039

King, J. M., & Nicklas, R. B. (2000). Tension on chromosomes increases the number of kinetochore microtubules but only within limits. *Journal of cell science*, *113 Pt 21*, 3815–3823. https://doi.org/10.1242/jcs.113.21.3815

Kirschner, M., & Mitchison, T. (1986). Beyond self-assembly: from microtubules to morphogenesis. *Cell*, *45*(3), 329–342. https://doi.org/10.1016/0092-8674(86)90318-1

Kitamura, E., Tanaka, K., Kitamura, Y., & Tanaka, T. U. (2007). Kinetochore microtubule interaction during S phase in Saccharomyces cerevisiae. *Genes & development*, *21*(24), 3319–3330. https://doi.org/10.1101/gad.449407

Koch, A., Maia, A., Janssen, A., and Medema, R.H. (2016). Molecular basis underlying resistance to Mps1/TTK inhibitors. *Oncogene* 35, 2518–2528. https://doi.org/10.1038/onc.2015.319.

Komaki, S., & Schnittger, A. (2016). The spindle checkpoint in plants-a green variation over a conserved theme?. *Current opinion in plant biology*, *34*, 84–91. https://doi.org/10.1016/j.pbi.2016.10.008

Krenn, V., & Musacchio, A. (2015). The Aurora B Kinase in Chromosome Bi-Orientation and Spindle Checkpoint Signaling. *Frontiers in oncology*, *5*, 225. https://doi.org/10.3389/fonc.2015.00225

Kwiatkowski, N., Jelluma, N., Filippakopoulos, P., Soundararajan, M., Manak, M.S., Kwon, M., Choi, H.G., Sim, T., Deveraux, Q.L., Rottmann, S., et al. (2010). Small-molecule kinase inhibitors provide insight into Mps1 cell cycle function. *Nat. Chem. Biol.* 6, 359–368. https://doi.org/10.1038/nchembio.345.

Lamb, J.R., Michaud, W.A., Sikorski, R.S., and Hieter, P.A. (1994). Cdc16p, Cdc23p and Cdc27p form a complex essential for mitosis. *EMBO J.* 13, 4321–4328. https://doi.org/10.1002/j.1460-2075.1994.tb06752.x.

Lampson, M.A., Renduchitala, K., Khodjakov, A., and Kapoor, T.M. (2004). Correcting improper chromosome-spindle attachments during cell division. *Nat. Cell Biol.* 6, 232–237. https://doi.org/10.1038/ncb1102.

Lampson, M. A., & Cheeseman, I. M. (2011). Sensing centromere tension: Aurora B and the regulation of kinetochore function. *Trends in cell biology*, *21*(3), 133–140. https://doi.org/10.1016/j.tcb.2010.10.007

Lampson, M. A., & Grishchuk, E. L. (2017). Mechanisms to Avoid and Correct Erroneous Kinetochore-Microtubule Attachments. *Biology*, *6*(1), 1. https://doi.org/10.3390/biology6010001

Lee, K., & Rhee, K. (2011). PLK1 phosphorylation of pericentrin initiates centrosome maturation at the onset of mitosis. *The Journal of cell biology*, *195*(7), 1093–1101. https://doi.org/10.1083/jcb.201106093

Li, C., Wen, A., Shen, B., Lu, J., Huang, Y., and Chang, Y. (2011). FastCloning: a highly simplified, purification-free, sequence- and ligation-independent PCR cloning method. *BMC Biotechnol.* 11, 92. https://doi.org/10.1186/1472-6750-11-92.

Li, S., Deng, Z., Fu, J., Xu, C., Xin, G., Wu, Z., Luo, J., Wang, G., Zhang, S., Zhang, B., Zou, F., Jiang, Q., & Zhang, C. (2015). Spatial Compartmentalization Specializes the Function of Aurora A and Aurora B. *The Journal of biological chemistry*, *290*(28), 17546–17558. https://doi.org/10.1074/jbc.M115.652453

Littlepage, L. E., Wu, H., Andresson, T., Deanehan, J. K., Amundadottir, L. T., & Ruderman, J. V. (2002). Identification of phosphorylated residues that affect the activity of the mitotic kinase Aurora-A. *Proceedings of the National Academy of Sciences of the United States of America*, *99*(24), 15440–15445. https://doi.org/10.1073/pnas.202606599

Liu, D., Vader, G., Vromans, M. J., Lampson, M. A., & Lens, S. M. (2009). Sensing chromosome bi-orientation by spatial separation of aurora B kinase from kinetochore substrates. *Science (New York, N.Y.)*, *323*(5919), 1350–1353. https://doi.org/10.1126/science.1167000

Liu, X., & Winey, M. (2012). The MPS1 family of protein kinases. *Annual review of biochemistry*, *81*, 561–585. https://doi.org/10.1146/annurev-biochem-061611-090435

Loncarek, J., Kisurina-Evgenieva, O., Vinogradova, T., Hergert, P., La Terra, S., Kapoor, T. M., & Khodjakov, A. (2007). The centromere geometry essential for keeping mitosis error free is controlled by spindle forces. *Nature*, *450*(7170), 745–749. https://doi.org/10.1038/nature06344

London, N., Ceto, S., Ranish, J. A., & Biggins, S. (2012). Phosphoregulation of Spc105 by Mps1 and PP1 regulates Bub1 localization to kinetochores. *Current biology : CB*, *22*(10), 900–906. https://doi.org/10.1016/j.cub.2012.03.052

Maciejowski, J., George, K.A., Terret, M.E., Zhang, C., Shokat, K.M., and Jallepalli, P.V. (2010). Mps1 directs the assembly of Cdc20 inhibitory complexes during interphase and mitosis to control M phase timing and spindle checkpoint signaling. *J. Cell Biol.* 190, 89–100. https://doi.org/10.1083/jcb.201001050.

Maciejowski, J., Drechsler, H., Grundner-Culemann, K., Ballister, E.R., Rodriguez-Rodriguez, J.A., Rodriguez-Bravo, V., Jones, M.J.K., Foley, E., Lampson, M.A., Daub, H., et al. (2017). Mps1 regulates kinetochore-microtubule attachment stability via the Ska complex to ensure error-free chromosome segregation. *Dev. Cell* 41, 143–156.e6. https://doi.org/10.1016/j.devcel.2017.03.025.

Macurek, L., Lindqvist, A., Lim, D., Lampson, M. A., Klompmaker, R., Freire, R., Clouin, C., Taylor, S. S., Yaffe, M. B., & Medema, R. H. (2008). Polo-like kinase-1 is activated by aurora A to promote checkpoint recovery. *Nature*, *455*(7209), 119–123. https://doi.org/10.1038/nature07185

Maiato, H., Rieder, C. L., & Khodjakov, A. (2004). Kinetochore-driven formation of kinetochore fibers contributes to spindle assembly during animal mitosis. *The Journal of cell biology*, *167*(5), 831–840. https://doi.org/10.1083/jcb.200407090

Maiato, H., Gomes, A. M., Sousa, F., & Barisic, M. (2017). Mechanisms of Chromosome Congression during Mitosis. *Biology*, *6*(1), 13. https://doi.org/10.3390/biology6010013

Magidson, V., Paul, R., Yang, N., Ault, J. G., O'Connell, C. B., Tikhonenko, I., McEwen, B. F., Mogilner, A., & Khodjakov, A. (2015). Adaptive changes in the kinetochore architecture facilitate proper spindle assembly. *Nature cell biology*, *17*(9), 1134–1144. https://doi.org/10.1038/ncb3223

Matthews, H. K., Bertoli, C., & de Bruin, R. A. (2022). Cell cycle control in cancer. *Nature reviews Molecular cell biology*, *23*(1), 74-88.

Maure, J. F., Kitamura, E., & Tanaka, T. U. (2007). Mps1 kinase promotes sister-kinetochore bi-orientation by a tension-dependent mechanism. *Current biology : CB*, *17*(24), 2175–2182. https://doi.org/10.1016/j.cub.2007.11.032

Maure, J. F., Komoto, S., Oku, Y., Mino, A., Pasqualato, S., Natsume, K., Clayton, L., Musacchio, A., & Tanaka, T. U. (2011). The Ndc80 loop region facilitates formation of kinetochore attachment to the dynamic microtubule plus end. *Current biology : CB*, *21*(3), 207–213. https://doi.org/10.1016/j.cub.2010.12.050

McAinsh, A. D., & Kops, G. J. P. L. (2023). Principles and dynamics of spindle assembly checkpoint signalling. *Nature reviews. Molecular cell biology*, *24*(8), 543–559. https://doi.org/10.1038/s41580-023-00593-z

Meng, L., Park, J. E., Kim, T. S., Lee, E. H., Park, S. Y., Zhou, M., Bang, J. K., & Lee, K. S. (2015). Bimodal Interaction of Mammalian Polo-Like Kinase 1 and a Centrosomal Scaffold, Cep192, in the Regulation of Bipolar Spindle Formation. *Molecular and cellular biology*, *35*(15), 2626–2640. https://doi.org/10.1128/MCB.00068-15

Meyer, R. E., Brown, J., Beck, L., & Dawson, D. S. (2018). Mps1 promotes chromosome meiotic chromosome biorientation through Dam1. *Molecular biology of the cell*, *29*(4), 479–489. https://doi.org/10.1091/mbc.E17-08-0503

Miller, S. A., Johnson, M. L., & Stukenberg, P. T. (2008). Kinetochore attachments require an interaction between unstructured tails on microtubules and Ndc80(Hec1). *Current biology : CB*, *18*(22), 1785–1791. https://doi.org/10.1016/j.cub.2008.11.007

Miranda, J. J., De Wulf, P., Sorger, P. K., & Harrison, S. C. (2005). The yeast DASH complex forms closed rings on microtubules. *Nature structural & molecular biology*, *12*(2), 138–143. https://doi.org/10.1038/nsmb896

Mitchison T. J. (1986). The role of microtubule polarity in the movement of kinesin and kinetochores. *Journal of cell science. Supplement*, *5*, 121–128. https://doi.org/10.1242/jcs.1986.supplement_5.7

Mitchison, T. J., & Salmon, E. D. (2001). Mitosis: a history of division. *Nature cell biology*, *3*(1), E17–E21. https://doi.org/10.1038/35050656

Mogilner, A., & Craig, E. (2010). Towards a quantitative understanding of mitotic spindle assembly and mechanics. *Journal of cell science*, *123*(Pt 20), 3435–3445. https://doi.org/10.1242/jcs.062208

Moura, M., Osswald, M., Leca, N., Barbosa, J., Pereira, A.J., Maiato, H., Sunkel, C.E., and Conde, C. (2017). Protein Phosphatase 1 inactivates Mps1 to ensure efficient spindle assembly checkpoint silencing. *eLife* 6, e25366. https://doi.org/10.7554/eLife.25366.

Moura, M., & Conde, C. (2019). Phosphatases in Mitosis: Roles and Regulation. *Biomolecules*, *9*(2), 55. https://doi.org/10.3390/biom9020055

Musacchio A. The Molecular Biology of Spindle Assembly Checkpoint Signaling Dynamics. Curr Biol. 2015 Oct 19;25(20):R1002-18. doi: 10.1016/j.cub.2015.08.051. Erratum in: Curr Biol. 2015 Nov 16;25(22):3017. PMID: 26485365.

Musacchio, A., & Desai, A. (2017). A Molecular View of Kinetochore Assembly and Function. *Biology*, *6*(1), 5. https://doi.org/10.3390/biology6010005

Naso, F. D., Boi, D., Ascanelli, C., Pamfil, G., Lindon, C., Paiardini, A., & Guarguaglini, G. (2021). Nuclear localisation of Aurora-A: its regulation and significance for Aurora-A functions in cancer. *Oncogene*, *40*(23), 3917–3928. https://doi.org/10.1038/s41388-021-01766-w

Naso, F. D., Polverino, F., Cilluffo, D., Latini, L., Stagni, V., Asteriti, I. A., Rosa, A., Soddu, S., & Guarguaglini, G. (2024). AurkA/TPX2 co-overexpression in nontransformed cells promotes genome instability through induction of chromosome mis-segregation and attenuation of the p53 signalling pathway. *Biochimica et biophysica acta. Molecular basis of disease*, *1870*(4), 167116. https://doi.org/10.1016/j.bbadis.2024.167116

Nezi, L., & Musacchio, A. (2009). Sister chromatid tension and the spindle assembly checkpoint. *Current opinion in cell biology*, *21*(6), 785–795. https://doi.org/10.1016/j.ceb.2009.09.007

Nicklas, R. B., & Koch, C. A. (1969). Chromosome micromanipulation. 3. Spindle fiber tension and the reorientation of mal-oriented chromosomes. *The Journal of cell biology*, *43*(1), 40–50. https://doi.org/10.1083/jcb.43.1.40

Nijenhuis, W., von Castelmur, E., Littler, D., De Marco, V., Tromer, E., Vleugel, M., van Osch, M. H., Snel, B., Perrakis, A., & Kops, G. J. (2013). A TPR domain-containing N-terminal module of MPS1 is required for its kinetochore localization by Aurora B. *The Journal of cell biology*, *201*(2), 217–231. https://doi.org/10.1083/jcb.201210033

Nurse P. (2000). The incredible life and times of biological cells. *Science (New York, N.Y.)*, *289*(5485), 1711–1716. https://doi.org/10.1126/science.289.5485.1711

Ohashi, S., Sakashita, G., Ban, R., Nagasawa, M., Matsuzaki, H., Murata, Y., Taniguchi, H., Shima, H., Furukawa, K., & Urano, T. (2006). Phospho-regulation of human protein kinase Aurora-A: analysis using anti-phospho-Thr288 monoclonal antibodies. *Oncogene*, *25*(59), 7691–7702. https://doi.org/10.1038/sj.onc.1209754

Olsen, J.V., Macek, B., Lange, O., Makarov, A., Horning, S., and Mann, M. (2007). Higher-energy C-trap dissociation for peptide modification analysis. *Nat. Methods* 4, 709–712. https://doi.org/10.1038/nmeth1060.

Pachis, S. T., & Kops, G. J. P. L. (2018). Leader of the SAC: molecular mechanisms of Mps1/TTK regulation in mitosis. *Open biology*, *8*(8), 180109. https://doi.org/10.1098/rsob.180109

Palazzo, R. E., Vogel, J. M., Schnackenberg, B. J., Hull, D. R., & Wu, X. (1999). Centrosome maturation. *Current topics in developmental biology*, *49*, 449–470. https://doi.org/10.1016/s0070-2153(99)49021-0

Pan, D., Klare, K., Petrovic, A., Take, A., Walstein, K., Singh, P., Rondelet, A., Bird, A.W., and Musacchio, A. (2017). CDK-regulated dimerization of M18BP1 on a Mis18 hexamer is necessary for CENP-A loading. *eLife* 6, e23352. https://doi.org/10.7554/eLife.23352.

Parnell, E.J., Jenson, E.E., and Miller, M.P. (2024). A conserved site on Ndc80 complex facilitates dynamic recruitment of Mps1 to yeast kinetochores to promote accurate chromosome segregation. *Curr. Biol.* 34, 2294–2307.e4. https://doi.org/10.1016/j.cub.2024.04.054.

Paul, R., Wollman, R., Silkworth, W. T., Nardi, I. K., Cimini, D., & Mogilner, A. (2009). Computer simulations predict that chromosome movements and rotations accelerate mitotic spindle assembly without compromising accuracy. *Proceedings of the National Academy of Sciences of the United States of America*, *106*(37), 15708–15713. https://doi.org/10.1073/pnas.0908261106

Perez-Riverol, Y., Bai, J., Bandla, C., García-Seisdedos, D., Hewapathirana, S., Kamatchinathan, S., Kundu, D.J., Prakash, A., Frericks-Zipper, A., Eisenacher, M., et al. (2022). The PRIDE database resources in 2022: A hub for mass spectrometry-based proteomics evidences. *Nucleic Acids Res.* 50, D543–D552. https://doi.org/10.1093/nar/gkab1038.

Pleuger, R., Cozma, C., Hohoff, S., Denkhaus, C., Dudziak, A., Kaschani, F., Kaiser, M., Musacchio, A., Vetter, I.R., and Westermann, S. (2024). Microtubule end-on attachment maturation regulates Mps1 association with its kinetochore receptor. *Curr. Biol.* 34, 2279–2293.e6. https://doi.org/10.1016/j.cub.2024.03.062.

Polverino, F., Naso, F. D., Asteriti, I. A., Palmerini, V., Singh, D., Valente, D., Bird, A. W., Rosa, A., Mapelli, M., & Guarguaglini, G. (2021). The Aurora-A/TPX2 Axis Directs Spindle Orientation in Adherent Human Cells by Regulating NuMA and Microtubule Stability. *Current biology : CB*, *31*(3), 658–667.e5. https://doi.org/10.1016/j.cub.2020.10.096

Polverino, F., Mastrangelo, A., & Guarguaglini, G. (2024). Contribution of AurkA/TPX2 Overexpression to Chromosomal Imbalances and Cancer. *Cells*, *13*(16), 1397. https://doi.org/10.3390/cells13161397

Posch, M., Khoudoli, G. A., Swift, S., King, E. M., Deluca, J. G., & Swedlow, J. R. (2010). Sds22 regulates aurora B activity and microtubule-kinetochore interactions at mitosis. *The Journal of cell biology*, *191*(1), 61–74. https://doi.org/10.1083/jcb.200912046

Primorac, I., Weir, J. R., Chiroli, E., Gross, F., Hoffmann, I., van Gerwen, S., Ciliberto, A., & Musacchio, A. (2013). Bub3 reads phosphorylated MELT repeats to promote spindle assembly checkpoint signaling. *eLife*, *2*, e01030. https://doi.org/10.7554/eLife.01030

Raisch, T., Ciossani, G., D'Amico, E., Cmentowski, V., Carmignani, S., Maffini, S., Merino, F., Wohlgemuth, S., Vetter, I.R., Raunser, S., et al. (2022). Structure of the RZZ complex and molecular basis of Spindly-driven corona assembly at human kinetochores. *EMBO J.* 41, e110411. https://doi.org/10.15252/embj.2021110411.

Rappsilber, J., Mann, M., and Ishihama, Y. (2007). Protocol for micro-purification, enrichment, pre-fractionation and storage of peptides for proteomics using StageTips. *Nat. Protoc.* 2, 1896–1906. https://doi.org/10.1038/nprot.2007.261.

Redli, P. M., Gasic, I., Meraldi, P., Nigg, E. A., & Santamaria, A. (2016). The Ska complex promotes Aurora B activity to ensure chromosome biorientation. *The Journal of cell biology*, *215*(1), 77–93. https://doi.org/10.1083/jcb.201603019

Renda, F., Miles, C., Tikhonenko, I., Fisher, R., Carlini, L., Kapoor, T.M., Mogilner, A., and Khodjakov, A. (2022). Non-centrosomal microtubules at kinetochores promote rapid chromosome biorientation during mitosis in human cells. *Curr. Biol.* 32, 1049–1063.e4. https://doi.org/10.1016/j.cub.2022.01.013.

Ritter, A., Kreis, N. N., Louwen, F., Wordeman, L., & Yuan, J. (2015). Molecular insight into the regulation and function of MCAK. *Critical reviews in biochemistry and molecular biology*, *51*(4), 228–245. https://doi.org/10.1080/10409238.2016.1178705

Rodrigues-Martins, A., Riparbelli, M., Callaini, G., Glover, D.M., and Bettencourt-Dias, M. (2007). Revisiting the role of the mother centriole in centriole biogenesis. *Science* 316, 1046–1050. https://doi.org/10.1126/science.1142950.

Roghi, C., Giet, R., Uzbekov, R., Morin, N., Chartrain, I., Le Guellec, R., Couturier, A., Dorée, M., Philippe, M., & Prigent, C. (1998). The Xenopus protein kinase pEg2 associates with the centrosome in a cell cycle-dependent manner, binds to the spindle microtubules and is involved in bipolar mitotic spindle assembly. *Journal of cell science*, *111 (Pt 5)*, 557–572. https://doi.org/10.1242/jcs.111.5.557

Ruff, E. F., Muretta, J. M., Thompson, A. R., Lake, E. W., Cyphers, S., Albanese, S. K., Hanson, S. M., Behr, J. M., Thomas, D. D., Chodera, J. D., & Levinson, N. M. (2018). A dynamic mechanism for allosteric activation of Aurora kinase A by activation loop phosphorylation. *eLife*, *7*, e32766. https://doi.org/10.7554/eLife.32766

Sacristan, C., & Kops, G. J. (2015). Joined at the hip: kinetochores, microtubules, and spindle assembly checkpoint signaling. *Trends in cell biology*, *25*(1), 21–28. https://doi.org/10.1016/j.tcb.2014.08.006

Santaguida, S., Tighe, A., D'Alise, A.M., Taylor, S.S., and Musacchio, A. (2010). Dissecting the role of MPS1 in chromosome biorientation and the spindle checkpoint through the small molecule inhibitor reversine. *J. Cell Biol.* 190, 73–87. https://doi.org/10.1083/jcb.201001036.

Santaguida, S., Vernieri, C., Villa, F., Ciliberto, A., & Musacchio, A. (2011). Evidence that Aurora B is implicated in spindle checkpoint signalling independently of error correction. *The EMBO journal*, *30*(8), 1508–1519. https://doi.org/10.1038/emboj.2011.70

Sarangapani, K. K., Akiyoshi, B., Duggan, N. M., Biggins, S., & Asbury, C. L. (2013). Phosphoregulation promotes release of kinetochores from dynamic microtubules via multiple mechanisms. *Proceedings of the National Academy of Sciences of the United States of America*, *110*(18), 7282–7287. https://doi.org/10.1073/pnas.1220700110

Sarangapani, K.K., Koch, L.B., Nelson, C.R., Asbury, C.L., and Biggins, S. (2021). Kinetochore-bound Mps1 regulates kinetochore-microtubule attachments via Ndc80 phosphorylation. *J. Cell Biol.* 220, e202106130. https://doi.org/10.1083/jcb.202106130.

Saurin, A. T., van der Waal, M. S., Medema, R. H., Lens, S. M., & Kops, G. J. (2011). Aurora B potentiates Mps1 activation to ensure rapid checkpoint establishment at the onset of mitosis. *Nature communications*, *2*, 316. https://doi.org/10.1038/ncomms1319

Schmidt, J. C., Arthanari, H., Boeszoermenyi, A., Dashkevich, N. M., Wilson-Kubalek, E. M., Monnier, N., Markus, M., Oberer, M., Milligan, R. A., Bathe, M., Wagner, G., Grishchuk, E. L., & Cheeseman, I. M. (2012). The kinetochore-bound Ska1 complex tracks depolymerizing microtubules and binds to curved protofilaments. *Developmental cell*, *23*(5), 968–980. https://doi.org/10.1016/j.devcel.2012.09.012

Schumacher, J. M., Ashcroft, N., Donovan, P. J., & Golden, A. (1998). A highly conserved centrosomal kinase, AIR-1, is required for accurate cell cycle progression and segregation of developmental factors in Caenorhabditis elegans embryos. *Development (Cambridge, England)*, *125*(22), 4391–4402. https://doi.org/10.1242/dev.125.22.4391

Schukken, K. M., & Foijer, F. (2018). CIN and Aneuploidy: Different Concepts, Different Consequences. *BioEssays : news and reviews in molecular, cellular and developmental biology*, *40*(1), 10.1002/bies.201700147. https://doi.org/10.1002/bies.201700147

Seki, A., Coppinger, J. A., Jang, C. Y., Yates, J. R., & Fang, G. (2008). Bora and the kinase Aurora a cooperatively activate the kinase Plk1 and control mitotic entry. *Science (New York, N.Y.)*, *320*(5883), 1655–1658. https://doi.org/10.1126/science.1157425

Sells, T., Ecsedy, J., Stroud, S., Janowick, D., Hoar, K., LeRoy, P., Wysong, D., Zhang, M., Huck, J., Silverman, L., Chen, W., Bembenek, M., Claiborne, C., & Manfredi, M. (2008). MLN8237: an orally active small molecule inhibitor of Aurora A kinase in phase I clinical trials. *Cancer research*, *68*(9_Supplement), 237-237.

Sells, T. B., Chau, R., Ecsedy, J. A., Gershman, R. E., Hoar, K., Huck, J., Janowick, D. A., Kadambi, V. J., LeRoy, P. J., Stirling, M., Stroud, S. G., Vos, T. J., Weatherhead, G. S., Wysong, D. R., Zhang, M., Balani, S. K., Bolen, J. B., Manfredi, M. G., & Claiborne, C. F. (2015). MLN8054 and Alisertib (MLN8237): Discovery of Selective Oral Aurora A Inhibitors. *ACS medicinal chemistry letters*, *6*(6), 630–634. https://doi.org/10.1021/ml500409n

Sessa, F., Mapelli, M., Ciferri, C., Tarricone, C., Areces, L. B., Schneider, T. R., Stukenberg, P. T., & Musacchio, A. (2005). Mechanism of Aurora B activation by INCENP and inhibition by hesperadin. *Molecular cell*, *18*(3), 379–391. https://doi.org/10.1016/j.molcel.2005.03.031

Shepperd, L. A., Meadows, J. C., Sochaj, A. M., Lancaster, T. C., Zou, J., Buttrick, G. J., Rappsilber, J., Hardwick, K. G., & Millar, J. B. (2012). Phosphodependent recruitment of Bub1 and Bub3 to Spc7/KNL1 by Mph1 kinase maintains the spindle checkpoint. *Current biology : CB*, *22*(10), 891–899. https://doi.org/10.1016/j.cub.2012.03.051

Sherwin, D., & Wang, Y. (2019). The Opposing Functions of Protein Kinases and Phosphatases in Chromosome Bipolar Attachment. *International journal of molecular sciences*, *20*(24), 6182. https://doi.org/10.3390/ijms20246182

Shimogawa, M. M., Graczyk, B., Gardner, M. K., Francis, S. E., White, E. A., Ess, M., Molk, J. N., Ruse, C., Niessen, S., Yates, J. R., 3rd, Muller, E. G., Bloom, K., Odde, D. J., & Davis, T. N. (2006). Mps1 phosphorylation of Dam1 couples kinetochores to microtubule plus ends at metaphase. *Current biology : CB*, *16*(15), 1489–1501. https://doi.org/10.1016/j.cub.2006.06.063

Simmons Kovacs, L. A., Nelson, C. L., & Haase, S. B. (2008). Intrinsic and cyclin-dependent kinase-dependent control of spindle pole body duplication in budding yeast. *Molecular biology of the cell*, *19*(8), 3243–3253. https://doi.org/10.1091/mbc.e08-02-0148

Sikirzhytski, V., Renda, F., Tikhonenko, I., Magidson, V., McEwen, B.F., and Khodjakov, A. (2018). Microtubules assemble near most kinetochores during early prometaphase in human cells. *J. Cell Biol.* 217, 2647–2659. https://doi.org/10.1083/jcb.201710094.

Sundin, L. J., Guimaraes, G. J., & Deluca, J. G. (2011). The NDC80 complex proteins Nuf2 and Hec1 make distinct contributions to kinetochore-microtubule attachment in mitosis. *Molecular biology of the cell*, *22*(6), 759–768. https://doi.org/10.1091/mbc.E10-08-0671

Tanaka, K., Kitamura, E., Kitamura, Y., & Tanaka, T. U. (2007). Molecular mechanisms of microtubule-dependent kinetochore transport toward spindle poles. *The Journal of cell biology*, *178*(2), 269–281. https://doi.org/10.1083/jcb.200702141

Tanaka, M., Ueda, A., Kanamori, H., Ideguchi, H., Yang, J., Kitajima, S., & Ishigatsubo, Y. (2002). Cell-cycle-dependent regulation of human aurora A transcription is mediated by periodic repression of E4TF1. *The Journal of biological chemistry*, *277*(12), 10719–10726. https://doi.org/10.1074/jbc.M108252200

Tanaka, T.U., Rachidi, N., Janke, C., Pereira, G., Galova, M., Schiebel, E., Stark, M.J.R., and Nasmyth, K. (2002). Evidence that the Ipl1-Sli15 (Aurora kinase-INCENP) complex promotes chromosome bi-orientation by altering kinetochore-spindle pole connections. *Cell* 108, 317–329. https://doi.org/10.1016/s0092-8674(02)00633-5.

Tanaka T. U. (2010). Kinetochore-microtubule interactions: steps towards bi-orientation. *The EMBO journal*, *29*(24), 4070–4082. https://doi.org/10.1038/emboj.2010.294

Tang, A., Gao, K., Chu, L., Zhang, R., Yang, J., & Zheng, J. (2017). Aurora kinases: novel therapy targets in cancers. *Oncotarget*, *8*(14), 23937–23954. https://doi.org/10.18632/oncotarget.14893

Tang, C. J., Lin, C. Y., & Tang, T. K. (2006). Dynamic localization and functional implications of Aurora-C kinase during male mouse meiosis. *Developmental biology*, *290*(2), 398–410. https://doi.org/10.1016/j.ydbio.2005.11.036

Tang, N. H., Takada, H., Hsu, K. S., & Toda, T. (2013). The internal loop of fission yeast Ndc80 binds Alp7/TACC-Alp14/TOG and ensures proper chromosome attachment. *Molecular biology of the cell*, *24*(8), 1122–1133. https://doi.org/10.1091/mbc.E12-11-0817

Tavernier, N., Noatynska, A., Panbianco, C., Martino, L., Van Hove, L., Schwager, F., Léger, T., Gotta, M., & Pintard, L. (2015). Cdk1 phosphorylates SPAT-1/Bora to trigger PLK-1 activation and drive mitotic entry in C. elegans embryos. *The Journal of cell biology*, *208*(6), 661–669. https://doi.org/10.1083/jcb.201408064

Tavernier, N., Thomas, Y., Vigneron, S., Maisonneuve, P., Orlicky, S., Mader, P., Regmi, S. G., Van Hove, L., Levinson, N. M., Gasmi-Seabrook, G., Joly, N., Poteau, M., Velez-Aguilera, G., Gavet, O., Castro, A., Dasso, M., Lorca, T., Sicheri, F., & Pintard, L. (2021a). Bora phosphorylation substitutes in trans for T-loop phosphorylation in Aurora A to promote mitotic entry. *Nature communications*, *12*(1), 1899. https://doi.org/10.1038/s41467-021-21922-w

Tavernier, N., Sicheri, F., & Pintard, L. (2021b). Aurora A kinase activation: Different means to different ends. *The Journal of cell biology*, *220*(9), e202106128. https://doi.org/10.1083/jcb.202106128

Thomas, G. E., Renjith, M. R., & Manna, T. K. (2017). Kinetochore-microtubule interactions in chromosome segregation: lessons from yeast and mammalian cells. *The Biochemical journal*, *474*(21), 3559–3577. https://doi.org/10.1042/BCJ20170518

Thomas, Y., Cirillo, L., Panbianco, C., Martino, L., Tavernier, N., Schwager, F., Van Hove, L., Joly, N., Santamaria, A., Pintard, L., & Gotta, M. (2016). Cdk1 Phosphorylates SPAT-1/Bora to Promote Plk1 Activation in C. elegans and Human Cells. *Cell reports*, *15*(3), 510–518. https://doi.org/10.1016/j.celrep.2016.03.049

Thompson, S. L., & Compton, D. A. (2011). Chromosome missegregation in human cells arises through specific types of kinetochore-microtubule attachment errors. *Proceedings of the National Academy of Sciences of the United States of America*, *108*(44), 17974–17978. https://doi.org/10.1073/pnas.1109720108

Tseng, T. C., Chen, S. H., Hsu, Y. P., & Tang, T. K. (1998). Protein kinase profile of sperm and eggs: cloning and characterization of two novel testis-specific protein kinases (AIE1, AIE2) related to yeast and fly chromosome segregation regulators. *DNA and cell biology*, *17*(10), 823–833. https://doi.org/10.1089/dna.1998.17.823

Tugendreich, S., Tomkiel, J., Earnshaw, W., and Hieter, P. (1995). CDC27Hs colocalizes with CDC16Hs to the centrosome and mitotic spindle and is essential for the metaphase to anaphase transition. *Cell* 81, 261–268. https://doi.org/10.1016/0092-8674(95)90336-4.

Umbreit, N. T., Gestaut, D. R., Tien, J. F., Vollmar, B. S., Gonen, T., Asbury, C. L., & Davis, T. N. (2012). The Ndc80 kinetochore complex directly modulates microtubule dynamics. *Proceedings of the National Academy of Sciences of the United States of America*, *109*(40), 16113–16118. https://doi.org/10.1073/pnas.1209615109

Vader, G., & Lens, S. M. (2008). The Aurora kinase family in cell division and cancer. *Biochimica et biophysica acta*, *1786*(1), 60–72. https://doi.org/10.1016/j.bbcan.2008.07.003

Valdez, V. A., Neahring, L., Petry, S., & Dumont, S. (2023). Mechanisms underlying spindle assembly and robustness. *Nature reviews. Molecular cell biology*, *24*(8), 523–542. https://doi.org/10.1038/s41580-023-00584-0

van der Waal, M.S., Saurin, A.T., Vromans, M.J.M., Vleugel, M., Wurzenberger, C., Gerlich, D.W., Medema, R.H., Kops, G.J.P.L., and Lens, S.M.A. (2012). Mps1 promotes rapid centromere accumulation of Aurora B. *EMBO Rep.* 13, 847–854. https://doi.org/10.1038/embor.2012.93.

Vigneron, S., Sundermann, L., Labbé, J. C., Pintard, L., Radulescu, O., Castro, A., & Lorca, T. (2018). Cyclin A-cdk1-Dependent Phosphorylation of Bora Is the Triggering Factor Promoting Mitotic Entry. *Developmental cell*, *45*(5), 637–650.e7. https://doi.org/10.1016/j.devcel.2018.05.005

Violin, J.D., Zhang, J., Tsien, R.Y., and Newton, A.C. (2003). A genetically encoded fluorescent reporter reveals oscillatory phosphorylation by protein kinase C. *J. Cell Biol.* 161, 899–909. https://doi.org/10.1083/jcb.200302125.

Vleugel, M., Omerzu, M., Groenewold, V., Hadders, M. A., Lens, S. M. A., & Kops, G. J. P. L. (2015). Sequential multisite phospho-regulation of KNL1-BUB3 interfaces at mitotic kinetochores. *Molecular cell*, *57*(5), 824–835. https://doi.org/10.1016/j.molcel.2014.12.036

Volkov, V. A., Huis In 't Veld, P. J., Dogterom, M., & Musacchio, A. (2018). Multivalency of NDC80 in the outer kinetochore is essential to track shortening microtubules and generate forces. *eLife*, *7*, e36764. https://doi.org/10.7554/eLife.36764

Walter, A. O., Seghezzi, W., Korver, W., Sheung, J., & Lees, E. (2000). The mitotic serine/threonine kinase Aurora2/AIK is regulated by phosphorylation and degradation. *Oncogene*, *19*(42), 4906–4916. https://doi.org/10.1038/sj.onc.1203847

Wang, E., Ballister, E. R., & Lampson, M. A. (2011). Aurora B dynamics at centromeres create a diffusion-based phosphorylation gradient. *The Journal of cell biology*, *194*(4), 539–549. https://doi.org/10.1083/jcb.201103044

Wang, F., Dai, J., Daum, J. R., Niedzialkowska, E., Banerjee, B., Stukenberg, P. T., Gorbsky, G. J., & Higgins, J. M. (2010). Histone H3 Thr-3 phosphorylation by Haspin positions Aurora B at centromeres in mitosis. *Science (New York, N.Y.)*, *330*(6001), 231–235. https://doi.org/10.1126/science.1189435

Wang, F., Ulyanova, N. P., Daum, J. R., Patnaik, D., Kateneva, A. V., Gorbsky, G. J., & Higgins, J. M. (2012). Haspin inhibitors reveal centromeric functions of Aurora B in chromosome segregation. *The Journal of cell biology*, *199*(2), 251–268. https://doi.org/10.1083/jcb.201205106

Weiss, E., & Winey, M. (1996). The Saccharomyces cerevisiae spindle pole body duplication gene MPS1 is part of a mitotic checkpoint. *The Journal of cell biology*, *132*(1-2), 111–123. https://doi.org/10.1083/jcb.132.1.111

Westermann, S., Avila-Sakar, A., Wang, H. W., Niederstrasser, H., Wong, J., Drubin, D. G., Nogales, E., & Barnes, G. (2005). Formation of a dynamic kinetochore- microtubule

interface through assembly of the Dam1 ring complex. *Molecular cell*, *17*(2), 277–290. https://doi.org/10.1016/j.molcel.2004.12.019

Westermann, S., Wang, H. W., Avila-Sakar, A., Drubin, D. G., Nogales, E., & Barnes, G. (2006). The Dam1 kinetochore ring complex moves processively on depolymerizing microtubule ends. *Nature*, *440*(7083), 565–569. https://doi.org/10.1038/nature04409

Wimbish, R. T., DeLuca, K. F., Mick, J. E., Himes, J., Jiménez-Sánchez, I., Jeyaprakash, A. A., & DeLuca, J. G. (2020). The Hec1/Ndc80 tail domain is required for force generation at kinetochores, but is dispensable for kinetochore-microtubule attachment formation and Ska complex recruitment. *Molecular biology of the cell*, *31*(14), 1453–1473. https://doi.org/10.1091/mbc.E20-05-0286

Willems, E., Dedobbeleer, M., Digregorio, M., Lombard, A., Lumapat, P. N., & Rogister, B. (2018). The functional diversity of Aurora kinases: a comprehensive review. *Cell division*, *13*, 7. https://doi.org/10.1186/s13008-018-0040-6

Yamagishi, Y., Honda, T., Tanno, Y., & Watanabe, Y. (2010). Two histone marks establish the inner centromere and chromosome bi-orientation. *Science (New York, N.Y.)*, *330*(6001), 239–243. https://doi.org/10.1126/science.1194498

Yamagishi, Y., Yang, C. H., Tanno, Y., & Watanabe, Y. (2012). MPS1/Mph1 phosphorylates the kinetochore protein KNL1/Spc7 to recruit SAC components. *Nature cell biology*, *14*(7), 746–752. https://doi.org/10.1038/ncb2515

Yang, K. T., Li, S. K., Chang, C. C., Tang, C. J., Lin, Y. N., Lee, S. C., & Tang, T. K. (2010). Aurora-C kinase deficiency causes cytokinesis failure in meiosis I and production of large polyploid oocytes in mice. *Molecular biology of the cell*, *21*(14), 2371–2383. https://doi.org/10.1091/mbc.e10-02-0170

Ye, A.A., Deretic, J., Hoel, C.M., Hinman, A.W., Cimini, D., Welburn, J.P., and Maresca, T.J. (2015). Aurora A kinase contributes to a pole-based error correction pathway. *Curr. Biol.* 25, 1842–1851. https://doi.org/10.1016/j.cub.2015.06.021.

Ye, A.A., and Maresca, T.J. (2015). It's all relative: Centromere- versus pole-based error correction. *Cell Cycle* 14, 3777–3778. https://doi.org/10.1080/15384101.2015.1105701.

Yoo, T. Y., Choi, J. M., Conway, W., Yu, C. H., Pappu, R. V., & Needleman, D. J. (2018). Measuring NDC80 binding reveals the molecular basis of tension-dependent kinetochore-microtubule attachments. *eLife*, *7*, e36392. https://doi.org/10.7554/eLife.36392

Zahm, J.A., and Harrison, S.C. (2024). A communication hub for phosphoregulation of kinetochore-microtubule attachment. *Curr. Biol.* 34, 2308–2318.e6. https://doi.org/10.1016/j.cub.2024.04.067.

Zaytsev, A. V., Sundin, L. J., DeLuca, K. F., Grishchuk, E. L., & DeLuca, J. G. (2014). Accurate phosphoregulation of kinetochore-microtubule affinity requires unconstrained molecular interactions. *The Journal of cell biology*, *206*(1), 45–59. https://doi.org/10.1083/jcb.201312107

Zaytsev, A. V., Mick, J. E., Maslennikov, E., Nikashin, B., DeLuca, J. G., & Grishchuk, E. L. (2015). Multisite phosphorylation of the NDC80 complex gradually tunes its microtubule-

binding affinity. *Molecular biology of the cell*, *26*(10), 1829–1844. https://doi.org/10.1091/mbc.E14-11-1539

Zaytsev, A. V., & Grishchuk, E. L. (2015). Basic mechanism for biorientation of mitotic chromosomes is provided by the kinetochore geometry and indiscriminate turnover of kinetochore microtubules. *Molecular biology of the cell*, *26*(22), 3985–3998. https://doi.org/10.1091/mbc.E15-06-0384

Zhang, G., Kelstrup, C. D., Hu, X. W., Kaas Hansen, M. J., Singleton, M. R., Olsen, J. V., & Nilsson, J. (2012). The Ndc80 internal loop is required for recruitment of the Ska complex to establish end-on microtubule attachment to kinetochores. *Journal of cell science*, *125*(Pt 13), 3243–3253. https://doi.org/10.1242/jcs.104208

Zorba, A., Buosi, V., Kutter, S., Kern, N., Pontiggia, F., Cho, Y. J., & Kern, D. (2014). Molecular mechanism of Aurora A kinase autophosphorylation and its allosteric activation by TPX2. *eLife*, *3*, e02667. https://doi.org/10.7554/eLife.02667

APPENDIX

ORIGINAL PUBLICATION

RightsLink

Sign in/Register



Proximity-based activation of AURORA A by MPS1 potentiates error correction

Author:
Nelson Leça,Francisca Barbosa,Sergi Rodriguez-Calado,Arianna Esposito Verza,Margarida Moura,Paulo D. Pedroso,Inês Pinto,Elena Artes,Tanja Bange,Claudio E. Sunkel,Marin Barisic,Thomas J. Maresca,Carlos Conde

Publication: Current Biology

Publisher: Elsevier

Date: 21 April 2025

© 2025 Elsevier Inc. All rights are reserved, including those for text and data mining, AI training, and similar technologies.

Journal Author Rights

Please note that, as the author of this Elsevier article, you retain the right to include it in a thesis or dissertation, provided it is not published commercially. Permission is not required, but please ensure that you reference the journal as the original source. For more information on this and on your other retained rights, please visit: https://www.elsevier.com/about/our-business/policies/copyright#Author-rights

BACK CLOSE WINDOW

© 2025 Copyright - All Rights Reserved | Copyright Clearance Center, Inc. | Privacy statement | Data Security and Privacy | For California Residents | Terms and ConditionsComments? We would like to hear from you. E-mail us at customercare@copyright.com

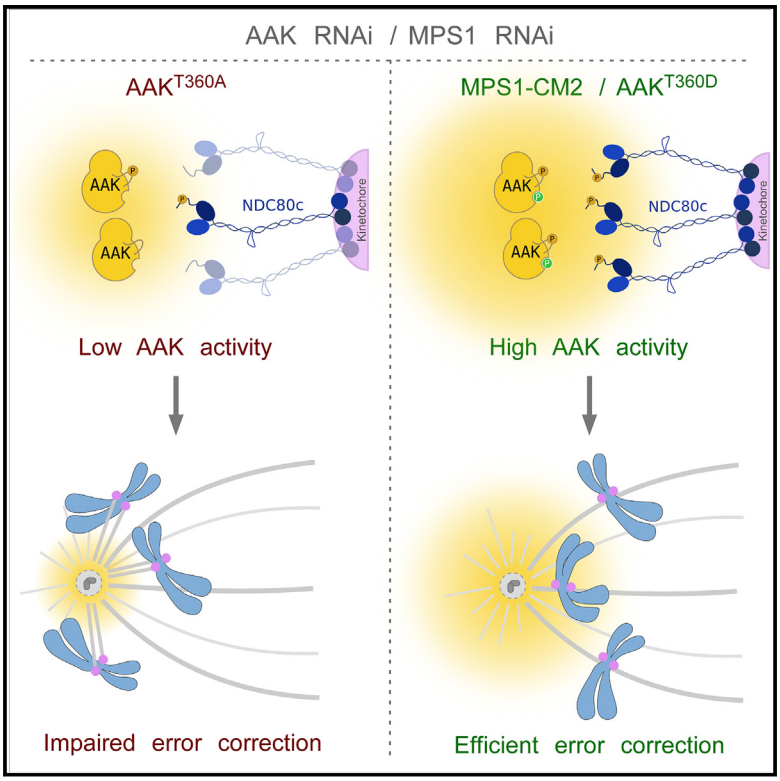
Privacy - Terms

Report

Current Biology

Proximity-based activation of AURORA A by MPS1 potentiates error correction

Graphical abstract



Authors

Nelson Leça, Francisca Barbosa, Sergi Rodriguez-Calado, ..., Marin Barisic, Thomas J. Maresca, Carlos Conde

Correspondence

tmaresca@umass.edu (T.J.M.), cconde@ibmc.up.pt (C.C.)

In brief

Leça et al. demonstrate that MPS1 on pole-proximal kinetochores phosphorylates AAK, enhancing its activation and potentiating a local gradient of AAK activity that destabilizes incorrect kinetochore-microtubule attachments. This finding highlights a crucial interplay between kinetochores and centrosomes in promoting error correction during mitosis.

Highlights

- Pole-proximal kinetochores activate centrosomal AAK in an MPS1-dependent manner
- MPS1 activates AAK through phosphorylation of a conserved residue at the C-lobe
- Potentiation of AAK by MPS1 ensures chromosome congression and error correction
- Proximity-based activation of AAK by MPS1 is conserved in human cells

Leça et al., 2025, Current Biology *35*, 1935–1947
April 21, 2025 © 2025 Elsevier Inc. All rights are reserved, including those for text and data mining, AI training, and similar technologies.
https://doi.org/10.1016/j.cub.2025.03.018

CellPress

Current Biology

CellPress

Report

Proximity-based activation of AURORA A by MPS1 potentiates error correction

Nelson Leça,[1,2,3] Francisca Barbosa,[1,2] Sergi Rodriguez-Calado,[4] Arianna Esposito Verza,[5] Margarida Moura,[1,2,3] Paulo D. Pedroso,[1,2] Inês Pinto,[1,2,3] Elena Artes,[6] Tanja Bange,[6] Claudio E. Sunkel,[1,2,7] Marin Barisic,[4,8] Thomas J. Maresca,[9,10,*] and Carlos Conde[1,2,7,11,*]

[1]i3S, Instituto de Investigação e Inovação em Saúde, Universidade do Porto, Rua Alfredo Allen 208, 4200-135 Porto, Portugal
[2]Instituto de Biologia Molecular e Celular, Universidade do Porto, Rua Alfredo Allen 208, 4200-135 Porto, Portugal
[3]Programa Doutoral em Biologia Molecular e Celular (MCbiology), Instituto de Ciências Biomédicas Abel Salazar (ICBAS), Rua de Jorge Viterbo Ferreira 228, 4050-313 Porto, Portugal
[4]Cell Division and Cytoskeleton, Danish Cancer Institute, Strandboulevarden 49, 2100 Copenhagen, Denmark
[5]Department of Mechanistic Cell Biology, Max-Planck-Institute of Molecular Physiology, Otto-Hahn-Str. 11, 44227 Dortmund, Germany
[6]Institute of Medical Psychology and Biomedical Center (BMC), Faculty of Medicine, Ludwig-Maximilians-Universität München, Goethestrasse 31, 80336 Munich, Germany
[7]Departamento de Biologia Molecular, ICBAS - Instituto de Ciências Biomédicas Abel Salazar, Rua de Jorge Viterbo Ferreira 228, 4050-313 Porto, Portugal
[8]Department of Cellular and Molecular Medicine, Faculty of Health and Medical Sciences, University of Copenhagen, Blegdamsvej 3B, 2200 Copenhagen, Denmark
[9]Biology Department, University of Massachusetts, 611 North Pleasant Street, Amherst, MA 01003-9297, USA
[10]Molecular and Cellular Biology Graduate Program, University of Massachusetts, 611 North Pleasant Street, Amherst, MA 01003-9297, USA
[11]Lead contact
*Correspondence: tmaresca@umass.edu (T.J.M.), cconde@ibmc.up.pt (C.C.)
https://doi.org/10.1016/j.cub.2025.03.018

SUMMARY

Faithful cell division relies on mitotic chromosomes becoming bioriented with each pair of sister kinetochores bound to microtubules oriented toward opposing spindle poles. Erroneous kinetochore-microtubule attachments often form during early mitosis but are destabilized through the phosphorylation of outer kinetochore proteins by centromeric AURORA B kinase (ABK) and centrosomal AURORA A kinase (AAK), thus allowing for re-establishment of attachments until biorientation is achieved.[1–9] MPS1-mediated phosphorylation of NDC80 has also been shown to directly weaken the kinetochore-microtubule interface in yeast.[10] In human cells, MPS1 has been proposed to transiently accumulate at end-on attached kinetochores[11] and phosphorylate SKA3 to promote microtubule release.[12] Whether MPS1 directly targets NDC80 and/or promotes the activity of AURORA kinases in metazoans remains unclear. Here, we report a novel mechanism involving communication between kinetochores and centrosomes, wherein MPS1 acts upstream of AAK to promote error correction. MPS1 on pole-proximal kinetochores phosphorylates the C-lobe of AAK, thereby increasing its activation at centrosomes. This proximity-based activation ensures the establishment of a robust AAK activity gradient that locally destabilizes mal-oriented kinetochores near spindle poles. Accordingly, MPS1 depletion from *Drosophila* cells causes severe chromosome misalignment and erroneous kinetochore-microtubule attachments, which can be rescued by tethering either MPS1 or constitutively active AAK mutants to centrosomes. Proximity-based activation of AAK by MPS1 also occurs in human cells to promote AAK-mediated phosphorylation of the NDC80 N-terminal tail. These findings uncover an MPS1-AAK crosstalk that is required for efficient error correction, showcasing the ability of kinetochores to modulate centrosome outputs to ensure proper chromosome segregation.

RESULTS

While it has long been appreciated that MPS1 contributes to error correction in human cells, defining whether it plays a direct or indirect role in the process has proven difficult. Initial evidence suggested that MPS1 could contribute to error correction indirectly via activation of centromeric AURORA B kinase (ABK)[13–15]; however, other studies concluded that MPS1 acted downstream of ABK[16] and reported that MPS1 inhibition did not reduce ABK's ability to phosphorylate known substrates in cells.[17,18] A direct role for kinetochore-associated MPS1 in error correction was later supported by the identification of kinetochore-microtubule attachment factors as MPS1 substrates in human and budding yeast. In humans, a pool of MPS1 localizes to end-on attached kinetochores prior to error correction[11] and MPS1-mediated phosphorylation of the SKA complex, which accumulates at end-on attachments to stabilize them, hinders its association with dynamic microtubules *in vitro*, and is required

All rights are reserved, including those for text and data mining, AI training, and similar technologies.

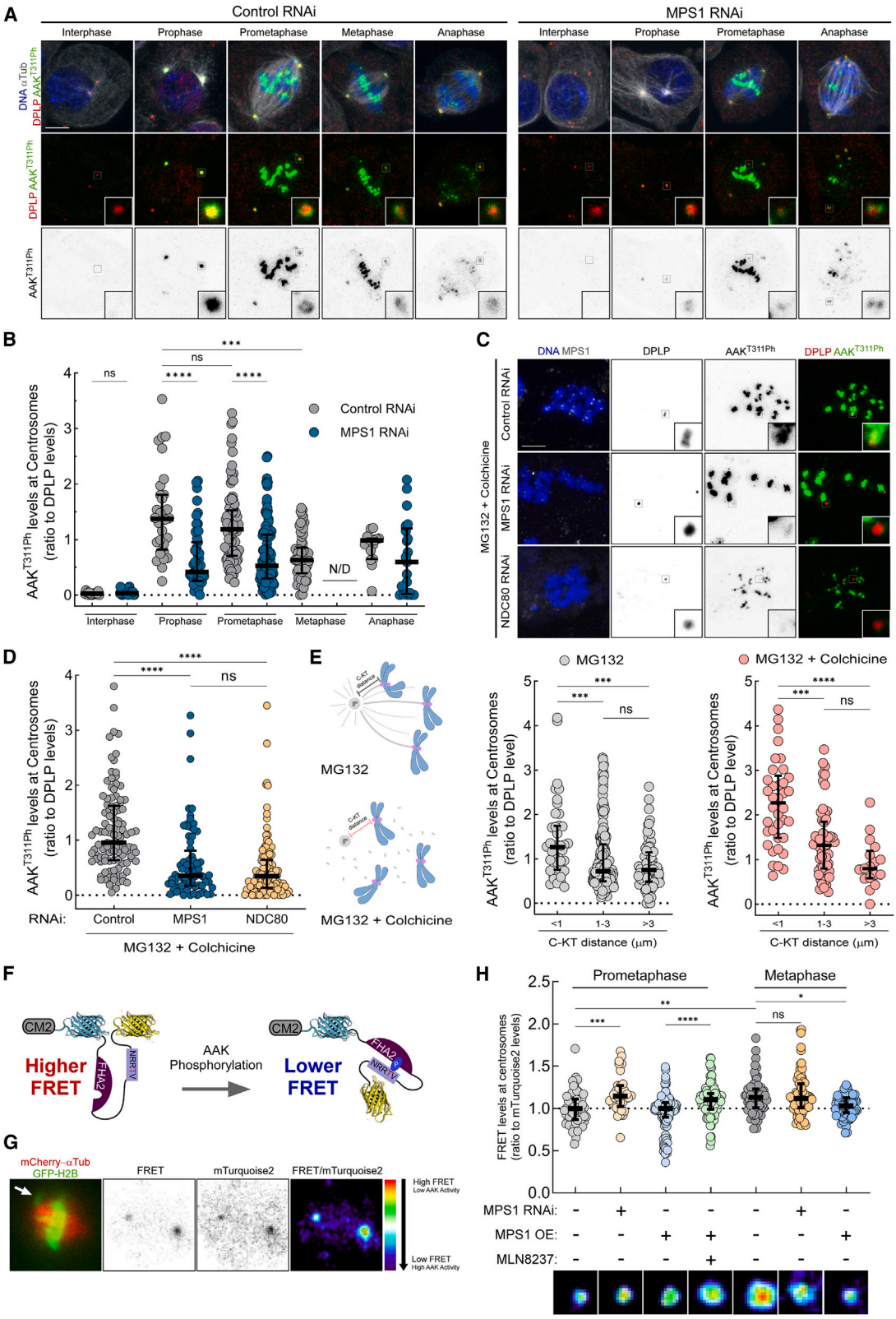


Figure 1. Polar chromosomes promote AAK activation at centrosomes in an MPS1-dependent manner

(A) Representative immunofluorescence images of AAK T311 phosphorylation (AAK^{T311Ph}) in control and MPS1-depleted *Drosophila* S2 cells in the indicated cell cycle stages. Insets depict magnifications of selected centrosomes.

(legend continued on next page)

for error correction in cells.[12] Similarly, in budding yeast, phosphorylation of the attachment factor NDC80 by kinetochore-associated MPS1 weakens the binding of kinetochore particles to microtubules *in vitro* and contributes to error correction and accurate chromosome segregation *in vivo*.[10] Thus, efficient error correction in yeast and humans relies on direct inputs from both MPS1 and AURORA kinases via phosphorylation of kinetochore-microtubule attachment factors. However, whether MPS1 directly targets NDC80 and/or promotes the activity of AURORA kinase in metazoans are open questions.

Drosophila melanogaster offers a unique model to further dissect error correction because key players in the pathway (MPS1, AURORA kinases, and the NDC80 complex) are conserved, but kinetochore composition in flies is divergent relative to human and budding yeast in notable ways. For example, flies do not have a functional SKA complex but, like humans, possess centrosome-enriched AURORA A kinase (AAK) and centromere/kinetochore-localized ABK, while budding yeast has a single AURORA kinase ortholog (Ipl1). AURORA kinases play a conserved role in error correction by targeting NDC80, but the localization of AAK and ABK imparts a spatial component to error correction that is likely absent in budding yeast. Indeed, AAK contributes to a polar error correction pathway in flies and mammals via phosphorylation of NDC80 at pole-proximal kinetochores.[7,8] In flies, MPS1 also localizes to microtubule-attached kinetochores,[19] but if it contributes to error correction, then it does so in the absence of the SKA complex and in the presence of spatial cues from AURORA kinases.

Polar chromosomes promote AAK activation at centrosomes in an MPS1-dependent manner

The activation status of AURORA kinases throughout the cell cycle was assessed in *D. melanogaster* S2 cells using antibodies against the phosphorylated T-loops of ABK (ABK^{T209Ph}) and AAK (AAK^{T311Ph}), the latter of which was distinguished from cross-reactive ABK^{T209Ph} by its colocalization with the *Drosophila* pericentrin-like protein (DPLP). Active AAK^{T311Ph} was undetectable at interphase centrosomes but increased significantly during mitosis, peaking in prophase and declining from prometaphase through metaphase and anaphase (Figures 1A and 1B). MG132-treated cells in prometaphase or co-treated with colchicine to depolymerize microtubules exhibited comparable levels of AAK^{T311Ph} that were significantly higher than AAK^{T311Ph} levels in MG132-arrested metaphase cells (Figures S1A and S1B). This suggests that AAK activation is increased by the presence of misaligned and unattached kinetochores, regardless of mitotic duration. Interestingly, robust activation of AAK required MPS1 activity as AAK^{T311Ph} levels at centrosomes remained low throughout mitosis in cells depleted of MPS1 relative to controls (Figures 1A, 1B, and S1C).

The effect of MPS1 depletion on AAK activation was next examined following depolymerization of microtubules with colchicine since MPS1 becomes enriched at unattached kinetochores via direct interaction with the NDC80 complex.[20–25] High levels of AAK^{T311Ph} were observed in control cells, but AAK activation was significantly compromised following depletion of either MPS1 or NDC80, which mislocalized MPS1 from kinetochores (Figures 1C, 1D, and S1D). Thus, kinetochore-associated MPS1 at misaligned and unattached kinetochores was required for the efficient activation of centrosomal AAK in mitosis. It was noteworthy that the effect of inhibiting MPS1 was specific to AAK because ABK^{T209Ph} levels at centromeres remained high throughout mitosis or following colchicine treatment in MPS1- and NDC80-depleted cells relative to control RNAi-treated cells (Figures S1E–S1H). Consistent with impaired AAK activity, the phosphorylation of D-TACC on S863, an established substrate of AAK,[26] and the accumulation of γ-tubulin[27–29] were reduced at centrosomes of MPS1-depleted prometaphase cells (Figures S1I–S1K).

(B) Quantification of the levels of AAK T311 phosphorylation (AAK^{T311Ph}) relative to DPLP at centrosomes of control and MPS1-depleted *Drosophila* S2 cells in the indicated cell cycle stages, as presented in (A). All values were normalized to the mean value determined for prometaphase control cells, which was set to 1. $n \geq 15$ centrosomes for each condition from 2 biological replicates.

(C) Representative immunofluorescence images of AAK T311 phosphorylation (AAK^{T311Ph}) in control, MPS1-depleted, or NDC80-depleted *Drosophila* S2 cells treated with 20 μM MG132 for 3 h and 30 μM colchicine for 2 h. Insets depict magnifications of selected centrosomes. Technical replicates were also stained for MPS1 and CID to quantify the kinetochore levels of MPS1. The quantification and the corresponding representative immunofluorescence images are presented in Figures S1D and S1E, respectively.

(D) Quantification of the levels of AAK T311 phosphorylation (AAK^{T311Ph}) relative to DPLP at centrosomes of control, MPS1-depleted, and NDC80-depleted *Drosophila* S2 cells treated with 20 μM MG132 for 3 h and 30 μM colchicine for 2 h in the indicated conditions, as presented in (C). All values were normalized to the mean value determined for control cells, which was set to 1. $n \geq 72$ centrosomes for each condition from 2 biological replicates.

(E) Quantification of the levels of AAK T311 phosphorylation (AAK^{T311Ph}) relative to DPLP at each centrosome versus the 3D distance between that centrosome and the closest kinetochore (measured as indicated in the schematic representation at the left) of control *Drosophila* S2 cells treated with 20 μM MG132 for 3 h or cells treated with and 20 μM MG132 for 3 h and 30 μM colchicine for 2 h, as presented in (Figures S1A and S1B). Centrosomes to kinetochore (C-KT) distances were organized in 3 different column ranges: less than 1 μm (<1), between 1 and 3 μm (1–3), and above 3 μm (>3). All values were normalized to the mean value determined for prometaphase control cells treated with 20 μM MG132 for 3 h, which was set to 1. $n \geq 17$ centrosomes for each condition from 2 biological replicates.

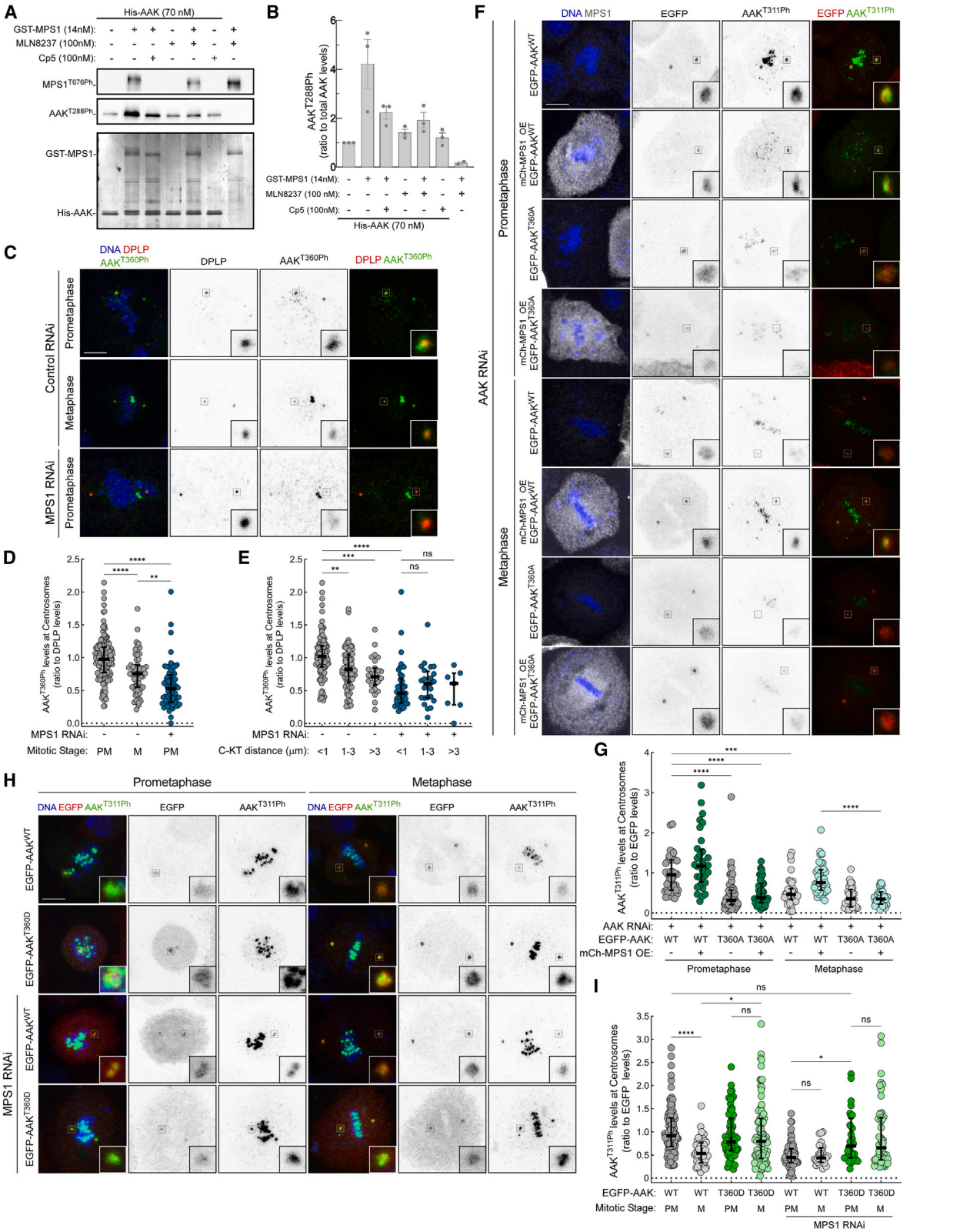
(F) Schematic of the centrosome-targeted CM2-AURORA FRET sensor used in (G) and (H).

(G) Representative images of the FRET reporter in a control cell with one polar chromosome (white arrow) near the left centrosome. The FRET emission ratio images "FRET/mTurquoise2" are pseudo-colored, according to the color wedge in display. All images are from a single selected Z-slice in the indicated channels.

(H) Quantification of the levels of FRET emission relative to total mTurquoise2 levels at centrosomes of cells and representative FRET emission ratio images FRET/mTurquoise2 pseudo-colored in the indicated conditions. All images are from a single selected Z-slice and depict magnifications of selected centrosomes from the indicated conditions. All values were normalized to the mean value determined for prometaphase control cells, which was set to 1. $n \geq 32$ centrosomes for each condition from 3 biological replicates.

Data in (B), (D), (E), and (H) are presented as median ± interquartile range. Statistical analysis was performed using a Kruskal-Wallis test for multiple comparisons. ns, not significant; $^{*}p < 0.05$, $^{**}p < 0.01$, $^{***}p < 0.001$, $^{****}p < 0.0001$. Scale bar, 5 μm.

See also Figure S1.



(legend on next page)

Centrosomal AAK^{T311Ph} levels were plotted as a function of distance to the nearest kinetochore to assess whether there was a spatial component to the MPS1-dependent activation of AAK. There was a clear correlation between the extent of AAK activation at centrosomes and proximity to kinetochores such that higher levels of centrosomal AAK^{T311Ph} were measured when kinetochores were present within an ~1 μm radius of the centrosome (Figure 1E). While the spatial effect was observed in both colchicine and untreated cells, the extent of kinetochore-proximal AAK activation was generally higher in colchicine-treated cells, consistent with there being elevated levels of MPS1 at unattached kinetochores.

A fluorescence resonance energy transfer (FRET)-based biosensor for AURORA kinase activity[8,30] was next used to study if MPS1-dependent activation of centrosomal AAK affected phosphorylation of downstream substrates. The reporter, which undergoes a conformational change upon phosphorylation that results in reduced FRET efficiency,[31] was tethered to centrosomes via an N-terminal fusion to the CM2 domain of centrosomin[32] (Figure 1F). Centrosome targeting put the reporter in close proximity to AAK, but higher phosphorylation (lower FRET) of the reporter was observed at centrosomes with nearby polar chromosomes (Figure 1G). Quantification of FRET emission ratios in prometaphase revealed a significant decrease in phosphorylation (higher FRET) of the reporter following MPS1 depletion (Figures 1H and S1C). FRET emission ratios were comparable in control and MPS1 overexpressing (MPS1 OE) prometaphase cells, suggesting that the centrosome-targeted sensor approaches maximal phosphorylation in prometaphase. Phosphorylation of the reporter in MPS1 OE prometaphase cells required AAK activity since treatment with the inhibitor MLN8237 at a concentration previously determined to specifically inhibit AAK in *Drosophila* S2 cells[8] decreased phosphorylation of the reporter to the same extent as that measured in MPS1-depleted cells (Figure 1H). Consistent with the prior observation of decreased AAK activation at centrosomes in metaphase (Figures 1A and 1B), the CM2-fused reporter exhibited reduced phosphorylation at metaphase centrosomes of control and MPS1-depleted cells (Figure 1H). However, overexpression of MPS1 increased phosphorylation of the reporter in metaphase to comparable levels as that measured in prometaphase cells (Figure 1H). Taken together, these findings support the conclusion that the proximity-based activation of AAK at centrosomes by MPS1 potentiates the phosphorylation of downstream AAK substrates.

MPS1-mediated phosphorylation of AAK C-lobe potentiates AAK auto-activation

In vitro kinase assays with purified human orthologs of His-AAK and GST-MPS1 were employed to gain mechanistic insights into how MPS1 activates AAK. Co-incubation of AAK with MPS1 resulted in an ~4-fold increase in the phosphorylation of AAK activation loop (AAK^{T288Ph}, equivalent to *Drosophila* AAK^{T311Ph}), which was reduced by half in the presence of the MPS1 inhibitor Cp5[33] (Figures 2A and 2B). The AAK inhibitor MLN8237 prevented MPS1-induced AAK activation, indicating that MPS1

Figure 2. MPS1-mediated phosphorylation of AAK C-lobe potentiates AAK auto-activation

(A) *In vitro* kinase assay with purified human orthologs of AAK and MPS1. Western blot analysis of human AAK T288 activating T-loop auto-phosphorylation (AAK^{T288Ph}) and human MPS1 T676 activating T-loop auto-phosphorylation (MPS1^{T676Ph}). Recombinant His6-AAK was incubated with 100 μM ATP during 30 min at 30°C in the indicated conditions. Total protein levels were assessed by gel silver staining.

(B) Quantification of human AAK T288 activating T-loop phosphorylation (AAK^{T288Ph}) blot intensity relative to total AAK levels in the indicated conditions, as presented in (A). All values were normalized to the mean value determined for basal AAK T288 phosphorylation, which was set to 1. The bars indicate the mean intensities, and the dots indicate the measurements from triplicates.

(C) Representative immunofluorescence images of AAK T360 phosphorylation (AAK^{T360Ph}) in prometaphase and metaphase control *Drosophila* S2 cells and prometaphase cells depleted of MPS1. Insets depict magnifications of selected centrosomes.

(D) Quantification of the levels of AAK T360 phosphorylation (AAK^{T360Ph}) relative to DPLP at centrosomes of prometaphase and metaphase control *Drosophila* S2 cells and prometaphase cells depleted of MPS1, as presented in (C). All values were normalized to the mean value determined for control prometaphase cells, which was set to 1. $n \geq 56$ centrosomes for each condition from 2 biological replicates.

(E) Quantification of the levels of AAK T360 phosphorylation (AAK^{T360Ph}) relative to DPLP at centrosomes of control *Drosophila* S2 cells and cells depleted of MPS1 in the indicated conditions. Centrosomes presented in (D) were organized in 3 different columns representing ranges of distance to the closest kinetochore: less than 1 μm (<1), between 1 and 3 μm (1–3), and above 3 μm (>3). All values were normalized to the mean value determined for control prometaphase cells, as presented in (D), which was set to 1. $n \geq 7$ centrosomes for each condition from 2 biological replicates.

(F) Representative immunofluorescence images of AAK T311 phosphorylation (AAK^{T311Ph}) in prometaphase or metaphase *Drosophila* S2 cells depleted of endogenous AAK and expressing EGFP-AAK^{WT} or EGFP-AAK^{T360A} in the indicated conditions. Insets depict magnifications of selected centrosomes. EGFP-AAK^{WT} cells expressing endogenous MPS1 or overexpressing mCherry-MPS1 (OE) were imaged in the same coverslip. EGFP-AAK^{T360A} cells expressing endogenous MPS1 or overexpressing mCherry-MPS1 (OE) were imaged in the same coverslip.

(G) Quantification of the levels of AAK T311 phosphorylation (AAK^{T311Ph}) relative to EGFP at centrosomes of prometaphase or metaphase *Drosophila* S2 cells depleted of endogenous AAK and expressing EGFP-AAK^{WT} or EGFP-AAK^{T360A} in the indicated conditions, as presented in (F). All values were normalized to the mean value determined for prometaphase cells expressing EGFP-AAK^{WT} and endogenous levels of MPS1, which was set to 1. $n \geq 32$ centrosomes for each condition from 2 biological replicates.

(H) Representative immunofluorescence images of AAK T311 phosphorylation (AAK^{T311Ph}) in prometaphase or metaphase *Drosophila* S2 cells expressing EGFP-AAK^{WT} or EGFP-AAK^{T360D} and expressing endogenous MPS1 or depleted of endogenous MPS1 in the indicated conditions. Insets depict magnifications of selected centrosomes.

(I) Quantification of the levels of AAK T311 phosphorylation (AAK^{T311Ph}) relative to EGFP at centrosomes of prometaphase or metaphase *Drosophila* S2 cells expressing EGFP-AAK^{WT} or EGFP-AAK^{T360D} and expressing endogenous MPS1 or depleted of endogenous MPS1 in the indicated conditions, as presented in (H). All values were normalized to the mean value determined for prometaphase cells expressing EGFP-AAK^{WT} and endogenous levels of MPS1, which was set to 1. $n \geq 27$ centrosomes for each condition from 2 biological replicates.

Data in (B) are presented as mean ± SD and in (D), (E), (G), and (I) are presented as median ± interquartile range. Statistical analysis in (D), (E), (G), and (I) was performed using a Kruskal-Wallis test for multiple comparisons. ns, not significant; $^{*}p < 0.05$, $^{**}p < 0.01$, $^{***}p < 0.001$, $^{****}p < 0.0001$. Scale bar, 5 μm.

See also Figure S2.

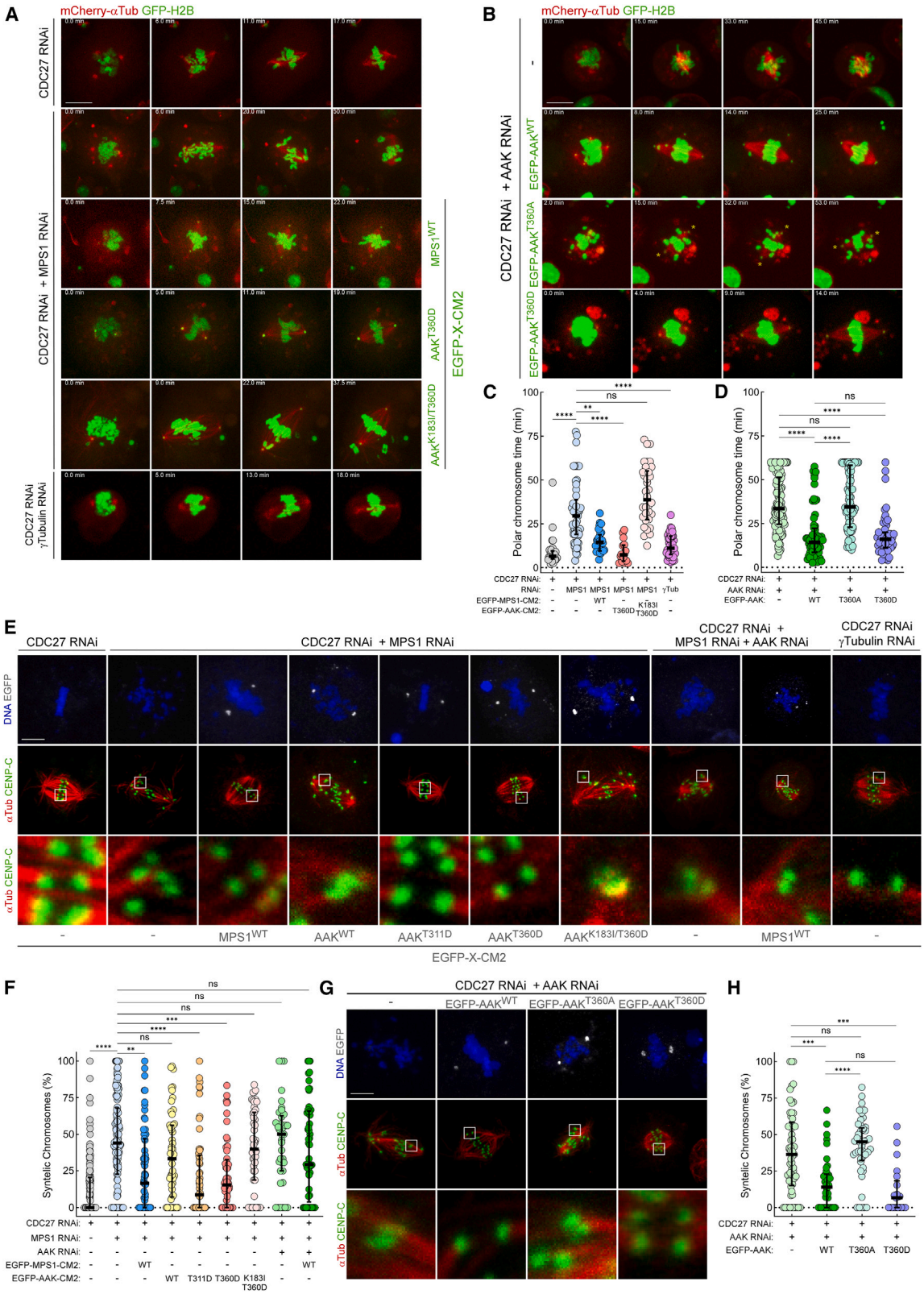


Figure 3. Activation of AAK by MPS1 is required for efficient error correction and chromosome congression

(A) Selected stills of representative mitotic progression movies of CDC27-depleted, CDC27/MPS1 co-depleted, or CDC27/γ-tubulin co-depleted *Drosophila* S2 cells stably expressing GFP-H2B, mCherry-α-tubulin, and the indicated EGFP-tagged and CM2-fused transgenes (EGFP-X-CM2).

(legend continued on next page)

CellPress

does not directly phosphorylate the T-loop (T288) but rather stimulates its auto-phosphorylation. Mass spectrometry of *in vitro* phosphorylated AAK identified a putative MPS1 target site located at a conserved residue (T337/T360 in human and *Drosophila* AAK, respectively) that is predicted by AlphaFold3 to be positioned in the C-lobe αG-helix with close proximity to the T-loop (Figures S2A–S2C). We raised a phospho-specific antibody that confirmed by immunoblotting the phosphorylation of AAK^{WT} at T337 (T337Ph) upon incubation with MPS1 *in vitro* (Figure S2D). As expected, the T337Ph signal failed to be detected when T337 was converted to alanine (AAK^{T337A}) or when Cp5 was added to the reaction (Figure S2D). To test if MPS1 phosphorylates AAK at T360 in *Drosophila* S2 cells, we used the phospho-specific antibody for immunofluorescence analysis. Centrosomal signal of T360 phosphorylation (T360Ph) was readily detected in prometaphase cells but became significantly reduced in metaphase or upon depletion of MPS1 (Figures 2C and 2D). Mirroring AAK T-loop activation, the levels of T360Ph at centrosomes were positively correlated with the proximity of kinetochores in an MPS1-dependent manner (Figures 2C and 2E). Depleting AAK, or replacing the endogenous protein with an unphosphorylatable mutant for T360 (T360A), also compromised T360Ph staining, which further validated the specificity of the antibody in S2 cells (Figures S2E and S2F). Collectively, these results support the conclusion that centrosomal AAK is phosphorylated at T360 by kinetochore-proximal MPS1.

A series of cell-based assays were next employed to test whether MPS1 stimulates AAK auto-phosphorylation of the T-loop (AAK^{T311Ph}) via phosphorylation of T360 in S2 cells. Consistent with the FRET results, OE MPS1 caused a significant increase in AAK^{T311Ph} at metaphase centrosomes relative to controls (Figures S2G and S2H). Loss of AAK activation upon MPS1 OE in AAK-depleted cells (Figures S2G and S2H) could be rescued by expression of wild type (WT) but not kinase-dead (K183I) AAK (Figures S2I and S2J). Importantly, expression of the AAK non-phosphorylatable T360A mutant (AAK^{T360A}), predicted to have a similar structure as AAK^{WT} (Figure S2K), also failed to rescue MPS1-mediated activation of AAK in either prometaphase or metaphase cells (Figures 2F and 2G). Conversely, the phospho-mimetic mutation of T360 to aspartic acid (AAK^{T360D}) was sufficient to retain elevated levels of AAK T-loop phosphorylation in metaphase and restore AAK activation in prometaphase cells depleted of MPS1 (Figures 2H and 2I). Thus, phosphorylation of the conserved AAK T360 residue by MPS1 promotes auto-phosphorylation of the AAK T-loop (T311) and hence efficient kinase activation *in vitro* and in cells.

Activation of AAK by MPS1 is required for efficient error correction and chromosome congression

The functional contributions of proximity-based activation of AAK by MPS1 to cell division were evaluated by live- and fixed-cell analyses of mitotic S2 cells. To isolate potential chromosome alignment and error correction functions of MPS1 from its role as a checkpoint kinase in *D. melanogaster*,[34] cells were arrested in mitosis via RNAi of the APC/C subunit CDC27.[35–37] Cells efficiently aligned their chromosomes on a metaphase plate upon depletion of CDC27; however, co-depleting MPS1 impaired timely chromosome congression and increased the abundance of persistent polar chromosomes (Figures 3A and 3C; Video S1). The congression defect in CDC27/MPS1 co-depleted cells was rescued by centrosomal targeting (via C-terminal fusions to CM2) of either WT MPS1 (MPS1^{WT}-CM2) or a phospho-mimetic mutant of AAK in which the previously identified MPS1 site (T360) was mutated to aspartic acid (AAK^{T360D}-CM2) (Figures 3A and 3C; Video S2). The rescue of chromosome alignment required AAK kinase activity since cells expressing a kinase-dead (K183I) version of AAK^{T360D}-CM2 (AAK$^{K183I/T360D}$-CM2) failed to effectively congress their chromosomes (Figures 3A and 3C; Video S2). As expected, co-depletion of AAK and CDC27 delayed chromosome congression (Figures 3B and 3D; Video S3). This defect was rescued by the expression of EGFP-AAK^{WT} and EGFP-AAK^{T360D} but not by the non-phosphorylatable T360A AAK mutant (EGFP-AAK^{T360A}) (Figures 3B and 3D; Video S3). These results support the conclusion that MPS1-mediated phosphorylation of AAK T360 is required for efficient chromosome congression.

The attachment status of kinetochores was next assessed by analyzing confocal Z-sections of chromosomes (DAPI), kinetochores (CENP-C), and microtubules (α-tubulin) in calcium-treated fixed cells to assess error correction (Figures 3E–3H and S3A–S3D). Chromosomes were scored as (1) bioriented when each sister kinetochore was clearly associated with

(B) Selected stills of representative mitotic progression movies of CDC27/AAK co-depleted *Drosophila* S2 cells stably expressing GFP-H2B, mCherry-α-tubulin, and the indicated transgenes. Asterisks indicate the centrosomes in the EGFP-AAK^{T360A} condition.
(C) Quantifications of the congression time of individual polar chromosomes (time each chromosome was retained near the spindle pole) in the conditions indicated in (A). $n \geq 16$ polar chromosomes followed through time for each condition from at least 2 biological replicates.
(D) Quantifications of the congression time of individual polar chromosomes (time each chromosome was retained near the spindle pole) in the conditions indicated in (B). $n \geq 51$ polar chromosomes followed through time for each condition from at least 3 biological replicates.
(E) Representative immunofluorescence images of mitotic *Drosophila* S2 cells expressing the indicated EGFP-tagged and CM2-fused transgenes (EGFP-X-CM2) and depleted of the indicated proteins. Insets depict magnifications of selected Z-steps of sister-kinetochores in amphitelic or syntelic attachment configurations.
(F) Percentage of syntelic kinetochore-microtubule attachments per cell in the indicated conditions, as presented in (E). Data corresponding to CDC27/γ-tubulin co-depleted cells are presented in Figure S3H. $n \geq 36$ cells for each condition from at least 2 biological replicates.
(G) Representative immunofluorescence images of CDC27/AAK co-depleted *Drosophila* S2 cells expressing EGFP-tagged AAK^{WT}, AAK^{T360A}, and AAK^{T360D}. Insets depict magnifications of selected Z-steps of sister-kinetochores in amphitelic or syntelic attachment configurations.
(H) Percentage of syntelic kinetochore-microtubule attachments per cell in the indicated conditions, as presented in (G). $n \geq 21$ cells for each condition from at least 2 biological replicates.
Data in (C), (D), (F), and (H) are presented as median ± interquartile range. Statistical analysis was performed using a Kruskal-Wallis test for multiple comparisons. ns, not significant; *$p < 0.05$, **$p < 0.01$, ***$p < 0.001$, ****$p < 0.0001$. Scale bar, 5 μm.
See also Figure S3 and Videos S1, S2, and S3.

microtubules oriented toward opposing spindle poles, (2) syntelic when sister kinetochore pairs were clearly attached to microtubules from the same spindle pole, and (3) pinned when the kinetochore pair was within 1 μm of the spindle pole regardless of whether its attachment status could be clearly discerned. While a vast majority of chromosomes were bioriented in CDC27-depleted cells, co-depletion of CDC27 and MPS1 resulted in a significant increase in the frequency of syntelic and pinned chromosomes, revealing that MPS1 is required for error correction in fly cells (Figures 3E, 3F, S3A, and S3B). The error correction defect in CDC27/MPS1 RNAi cells could be rescued by expressing centrosome-tethered MPS1^{WT}-CM2 but not AAK^{WT}-CM2 (Figures 3E, 3F, S3A, and S3B). Co-depletion of AAK hindered MPS1^{WT}-CM2 capacity to promote chromosome alignment and biorientation, further supporting the conclusion that MPS1 acts upstream of AAK in the pole-based error correction pathway (Figures 3E, 3F, S3A, and S3B). The requirement for MPS1 to potentiate AAK-mediated error correction could be bypassed in CDC27/MPS1 co-depleted cells by centrosomal targeting of either the T-loop (T311D) or C-lobe (T360D) AAK-CM2 phospho-mimetic mutants but not the catalytic dead AAK$^{K183I/T360D}$-CM2 version (Figures 3E, 3F, S3A, and S3B).

To directly test the requirement of AAK T360 phosphorylation for error correction, we co-depleted CDC27 and endogenous AAK and evaluated kinetochore-microtubule attachments upon the expression of untethered versions of AAK. Contrasting with EGFP-AAK^{WT} and EGFP-AAK^{T360D}, the non-phosphorylatable EGFP-AAK^{T360A} mutant failed to restore chromosome biorientation and alignment in S2 cells depleted of endogenous AAK (Figures 3G, 3H, S3C, and S3D). Given that MPS1 depletion hindered the accumulation of γ-tubulin and D-TACC^{S863} phosphorylation at centrosomes (Figures S1I–S1K), it was possible that the mitotic defects observed in the absence of MPS1-dependent AAK activation stemmed from an attenuation of centrosome maturation and function. However, S2 cells partially depleted of γ-tubulin, which formed abnormal mitotic spindles (Figure 3A) but maintained robust AAK activation (Figures S3E–S3G), successfully aligned their chromosomes and established proper kinetochore-microtubule attachments as efficiently as control cells (Figures 3A, 3C, and S3H–S3J; Video S1). This finding suggests that compromised microtubule nucleation and polymerization at the centrosome play a minor role in the observed accumulation of erroneous kinetochore-microtubule attachments and chromosome misalignment in S2 cells that fail to fully activate AAK.

Collectively, the data demonstrate that the AAK-mediated error correction pathway is impaired in cells depleted of MPS1 or expressing AAK harboring the T360A mutation. AAK targets a number of the same sites on the N-terminal tail of NDC80 as ABK, but S69 on HEC1 (human NDC80) is preferentially phosphorylated by AAK.[9] Thus, we used a phospho-specific antibody against the equivalent phosphorylation on *Drosophila* NDC80 (NDC80^{S67Ph}) to evaluate whether it requires MPS1-mediated phosphorylation of AAK T360. Kinetochore levels of NDC80^{S67Ph} were elevated in prometaphase cells and decreased as chromosomes congressed to the metaphase plate (Figures S3K and S3L). Consistent with impaired error correction, depletion of MPS1 or expression of the EGFP-AAK^{T360A} mutant significantly compromised the phosphorylation of NDC80 at S67 regardless of kinetochore proximity to the spindle pole (Figures S3K–S3M). To test whether MPS1 directly potentiates AAK-mediated phosphorylation of NDC80/HEC1 N-terminal tail, we performed an *in vitro* kinase assay with recombinant bonsai NDC80 complex as a substrate[38] and probed for the phosphorylation of HEC1 at S55, another well-established AAK phosphorylation site.[9] In accordance with its activation status, AAK capacity to phosphorylate S55 increased dramatically when co-incubated with MPS1 (Figures S3N and S3O). These findings support the conclusion that pole-based error correction in fly cells is carried out by AAK activated via phosphorylation of its C-lobe (T360) by MPS1 and further validate results from the FRET reporter, indicating that phosphorylation of downstream AAK targets is potentiated by MPS1.

Proximity-based activation of AAK by MPS1 is conserved in human cells

To examine if proximity-based activation of AAK by MPS1 is conserved outside *D. melanogaster*, the extent of AAK activation was evaluated under experimental conditions where the positioning of kinetochores relative to centrosomes/spindle poles could be manipulated in human RPE-1 cells.[39] When compared with control monopolar spindles (S-trityl-L-cysteine [STLC] treatment), kinetochores were positioned closer to the monopole center upon inhibition of the kinetochore-associated motor CENP-E with GSK923295 (CENP-Ei), while depletion of the Dynein adaptor Spindly (siSpindly) positioned kinetochores further from the monopole center (Figures 4A–4C). Consistent with there being spatial crosstalk between kinetochores and centrosomes, AAK activation (AAK^{T288Ph}) levels at centrosomes/spindle poles were significantly increased in the CENP-Ei cells and significantly reduced in the siSpindly cells relative to control cells (Figures 4D and 4E). Active AAK^{T288Ph} signal at centrosomes was significantly reduced compared with controls in nocodazole- (Figures S4A and S4B) and STLC-treated cells (Figures 4F and 4G) when MPS1 was inhibited with Cp5 (MPS1i). Importantly, inhibiting MPS1 prevented the increase in AAK activation in CENP-Ei monopoles (Figures 4F and 4G). Thus, the potentiation in AAK activation observed when kinetochores were positioned closer to centrosomes in human RPE-1 cells required MPS1 activity. Accordingly, the activation of AAK at centrosomes during an unperturbed mitosis peaked in prometaphase in an MPS1-dependent manner and decreased significantly in metaphase (Figures S4C and S4D). While the observations of centrosomal AAK activation in RPE-1 cells were broadly consistent with those from fly cells, one notable difference was in prophase cells, where AAK activation at centrosomes was high in fly cells but low in RPE-1 cells (Figures S4C and S4D). It is unclear why this is the case or if the AAK activation status fulfills unique prophase functions in fly versus human cells.

We then measured the extent of HEC1 phosphorylation at S69 (HEC1^{S69Ph}) as a function of kinetochore positioning within monopolar spindles. Consistent with the extent of AAK activation (AAK^{T288Ph} levels), phosphorylation of HEC1-S69 was increased in CENP-Ei cells and reduced in siSpindly cells relative to controls (Figures 4H and 4I). In nocodazole-treated cells, HEC1^{S69Ph} levels were reduced to the same extent following inhibition of either MPS1 or AAK and to a lesser extent upon ABK

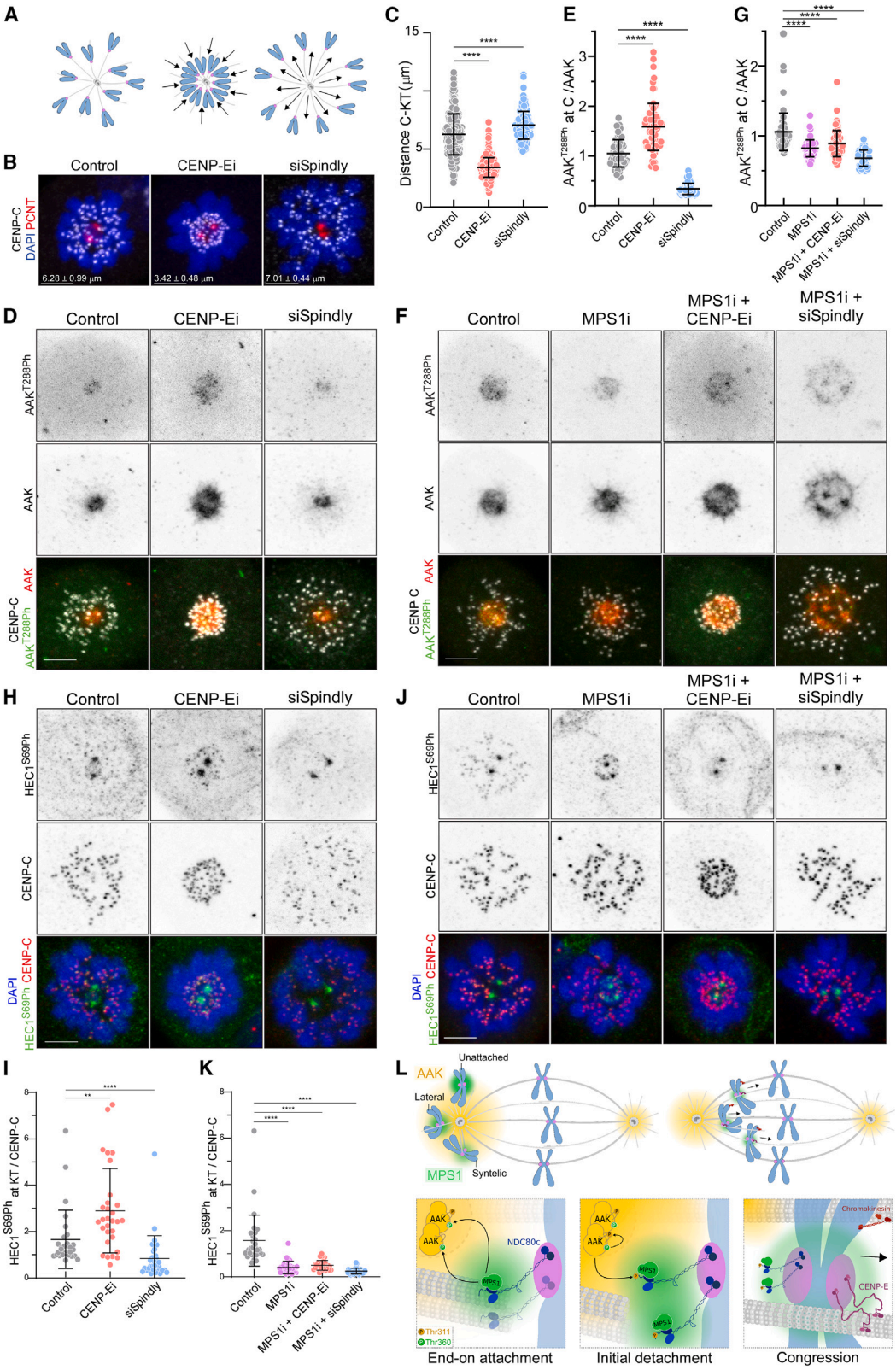


Figure 4. Proximity-based activation of AAK by MPS1 is conserved in human cells

(A) Schematic representation of the monopolar spindle assay used to assess AAK^{T288Ph} and HEC1^{S69Ph} changes in response to the distance between centrosomes and kinetochores.

(legend continued on next page)

inhibition, reflecting an upstream role of MPS1 in the preferential phosphorylation of HEC1-S69 by AAK (Figures S4E and S4F). Importantly, HEC1^{S69Ph} levels were significantly reduced when MPS1 was inhibited, including in CENP-Ei cells that normally exhibited a significant increase in HEC1^{S69Ph} levels (Figures 4J and 4K). Altogether, the data support the conclusion that kinetochore proximity-based activation of AAK by MPS1 potentiates phosphorylation of the bona fide error correction substrate HEC1 in human cells.

DISCUSSION

We propose a model whereby a proximity-dependent crosstalk between kinetochores and centrosomes/spindle poles promotes error correction (Figure 4L). The model envisions that as erroneous kinetochore-microtubule interactions (e.g., a syntelic attachment) become positioned within the vicinity (~1 μm) of the spindle pole, kinetochore-recruited MPS1 phosphorylates AAK on a conserved site (T360 in flies) located in the αG-helix of the kinase C-lobe. Phosphorylation of the C-lobe, in turn, triggers auto-catalytic phosphorylation of the AAK T-loop to amplify an ~2 μm radius activity gradient[7,8,40] to locally promote microtubule detachment via phosphorylation of kinetochore substrates such as the NDC80 complex. AlphaFold3 predicts that phosphorylation of T360 causes an outward stretch of the αG-helix that pulls on the T-loop by interacting with D317 in a manner that could render the T-loop more flexible and leave the activating T311 more exposed for phosphorylation (Figures S2L–S2N). Further investigation into the structural basis of this novel activation mechanism is warranted.

It has been proposed that the establishment of stable end-on attachments prevents recruitment of MPS1 to kinetochores because of mutually exclusive binding to either microtubules or MPS1 by the CH-domains of the NDC80 complex.[20–22] However, a pool of MPS1 still localizes to microtubule-attached kinetochores either through association with the NDC80 complex or other kinetochore receptors.[11,19] Three recent studies in budding yeast showed that MPS1 binds to regions in the CH-domains of the NDC80 complex that are on the opposite side of the microtubule binding region[23–25] and, accordingly, purified budding yeast NDC80 complex was shown to simultaneously bind microtubules and MPS1 *in vitro*.[24] It has been suggested that this interaction interface is conserved.[25] If so, then this mechanism could explain how a population of MPS1 remains at microtubule-attached metazoan kinetochores. Regardless of how it is recruited, we hypothesize that the residual MPS1 population on erroneously attached polar kinetochores activates AAK to promote their own correction.

An interesting feature of the crosstalk pathway described here is that it contains an intrinsic positive feedback loop since the destabilization of kinetochore-microtubule interactions by AAK-mediated phosphorylation of NDC80 would recruit more MPS1. Such a spatio-chemical feedback loop would heavily disfavor the production of end-on attached kinetochores in the vicinity of spindle poles. Thus, we speculate that MPS1-driven potentiation of AAK activity following nuclear envelope breakdown is important to minimize the formation of end-on attachments near the centrosomes, where syntelic attachments would otherwise be prone to accumulate due to the high density of nucleated microtubules. Instead, robust activation of AAK favors the formation of lateral attachments and facilitates motor activation of CENP-E[41] to ensure timely chromosome congression toward the cell equator, where amphitelic attachments can form synchronously as a result of interactions between non-centrosomal short microtubules

(B) Representative immunofluorescence images of STLC-treated RPE-1 cells in control, CENP-E inhibited (CENP-Ei), and Spindly depleted (siSpindly) conditions.
(C) Quantification of centrosome (PCNT)-kinetochore (CENP-C) (C-KT) distances of STLC-treated RPE-1 cells in the indicated conditions, as presented in (B).
(D) Representative immunofluorescence images of AAK T288 phosphorylation (AAK^{T288Ph}) and AAK levels in STLC-treated RPE-1 cells in control, CENP-E inhibited (CENP-Ei), and Spindly depleted (siSpindly) conditions.
(E) Quantification of the levels of AAK T288 phosphorylation (AAK^{T288Ph}) relative to total AAK levels at centrosomes of STLC-treated RPE-1 cells in the indicated conditions, as presented in (D). All values were normalized to the median value determined for control cells, which was set to 1.
(F) Representative immunofluorescence images of AAK T288 phosphorylation (AAK^{T288Ph}) and AAK levels in STLC-treated RPE-1 cells in control, MPS1 inhibited (MPS1i), MPS1/CENP-E co-inhibited (MPS1i + CENP-Ei), and MPS1 inhibited in Spindly depleted background (MPS1i + siSpindly). In all conditions, the proteasome was inhibited with MG132.
(G) Quantification of the levels of AAK T288 phosphorylation (AAK^{T288Ph}) relative to total AAK levels at centrosomes of STLC-treated RPE-1 cells in the indicated conditions, as presented in (F). All values were normalized to the median value determined for control cells, which was set to 1.
(H) Representative immunofluorescence images of HEC1 S69 phosphorylation (HEC1^{S69Ph}) and CENP-C levels in STLC-treated RPE-1 cells in control, CENP-E inhibited (CENP-Ei), and Spindly depleted (siSpindly) conditions.
(I) Quantification of the levels of HEC1 S69 phosphorylation (HEC1^{S69Ph}) relative to CENP-C levels at kinetochores of STLC-treated RPE-1 cells in the indicated conditions, as presented in (H). All values were normalized to the median value determined for control cells, which was set to 1.
(J) Representative immunofluorescence images of HEC1 S69 phosphorylation (HEC1^{S69Ph}) and CENP-C levels in STLC-treated RPE-1 cells in control, MPS1 inhibited (MPS1i), MPS1/CENP-E co-inhibited (MPS1i + CENP-Ei), and MPS1 inhibited in Spindly depleted background (MPS1i + siSpindly). In all conditions the proteasome was inhibited with MG132.
(K) Quantification of the levels of HEC1 S69 phosphorylation (HEC1^{S69Ph}) relative to CENP-C levels at kinetochores of STLC-treated RPE-1 cells the indicated conditions, as presented in (J). All values were normalized to the median value determined for control cells, which was set to 1.
(L) Proposed model for proximity-based activation of AAK by MPS1 as a strategy to potentiate error correction of polar chromosomes and ensure chromosome congression. A pool of MPS1 recruited to kinetochores of polar chromosomes indirectly contributes to pole-based error correction by phosphorylating AAK on the conserved residue T360. This potentiates AAK activation at centrosomes and thereby its capacity to phosphorylate the N-terminal tail of HEC1/NDC80 at kinetochores to destabilize end-on attachments. This mechanism corrects and prevents syntelic kinetochore-microtubule interactions in the vicinity of centrosomes and ensures efficient chromosome congression.
Data are presented in (C), (E), (G), (I), and (K) as mean ± SD. Statistical analysis was performed using a Mann-Whitney non-parametric t test. ns, not significant; $^{*}p < 0.05$, $^{**}p < 0.01$, $^{***}p < 0.001$, $^{****}p < 0.0001$. $n \geq 75$ cells for each condition. Scale bar, 5 μm.
See also Figure S4.

emanating from kinetochores and bundles of antiparallel microtubules.[42–44]

Overall, our findings support the conclusion that a pool of MPS1 at kinetochores indirectly contributes to pole-based error correction. This model is consistent with an earlier proposal that MPS1 plays an indirect role in error correction, with a notable difference being that the relevant downstream target of MPS1 is AAK rather than ABK.[13–15] MPS1 clearly activated AAK in our cell-based assays, but consistent with prior findings,[16–18] we did not see evidence of MPS1-mediated ABK activation in cells despite the facts that (1) the centromere/kinetochore-localized ABK is closer than centrosomal AAK to kinetochore-bound MPS1, (2) the C-lobe threonine is present in ABK αG-helix, and (3) ABK is phosphorylated and activated by MPS1 *in vitro* (data not shown). Since constitutive ABK activation would be detrimental to forming stable attachments, kinetochore/centromere-associated protein phosphatases likely protect ABK from MPS1-mediated activation in cells. Direct and indirect roles for MPS1 in error correction need not be mutually exclusive. In fact, it now appears that diverse organisms rely on each mechanism to different extents in carrying out error correction. Budding yeast utilize MPS1 to directly target the NDC80 complex without indirectly inducing error correction through activation of AURORA kinase.[10] Conversely, our work shows that activation of AAK-mediated error correction by kinetochore-recruited MPS1 is the dominant pathway in flies, although a direct role for MPS1 in error correction cannot be ruled out. Since we observed proximity-based activation of AAK by MPS1 in RPE-1 cells, efficient error correction in humans likely requires both indirect and direct pathways via MPS1-mediated phosphorylation of AAK and kinetochore-microtubule attachment factors, respectively. Future efforts to dissect the relative contributions of direct versus indirect roles of MPS1 in error correction are warranted, but the findings presented here define a novel and conserved mechanism by which polar kinetochores modulate centrosome-based activities to promote accurate chromosome segregation.

RESOURCE AVAILABILITY

Lead contact

Further information and requests for resources and reagents should be directed to and will be fulfilled by the lead contact, Carlos Conde (cconde@ibmc.up.pt).

Materials availability

All unique/stable reagents generated in this study will be made available on request.

Data and code availability

The mass spectrometry proteomics data have been deposited in the ProteomeXchange Consortium via the PRIDE[45] partner repository with the dataset identifier PRIDE: PXD056173. This study did not generate code.

ACKNOWLEDGMENTS

We thank Geert Kops, Jennifer DeLuca, Mónica Bettencourt-Dias, René Medema, Christian Lehner, and Scott Hawley for reagents. We thank Andrea Musacchio for critically discussing the data. Work in C.C.'s and C.E.S.'s lab was funded by National Funds through FCT—Fundação para a Ciência e a Tecnologia, I.P., under the project UIDB/04293/2020 and by the project "Cancer Research on Therapy Resistance: From Basic Mechanisms to Novel Targets" – NORTE-01-0145-FEDER-000051, supported by Norte Portugal Regional Operational Programme (NORTE 2020), under the PORTUGAL 2020 Partnership Agreement, through the European Regional Development Fund (ERDF). C.C. was supported by a Scientific Employment Stimulus contract (2020.00067.CEECIND) from Fundação para a Ciência e a Tecnologia. N.L. (SFRH/BD/136526/2018), M.M. (SFRH/BD/123306/2016), and I.P. (2024.02612.BD) were supported by PhD fellowships from Fundação para a Ciência e a Tecnologia. This work was supported by an NIH grant (GM107026) to T.J.M. International collaboration was supported with Fulbright Awards to T.J.M. and N.L. Work in T.B.'s lab was supported by funding from the Deutsche Forschungsgemeinschaft (DFG) (project number: 5041140321) and from the Friedrich-Baur Stiftung. T.B. is also thankful for funding by LMU Munich's Institutional Strategy LMUexcellent within the framework of the German Excellence Initiative and MS instrumentation by the DFG (INST 86/1800-1 FUGG for MSR). Work in M.B.'s lab was supported by the Novo Nordisk Foundation (NNF19OC0058504), the Independent Research Fund Denmark (3101-00075B), and the Lundbeck Foundation (R434-2023-431). The authors acknowledge the i3S Scientific Platform ALM, member of the national infrastructure Portuguese Platform of Bioimaging, for excellent support.

AUTHOR CONTRIBUTIONS

C.C. conceptualized the study, and T.J.M. wrote the original manuscript draft with contributions from C.C. C.C. and T.J.M. coordinated the work. C.C. designed the experiments, with contributions from N.L., C.E.S., M.B., and T.J.M. Data acquisition: N.L. performed the major experiments presented in Figures 1, 2, 3, and S1–S3, with contributions from F.B., M.M., and I.P.; S.R.-C. performed the experiments presented in Figures 4 and S4; E.A. and T.B. performed the mass spectrometry analysis; and P.D.P. generated the Alphafold models. Data analysis and interpretation, N.L., F.B., M.M., P.D.P., I.P., A.E.V., E.A., T.B., C.E.S., M.B., T.J.M., and C.C. Supervision, C.E.S., M.B., T.J.M., and C.C. Funding acquisition, C.E.S., T.B., M.B., T.J.M., and C.C. N.L. assembled Figures 1, 2, 3, and S1–S3 and Videos S1, S2, and S3, and S.R.-C. and M.B. assembled Figures 4 and S4. All authors reviewed the manuscript and agreed with its contents.

DECLARATION OF INTERESTS

The authors declare no competing interests.

STAR★METHODS

Detailed methods are provided in the online version of this paper and include the following:

- KEY RESOURCES TABLE
- EXPERIMENTAL MODELS AND STUDY PARTICIPANT DETAILS
  - *Drosophila* Cell Lines
  - Human Cell Lines
- METHOD DETAILS
  - RNAi-mediated depletion and drug treatments
  - Transgene constructs and S2 cell transfection
  - FRET-based AURORA kinase sensor
  - Live cell imaging
  - Immunofluorescence imaging and analysis
  - Antibodies
  - Recombinant Protein Production
  - *In vitro* kinase assay and mass-spectrometry
  - *In vitro* AAK T337/T360 antibody validation
  - NDC80 Bonsai phosphorylation assay
  - Western blotting and gel staining
  - AlphaFold 3 predictions
- QUANTIFICATION AND STATISTICAL ANALYSIS
  - Statistical analysis

SUPPLEMENTAL INFORMATION

Supplemental information can be found online at https://doi.org/10.1016/j.cub.2025.03.018.

Received: June 11, 2024
Revised: January 29, 2025
Accepted: March 12, 2025
Published: April 8, 2025

REFERENCES

1. Biggins, S., Severin, F.F., Bhalla, N., Sassoon, I., Hyman, A.A., and Murray, A.W. (1999). The conserved protein kinase Ipl1 regulates microtubule binding to kinetochores in budding yeast. Genes Dev. *13*, 532–544. https://doi.org/10.1101/gad.13.5.532.
2. Tanaka, T.U., Rachidi, N., Janke, C., Pereira, G., Galova, M., Schiebel, E., Stark, M.J.R., and Nasmyth, K. (2002). Evidence that the Ipl1-Sli15 (Aurora kinase-INCENP) complex promotes chromosome bi-orientation by altering kinetochore-spindle pole connections. Cell *108*, 317–329. https://doi.org/10.1016/s0092-8674(02)00633-5.
3. Lampson, M.A., Renduchitala, K., Khodjakov, A., and Kapoor, T.M. (2004). Correcting improper chromosome-spindle attachments during cell division. Nat. Cell Biol. *6*, 232–237. https://doi.org/10.1038/ncb1102.
4. Cheeseman, I.M., Chappie, J.S., Wilson-Kubalek, E.M., and Desai, A. (2006). The conserved KMN network constitutes the core microtubule-binding site of the kinetochore. Cell *127*, 983–997. https://doi.org/10.1016/j.cell.2006.09.039.
5. Cimini, D., Wan, X., Hirel, C.B., and Salmon, E.D. (2006). Aurora kinase promotes turnover of kinetochore microtubules to reduce chromosome segregation errors. Curr. Biol. *16*, 1711–1718. https://doi.org/10.1016/j.cub.2006.07.022.
6. DeLuca, J.G., Gall, W.E., Ciferri, C., Cimini, D., Musacchio, A., and Salmon, E.D. (2006). Kinetochore microtubule dynamics and attachment stability are regulated by Hec1. Cell *127*, 969–982. https://doi.org/10.1016/j.cell.2006.09.047.
7. Chmátal, L., Yang, K., Schultz, R.M., and Lampson, M.A. (2015). Spatial regulation of kinetochore microtubule attachments by destabilization at spindle poles in meiosis I. Curr. Biol. *25*, 1835–1841. https://doi.org/10.1016/j.cub.2015.05.013.
8. Ye, A.A., Deretic, J., Hoel, C.M., Hinman, A.W., Cimini, D., Welburn, J.P., and Maresca, T.J. (2015). Aurora A kinase contributes to a pole-based error correction pathway. Curr. Biol. *25*, 1842–1851. https://doi.org/10.1016/j.cub.2015.06.021.
9. DeLuca, K.F., Meppelink, A., Broad, A.J., Mick, J.E., Peersen, O.B., Pektas, S., Lens, S.M.A., and DeLuca, J.G. (2018). Aurora A kinase phosphorylates Hec1 to regulate metaphase kinetochore-microtubule dynamics. J. Cell Biol. *217*, 163–177. https://doi.org/10.1083/jcb.201707160.
10. Sarangapani, K.K., Koch, L.B., Nelson, C.R., Asbury, C.L., and Biggins, S. (2021). Kinetochore-bound Mps1 regulates kinetochore-microtubule attachments via Ndc80 phosphorylation. J. Cell Biol. *220*, e202106130. https://doi.org/10.1083/jcb.202106130.
11. Hayward, D., Roberts, E., and Gruneberg, U. (2022). MPS1 localizes to end-on microtubule-attached kinetochores to promote microtubule release. Curr. Biol. *32*, 5200–5208.e8. https://doi.org/10.1016/j.cub.2022.10.047.
12. Maciejowski, J., Drechsler, H., Grundner-Culemann, K., Ballister, E.R., Rodriguez-Rodriguez, J.A., Rodriguez-Bravo, V., Jones, M.J.K., Foley, E., Lampson, M.A., Daub, H., et al. (2017). Mps1 regulates kinetochore-microtubule attachment stability via the Ska complex to ensure error-free chromosome segregation. Dev. Cell *41*, 143–156.e6. https://doi.org/10.1016/j.devcel.2017.03.025.
13. Jelluma, N., Brenkman, A.B., van den Broek, N.J.F., Cruijsen, C.W.A., van Osch, M.H.J., Lens, S.M.A., Medema, R.H., and Kops, G.J.P.L. (2008). Mps1 phosphorylates Borealin to control Aurora B activity and chromosome alignment. Cell *132*, 233–246. https://doi.org/10.1016/j.cell.2007.11.046.
14. Kwiatkowski, N., Jelluma, N., Filippakopoulos, P., Soundararajan, M., Manak, M.S., Kwon, M., Choi, H.G., Sim, T., Deveraux, Q.L., Rottmann, S., et al. (2010). Small-molecule kinase inhibitors provide insight into Mps1 cell cycle function. Nat. Chem. Biol. *6*, 359–368. https://doi.org/10.1038/nchembio.345.
15. van der Waal, M.S., Saurin, A.T., Vromans, M.J.M., Vleugel, M., Wurzenberger, C., Gerlich, D.W., Medema, R.H., Kops, G.J.P.L., and Lens, S.M.A. (2012). Mps1 promotes rapid centromere accumulation of Aurora B. EMBO Rep. *13*, 847–854. https://doi.org/10.1038/embor.2012.93.
16. Santaguida, S., Tighe, A., D'Alise, A.M., Taylor, S.S., and Musacchio, A. (2010). Dissecting the role of MPS1 in chromosome biorientation and the spindle checkpoint through the small molecule inhibitor reversine. J. Cell Biol. *190*, 73–87. https://doi.org/10.1083/jcb.201001036.
17. Hewitt, L., Tighe, A., Santaguida, S., White, A.M., Jones, C.D., Musacchio, A., Green, S., and Taylor, S.S. (2010). Sustained Mps1 activity is required in mitosis to recruit O-Mad2 to the Mad1-C-Mad2 core complex. J. Cell Biol. *190*, 25–34. https://doi.org/10.1083/jcb.201002133.
18. Maciejowski, J., George, K.A., Terret, M.E., Zhang, C., Shokat, K.M., and Jallepalli, P.V. (2010). Mps1 directs the assembly of Cdc20 inhibitory complexes during interphase and mitosis to control M phase timing and spindle checkpoint signaling. J. Cell Biol. *190*, 89–100. https://doi.org/10.1083/jcb.201001050.
19. Moura, M., Osswald, M., Leça, N., Barbosa, J., Pereira, A.J., Maiato, H., Sunkel, C.E., and Conde, C. (2017). Protein Phosphatase 1 inactivates Mps1 to ensure efficient spindle assembly checkpoint silencing. eLife *6*, e25366. https://doi.org/10.7554/eLife.25366.
20. Dou, Z., Liu, X., Wang, W., Zhu, T., Wang, X., Xu, L., Abrieu, A., Fu, C., Hill, D.L., and Yao, X. (2015). Dynamic localization of Mps1 kinase to kinetochores is essential for accurate spindle microtubule attachment. Proc. Natl. Acad. Sci. USA *112*, E4546–E4555. https://doi.org/10.1073/pnas.1508791112.
21. Hiruma, Y., Sacristan, C., Pachis, S.T., Adamopoulos, A., Kuijt, T., Ubbink, M., von Castelmur, E., Perrakis, A., and Kops, G.J.P.L. (2015). CELL DIVISION CYCLE. Competition between MPS1 and microtubules at kinetochores regulates spindle checkpoint signaling. Science *348*, 1264–1267. https://doi.org/10.1126/science.aaa4055.
22. Ji, Z., Gao, H., and Yu, H. (2015). CELL DIVISION CYCLE. Kinetochore attachment sensed by competitive Mps1 and microtubule binding to Ndc80C. Science *348*, 1260–1264. https://doi.org/10.1126/science.aaa4029.
23. Parnell, E.J., Jenson, E.E., and Miller, M.P. (2024). A conserved site on Ndc80 complex facilitates dynamic recruitment of Mps1 to yeast kinetochores to promote accurate chromosome segregation. Curr. Biol. *34*, 2294–2307.e4. https://doi.org/10.1016/j.cub.2024.04.054.
24. Pleuger, R., Cozma, C., Hohoff, S., Denkhaus, C., Dudziak, A., Kaschani, F., Kaiser, M., Musacchio, A., Vetter, I.R., and Westermann, S. (2024). Microtubule end-on attachment maturation regulates Mps1 association with its kinetochore receptor. Curr. Biol. *34*, 2279–2293.e6. https://doi.org/10.1016/j.cub.2024.03.062.
25. Zahm, J.A., and Harrison, S.C. (2024). A communication hub for phosphoregulation of kinetochore-microtubule attachment. Curr. Biol. *34*, 2308–2318.e6. https://doi.org/10.1016/j.cub.2024.04.067.
26. Barros, T.P., Kinoshita, K., Hyman, A.A., and Raff, J.W. (2005). Aurora A activates D-TACC-Msps complexes exclusively at centrosomes to stabilize centrosomal microtubules. J. Cell Biol. *170*, 1039–1046. https://doi.org/10.1083/jcb.200504097.
27. Hannak, E., Kirkham, M., Hyman, A.A., and Oegema, K. (2001). Aurora-A kinase is required for centrosome maturation in Caenorhabditis elegans. J. Cell Biol. *155*, 1109–1116. https://doi.org/10.1083/jcb.200108051.
28. Berdnik, D., and Knoblich, J.A. (2002). Drosophila Aurora-A is required for centrosome maturation and actin-dependent asymmetric protein localization during mitosis. Curr. Biol. *12*, 640–647. https://doi.org/10.1016/s0960-9822(02)00766-2.
29. Giet, R., McLean, D., Descamps, S., Lee, M.J., Raff, J.W., Prigent, C., and Glover, D.M. (2002). Drosophila Aurora A kinase is required to localize D-TACC to centrosomes and to regulate astral microtubules. J. Cell Biol. *156*, 437–451. https://doi.org/10.1083/jcb.200108135.

30. Fuller, B.G., Lampson, M.A., Foley, E.A., Rosasco-Nitcher, S., Le, K.V., Tobelmann, P., Brautigan, D.L., Stukenberg, P.T., and Kapoor, T.M. (2008). Midzone activation of aurora B in anaphase produces an intracellular phosphorylation gradient. Nature *453*, 1132–1136. https://doi.org/10.1038/nature06923.

31. Violin, J.D., Zhang, J., Tsien, R.Y., and Newton, A.C. (2003). A genetically encoded fluorescent reporter reveals oscillatory phosphorylation by protein kinase C. J. Cell Biol. *161*, 899–909. https://doi.org/10.1083/jcb.200302125.

32. Feng, Z., Caballe, A., Wainman, A., Johnson, S., Haensele, A.F.M., Cottee, M.A., Conduit, P.T., Lea, S.M., and Raff, J.W. (2017). Structural basis for mitotic centrosome assembly in flies. Cell *169*, 1078–1089.e13. https://doi.org/10.1016/j.cell.2017.05.030.

33. Koch, A., Maia, A., Janssen, A., and Medema, R.H. (2016). Molecular basis underlying resistance to Mps1/TTK inhibitors. Oncogene *35*, 2518–2528. https://doi.org/10.1038/onc.2015.319.

34. Conde, C., Osswald, M., Barbosa, J., Moutinho-Santos, T., Pinheiro, D., Guimarães, S., Matos, I., Maiato, H., and Sunkel, C.E. (2013). Drosophila Polo regulates the spindle assembly checkpoint through Mps1-dependent BubR1 phosphorylation. EMBO J. *32*, 1761–1777. https://doi.org/10.1038/emboj.2013.109.

35. Lamb, J.R., Michaud, W.A., Sikorski, R.S., and Hieter, P.A. (1994). Cdc16p, Cdc23p and Cdc27p form a complex essential for mitosis. EMBO J. *13*, 4321–4328. https://doi.org/10.1002/j.1460-2075.1994.tb06752.x.

36. Tugendreich, S., Tomkiel, J., Earnshaw, W., and Hieter, P. (1995). CDC27Hs colocalizes with CDC16Hs to the centrosome and mitotic spindle and is essential for the metaphase to anaphase transition. Cell *81*, 261–268. https://doi.org/10.1016/0092-8674(95)90336-4.

37. Huang, J.Y., and Raff, J.W. (2002). The dynamic localisation of the Drosophila APC/C: evidence for the existence of multiple complexes that perform distinct functions and are differentially localised. J. Cell Sci. *115*, 2847–2856. https://doi.org/10.1242/jcs.115.14.2847.

38. Ciferri, C., Pasqualato, S., Screpanti, E., Varetti, G., Santaguida, S., Dos Reis, G., Maiolica, A., Polka, J., De Luca, J.G., De Wulf, P., et al. (2008). Implications for kinetochore-microtubule attachment from the structure of an engineered Ndc80 complex. Cell *133*, 427–439. https://doi.org/10.1016/j.cell.2008.03.020.

39. Barisic, M., Aguiar, P., Geley, S., and Maiato, H. (2014). Kinetochore motors drive congression of peripheral polar chromosomes by overcoming random arm-ejection forces. Nat. Cell Biol. *16*, 1249–1256. https://doi.org/10.1038/ncb3060.

40. Ye, A.A., and Maresca, T.J. (2015). It's all relative: Centromere- versus pole-based error correction. Cell Cycle *14*, 3777–3778. https://doi.org/10.1080/15384101.2015.1105701.

41. Eibes, S., Rajendraprasad, G., Guasch-Boldu, C., Kubat, M., Steblyanko, Y., and Barisic, M. (2023). CENP-E activation by Aurora A and B controls kinetochore fibrous corona disassembly. Nat. Commun. *14*, 5317. https://doi.org/10.1038/s41467-023-41091-2.

42. Sikirzhytski, V., Renda, F., Tikhonenko, I., Magidson, V., McEwen, B.F., and Khodjakov, A. (2018). Microtubules assemble near most kinetochores during early prometaphase in human cells. J. Cell Biol. *217*, 2647–2659. https://doi.org/10.1083/jcb.201710094.

43. Chakraborty, M., Tarasovetc, E.V., Zaytsev, A.V., Godzi, M., Figueiredo, A.C., Ataullakhanov, F.I., and Grishchuk, E.L. (2019). Microtubule end conversion mediated by motors and diffusing proteins with no intrinsic microtubule end-binding activity. Nat. Commun. *10*, 1673. https://doi.org/10.1038/s41467-019-09411-7.

44. Renda, F., Miles, C., Tikhonenko, I., Fisher, R., Carlini, L., Kapoor, T.M., Mogilner, A., and Khodjakov, A. (2022). Non-centrosomal microtubules at kinetochores promote rapid chromosome biorientation during mitosis in human cells. Curr. Biol. *32*, 1049–1063.e4. https://doi.org/10.1016/j.cub.2022.01.013.

45. Perez-Riverol, Y., Bai, J., Bandla, C., García-Seisdedos, D., Hewapathirana, S., Kamatchinathan, S., Kundu, D.J., Prakash, A., Frericks-Zipper, A., Eisenacher, M., et al. (2022). The PRIDE database resources in 2022: A hub for mass spectrometry-based proteomics evidences. Nucleic Acids Res. *50*, D543–D552. https://doi.org/10.1093/nar/gkab1038.

46. Heeger, S., Leismann, O., Schittenhelm, R., Schraidt, O., Heidmann, S., and Lehner, C.F. (2005). Genetic interactions of separase regulatory subunits reveal the diverged Drosophila Cenp-C homolog. Genes Dev. *19*, 2041–2053. https://doi.org/10.1101/gad.347805.

47. Gilliland, W.D., Hughes, S.E., Cotitta, J.L., Takeo, S., Xiang, Y., and Hawley, R.S. (2007). The multiple roles of mps1 in Drosophila female meiosis. PLoS Genet. *3*, e113. https://doi.org/10.1371/journal.pgen.0030113.

48. Rodrigues-Martins, A., Riparbelli, M., Callaini, G., Glover, D.M., and Bettencourt-Dias, M. (2007). Revisiting the role of the mother centriole in centriole biogenesis. Science *316*, 1046–1050. https://doi.org/10.1126/science.1142950.

49. Jelluma, N., Brenkman, A.B., McLeod, I., Yates, J.R., 3rd, Cleveland, D.W., Medema, R.H., and Kops, G.J.P.L. (2008). Chromosomal instability by inefficient Mps1 auto-activation due to a weakened mitotic checkpoint and lagging chromosomes. PLoS One *3*, e2415. https://doi.org/10.1371/journal.pone.0002415.

50. Raisch, T., Ciossani, G., D'Amico, E., Cmentowski, V., Carmignani, S., Maffini, S., Merino, F., Wohlgemuth, S., Vetter, I.R., Raunser, S., et al. (2022). Structure of the RZZ complex and molecular basis of Spindly-driven corona assembly at human kinetochores. EMBO J. *41*, e110411. https://doi.org/10.15252/embj.2021110411.

51. Pan, D., Klare, K., Petrovic, A., Take, A., Walstein, K., Singh, P., Rondelet, A., Bird, A.W., and Musacchio, A. (2017). CDK-regulated dimerization of M18BP1 on a Mis18 hexamer is necessary for CENP-A loading. eLife *6*, e23352. https://doi.org/10.7554/eLife.23352.

52. Abramson, J., Adler, J., Dunger, J., Evans, R., Green, T., Pritzel, A., Ronneberger, O., Willmore, L., Ballard, A.J., Bambrick, J., et al. (2024). Accurate structure prediction of biomolecular interactions with AlphaFold 3. Nature *630*, 493–500. https://doi.org/10.1038/s41586-024-07487-w.

53. Li, C., Wen, A., Shen, B., Lu, J., Huang, Y., and Chang, Y. (2011). FastCloning: a highly simplified, purification-free, sequence- and ligation-independent PCR cloning method. BMC Biotechnol. *11*, 92. https://doi.org/10.1186/1472-6750-11-92.

54. Kapoor, T.M., Mayer, T.U., Coughlin, M.L., and Mitchison, T.J. (2000). Probing spindle assembly mechanisms with monastrol, a small molecule inhibitor of the mitotic kinesin, Eg5. J. Cell Biol. *150*, 975–988. https://doi.org/10.1083/jcb.150.5.975.

55. Gibson, D.G., Young, L., Chuang, R.Y., Venter, J.C., Hutchison, C.A., 3rd, and Smith, H.O. (2009). Enzymatic assembly of DNA molecules up to several hundred kilobases. Nat. Methods *6*, 343–345. https://doi.org/10.1038/nmeth.1318.

56. Rappsilber, J., Mann, M., and Ishihama, Y. (2007). Protocol for micro-purification, enrichment, pre-fractionation and storage of peptides for proteomics using StageTips. Nat. Protoc. *2*, 1896–1906. https://doi.org/10.1038/nprot.2007.261.

57. Olsen, J.V., Macek, B., Lange, O., Makarov, A., Horning, S., and Mann, M. (2007). Higher-energy C-trap dissociation for peptide modification analysis. Nat. Methods *4*, 709–712. https://doi.org/10.1038/nmeth1060.

58. Cox, J., and Mann, M. (2008). MaxQuant enables high peptide identification rates, individualized p.p.b.-range mass accuracies and proteome-wide protein quantification. Nat. Biotechnol. *26*, 1367–1372. https://doi.org/10.1038/nbt.1511.

STAR★METHODS

KEY RESOURCES TABLE

REAGENT or RESOURCE	SOURCE	IDENTIFIER
Antibodies		
Anti Aurora A T360Ph, rabbit	This paper	N/A
Anti α-Tubulin B512, mouse	Sigma-Aldrich	RRID: AB_477582
Anti CID, rat	Conde et al.[34]	Clone Rat4
Anti GFP, chicken	Abcam	RRID: AB_300798
Anti CENP-C, rabbit	Heeger et al.[46]	Clone Rb1
Anti MPS1, guinea pig	Gilliland et al.[47]	RRID: AB_2567774
Anti Aurora B T232Ph, rabbit	Rockland	RRID: AB_2061641
Anti Aurora A T288Ph, rabbit	Cell Signaling Technology	RRID: AB_2061481
Anti DPLP, chicken	Rodrigues-Martins et al.[48]	N/A
Anti FLAG, mouse	Sigma-Aldrich	RRID: AB_262044
Anti γ-Tubulin GTU-88, mouse	Sigma-Aldrich	RRID: AB_532292
Anti D-TACC S863Ph, rabbit	Barros et al.[26]	N/A
Anti CENP-C, guinea pig	MBL	RRID: AB_10693556
Anti Pericentrin, mouse	Abcam	RRID: AB_2160664
Anti Aurora A, mouse	Abcam	RRID: AB_300667
Anti Hec1 S69Ph, rabbit	DeLuca et al.[9]	N/A
Anti MPS1 T676Ph, rabbit	Jelluma et al.[49]	N/A
Anti α-Tubulin DM1a, mouse	Santa Cruz Biotechnology	RRID: AB_628412
Anti Aurora A, mouse	BD	RRID: AB_398252
Anti Aurora B T232Ph, rabbit	Cell Signaling Technology	RRID: AB_2061631
Anti GST, mouse	Sigma-Aldrich	RRID: AB_10807767
Anti NDC80, mouse	Gene Tex	RRID: AB_371632
Anti NDC80 S55Ph, rabbit	Invitrogen	RRID: AB_2792966
Anti chicken Alexa Fluor 488	Invitrogen	RRID: AB_142924
Anti chicken Alexa Fluor 647	Invitrogen	RRID: AB_2535866
Anti rabbit Alexa Fluor 488	Invitrogen	RRID: AB_2576217
Anti rabbit Alexa Fluor 568	Invitrogen	RRID: AB_10563566
Anti rabbit Alexa Fluor 647	Invitrogen	RRID: AB_2536183
Anti rat Alexa Fluor 647	Invitrogen	RRID: AB_141778
Anti guinea pig Alexa Fluor 488	Invitrogen	RRID: AB_2534117
Anti guinea pig Alexa Fluor 568	Invitrogen	RRID: AB_141954
Anti guinea pig Alexa Fluor 647	Invitrogen	RRID: AB_141882
Anti mouse Alexa Fluor 488	Invitrogen	RRID: AB_2534088
Anti mouse Alexa Fluor 568	Invitrogen	RRID: AB_144696
Anti mouse Alexa Fluor 647	Invitrogen	RRID: AB_162542
Anti rabbit HRP conjugated	Jackson ImmunoResearch	RRID: AB_2313567
Anti guinea pig HRP conjugated	Invitrogen	RRID: AB_2535546
Anti mouse HRP conjugated	Jackson ImmunoResearch	RRID: AB_10015289
Anti rabbit HRP conjugated	GE Healthcare	RRID: AB_772191
Anti mouse HRP conjugated	GE Healthcare	RRID: AB_772193
Bacterial and virus strains		
E. coli BL21CodonPlus(DE3)-RIL	Agilent Products	CAT#200131
E. coli DH5α competent cells	ThermoFischer	CAT#EC0112

(*Continued on next page*)

Continued

REAGENT or RESOURCE	SOURCE	IDENTIFIER
E. coli Omnimax competent bacteria	Invitrogen	CAT#C854003
E. coli BL21(DE3) competente bacteria	ThermoFischer	CAT#C601003
Chemicals, peptides, and recombinant proteins		
Protease inhibitors cOmplete cocktail	Roche	CAT#11697498001
Phosphatase inhibitor cocktail 3	Sigma-Aldrich	CAT#P0044
MG132 proteasome inhibitor	Sigma-Aldrich	CAS 133407
Colchicine	Sigma-Aldrich	CAS 64-86-8
Nocodazole	Sigma-Aldrich	CAS 31430-18-9
MLN8054	Selleck Chemicals	CAT#S1100
MLN8237	Selleck Chemicals	CAT#S1133
Compound5 (Cp5)	Koch et al.[33]	N/A
ZM447439	AstraZeneca	CAS 331771-20-1
GSK923295	MedChemExpress	CAT#HY-10299
STLC Eg-5 inhibitor	Santa Cruz Biotechnology	CAS 2799-07-7
Aurora A Protein, active	Merck, Millipore	CAT#14-511
Recombinant Human Mps1/TTK Protein	SignalChem	CAT#T20-10G
Vectashield Antifade Mounting Medium with DAPI	Vector Laboratories	CAT#H-1200
$NDC80^{bonsai}$	Cifferi et al.[38]	N/A
MBP-AAK WT	This paper	N/A
MBP-AAK T337A	This paper	N/A
mCherry-MPS1	Raisch et al.[50]	N/A
GST-MPS1-6xHis	Raisch et al.[50]	N/A
Concanavalin A	SigmaAldrich	CAT#C5275
Deposited data		
Mass spectrometry data	This paper	PRIDE: PXD056173
Experimental models: Cell lines		
Drosophila: S2 cells	DGRC	RRID: CVCL_TZ72
Human: hTERT RPE-1	ATCC	RRID: CVCL_4388
Oligonucleotides		
For oligonucleotides used in this study, see Table S1.	N/A	N/A
Recombinant DNA		
pGFP-Histone2B	Conde et al.[34]	N/A
pAc-mCherry-αTubulin	Conde et al.[34]	N/A
pCENP-C-CM2-AuroraFRETsensor	This paper	N/A
$pHGW\text{-}AAK^{WT}$	This paper	N/A
pMT-mCherry-MPS1	This paper	N/A
$pHGW\text{-}AAK^{T360A}$	This paper	N/A
$pHGW\text{-}AAK^{T360D}$	This paper	N/A
$pMT\text{-}EGFP\text{-}MPS1^{WT}\text{-}CM2$	This paper	N/A
$pHGW\text{-}AAK^{WT}\text{-}CM2$	This paper	N/A
$pHGW\text{-}AAK^{T311D}\text{-}CM2$	This paper	N/A
$pHGW\text{-}AAK^{T360D}\text{-}CM2$	This paper	N/A
$pHGW\text{-}AAK^{K183I/T360D}\text{-}CM2$	This paper	N/A
$pHFMW\text{-}AAK^{WT}$	This paper	N/A
$pHFMW\text{-}AAK^{K183I}$	This paper	N/A
pMT-EGFP-MPS1	Conde et al.[34]	N/A
pMalc-AAK 126-403	This paper	N/A
pMalc-AAK 126-403 K162I	This paper	N/A

(*Continued on next page*)

Continued		
REAGENT or RESOURCE	SOURCE	IDENTIFIER
pMalc-AAK 144-411	This paper	N/A
pMalc-AAK 144-411 K183I	This paper	N/A
pETDuet-AAK WT	Pan et al.[51]	N/A
pETDuet-AAK T337A	This paper	N/A
pLIB-GST-MPS1	Raisch et al.[50]	N/A
pLIB-mCherry-MPS1	Raisch et al.[50]	N/A
pGEX6P-2rbs-NDC80^{bonsai}	Ciferri et al.[38]	N/A
Software and algorithms		
Fiji software	ImageJ	RRID: SCR_002285
AlphaFold3	Abramson et al.[52]	RRID: SCR_025454
GraphPad Prism 10.2.3	GraphPad Software Inc.	RRID: SCR_002798
KT-SP distance measurement custom routine	Barisic et al.[39]	N/A
Other		
μ-Dish 35mm, high Glass Bottom	Ibidi	CAT#81158
35 mm glass bottom petri dishes	Cellvis	CAT#D35-20-0-N
12 mm round cover glasses	Menzel Glaser	CAT#MENZCB00120RA020
Superdex 200 SEC column	GE Healthcare	CAT#GE28-9909-44
TranscriptAid T7 High Yield Transcription Kit	(ThermoFischer)	CAT#K0441
MBP amylose magnetic beads	New England Biolabs	CAT#E8035S

EXPERIMENTAL MODELS AND STUDY PARTICIPANT DETAILS

Drosophila Cell Lines

The experiments have been conducted in male *Drosophila* S2 cells (S2-DGRC, RRID: CVCL_TZ72) cultured at 25°C in Schneider's Insect Medium (Sigma-Aldrich) supplemented with 10% FBS. This cell line has been authenticated by DGRC.

Human Cell Lines

The experiments have been conducted in female hTERT RPE-1 (ATCC, RRID: CVCL_4388) cultured in DMEM/F12 supplemented with 10% FBS and cultured at 37°C in humidified conditions with 5% CO2. This cell line has been authenticated by ATCC.

METHOD DETAILS

RNAi-mediated depletion and drug treatments

For protein depletion in *Drosophila* S2 cells, dsRNA synthesis was performed using TranscriptAid T7 High Yield Transcription Kit (ThermoFischer), according to the manufacturer's instructions, at 37°C for 16h. The incubation with dsRNA was performed at 25°C for 1h in non-supplemented Schneider's Insect Medium (Sigma-Aldrich) followed by 96h-120h of cell culture in Schneider's Insect Medium (Sigma-Aldrich) supplemented with 10% FBS, as previously described.[34] The PCR product used as template to produce MPS1 RNAi was amplified with the set of primers MPS1F (5′-TAATACGACTCACTATAGGGTCTTCCAAACACCTATGACG-3′) and MPS1R (5′-TAATACGACTCACTATAGGGCGTTTAGATATCCCTGCACCA-3′) (Table S1). The PCR product used as template to produce AAK 5′UTR RNAi was amplified with AAK5′_F (5′-TAATACGACTCACTATAGGGAGAACTTGCCATTCGCCTCATC-3′) and AAK5′_R (5′-TAATACGACTCACTATAGGGAGAGACGGCACGGCACAGGCACTCG-3′) (Table S1). The PCR product used as template to produce AAK 3′UTR RNAi was amplified with AAK3′_F (5′-TAATACGACTCACTATAGGGAGAACACATTCTTGTTTA ATTTTC-3′) and AAK3′_R (5′-TAATACGACTCACTATAGGGAGAGAAAACACACACAAACTTT-3′) (Table S1). The PCR product used as template to produce NDC80 RNAi was amplified with NDC80F (5′-TAATACGACTCACTATAGGGTTTGATCCGGATGTTT TGTTGTAGTTC-3′) and NDC80R (5′-TAATACGACTCACTATAGGGTTTTTTAATTTGAAAACAAAGAATACTCTT-3′) (Table S1). The PCR product used as template to produce CDC27 RNAi was amplified with CDC27F (5′-TAATACGACTCACTATAGGGAACAAT AGC-3′) and CDC27R (5′-TAATACGACTCACTATAGGGTCTTCATGTAGAATTGCATGGC-3′) (Table S1). The PCR product used as template to produce γTubulin RNAi was amplified with γTub RNAiF (5'-TAATACGACTCACTATAGTTTTCTCATGACAGGCTAC ACG-3') and γTub RNAiR (5'-TAATACGACTCACTATAGGGTCACAGATCGACTATCCTCC-3') (Table S1). At selected time points, cells were collected and processed for immunofluorescence or time-lapse microscopy. When required, cells were subjected to

several drug treatments before being collected and processed for analysis. To promote microtubule depolymerization, cells were incubated for 2 h with 30 μM colchicine (Sigma-Aldrich). To inhibit the proteasome, cells were incubated for 3 h with 20 μM MG132 (Calbiochem).

For siRNA-mediated depletion experiments in human RPE-1 cells, cells were transfected in OptiMEM (Thermo Fisher) with Lipofectamine RNAiMAX (Thermo Fisher) with 40 nM siRNAs for 48 h – siSpindly: 5′-GAAAGGGUCUCAAACUGAA-3′, siControl (non-targeting control siRNA): 5′- UGGUUUACAUGUCGACUAA-3′ (Table S1). Where indicated, monopolar spindles were induced by inhibiting Eg5 using 5 μM S-Trityl-L-Cysteine (STLC; Santa Cruz Biotechnology) which was added to the medium 5 h before fixation. CENP-E was inhibited by adding 200 nM GSK923295 (MedChemExpress) to the medium 1 h before fixation. MPS1 was inhibited by adding 500 nM Cp5[33] (a gift from René Medema, Oncode Institute, The Netherlands Cancer Institute, The Netherlands) to the medium 1 h before fixation. To avoid mitotic exit after MPS1 inhibition, the proteasome was inhibited by adding 5 μM MG132 (Sigma) to the medium 1 h before MPS1 inhibition. To depolymerize microtubules, 2 μM nocodazole (Sigma) was added 2 h before fixation. For inhibition of AAK and ABK, 250 nM MLN-8054 (Selleck Chemicals) and 4 μM ZM447439 (AstraZeneca) were respectively added to the cells 2 h before fixation.

Transgene constructs and S2 cell transfection

EGFP-MPS1^{WT}, H2B-GFP and mCherry-α-Tubulin constructs were previously characterized.[34] For the generation of the expression vector mCherry-MPS1^{WT}, mCherry cDNA was amplified by PCR and inserted into the EGFP-MPS1 construct, by FastCloning,[53] in replacement of previously removed EGFP. EGFP-AAK^{WT} and FLAG-AAK^{WT} constructs were generated by PCR amplification of AAK cDNA and insertion into modified versions of pENTR entry vector through FastCloning.[53] Entry clones were then used for Gateway recombination (Thermo Fischer Scientific) together with pHGW (for EGFP-AAK constructs) or pHFMW (for FLAG-AAK constructs) destination vectors (heat-shock inducible promoter, N-terminal EGFP or FLAG tag, respectively). To generate FLAG-AAK^{K183I}, EGFP-AAK^{T311D}, EGFP-AAK^{T360A}, EGFP-AAK^{T360D} and EGFP-AAK$^{K183I/T360D}$ versions, either FLAG-AAK^{WT} or EGFP-AAK^{WT} expression vectors had their codons corresponding to K183, T311, T360, T360 and K183 and T360 changed by site-directed mutagenesis with a primer harboring the desired mutation to Isoleucine (I), Aspartate (D), Alanine (A), Aspartate (D) and Isoleucine (I) and Aspartate (D), respectively. The PCR reactions were performed with Phusion polymerase (Thermo Fisher Scientific). To generate the EGFP-MPS1^{WT}-CM2 and EGFP-AAK-CM2 constructs, the CM2 domain of Centrosomin (CNN) cDNA was amplified by PCR and was inserted in the C-terminal region of the available EGFP-MPS1^{WT} and EGFP-AAK constructs, respectively, by FastCloning.[53] Stable transfection of indicated vectors into S2 cells was performed using Effectene Transfection Reagent (Qiagen, Hilden, Germany), according to the manufacturer's instructions. To induce EGFP-MPS1^{WT}, mCh-MPS1^{WT} and EGFP-MPS1^{WT}-CM2 expression, S2 cells were incubated overnight with 200 μM $CuSO_4$ at 25°C. To induce the expression of either AAK constructs cells were heat-shocked for 30 min at 37°C and allowed to rest for at least 6 h before being processed for immunofluorescence or live cell imaging.

FRET-based AURORA kinase sensor

S2 cells stably expressing the CM2-FRET reporter, GFP-H2B and either mCherry-α-tubulin or mCherry-MPS1 were seeded onto Concanavalin A- (ConA) (Sigma-Aldrich) treated 35 mm glass bottom petri dishes (Cellvis) for 1 hour prior to bringing the volume of Schneider's media up to 2 mL. Cells were then imaged at 24°C on a TiE inverted microscope (Nikon) equipped with an iXON EMCCD camera (Andor Technology) using a 100x 1.4 NA Plan Apo violet-corrected series differential interference contrast objective (Nikon). Metamorph software (Molecular Devices) was used to control the imaging system. Mitotic cells and the best focal plane were identified on the RFP channel (mCherry-α-tubulin or mCherry-MPS1). After acquiring the RFP image, sequential images of mTurquoise2, mVenus, and FRET (ECFP excitation, EYFP emission) were taken with equal exposure times (200 ms). Overexpression of MPS1 was induced by overnight incubation with 200 μM $CuSO_4$. AAK was inhibited by treating the seeded cells in the chamber for 1 hour in 100 nM MLN8237 (Selleck Chemicals) prior to FRET imaging. Background-corrected fluorescence intensities for mTurquoise2 and FRET were measured in Metamorph software by subtraction of local background using a duplicate area. The reported FRET emission ratios represent the ratios of the background corrected FRET signal over the background corrected mTurquoise2 signal and values were normalized against the mean prometaphase FRET emission ratio for each biological replicate.

Live cell imaging

For live imaging of S2 cells, cells were plated onto μ-Dish 35mm, high Glass Bottom dishes (Ibidi) previously treated with 0.2 mg/mL ConA (Sigma-Aldrich). Images were obtained at 30s intervals up to a maximum of 90min. All images were acquired at 25°C with either a spinning disc confocal system (Revolution; Andor) equipped with an electron multiplying charge-coupled device camera (iXonEM+; Andor) and a CSU-22 unit (Yokogawa) based on an inverted microscope (IX81; Olympus) driven by iQ software (Andor) or a Nikon ECLIPSE Ti2 (Nikon, Japan) equipped with Crest X-Light V3 spinning disk confocal system (Crest CrestOptics, Italy) and Kinetix 25 (Photometrics) camera driven by NIS elements 5.5 (Nikon, Japan) software. The microscopes are served with two laser lines, 488 and 561 nm, for the excitation of EGFP/GFP and mCherry, respectively. Time-lapse imaging of z stacks with 0.8 μm steps covering the entire volume of the cell was collected, and image sequence analysis and video assembly were done with Fiji software (https://fiji.sc/). The time each polar chromosome spent closer to the spindle pole than to the metaphase plate was quantified.

Immunofluorescence imaging and analysis

For immunofluorescence analysis of kinetochore-microtubule attachments in S2 cells, 10^5 cells were seeded onto coverslips previously treated with 0.2 mg/mL ConA (Sigma-Aldrich). For detection of calcium-stable k-fibers, cells were permeabilized for 120 seconds in a buffer containing 100 mM Pipes (pH 6.8), 1 mM MgCl2, 0.1 mM $CaCl_2$, and 0.1% Triton X-100 and then fixed for 10 min in the same buffer supplemented with 4% formaldehyde as previously described[54] followed by immunostaining. For immunofluorescence analysis of AAK^{T311Ph}, AAK^{T360Ph} or $NDC80^{S67Ph}$ levels in correlation to the distance between the centrosome and its closest kinetochore in S2 cells, 10^5 cells were seeded onto coverslips previously treated with 0.2 mg/mL ConA (Sigma-Aldrich), processed for fixation in 4% paraformaldehyde in PBS for 12 min and further extracted for 8 min with 0.1% Triton X-100 in PBS, followed by immunostaining. For immunofluorescence analysis of AAK^{T311Ph} and ABK^{T209Ph} levels, 10^5 cells were centrifuged onto slides for 5 min, at 239 g, and processed for fixation in 4% paraformaldehyde in PBS for 12 min and further extracted for 8 min with 0.1% Triton X-100 in PBS, followed by immunostaining. Immunostaining of S2 cells was performed as previously described.[34] Blocking was performed in 1xPBS, 10% fetal bovine serum, 0.05% Tween 20 at room temperature for 1h. Primary antibody incubations were prepared in blocking solution and incubated at 4°C overnight, followed by three 10-min washes in 1xPBS, 0.05% Tween. Secondary antibody incubations were prepared in blocking solution and incubated at room temperature for 1h, followed by three 10-min washes in 1xFBS, 0,05% Tween. Slides were then mounted using Vectashield mounting medium for fluorescence with DAPI (Vector Laboratories, Burlingame, CA). Images were collected in a Leica Scanning Confocal SP8 inverted microscope (Leica Microsystems). For immunofluorescence analysis of human cells, cells were grown on 12 mm round cover glasses (Menzel Glaser) and fixed by ice-cold methanol at -20°C for 4 minutes. DAPI was used at 1 μg/mL (Sigma) for DNA counterstaining. For quantification of centrosome to kinetochore distance, as well as for AAK and HEC1 phosphorylation status, images were acquired using a Plan-Apochromat DIC 63x/1.4 NA oil objective mounted on an inverted Zeiss Axio Observer Z1 microscope (Marianas Imaging Workstation from 3i-Intelligent Imaging and Innovations Inc.) equipped with a Hamamatsu ORCA-Flash4.0 v2 sCMOS Camera (Hamamatsu Photonics). Representative images were acquired using LSM700 confocal microscope (Carl Zeiss Inc.) mounted on a Zeiss-Axio imager Z1 equipped with alpha-Plan-Apochromat 100x/1.46 oil DIC M27 and plan-apochromat 63×/1.40 oil DIC M27 objective (Carl Zeiss Inc.) and Zen 2010 B SP1 software (Carl Zeiss, Inc.). In S2 cells, the distance (in 3D) between the centrosome and its closest kinetochore was calculated using the measured values of the distance in the XY plane and the distance in the Z-axis (number of slices x Z-step). For immunofluorescence quantification, the mean fluorescence intensity of kinetochore or centrosome proteins was measured within a specific predefined region of interest (ROI) where individual kinetochores or centrosomes could fit. The kinetochores were identified based on their constitutive marker CID. The centrosomes were identified based on either their constitutive marker DPLP or, when stated, the transfected FLAG-AAK or EGFP-AAK versions. After background subtraction, identified as a region in the cell with no kinetochores or centrosomes, the intensities of the proteins of interest were determined relative to the respective constitutive markers, unless stated otherwise. Control values were averaged and used for normalization of values determined in the different biological conditions tested.

In human cells, kinetochore to centrosome distance and $HEC1^{S69Ph}$ signal quantification on kinetochores in fixed cells were both measured using a custom routine written in MATLAB 8.2 (Mathworks). For analysis of kinetochore to centrosome distance, Pericentrin signal at centrosomes and CENP-C signal at kinetochores were used to determine the three-dimensional distance between the midpoint between the centrioles and the centroids of a kinetochore. For $HEC1^{S69Ph}$ quantification on kinetochores, intensities were determined by quantification of pixel gray levels of the focused z plane within a ROI. Background fluorescence was measured outside the ROI and subtracted. For quantifications at kinetochores, the ROI encompassed a single kinetochore measuring the signal intensity of $HEC1^{S69Ph}$ at the kinetochores. $HEC1^{S69Ph}$ intensity was quantified relative to CENP-C fluorescence. $HEC1^{S69Ph}$/CENP-C intensity ratios were subsequently normalized to control median value. At least 200 kinetochores from 10 different cells in each of three independent experiments were measured in both quantifications.

For AAK^{T288Ph} quantification at centrosomes, intensities were determined by measuring the signal intensity of AAK^{T288Ph} and total AAK in ImageJ software. Protein signal was quantified by drawing a circle closely along the total AAK staining at centrosomes and using the same ROI for AAK^{T288Ph} quantification. The ROI were adjusted in every cell to accurately match the total AAK staining. AAK^{T288Ph} intensity was quantified relative to total AAK fluorescence. AAK^{T288Ph}/AAK intensity ratios were subsequently normalized to control median value. At least 25 cells in each of three independent experiments were used for the quantifications.

Antibodies

Rabbit polyclonal anti-phospho(ph)Thr360-AAK (AAK^{T360Ph}) was raised against a phosphorylated peptide SKNYDE[pT]YKKIL, generated by Eurogentec, Seraing, Belgium. The primary antibodies used for immunofluorescence in S2 cells were rabbit anti-phosphorylated Thr360-Aurora A (AAK^{T360Ph}, this study) used at 1:500; mouse anti-α-tubulin B512 (Sigma-Aldrich) used at 1:5000; rat anti-CID (Rat4) used at 1:500; chicken anti-GFP (#ab13970, Abcam, Cambridge, UK) used at 1:2000; rabbit anti-CENP-C (Rb1[46]; a gift from Christian Lehner, University of Zurich, Switzerland) used at 1:3000; guinea pig anti-MPS1 (Gp15[47]; RRID:AB_2567774; a gift from Scott Hawley, The Stowers Institute for Medical Research, USA) used at 1:250; rabbit anti-phosphorylated Thr232-Aurora B (ABK^{T232Ph}, Rockland, Lim-erik, PA) used at 1:1000; rabbit anti-phosphorylated Thr288-Aurora A (AAK^{T288Ph}, C39D8, mAb #3079, Cell Signaling Technology, Danvers, MA, USA) used at 1:500; chicken anti-DPLP[48] (a gift from Mónica Bettencourt-Dias, Instituto Gulbenkian de Ciencia, Portugal) used at 1:2000; mouse anti-FLAG (F1804, Sigma-Aldrich) used at 1:500; mouse anti-γTubulin (GTU-88, T5326 Sigma-Aldrich) used at 1:250; rabbit anti-phosphorylated Ser863-D-TACC (D-$TACC^{S863Ph}$,[26]; a gift from Jordan Raff) used at 1:500. Alexa secondary antibodies were used according to the manufacturer's instructions.

The primary antibodies used for immunofluorescence in human cells were guinea pig anti-CENP-C (PD030, MBL) used at 1:1000, mouse anti-Pericentrin (ab28144, Abcam) used at 1:1000, mouse anti-Aurora A (ab13824, Abcam) used at 1:200, rabbit anti-phosphorylated Thr288 Aurora A (AAK^{T288Ph}) (C39D8 #3079, Cell Signalling) used at 1:1600 and rabbit anti-phosphorylated Ser69-HEC1 ($HEC1^{S69Ph}$,[9]; a gift from Jennifer DeLuca, Colorado State University, USA) used at 1:3000. Goat anti-Mouse IgG (H + L) Highly Cross-Adsorbed Secondary Antibody, Alexa Fluor 568; Goat anti-Rabbit IgG (H + L) Highly Cross-Adsorbed Secondary Antibody, Alexa Fluor 488; and Goat anti-Guinea Pig IgG (H + L) Highly Cross-Adsorbed Secondary Antibody, Alexa Fluor 647 (Invitrogen) secondary antibodies were used at 1:1000.

The primary antibodies used for Western blotting analysis were rabbit anti-phosphorylated Thr360-Aurora A (AAK^{T360Ph}, this study) used at 1:250, rabbit anti-phosphorylated Thr676-MPS1 ($MPS1^{T676Ph}$,[49]; a gift from Geert Kops, Oncode Institute, Hubrecht Institute, The Netherlands) used at 1:2000; rabbit anti-phosphorylated Thr288-Aurora A (AAK^{T288Ph}, C39D8, mAb #3079, Cell Signaling Technology, Danvers, MA, USA) used at 1:1000; mouse anti-αTubulin (DM1a, sc-32293, Santa Cruz Biotechnology) used at 1:10000; guinea pig anti-MPS1 (Gp15,[47]; RRID:AB_2567774; a gift from Scott Hawley, The Stowers Institute for Medical Research, USA) used at 1:5000; mouse anti-AURKA antibody (BD #610938, 4/IAK1) used at 1:1000, rabbit anti-AURKA pT288, AURKB pT232, AURKC pT198 (Cell Signalling #2914, D13A11) used at 1:1000, mouse anti-GST (Novagen/Millipore #71097-3) used at 1:1000, mouse anti-NDC80 (Gene Tex (via Biozol) # GTX 70268-100, 9G3.23), rabbit anti-phosphorylated Ser55-NDC80 ($NDC80^{S55Ph}$, Invitogen #PA5-85846) used at 1:1000.

Recombinant Protein Production

For the mass spectrometry analysis, the catalytic domain of either human or *Drosophila* AAK wild-type or kinase-dead (AAK^{K162I} in human or AAK^{K183I} in *Drosophila*) were fused with N-terminal MBP. To generate these constructs, human and *Drosophila* AAK cDNAs were used as template to amplify the regions corresponding to the amino acids 126-403 and 144-411, respectively. The PCR products were introduced in pMal-c2 (New England Biolabs) expression vector through FastCloning.[53] Recombinant vectors were subsequently transformed into BL21-star competent cells, and expression was induced overnight at 15°C by the addition of 0.05 mM IPTG. Lysates were sonicated and clarified by centrifugation at 4°C. The recombinant proteins were then incubated with MBP amylose magnetic beads (New England Biolabs) for 1 h at 4°C and washed with 200 mM NaCl, 20 mM Tris–HCl, 1 mM EDTA, 1 mM DTT, pH 7.4 and eluted in Column Buffer supplemented with 10 mM Maltose. The same protocol was followed for expression and purification of MBP protein alone.

To produce human MBP-AAK-8xHis for *in vitro* kinase assays with bonsai NDC80 complex, a PCR product containing the sequence encoding full length human AAK was inserted into the BamHI/XhoI sites of a pETDuet-1 vector modified as described in Pan et al.[51] by Gibson assembly.[55] All PCR amplifications were performed with Phusion High Fidelity PCR master mix (Thermo Fisher Scientific, Waltham, US-MA). The ligation and PCR products were used to transform Omnimax competent bacteria (Invitrogen Corporation, Waltham, US-MA), and cells harboring plasmids were kept under antibiotic selection. The final DNA construct was validated by Sanger sequencing. The sequence encoding GST-MPS1-6xHis was subcloned into BamHI/HindIII sites of a pLIB vector for insect cell expression. The construct expressing bonsai NDC80 complex was generated previously.[38]

Expression of human wild-type (WT) and non-phosphorylatable T337 mutant (T337A) MBP-AAK-6xHis was carried out in *E. coli* BL21CodonPlus(DE3)-RIL cells (Agilent Products, Santa Clara, US-CA) grown in 2 L Terrific Broth (TB). Protein expression was induced with 0.1 mM IPTG at 18°C for 18 hours. Cells were pelleted, snap-frozen, and stored at -80°C. All purification steps were performed on ice or at 4°C. Cells expressing MBP-AAK-6xHis were resuspended in purification buffer (20 mM Tris-HCl pH 8, 500 mM NaCl, 1 mM TCEP) with added DNase (Roche, Basel, Switzerland) and protease inhibitors (Serva Electrophoresis GmbH, Heidelberg, Germany). Cells were lysed via sonication, and the lysate clarified by centrifugation (85,000×g, 30 min). The supernatant was incubated with 2 mL cOmplete His-tag NiNTA beads (Roche) pre-equilibrated in purification buffer for 2 hours with agitation. Beads were washed with 60 mL wash buffer (20 mM Tris-HCl pH 8, 500 mM NaCl, 1 mM TCEP, 20 mM Imidazole) using a 10-mL gravity column (Thermo Fisher Scientific). Protein was eluted using 300 mM imidazole in purification buffer. Following concentration by centrifugation, the protein was injected into a Superdex 200 10/600 (Cytiva, Marlborough, US-MA). Eluted fractions were analyzed by SDS-PAGE and Coomassie blue staining; the purest fractions were concentrated, spun down and snap-frozen to be stored at -80°C. GST-MPS1-6xHis and mCherry-MPS1-6xHis had been previously expressed and purified as described in Raische et al.[50] Expression and purification of $NDC80^{bonsai}$ had been previously done in Ciferri et al.[38]

In vitro kinase assay and mass-spectrometry

For *in vitro* kinase assays, recombinant human or *Drosophila* MBP-fused catalytic domain of wild-type or kinase-dead AAK, or 70nM of N-terminal His6-tagged, recombinant full-length human active AAK (#14-511 Merck Millipore, Germany) were incubated either in the presence or the absence of 14nM of N-terminal GST-fused active HsMPS1/TTK (SignalChem, Richmond, Canada) at 30°C for 30 min in a total volume of 30 μL kinase reaction buffer (5 mM MOPS, pH 7.2, 2.5 mM b-glycerol-phosphate, 5 mM $MgCl_2$, 1 mM EGTA, 0.4 mM EDTA, 0.25 mM DTT, 0.1 mM ATP. For inhibition of HsMPS1/TTK activity, Compound 5 (Cp5)[33] (gift from René Medema, Oncode Institute, The Netherlands Cancer Institute, The Netherlands) was added to the reaction at a final concentration of 100 nM. For AAK inhibition, MLN8237 (Selleck Chemicals) was added to the reaction at a final concentration of 100 nM. For Western blot analysis of AAK phosphorylation levels, reactions were stopped by addition of Laemmli sample buffer (4% SDS, 10% mercaptoetanol, 0.125 M Tris-HCl, 20% glycerol, 0.004% bromophenol blue) and heated for 5 min at 95°C. Peptides were resolved in a 10% SDS-PAGE. The activating autophosphorylation on T676 of human MPS1/TTK and the activating autophosphorylation on T288 of

human AAK were detected by western blotting with phospho-specific antibodies. Total protein levels were detected by silver staining of the gel.

For identification of phosphorylated residues, the reaction was stopped by addition of 6 M urea and analyzed by liquid chromatography (LC) coupled to a mass spectrometer (LC/MS-MS). Samples were digested with LysC/Trypsin and prepared for LC-MS/MS analysis as previously described.[56] Peptides (100 ng) were separated on an EASY-nLC 1000 HPLC system (Thermo Fisher Scientific) with a 45 min gradient from 5–60% acetonitrile with 0.1% formic acid and directly sprayed via a nano-electrospray source in an Orbitrap Exploris 480 (Thermo Fisher Scientific). The MS was operated in data-dependent mode, acquiring one survey scan and subsequently 20 MS/MS scans.[57] Resulting raw files were processed with MaxQuant software (v.2.0.1.0) using a database composed of the BL21-DE3 proteome (uniprot release 2024), Drosophila AAK, human TTK and common contaminants. Oxidation (M) and phosphorylation (STY) were given as variable modifications and carbamidomethylation (C) as fixed modification.[58] A false discovery rate cut-off of 1% was applied at the peptide, and protein levels and as well on phosphorylated peptides. Samples were run at least twice as technical replicates. Phosphosites were extracted from the phosphor(STY).txt output table. The MS/MS spectrum of pT360 was visualized and exported from MaxQuant.

In vitro AAK T337/T360 antibody validation

To test the sensitivity and specificity of the T337/T360 antibody produced in this study in detecting the AAK phosphorylation by MPS1, 200 nM of MBP-AAK (WT or T337A) was incubated either in the presence or absence of 200 nM mCherry-MPS1 (previously obtained in Raisch et al.[50]) at 30°C for 30 min in a total volume of 40 μL kinase reaction buffer (5 mM MOPS, pH 7.2, 2.5 mM b-glycerol-phosphate, 5 mM $MgCl_2$, 1 mM EGTA, 0.4 mM EDTA, 0.25 mM DTT, 0.1 mM ATP. For inhibition of HsMPS1/TTK activity, Cp5[33] (gift from René Medema, Oncode Institute, The Netherlands Cancer Institute, The Netherlands) was added to the reaction at a final concentration of 100 nM. For Western blot analysis of AAK T337/T360 phosphorylation levels, reactions were stopped by addition of Laemmli sample buffer (4% SDS, 10% mercaptoetanol, 0.125 M Tris-HCl, 20% glycerol, 0.004% bromophenol blue) and heated for 5 min at 95°C. Peptides were resolved in an 8% SDS-PAGE. The T337 AAK phosphorylation by MPS1 was detected by Western blotting with the phospho-specific antibody produced in this study. Total protein levels were detected by Coomassie staining.

NDC80 Bonsai phosphorylation assay

To test *in vitro* MPS1-mediated potentiation of HEC1/NDC80 phosphorylation by AAK, recombinant MBP-AAK-8xHis at a concentration of 5 μM was pre-incubated for 18 hours at 10°C with 1 mM MnCl2 and 200 nM λ-PP (produced in house) to remove T-loop phosphorylation. Subsequently, MBP-AAK-8xHis was diluted at a final concentration of 70 nM and incubated with $NDC80^{Bonsai}$ (500 nM), with or without GST-MPS1 (70 nM) for 30 min. Reactions were carried out at 30°C in the presence of 5 μM sodium orthovanadate, and started by adding a mix of ATP (final concentration of 2.5 mM) and MgCl2 (5 mM) to a 40 μL solution of proteins in reaction buffer (50 mM Hepes, pH 7.5, 150 mM NaCl, 1 mM TCEP). Reactions were stopped by addition of 5x Laemmli sample buffer (4% SDS, 10% β-mercaptoethanol, 0.125 M Tris-HCl, 20% glycerol, 0.004% bromophenol blue). Proteins were resolved by 15% SDS-PAGE. The autophosphorylation of T288 on MBP-AAK-8xHis and the phosphorylation of S55 on HEC1 were detected by Western blotting with phospho-specific antibodies. Total protein levels were detected by Western blotting or Coomassie blue staining of the gel.

Western blotting and gel staining

For *in vitro* kinase assays in Figure 2A, Coomassie staining of proteins resolved by SDS–PAGE was first conducted to determine comparable amounts of recombinant protein in solution to be used in the kinase assays. For Western blotting analysis, resolved proteins were transferred to a nitrocellulose membrane, using the iBlot Dry Blotting System (Thermo Fisher Scientific) according to the manufacturer's instructions. Membranes were incubated for at least 1 h at room temperature in blocking solution (5% powder milk in PBS1×, 0.05% Tween 20). All primary and secondary antibodies were diluted in the blocking solution. Membranes were incubated with primary antibody solutions overnight at 4°C under constant stirring and washed three times in PBS1×, 0.05% Tween 20 for 10 min each. Then, membranes were incubated with secondary antibody solutions for 1 h at room temperature under constant stirring. Secondary antibodies were conjugated to horseradish peroxidase (Jackson Immuno Research, UK). The blots were visualized by ECL detection and exposure to X-ray films (Fuji Medical X-Ray Film). Silver staining was conducted by gel fixation (in 30% ethanol, 10% acetic acid solution) for 2 h, followed by washing in 20% ethanol solution for 20 min and washing in water for 10 min. Then, the gel was incubated for 1min in 0,2g/L sodium thiosulfate, followed by a quick rinse with water and a 30 min incubation with 2g/L silver nitrate at 4°C. After a quick rinse with water, the gel was incubated with developer solution (10mg/L sodium thiosulfate, 0,025% formaldehyde, 30g/L sodium carbonate). When the adequate degree of staining was achieved, the development was stopped by adding a 50g/L Tris-base, 2,5% acetic acid solution.

For *in vitro* $NDC80^{Bonsai}$ phosphorylation assays in Figure S3N, proteins were transferred onto nitrocellulose membranes using the TransBlot Turbo transfer system (BioRad Laboratories, Hercules, US-CA) as per the manufacturer's protocol. Membranes were blocked for 1 hour at room temperature in 5% milk dissolved in TBS 1x, 0.1% Tween 20. Primary antibodies, diluted in the blocking solution, were incubated overnight at 4°C with constant stirring. Membranes were washed three times (10 min each) with TBS 1×, 0.1% Tween 20, followed by a 1-hour incubation at room temperature with horseradish peroxidase-conjugated secondary antibodies (Amersham/Cytiva, catalog #NXA931-1ML, 1:10000 dilution) in TBS 1×, 0.1% Tween 20. Blots were visualized via ECL detection, and images were acquired using the ChemiDoc MP System (BioRad) with Image Lab 5.1 software.

AlphaFold 3 predictions

AlphaFold 3[52] was used to model the structure of *Drosophila melanogaster* AAK and the impact of T360 phosphorylation and T360A and T360D mutations. Models were obtained by inputting the kinase domain sequence (154-406 amino acids) of *Drosophila* AAK (Q9VGF9) as a single copy 'Protein' together with a single ADP 'Ligand' and two Mg2+ 'Ion' copies. Similarly, the mutants were obtained in the same conditions, but with either Alanine (A) or Aspartic acid (D) replacing Threonine (T) in amino acid position 360. For the Phospho-threonine (pT) model, the appropriate PTM was added onto the original sequence. For each of the five output models, ClashScore analysis and T-loop Confidence scores were assessed in SwissModel to determine the best model for each prediction. Confidence scores can be found in Figure S2N. All images of structures were processed on RCSB PBD - 3D view, where alignments are overall cartoon chain superpositions with ball and stick highlights on aa360, aa317, aa311 and molecular surface of the structure. The color coding was set as cyan blue for AAK^{WT}, yellow for AAK^{T360A}, red for AAK^{T360D} and orange for AAK^{pT360}.

QUANTIFICATION AND STATISTICAL ANALYSIS

Statistical analysis

All statistical analysis was performed using GraphPad Prism V10.0 (GraphPad Software, Inc.). Values were considered statistically different whenever $P < 0.05$. P values: ns, not significant; *< 0.05; **< 0.01; ***< 0.001; ****< 0.0001. *Drosophila* cells and western blot data are presented as median ± interquartile range or mean ± SD. Statistical analysis were performed using a Kruskal–Wallis test for multiple comparisons or Mann-Whitney test when comparing between two conditions. Details on the specific test, the sample sizes and what is shown are indicated in the respective figure legends. Human cells data points were assessed for normality using the D'Agostino & Pearson test. Based on the results, statistical significance was evaluated either by Student's t-test (unpaired, two-tailed for normally distributed data) or the Mann-Whitney U-test (unpaired, two-tailed for non-normally distributed data). Variances were compared using the F-test, and Welch's correction was applied when variances were unequal. Detailed information on statistical significance for each condition can be found in the figures and their legends.

Current Biology, Volume *35*

Supplemental Information

Proximity-based activation of AURORA A by MPS1 potentiates error correction

Nelson Leça, Francisca Barbosa, Sergi Rodriguez-Calado, Arianna Esposito Verza, Margarida Moura, Paulo D. Pedroso, Inês Pinto, Elena Artes, Tanja Bange, Claudio E. Sunkel, Marin Barisic, Thomas J. Maresca, and Carlos Conde

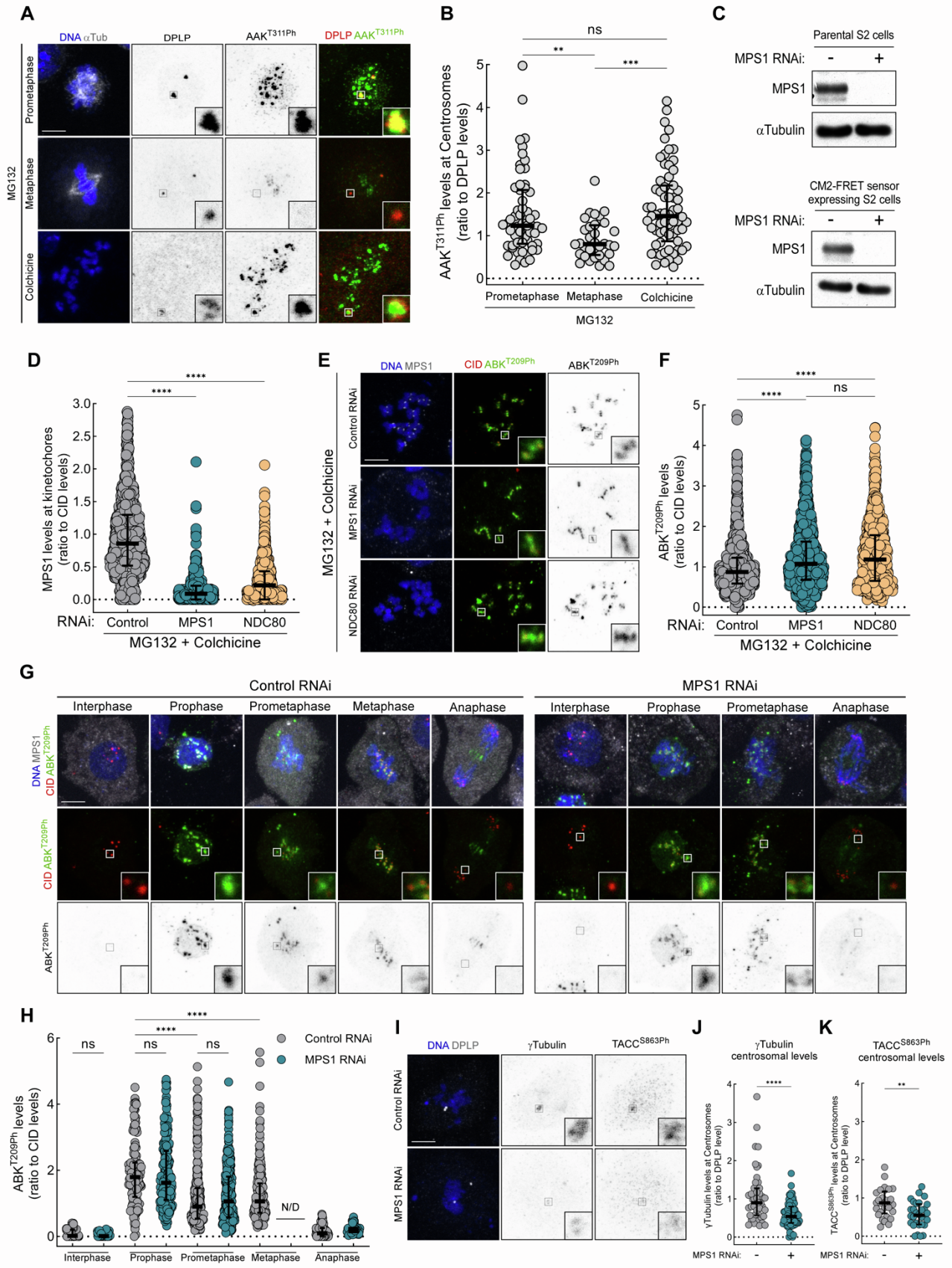


FIGURE S1. MPS1 is required for mitotic activation of AAK at centrosomes but dispensable for ABK activation at centromeres. Related to Figure 1.

(A) Representative immunofluorescence images of AAK T311 phosphorylation (AAK^{T311Ph}) levels in MG132-treated *Drosophila* S2 cells in the indicated conditions. Insets depict magnifications of selected centrosomes.

(B) Quantification of the levels of AAK T311 phosphorylation (AAK^{T311Ph}) relative to DPLP at centrosomes in the indicated conditions, as presented in (A). All values were normalized to the mean value determined for prometaphase control cells treated with MG132, which was set to 1. n ≥ 32 centrosomes for each condition from 2 biological replicates.

(C) Western blot showing MPS1 depletion in parental *Drosophila* S2 cells as presented in Figure 1A and in S2 cells expressing and CM2-FRET sensor as presented in Figure 1H.

(D) Quantification of the levels of MPS1 relative to CID at kinetochores in MG132 and colchicine-treated *Drosophila* S2 cells in the indicated conditions, as presented in (E). All values were normalized to the mean value determined for control cells treated with MG132 and colchicine, which was set to 1. n ≥ 796 kinetochores for each condition from 2 biological replicates.

(E) Representative immunofluorescence images of ABK T209 phosphorylation (ABK^{T209Ph}) and MPS1 levels in MG132 and colchicine-treated *Drosophila* S2 cells in the indicated conditions. Insets depict magnifications of selected kinetochores. This immunofluorescence staining was performed in technical replicates that were used for the immunofluorescence and quantification of AAK^{T311ph} centrosomal levels presented in Figure 1C and 1D.

(F) Quantification of the levels of ABK T209 phosphorylation (ABK^{T209Ph}) relative to CID at kinetochores/centromeres in the indicated conditions, as presented in (E). All values were normalized to the mean value determined for control cells treated with MG132 and colchicine, which was set to 1. n ≥ 796 kinetochores for each condition, from 2 biological replicates.

(G) Representative immunofluorescence images of ABK T209 phosphorylation (ABK^{T209Ph}) in control and MPS1-depleted *Drosophila* S2 cells in the indicated cell cycle stages. Insets depict magnifications of selected kinetochores/centromeres.

(H) Quantification of the levels of ABK T209 phosphorylation (ABK^{T209Ph}) relative to CID at kinetochores/centromeres of control and MPS1-depleted *Drosophila* S2 cells in the indicated cell cycle stages, as presented in (G). All values were normalized to the mean value determined for prometaphase control cells, which was set to 1. n ≥ 45 kinetochores for each condition from 2 biological replicates.

(I) Representative immunofluorescence images of γTubulin and TACC phosphorylation at S863 ($TACC^{S863Ph}$) in prometaphase control and MPS1-depleted *Drosophila* S2 cells. Insets depict magnifications of selected centrosomes.

(J) Quantification of the levels of γTubulin relative to DPLP at centrosomes of prometaphase control and MPS1-depleted *Drosophila* S2 cells, as presented in (I). All values were normalized to the mean value determined for prometaphase control cells, which was set to 1. n ≥ 29 centrosomes for each condition from 2 biological replicates.

(K) Quantification of the levels of TACC phosphorylation at S863 ($TACC^{S863Ph}$) relative to DPLP at centrosomes of prometaphase control and MPS1-depleted *Drosophila* S2 cells, as presented in (I). All values were normalized to the mean value determined for prometaphase control cells, which was set to 1. n ≥ 44 centrosomes for each condition, from 2 biological replicates.

Data information: Data in (B), (D), (F), (H), (J) and (K) are presented as median ± interquartile range. Statistical analysis in (B), (D), (F) and (H) was performed using a Kruskal–Wallis test for multiple comparisons. Statistical analysis in (J) and (K) was performed using a Mann-Whitney test. P values: ns, not significant; *< 0.05; **< 0.01; ***< 0.001; ****< 0.0001. Scale bar: 5 μm.

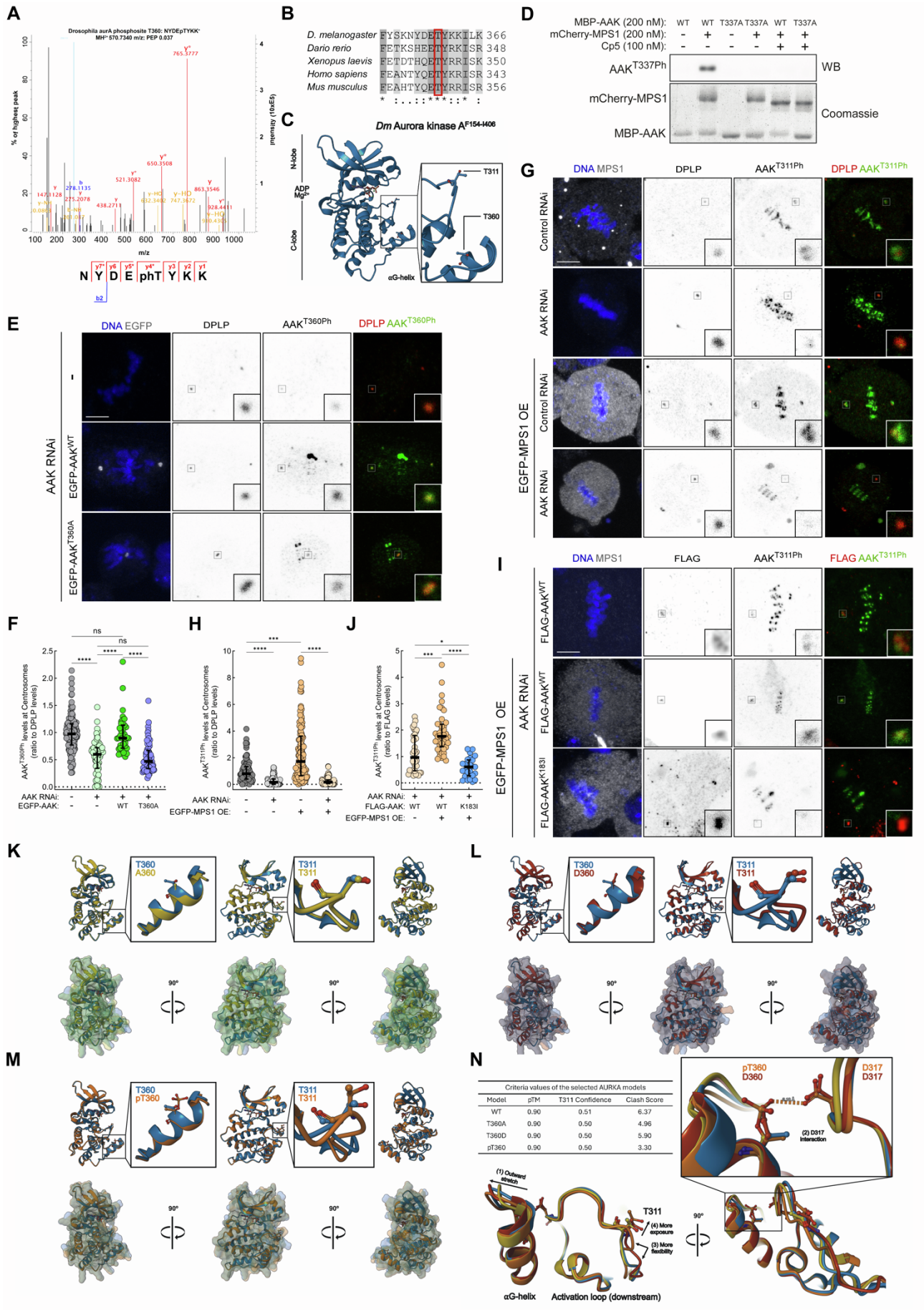


FIGURE S2. Phosphorylation of AAK T360 by MPS1 potentiates AAK T-loop autophosphorylation. Related to Figure 2.

(A) MS/MS spectrum of the phosphorylated T360 peptide of *Drosophila* AAK. *In vitro* phosphorylation of AAK by MPS1 was analyzed by MS and the MS/MS spectra were extracted from MaxQuant. Peaks corresponding to b- (blue) and y- (red and yellow) ions are annotated in the spectrum and peptide below. Fragment ions are labelled with their corresponding m/z value. Ions marked * indicate neutral losses (water or ammonia) or posttranslational modifications. The highest peak was set to 100%. Peptide mass, phosphorylation site and PEP (posterior error probability) are indicated.

(B) Clustal Omega (EMBL-EBI) local sequence alignment for the indicated AAK orthologues. Residues conservation: (*), fully conserved; (:), strongly similar properties; (.), weakly similar properties. MPS1-mediated phosphorylation of Threonine 360 (T360) in *Drosophila* AAK was identified by MS analysis after *in vitro kinase* assays. The identified residue is conserved in AAK orthologues (red rectangular box).

(C) AlphaFold 3 model of the kinase domain (154-406aa) of *Drosophila melanogaster* AAK (Q9VGF9) in crystal-like conditions (ADP and two Mg2+ ions).

(D) *In vitro* kinase assay with purified human MBP-AAK and mCherry-MPS1. Western blot analysis of AAK T337 phosphorylation (AAK^{T337Ph}) using the phospho-specific antibody produced in this study. Recombinant human wild-type (WT) or non-phosphorylatable T337 mutant (T337A) MBP-AAK was incubated with or without human mCherry-MPS1 for 30 min at 30ºC. MPS1 was inhibited (when indicated) with Cp5. Total protein levels were detected by Coomassie staining.

(E) Representative immunofluorescence images of AAK T360 phosphorylation (AAK^{T360Ph}) levels in prometaphase *Drosophila* S2 cells depleted of endogenous AAK and expressing EGFP-AAK^{WT} or EGFP-AAK^{T360A}. Insets depict magnifications of selected centrosomes. These results are part of the experiment presented in Figure 2C-E. The immunofluorescence image of the control parental S2 cell is presented in Figure 2C.

(F) Quantification of the levels of AAK T360 phosphorylation (AAK^{T360Ph}) relative to DPLP at centrosomes of prometaphase control *Drosophila* S2 cells, cells depleted of endogenous AAK and cells depleted of endogenous AAK and expressing EGFP-AAK^{WT} or EGFP-AAK^{T360A}, as presented in (E). These results are part of the experiment presented in Figure 2C-E. The values for controls are the same as presented in Figure 2C and 2D. All values were normalized to the mean value determined for prometaphase control cells, which was set to 1. n ≥ 39 centrosomes for each condition, from 2 biological replicates.

(G) Representative immunofluorescence images of AAK T311 phosphorylation (AAK^{T311Ph}) levels in metaphase *Drosophila* S2 cells in the indicated conditions. Insets depict magnifications of selected centrosomes.

(H) Quantification of the levels of AAK T311 phosphorylation (AAK^{T311Ph}) relative to DPLP at centrosomes of metaphase *Drosophila* S2 cells in the indicated conditions, as presented in (G). All values were normalized to the mean value determined for control cells expressing endogenous levels of MPS1, which was set to 1. n ≥ 71 centrosomes for each condition, from 2 biological replicates.

(I) Representative immunofluorescence images of AAK T311 phosphorylation (AAK^{T311Ph}) in metaphase *Drosophila* S2 cells depleted of endogenous AAK and expressing FLAG-AAK^{WT} or FLAG-AAK^{K183I} in the indicated conditions. Insets depict magnifications of selected centrosomes.

(J) Quantification of the levels of AAK T311 phosphorylation (AAK^{T311Ph}) relative to FLAG at centrosomes of metaphase *Drosophila* S2 cells depleted of endogenous AAK and expressing FLAG-AAK^{WT} or FLAG-AAK^{K183I} in the indicated conditions, as presented in (I). All values were normalized to the mean value determined for cells expressing FLAG-AAK^{WT} and endogenous levels of MPS1, which was set to 1. n ≥ 25 centrosomes for each condition, from 2 biological replicates.

(K) Superposed AlphaFold 3 models of *Drosophila* AAK^{WT} (cyan) and AAK^{T360A} (yellow) showing that the T360A mutation is not predicted to induce structural changes on the αG-helix, nor on the T-loop.

(L) Superposed AlphaFold 3 models of *Drosophila* AAK^{WT} (cyan) and AAK^{T360D} (red) showing that the T360D mutation is predicted to cause a displacement in the αG-helix, opening room for more flexibility of the T-loop and exposure of T311.

(M) Superposed AlphaFold 3 models of *Drosophila* AAK^{WT} (cyan) and AAK^{WT} phosphorylated in T360 (AAK^{pT360}) (orange) predicting that the phospho-threonine causes steric hindrance leading to αG-helix displacement and increased T-loop flexibility and exposure.

(N) The table shows the overall structure pTM, T-loop Confidence and ClashScore for the best models and underneath is presented the predicted model by which phosphorylation of T360 facilitates AAK T311 autophosphorylation. This model consists of four steps, (1) an outward stretch of the αG-helix that pulls on the T-loop by (2) interacting with D317 in manner that could (3) render the T-loop more flexible and (4) leave the activating T311 more exposed for phosphorylation.

Data information: Data in (F), (H) and (J) are presented as median ± interquartile range. Statistical analysis was performed using a Kruskal–Wallis test for multiple comparisons. P values: ns, not significant; *< 0.05; **< 0.01; ***< 0.001; ****< 0.0001. Scale bar: 5 μm.

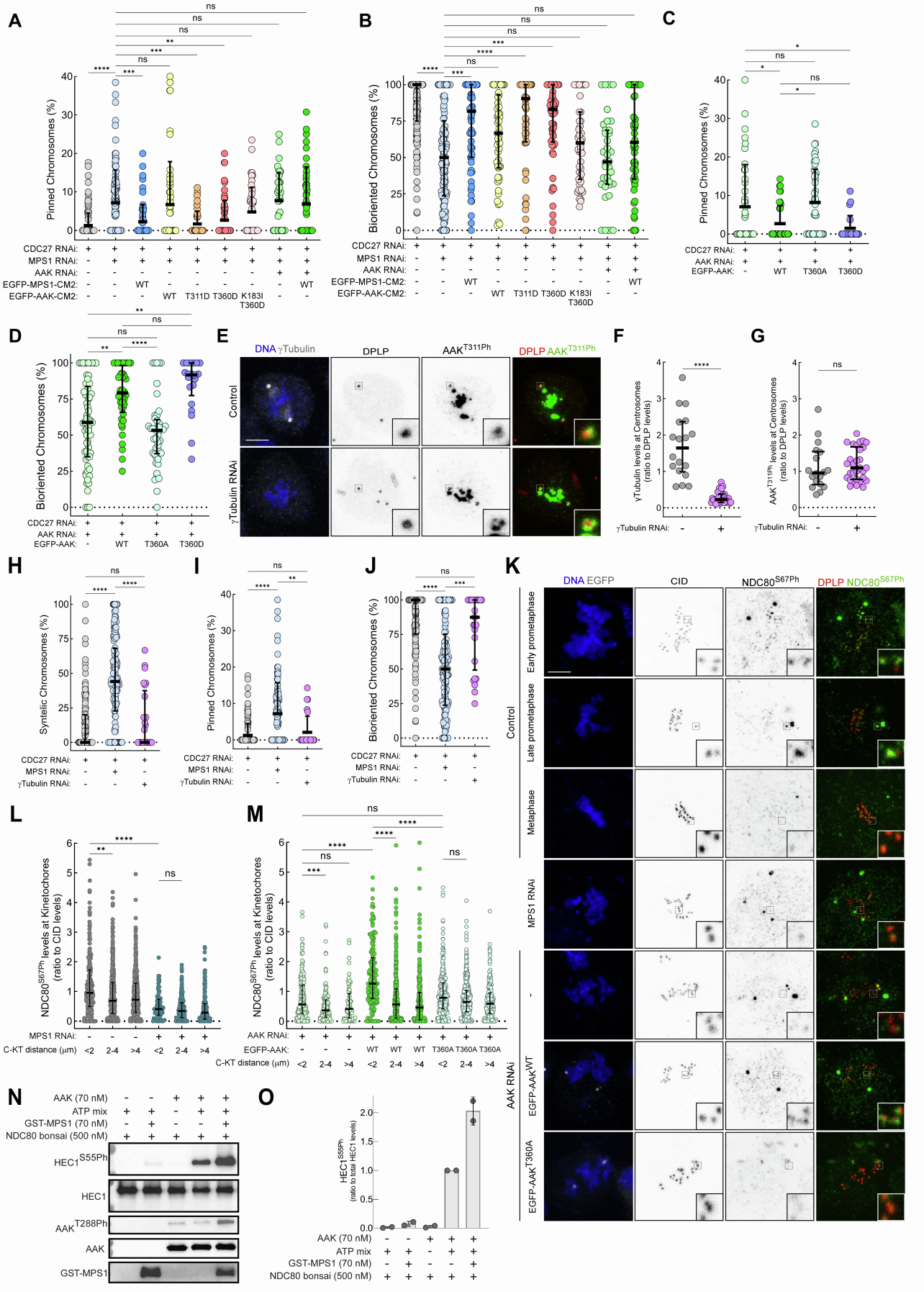


FIGURE S3. Activation of AAK by MPS1 is required for chromosome congression and biorientation in *Drosophila* S2 cells. Related to Figure 3.

(A) Percentage of chromosomes pinned to centrosomes/spindle poles per cell in the indicated conditions, as presented in Figure 3E. n ≥ 36 cells for each condition from at least 2 biological replicates.

(B) Percentage of bioriented chromosomes per cell in the indicated conditions, as presented in Figure 3E. n ≥ 36 cells for each condition from at least 2 biological replicates.

(C) Percentage of chromosomes pinned to centrosomes/spindle poles per cell in the indicated conditions, as presented in Figure 3G. n ≥ 21 cells for each condition, from at least 2 biological replicates.

(D) Percentage of bioriented chromosomes per cell in the indicated conditions, as presented in Figure 3G. n ≥ 21 cells for each condition from at least 2 biological replicates.

(E) Representative immunofluorescence images of AAK T311 phosphorylation (AAK^{T311Ph}) and γTubulin in prometaphase *Drosophila* S2 cells in the indicated conditions. Insets depict magnifications of selected centrosomes.

(F) Quantification of the levels of γTubulin relative to DPLP at centrosomes of prometaphase *Drosophila* S2 control cells in the indicated conditions, as presented in (E). All values were normalized to the mean value determined for prometaphase control cells, which was set to 1. n ≥ 18 centrosomes for each condition from 2 biological replicates.

(G) Quantification of the levels of AAK T311 phosphorylation (AAK^{T311Ph}) relative to DPLP at centrosomes of prometaphase *Drosophila* S2 in the indicated conditions, as presented in (E). All values were normalized to the mean value determined for prometaphase control cells, which was set to 1. n ≥ 18 centrosomes for each condition from 2 biological replicates.

(H) Percentage of syntelic kinetochore-microtubule attachments per cell in the indicated conditions as presented in Figure 3E. These results are part of the experiment presented in Figure 3E and 3F. The values for controls and MPS1-depleted cells are the same as presented in Figure 3F and are depicted to facilitate comparison. n ≥ 25 cells for each condition from at least 2 biological replicates.

(I) Percentage of chromosomes pinned to centrosomes/spindle poles per cell in the indicated conditions, as presented in Figure 3E. These results are part of the experiment presented in Figure 3E and S3A. The values for controls and MPS1-depleted cells are the same as presented in Figure S3A and are depicted to facilitate comparison. n ≥ 25 cells for each condition from at least 2 biological replicates.

(J) Percentage of bioriented chromosomes per cell in the indicated conditions, as presented in Figure 3E. These results are part of the experiment presented in Figure 3E and S3B. The values for controls and MPS1-depleted cells are the same as presented in Figure S3B and are depicted to facilitate comparison. n ≥ 25 cells for each condition from at least 2 biological replicates.

(K) Representative immunofluorescence images of NDC80 S67 phosphorylation ($NDC80^{S67Ph}$) in control *Drosophila* S2 in early prometaphase, late prometaphase and metaphase cells, prometaphase cells depleted of MPS1 or prometaphase cells depleted of AAK and expressing EGFP-AAK^{WT} or EGFP-AAK^{T360A}. Insets depict magnifications of selected centrosomes.

(L) Quantification of the levels of NDC80 S67 phosphorylation ($NDC80^{S67Ph}$) relative to CID at kinetochores of prometaphase and metaphase *Drosophila* S2 control cells and cells depleted of MPS1 in the indicated conditions, as presented in (K). Kinetochores were organized in 3 different columns representing ranges of distance to the closest centrosome: less than 2μm (<2); between 2μm and 4μm (2-4) and above 4μm (>4). All values were normalized to the mean value determined for prometaphase control cells, which was set to 1. n ≥ 72 kinetochores for each condition from 2 biological replicates.

(M) Quantification of the levels of NDC80 S67 phosphorylation ($NDC80^{S67Ph}$) relative to CID at kinetochores of prometaphase and metaphase *Drosophila* S2 depleted of endogenous AAK or depleted of endogenous AAK and expressing either AAK^{WT} or AAK^{T360A} in the indicated conditions, as presented in (K). Kinetochores were organized in 3 different columns representing ranges of distance to the closest centrosome: less than 2μm (<2); between 2μm and 4μm (2-4) and above 4μm (>4). All values were normalized to the mean value determined for prometaphase control cells,

as presented in (L), which was set to 1. n ≥ 72 kinetochores for each condition from 2 biological replicates.

(N) *In vitro* kinase assay with purified human orthologues of AAK and MPS1 and $NDC80^{bonsai}$. Western blot analysis of human AAK T288 activating T-loop autophosphorylation (AAK^{T288Ph}) and human HEC1 S55 phosphorylation ($HEC1^{S55Ph}$) using phospho-specific antibodies. Previously dephosphorylated recombinant MBP-AAK-8xHis was incubated with $NDC80^{Bonsai}$, with or without GST-MPS1 for 30 min at 30ºC. Total protein levels were detected by Western blotting.

(O) Quantification of HEC1 S55 phosphorylation ($HEC1^{S55Ph}$) blot intensity relative to total HEC1 levels in the indicated conditions, as presented in (N). All values were normalized to the mean value determined for HEC1 S55 phosphorylation in the presence of AAK and ATP and in the absence of MPS1 (lane 4), which was set to 1. The bars indicate the mean intensities; the dots indicate the measurements from duplicates.

Data information: Data in (A), (C), (I) and (O) are presented as mean ± SD; and in (B), (D), (F), (G), (H), (J), (L) and (M) as median ± interquartile range. Statistical analysis in (A), (B), (C), (D), (H), (I), (J), (L), (M) was performed using a Kruskal–Wallis test for multiple comparisons. Statistical analysis in (F) and (G) was performed using a Mann-Whitney test. P values: ns, not significant; *< 0.05; **< 0.01; ***< 0.001; ****< 0.0001. Scale bar: 5 μm.

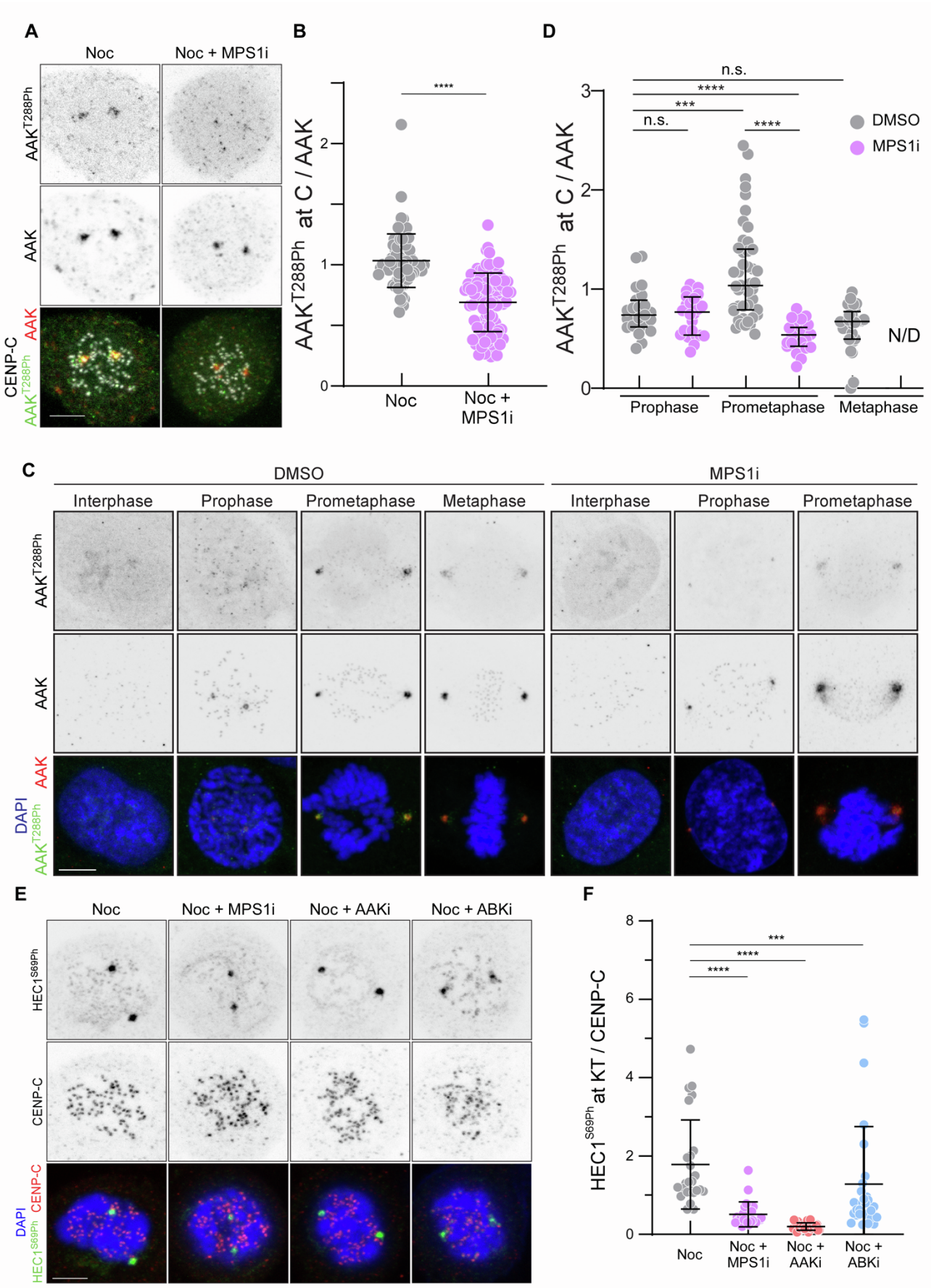


Figure S4. Inhibition of MPS1 impairs AAK activation at centrosomes and HEC1 S69 phosphorylation at unattached kinetochores in RPE-1 cells. Related to Figure 4.

(A) Representative immunofluorescence images of AAK T288 phosphorylation (AAK^{T288Ph}) and AAK levels in nocodazole-treated RPE-1 cells in control and MPS1-inhibited (MPS1i) conditions. Proteasome was inhibited by MG132 to prevent mitotic exit after MPS1 inhibition.

(B) Quantification of the levels of AAK T288 phosphorylation (AAK^{T288Ph}) relative to total AAK levels at centrosomes of nocodazole-treated RPE-1 cells in the indicated conditions as presented in (A). All values were normalized to the median value determined for control cells, which was set to 1.

(C) Representative immunofluorescence images of AAK T288 phosphorylation (AAK^{T288Ph}) and AAK levels in RPE-1 cells in control and MPS1-inhibited (MPS1i) conditions in the indicated cell cycle stage.

(D) Quantification of the levels of AAK T288 phosphorylation (AAK^{T288Ph}) relative to total AAK levels at centrosomes of RPE1 cells in control and MPS1-inhibited (MPS1i) conditions in the indicated mitotic stages, as presented in (C). All values were normalized to the median value determined for control cells, which was set to 1.

(E) Representative immunofluorescence images of HEC1 S69 phosphorylation ($HEC1^{S69Ph}$) and CENP-C levels in nocodazole-treated RPE-1 cells in control, MPS1-inhibited (MPS1i), AAK-inhibited (AAKi) and ABK-inhibited (ABKi) conditions. Proteasome was inhibited by MG132 to prevent mitotic exit after MPS1 inhibition.

(F) Quantification of the levels of HEC1 S69 phosphorylation ($HEC1^{S69Ph}$) relative to CENP-C levels at kinetochores of nocodazole-treated RPE-1 cells in the indicated conditions as presented in (E). All values were normalized to the median value determined for control cells, which was set to 1.

Data information: Data are presented in (B), (D) and (F) as mean ± SD. Statistical analysis was performed using a Mann-Whitney non-parametric t-test. P values: ns, not significant; *< 0.05; **< 0.01; ***< 0.001; ****< 0.0001. n ≥ 25 cells for each condition. Scale bar 5 μm.

REAGENT or RESOURCE	SOURCE	IDENTIFIER
Oligonucleotides		
MPS1F: 5'- TAATACGACTCACTATAGGGTC TTCCAAACACCTATGACG-3′	This paper	N/A
MPS1R: 5′-TAATACGACTCACTATAGGGCGTT TAGATATCCCTGCACCA-3′	This paper	N/A
AAK5′_F; 5′-TAATACGACTCACTATAGGGAGAA CTTGCCATTCGCCTCATC-3′	This paper	N/A
AAK5′_R: 5′-TAATACGACTCACTATAGGGAGA GACGGCACGGCACAGGCACTCG-3′	This paper	N/A
AAK3′_F: 5′-TAATACGACTCACTATAGGGAGA ACACATTCTTGTTTAATTTTC-3′	This paper	N/A
AAK3′_R: 5′-TAATACGACTCACTATAGGGAGA GAAAACACACACAAACTTT-3′	This paper	N/A
NDC80F: 5′-TAATACGACTCACTATAGGGTTTG ATCCGGATGTTTTGTTGTAGTTC-3′	This paper	N/A
NDC80R: 5′-TAATACGACTCACTATAGGGTTTT TTAATTTGAAAACAAAGAATACTCTT-3′	This paper	N/A
CDC27F: 5′-TAATACGACTCACTATAGGGAACA ATAGC-3′	This paper	N/A
CDC27R: 5′-TAATACGACTCACTATAGGGTCTT CATGTAGAATTGCATGGC-3′	This paper	N/A
γTub RNAiF: 5'-TAATACGACTCACTATAGTTTT CTCATGACAGGCTACACG-3'	This paper	N/A
γTub RNAiR: 5'-TAATACGACTCACTATAGGGT CACAGATCGACTATCCTCC-3'	This paper	N/A
siSpindly: 5′- GAAAGGGUCUCAAACUGAA-3′	Eibes et al[S1]	N/A
siControl: 5′- UGGUUUACAUGUCGACUAA-3′	Eibes et al[S1]	N/A

Table S1. Oligonucleotides used in the study. Related to STAR Methods.

Supplemental Reference

S1. Eibes S, Rajendraprasad G, Guasch-Boldu C, Kubat M, Steblyanko Y, Barisic M. (2023) CENP-E activation by Aurora A and B controls kinetochore fibrous corona disassembly. Nat Commun. 14(1):5317. doi: 10.1038/s41467-023-41091-2. PMID: 37658044; PMCID: PMC10474297.